Arsenic removal by household sand filters

Dissertation

der Mathematisch-Naturwissenschaftlichen

Fakultät der Eberhard Karls Universität Tübingen

zur Erlangung des Grades eines

Doktors der Naturwissenschaften

(Dr. rer. nat.)

Vorgelegt von

M.Sc. Anh Van Le

Aus Hanoi, Vietnam

Tübingen

2023

Gedruckt mit Genehmigung der Mathematisch-Naturwissenschaftlichen Fakultät der Eberhard Karls Universität Tübingen.

Tag der mündlichen Qualifikation: 23.06.2023

Dekan :	Prof. Dr. Thilo Stehle
1. Berichterstatter:	Prof. Dr. Andreas Kappler
2. Berichterstatter:	Assoc. Prof. Dr. James M Byrne

Source: the United Nations Water

Table of contents

Acknowledgment

First, I would like to thank Prof. Dr. Andreas Kappler, my main supervisor, for his continuous support and guidance during my Ph.D. The way Andreas led the Geomicrobiology group, involved people in discussions, exchanging ideas, and learning from each other has opened my mind. His passion for science and the motivated and friendly conversations were inspiring. I thank Andreas for his trust and the freedom I had to develop the Ph.D. project independently. Ultimately, we could answer all our research questions. He is truly a unique boss that I always enjoy working with.

Second, I am grateful to my co-supervisor Dr. Stephan Hug for his support during my short stay at Eawag for XRF analysis and his comments on my Ph.D. outlines and manuscripts.

Third, this thesis would only be done with the help of Assoc. Prof. Dr. Marie Muehe regarding all synchrotron analysis. Despite the technical challenges and time differences when running the beamline remotely, Marie put a lot of effort into collecting “decent signals” for all my samples. Thank you so much, Marie!

Next, I would like to express my gratitude to my Vietnamese collaborators: Prof. Viet, Prof. Trang, Duyen, The Anh, Vy Anh at Hanoi University of Science, who provided the field supports and laboratory equipment to ensure that the field campaigns 2018 and 2020 went smoothly.

I also want to thank all the junior group leaders in Geomicrobiology, including James, Casey, Caroline, Muammar, and Parchi, for your suggestions/feedback and for always being available for any questions.

I am grateful to Ulf, Natalia, and Stefie, who had to work extra hours at night to proofread this thesis and help me quickly translate the English abstract to German.

My most enormous acknowledgment is for the “Kappler family” - all the geomicrobiology group members who directly or indirectly contributed to this Ph.D. thesis. I want to thank our excellent technicians, Ellen, Franziska, and Lars, who helped with the analysis and patiently answered all my questions (even on the weekend). My time in Tuebingen was unforgettable because of my office mates: “the one and only” Stefanie Becker, Timm Bayer, and our “honored member” Natalia Jakus. I am also grateful for the time spent with others; Sergey, Ulf, Verena, Kate, Anjela,

Yuming, Yuge, Hanna, Katrin, Ankita, Christopher, Martyna, Lea, Manuel, Dr. Alison, and people from the 6th floor: Lucile, Ran, Victor. Thanks for all the scientific and non-scientific conversations and events. Many of you colleagues have become my friends for life!

Further, I want to thank my students and student assistants (Hiwis) involved in this project: Elly, Caro, Mario, Sophie, and Thomas.

I want to acknowledge my family, who always encourages me to thrive harder, get out of my comfort zone and explore the world. This is a dream that my parents did not have a chance to do so during their young age. My parents (bố Lê Công Hùng, mẹ Lê Thị Nga) and my brother (Quốc Anh – Mít) never doubt my (personal and professional) choices but support me unconditionally and patiently.

Cảm ơn cả nhà đã luôn ủng hộ Vân béo trên còn đường khoa học chông gai hiểm hóc này. Vân béo đã làm được rồi!

Last but not least, I would like to express my highest appreciation to my life companion - my husband - Mohammad Azari, who has been sharing all the highs and lows with me. Thanks for traveling almost every week from Essen to Tuebingen to visit me for the last three years. My highest motivation to finish this journey was his support, understanding, patience, and love. دوستت دارم!

Summary

Arsenic (As) contamination in groundwater is threatening the health of 220 million people worldwide, especially in low-income regions such as West Bengal, Bangladesh, and Vietnam. The capacities of centralized water treatment facilities are insufficient, forcing people in rural areas to rely on simple household sand filtration systems. Recent studies in Vietnam reported that 2.5 million people use sand filters to treat As-contaminated groundwater. However, there have been limited studies on the stability and efficiency of As and co-contaminants (such as Fe, Mn, and NH_4^+) and on the evaluation of the environmental risks of using household sand filters.

Therefore, in the framework of this Ph.D. thesis, we aim to expand our understanding on different mechanisms controlling the retention of As in household sand filters in the Red River delta, Vietnam, and provide the first insights into potential environmental risks caused by open disposal of filter materials. Our research strategy was a combination of field and lab work, applying a wide range of chemical and microbial analyses to tackle three main aspects:

i) Contribution of microbial oxidation processes to Fe(II), As(III), Mn(II), and NH_4^+ removal efficiency of sand filters under different geochemical conditions.
ii) Monitoring long-term filter performances and characterizing spatiotemporal changes of solid-associated Fe, As, and Mn in sand columns mimicking household filters under unsaturated and saturated conditions.
iii) Evaluating the environmental risk of As re-mobilization from disposed As-bearing filter materials to the soils.

The general outcome of the project enabled us to draw several conclusions as follows:

i) Core microbial communities shared amongst household sand filters indicated that Fe(II) -, Mn(II) -, NH_4^+ -, and NO_2^- -oxidizing microorganisms were prevalent and correlated with key functional processes in sand filters. Due to the complementation of microbial processes, the removal efficiency of Fe, Mn, and As reached (on average) 96 ± 3.8%, 92.2 ± 13.9%, and 92.8 ± 7.2%, respectively. Additionally, NH_4^+ was transformed by ammonium-oxidizing archaea (*Nitrosotaleacea*e) and ammonium-oxidizing bacteria (*Nitrosomonas*), followed by nitrite-oxidizing bacteria (*Nitrospira*) to NO_3^- to a large extent, with a removal efficiency of 74.7 ± 29.8 %. Unexpectedly, a substantial amount of putative methane oxidizer sequences and methane

monooxygenase genes (*pmoA*) were detected in all samples, suggesting microbial methane oxidation in household sand filters.

ii) A series of column experiments mimicking household sand filters in the field and lab was established to follow Fe, As, and Mn removal over time and their elemental distribution and speciation on sand surfaces under unsaturated (fully oxic) and saturated (O_2-depleted) conditions in sand filters.

In average, 99 ± 0.2%, 93 ± 0.7%, and 91 ± 8% of dissolved Fe(II), As(III), and Mn(II) was removed by filtration under unsaturated conditions. Under saturated conditions, Fe and As removal remained the same (99 ± 0.4% and 95 ± 1.7%), while an elevated amount of dissolved Mn(II) was leached from the sand column. The effluent's Mn(II) concentration was detected to be 2-5 times higher than the inflow. Solid phase analysis of spatial distribution and speciation of Fe, As, and Mn on the sand particle surfaces indicated Fe(III), As(V), and Mn(III)/(IV) dominated in unsaturated sand materials. Inversely, under saturated conditions, up to 46 and 15% of Fe(III) and As(V) were reduced in the anoxic zone (5-10 cm depth), and the presence of reduced Mn(II) was confirmed.

Our observations indicated that Mn oxides formed during the oxic flow (unsaturated conditions) were acting as a secondary hosting phase and oxidant for both Fe(II) and As(III)/(V) under saturated conditions. The mechanisms included following steps: (1) Microbial reduction of As-bearing Fe(III) (oxyhydr)oxide under O_2-depleted conditions led to an increase of Fe(II) and desorption of As(III)/(V) from Fe(III) phases. (2) Re-adsorption of reduced Fe(II) and desorbed As(III)/(V) to remaining Fe(III) (oxyhydr)oxide and Mn oxides surfaces. (3) Abiotic Fe(II) oxidation by Mn oxides resulting in formation of new Fe(III) phases that sequester As(III)/(V) to the solid phase.

iii) Finally, dumping disposed sand filter materials into soils was shown to mobilize As from sand materials into the pore water under reducing conditions. Results from microcosm experiments revealed that microbially-mediated Fe(III)/As(V) reduction led to 210 µg/L of As mobilization in the mixture of sand materials with soil. In the solid phase, we detected that up to 10% Fe(III), and 32% As(V) was reduced in the mixture microcosm mimicking filter materials' interaction with the soil. Additionally, the optimization of single-particle ICP-MS detected the mass concentration of colloidal Fe

and As in our microcosms. The results indicated that 77-100% of Fe and As concentrations in the colloidal fraction were quickly decreased with the highest reduction rate after 30 days. The finding highlights that As mobilization as colloids is essential, especially after onset of the reducing conditions, but its importance decreases over time.

Overall, the Ph.D. thesis greatly expands our knowledge on factors contributing to As, Fe, Mn, and NH_4^+ removal in household sand filters and the potential risk of disposing filter materials to the environment. Results from the thesis can be transferred as recommended guidelines for the safe and sustainable use of household sand filters. As a future vision to achieve sustainable development goals of the United Nations by 2030, this work can be a model approach to expand studies on sand filter-based technologies applied to other As-affected areas. Such an approach can enhance the water quality and help to minimize the mortality rate of using unsafe water for humankind.

Zusammenfassung

Die Verunreinigung des Grundwassers mit Arsen (As) bedroht die Gesundheit von 220 Millionen Menschen weltweit, insbesondere in einkommensschwachen Regionen wie Westbengalen, Bangladesch und Vietnam. Hier müssen sich die Menschen aus ländlichen Gebieten auf einfache Sandfiltersysteme für den Haushalt stützen, da konventionelle zentrale Wasseraufbereitungsanlagen nicht ausreichend vorhanden sind. Jüngste Studien aus Vietnam haben ergeben, dass 2,5 dort Millionen Menschen Sandfilter zur Aufbereitung von As-verunreinigtem Grundwasser verwenden. Es gibt jedoch nur begrenzt Studien zur Effizienz und der Haltbarkeit der Filter bei der Entfernung von As- und Co-Kontaminanten (wie Fe, Mn und NH_4^+), sowie zur Evaluation eines potenziellen Umweltrisikos, welches durch die Verwendung von Haushaltssandfiltern entsteht.

Im Rahmen dieser Doktorarbeit wollen wir daher unser Verständnis der verschiedenen Mechanismen, die die Rückhaltung von As in Haushaltssandfiltern bewirken, erweitern und erste Einblicke in mögliche Umweltrisiken durch die Verwendung von Sandfiltern geben. Unser Forschungsansatz war eine Kombination aus Feld- und Laborarbeit, wobei wir eine Vielzahl von chemischen und mikrobiellen Analysen einsetzten, um drei Hauptaspekte zu untersuchen:

i) Beitrag der mikrobiellen Oxidationsprozesse zum Wirkungsgrad von Sandfiltern bei der Entfernung von Fe(II), As(III), Mn(II) und NH_4^+ unter verschiedenen geochemischen Bedingungen.

ii) Langzeitüberwachung der Filterleistung und Charakterisierung der räumlich-zeitlichen Veränderungen von feststoffassoziiertem Fe, As und Mn in Sandsäulen, welche Haushaltsfilter unter ungesättigten und gesättigten Bedingungen simulieren.

iii) Evaluierung von Umweltrisiken durch die Remobilisierung von As aus entsorgten As-haltigen Filtermaterialien in die Böden.

Das Hauptergebnis des Projekts ermöglichte es uns, mehrere Schlussfolgerungen zu ziehen:

i) Die Identifizierung der wichtigen mikrobiellen Gemeinschaften in Haushaltssandfiltern zeigte, dass Fe(II) -, Mn(II) -, NH_4^+ - und NO_2^- - oxidierende Mikroorganismen überwiegen und mit den funktionellen Schlüsselvorgängen in Sandfiltern korrelieren. Aufgrund der gegenseitigen Ergänzung der mikrobiellen

Prozesse, erreichte die Wirksamkeit der Entfernung von Fe, Mn und As (im Durchschnitt) 96 ± 3,8%, 92,2 ± 13,9% bzw. 92,8 ± 7,2%. Darüber hinaus wurde NH_4^+ von Ammonium-oxidierenden Archaeen (Nitrosotaleaceae) und Ammonium-oxidierenden Bakterien (Nitrosomonas), und weiter von Nitrit-oxidierenden Bakterien (Nitrospira) zu einem großen Teil in NO_3^- umgewandelt, mit einer Wirksamkeit von 74,7 ± 29,8%. Unvermutet wurde in allen Proben eine beachtliche Menge an vermeintlichen Methanoxidationssequenzen und Methanmonooxygenase-Genen (pmoA) nachgewiesen, was auf eine mikrobielle Methanoxidation in Haushaltssandfiltern schließen lässt.

ii) Es wurde eine Reihe von Säulenexperimenten als Feldstudie und im Labor durchgeführt, um die Entfernung von Fe, As und Mn im Laufe der Zeit sowie deren elementare Verteilung und Spezies auf Sandoberflächen unter ungesättigten (mit Sauerstoff) und gesättigten (ohne Sauerstoff) Bedingungen in Sandfiltern zu bestimmen.

Durchschnittlich 99 ± 0,2%, 93 ± 0,7% und 91 ± 8% des gelösten Fe(II), As(III) und Mn(II) wurden durch Filtration unter ungesättigten Bedingungen entfernt. Unter gesättigten Bedingungen blieb die Fe- und As-Entfernung gleich (99 ± 0,4% und 95 ± 1,7%), während eine erhöhte Menge an gelöstem Mn(II) aus der Sandsäule ausgewaschen wurde. Die Mn(II)-Konzentration des Ausflusses war 2-5 mal höher als die des Zuflusses. Die Festphasenanalyse der räumlichen Verteilung und der Spezies von Fe, As und Mn auf den Sandpartikeloberflächen ergab, dass Fe(III), As(V) und Mn(III)/(IV) in ungesättigten Sandmaterialien dominieren. Umgekehrt wurden unter gesättigten Bedingungen bis zu 46% Fe(III) und 15% As(V) in der anoxischen Zone (5-10 cm Tiefe) reduziert, und das und Vorhandensein von reduziertem Mn(II) wurde bestätigt.

Unsere Beobachtung deutet darauf hin, dass die während des oxischen Flusses (ungesättigte Bedingungen) gebildeten Mn-Oxide als sekundäre Trägerphase und Oxidationsmittel für Fe(II) und As(III)/(V) unter gesättigten Bedingungen nach folgenden Mechanismen wirken: i) reduziertes Fe(II) und desorbiertes As(III)/(V) wurden an die verbleibenden Fe(III)-(Oxyhyr)oxid- und Mn-Oxid-Mineraloberflächen erneut adsorbiert. ii) Fe(II) wurde abiotisch durch Mn-Oxide oxidiert, die neue Fe(III)-Phasen bilden, welche As(III)/(V) an die feste Phase binden.

Schließlich wurde gezeigt, dass durch das Ausbringen von erschöpften Sandfiltermaterialien in den Erdboden, unter reduzierenden Bedingungen, das As aus den Sandmaterialien in das Porenwasser ausgespült werden kann. Die Ergebnisse von Mikrokosmos-Experimenten zeigten, dass die mikrobiell bedingte Fe(III)/As(V)-Reduktion zu einer As-Mobilisierung von 210 µg/L in einer Sand-Erde-Mischung führte. In der Festphase konnten wir bis zu 10% Fe(III) nachweisen, und 32% As(V) wurden im gemischten Mikrokosmos, der die Interaktion der Filtermaterialien mit dem Erdboden imitiert, reduziert. Zusätzlich wurde durch die Optimierung der Einzelteilchen-Massenspektrometrie mit induktiv gekoppeltem Plasma die Massenkonzentration von kolloidalem Fe und As in unseren Mikrokosmen ermittelt. Die Ergebnisse zeigten, dass 77-100% der Fe- und As-Konzentrationen in der kolloidalen Fraktion im Vergleich zum Beginn der reduzierenden Bedingungen schnell abnahmen. Das Ergebnis unterstreicht, dass die Mobilisierung von As in Form von Kolloiden von wesentlicher Bedeutung ist, insbesondere direkt nach Beginn der reduzierenden Bedingungen, wobei ihre Bedeutung mit der Zeit abnimmt.

Zusammenfassend lässt sich sagen, dass die Doktorarbeit durch eine Reihe von durchgeführten Studien, unser Verständnis über die Faktoren, die zur Entfernung von As, Fe, Mn und NH_4^+ durch Haushaltssandfilter, sowie über ein potenzielles Umweltrisiko durch die Entsorgung von Filtermaterialien erweitert wurde. Die Ergebnisse dieser Arbeit können als empfohlene Richtlinien für den sicheren und nachhaltigen Einsatz von Haushaltssandfiltern verwendet werden. Vorausblickend, kann diese Arbeit als Modellversuch angesehen werden, um Studien über Sandfiltertechnologien auf andere von Armut betroffenen Gebiete auszuweiten, dies wiederum würde zur Realisierung von Entwicklungszielen der Vereinten Nationen bis 2030 nachhaltig beitragen. Ein solcher Schritt könnte die Wasserqualität verbessern und die Sterblichkeitsrate aufgrund der Verwendung von unsicherem Wasser für die Menschheit vermindern.

Chapter 1. Introduction

Arsenic (As) is known as the "king of poisons" (Parascandola, 2012). The acute toxicity of inorganic arsenic is ranked number one on the substance priority list announced by the agency for toxic substances and disease registry (ATSDR) (ATSDR, 2022). An elevated As concentration in the groundwater in Asia has been reported since the beginning of the 1990s. The As mobilization processes have naturally occurred in unconsolidated sediment aquifers worldwide (Smedley and Kinniburgh, 2002). Due to a lack of centralized water treatment facilities in Southeast Asia, millions must lean on As-contaminated private wells as a primary water source (Podgorski and Berg, 2020). For many years, sand filters are a popular household treatment method to enhance drinking water quality in such areas, due to their practicability, simplicity, and affordability. However, household sand filters usually experience low maintenance and lack water quality monitoring (Kabir and Chowdhury, 2017).

In another context, ensuring As-safe drinking water is one of the key priorities in the United Nation's 2030 Sustainable Development Goals (SDGs) (Bundschuh et al., 2022). More specifically, SDG 6 targeting 6.1 and 6.3 calls for achieving **"universal and equitable access to safe and affordable drinking water"** as well as **"to improve water quality by reducing pollution, eliminating dumping and minimizing release of hazardous chemicals and materials"** (UN, 2018). Therefore, for developing countries to fulfill mentioned goals, tremendous and urgent efforts are required to improve current sand filtration technologies to reduce As to lower than 10 µg/L (world health organization - WHO standard for drinking water) and minimize their potential environmental risk.

1.1. Arsenic contamination in the groundwater

The geogenic occurrence of As is the primary source of As contamination globally, affecting human health (Zheng, 2020). Metamorphic rocks containing As from the Himalayan mountains were eroded and weathered in Asia. These processes formed adsorbed As on iron (oxyhydr)oxides coating on sand particles, which were delivered downstream and associated with river delta sediments (McArthur et al., 2001; Mukherjee et al., 2019). Over thousands of years, sediment transportation has built

up at the delta with depths of several hundred meters that buried As from Himalayan-derived sediments under anoxic conditions (Polizzotto et al., 2008).

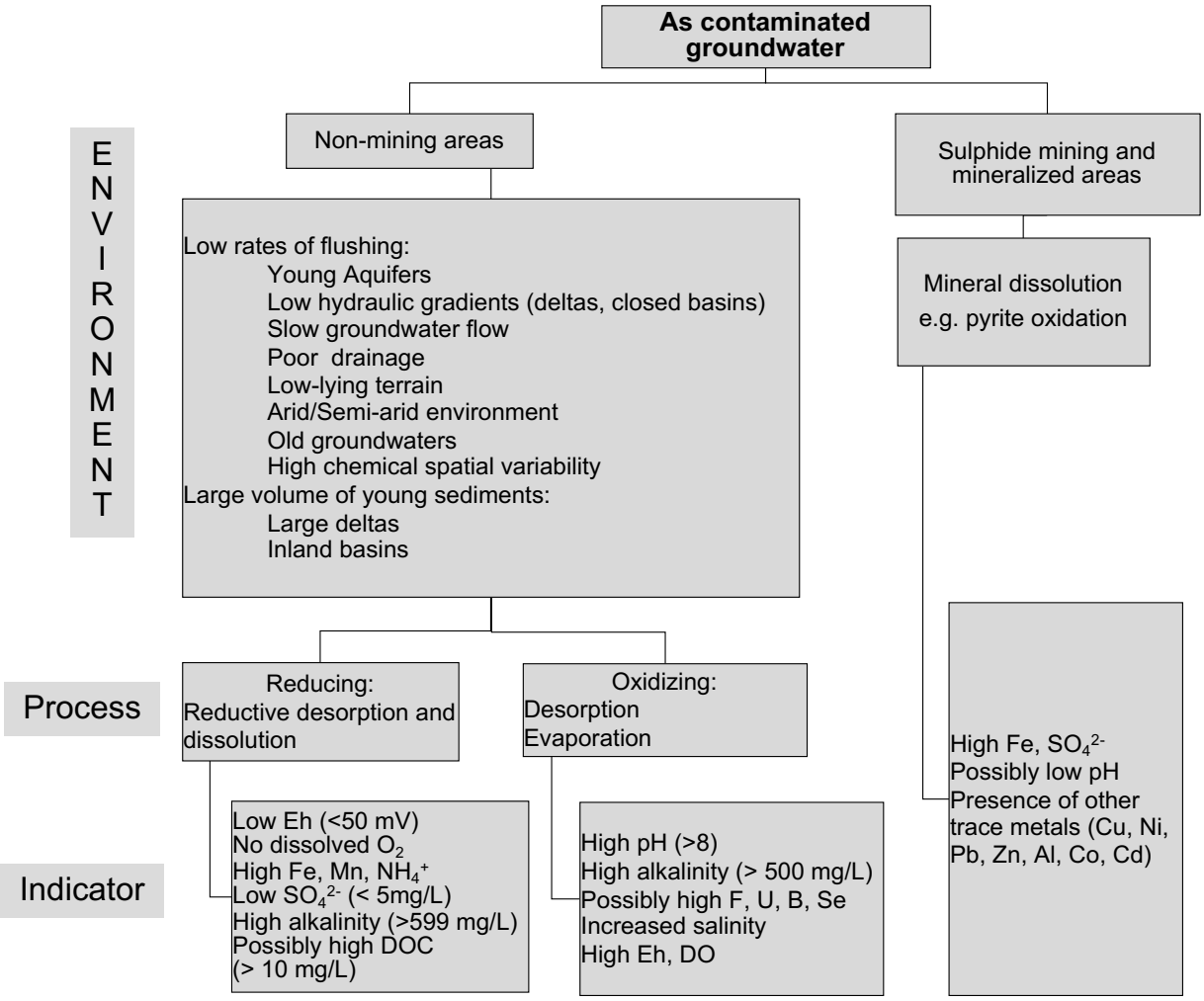

Figure 1. Summary of groundwater conditions prone to As mobilization with proposed processes and indicators adapted from (Smedley and Kinniburgh, 2002).

Although the mechanisms of the natural occurrence of As are widely accepted, the mechanism of As mobilization to the groundwater is under debate. The mobilization processes highly depend on the hydrological and biogeochemical conditions of the aquifer/aquitard (Muehe and Kappler, 2014). Groundwater characteristics that indicate a potential for As mobilisation were proposed by (Smedley and Kinniburgh, 2002), and summarized in Figure 1. The first proposed mechanism of As mobilization is due to extensive groundwater abstraction. The aquifer conditions turn to oxic, consequently leading to an oxidation of the As-rich pyrite aquifer (Chowdhury et al., 1999; Das et al., 1996; Mandal et al., 1996). Another proposed mechanism is the As release due to the competition with phosphate, carbonate, or organic carbon for sorption sites on ferrihydrite (Islam et al., 2004; Smedley and Kinniburgh, 2002). The two most

commonly accepted mechanisms are a combination of microbial reduction of As-bearing Fe(III) (oxyhydr)oxides (Harvey et al., 2002; Islam et al., 2004), and direct reduction of As(V) by As-reducing bacteria (AsRB) to form toxic As(III) (Oremland and Stolz, 2003). Since As(III) has a lower sorption affinity to Fe(III) (oxyhydr)oxides than As (V), it is thus more amenable to being mobilized to the solution (Leupin and Hug, 2005).

1.2. Arsenic treatment technologies with focus on household application

Arsenic treatment technologies have been implemented at full-scale and household scale levels, which serve different communities/ areas worldwide (Figure 2). Full-scale water treatment plants commonly use adsorptive media to eliminate As at coagulation or filtration steps (Hering et al., 2017). The media can sequester As and other contaminants such as Fe, Mn, and PO_4^{3-}. In some treatment plants, oxidants such as NaOCl or $KMnO_4$ are injected into the treatment processes to enhance the oxidation efficiency of As(III) (Sorlini and Gialdini, 2010). Fewer drinking water treatment plants have used ion exchange or reverse osmosis (RO) to remove As (Hering et al., 2017; Koley, 2022). In general, the full-scale As treatment requires operation, maintenance, and high cost at initial investment and maintenance. Therefore, the methods/ concepts suit high- to middle- income countries.

Figure 2. Arsenic affected areas worldwide marked as red dots and pictures of As treatment technologies are used in these areas (Muehe and Kappler, 2014).

In low-income countries, household sand filter (SFs) is a popular arsenic treatment method recommended by the world health organization (WHO) to increase access to safe drinking water (WHO, 2011). The sand filters usually contain a reactive sand layer and separation and drainage layers. The water is fed from the top, and the effluent is collected at the bottom (see examples of "SONO" filters in Bangladesh and normal household sand filters in Vietnam in Figure 2). Depending on the groundwater composition, the sand filter materials can be mixed with different adsorptive media to enhance the As removal. For example, "Alcan" filters implemented in India contain layers of aluminum hydroxide in the filter bed, and "SONO" filters in Bangladesh include layers of a composite iron matrix (Table 1). However, when the groundwater contains high Fe/As ratios, such as in the case of the Red River delta, in Vietnam, fine sand materials collected locally can effectively remove As, Fe, Mn, and NH_4^+ (Nitzsche et al., 2015a; Van Le et al., 2022b). The cost-effectiveness of the household filters mainly depends on adsorbent media, low-cost media such as aluminum oxides (5.7 US $/kg), and ferric hydroxide (6 US $/kg) can effectively remove As bringing the treatment cost to even less than 0.2 US $/m3 (Table 1) (Kabir and Chowdhury, 2017).

Table 1. List of household filters applied to remove arsenic in low-income countries adapted from (Kabir and Chowdhury, 2017).

	Name/ method	Description	Cost ($ US/m^3)	References
1	BUET filter	Filter fill with activated aluminum oxides. As inflow = 176–402 µg/L As outflow = 2–8 µg/L	0.7–1.2	(Ahmed, 2001; Chappell et al., 2001)
2	Iron oxide-coated sand filter	7100 cm^3 of Fe-coated sand treat at least 2500 L of inflow water 25-mg Fe/g sand can effectively reduce arsenic from 300 µg/L to below 50 µg/L	0.7	(Ahmed et al., 2005; Chappell et al., 2001; Joshi and Chaudhuri, 1996)
3	Filtration with zero-valent iron	Add a layer of ZVI (such as iron nails) between sand layers. 90% arsenic removal	1.2	(Hug and Leupin, 2003; Leupin and Hug, 2005)
4	Alcan filter	Pre-aeration of groundwater and aluminum oxides act as adsorptive media attached to the tube well Up to 100% removal	< 0.3	(Ahmed, 2001; Chappell et al., 2001)
5	Apyron filter	Inorganic granular mixed metal oxides-based filter media	< 0.12	(Ahmed et al., 2005; Ahmed, 2001)

		Efficiency 95%, final arsenic < 50 µg/L		
6	SONO filter	A layer of composite iron matrix fillings mix with layers of coarse and fine sand 90–95% arsenic removal	0.2–0.25	(Hussam and Munir, 2007)
7	Garnet filter	Use brick chips and sand as filter media. 70–90% removal efficiency	0.71	(Ahmed, 2001; Chappell et al., 2001)
8	Shafi filter	Adapted ceramic filters. Bijoypur clay and treated cellulose act as filter media. As outflow < 100 µg/L	0.85	(Ahmed, 2001; Chappell et al., 2001)
9	Shapla filter	Bricks treated by ferrous sulfate 80–90% arsenic removal	0.73	(Ahmed et al., 2005)
10	Kachan™ filter	Combines slow sand filtration with iron nails installed at top of the filter unit 85–95% removal rate	1.0	(Mueller et al., 2021; Ngai et al., 2007)
11	Read-Fi filter	Hydrous cerium oxide (CeO_2. nH_2O) act as adsorbent for As removal	2.0	(Ahmed et al., 2005; Hanchett et al., 2011)

1.3 Household sand filters in Vietnam applied to remove As(III), Fe(II), Mn(II) and NH_4^+

In Vietnam, from the early 1990s, household SFs represent a conventional and popular treatment method to eliminate Fe and As from the groundwater (Berg et al., 2006). Groundwater in Vietnam typically contains <0.01–48 mg/L of Fe(II), 0.05–3.3 mg/L of Mn(II), 10–382 µg/L of As(III), and < 0.25–96 mg-N/L of NH_4^+ (Winkel et al., 2011). The As removal efficiency depends on Fe : As : P ratios from the groundwater. Accounting for the competition of P and As for sorption on the Fe mineral surface, the mass ratio of (Fe-1.8P)/As has to be higher than 50 to ensure efficient As removal (Berg et al., 2006; Hug et al., 2008). The groundwater is pumped intermittently into a top compartment and trickles through the filter driven by gravity. Outflow water is collected in a lower basin and used for drinking and cleaning (Figure 3A) (Nitzsche et al., 2015a).

Fe(II), Mn(II), As(III), and NH_4^+ removal mechanisms in household SFs are governed by a complex interplay of biogeochemical processes. Abiotic Fe(II) oxidation by atmospheric O_2 forms poorly crystalline Fe(III) (oxyhydr)oxide minerals coated on

sand grains (Nitzsche et al., 2015a; Voegelin et al., 2014). This process also mediates the co-oxidation of As(III) to As(V), which strongly adsorbs on Fe(III) (oxyhydr)oxide (Hug and Leupin, 2003; Voegelin et al., 2014). Mn(II) oxidation processes occur either by activities of manganese oxidizing bacteria (Hansel, 2017; Tebo et al., 2005) or by abiotic reaction with O_2 at the Fe(III) (oxyhydr)oxides surface (Davies and Morgan, 1989; Ross and Bartlett, 1981). Additionally, microbial ammonium oxidation forming nitrate (NO_3^-) was demonstrated in a previous study (Nitzsche et al., 2015b).

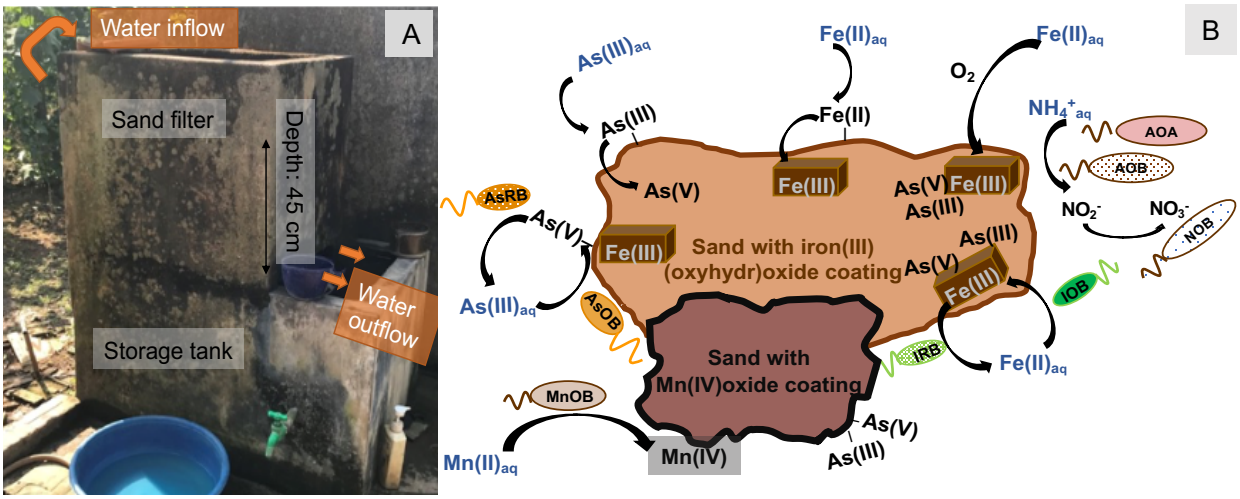

Figure 3: (A) Household sand filter in Vietnam; (B) main processes in sand filters suggested by (Nitzsche et al., 2015a; Voegelin et al., 2014).

The operation of the sand filter starts with the unsaturated flow when sand layers maintain oxic and is followed by saturated flow when an oxygen gradient is formed along the sand column creating semi-oxic (top layer) and anoxic zones (bottom layer). Due to the precipitation of carbonate minerals and metal (oxyhydr)oxides on the filter surface, the filter is clogged (every 3-6 months), 10- 20 cm of top sand is scraped off for unclogging (Nitzsche et al., 2015a). Thus, sand filters are usually operated under alternating unsaturated and saturated flow for many years.

For decades, As-bearing sand materials have been disposed in backyard gardens (floodplain soil) and along riverbanks. Considering a sand filter described in (Voegelin et al., 2014) with a surface area of 0.47 m^2 in which at least 10 cm of sand layer needs to be removed (with a bulk density of 1470 kg/m^3 and porosity of 35%), this equals to the disposal of around 70 kg of As-bearing sand materials from one household. During the monsoon season, with frequent and heavy rainfall and potential flood events, the disposed sand materials turn anoxic and reduce, leading to a high risk of As release to porewater.

1.4. Knowledge gaps

Previous works analyzing filtration efficiency, solid-phase composition, and microbial community of one household sand filter have given solid background information on mechanisms controlling the retention and transformation of As, Fe, Mn and NH_4^+. However, there are still open questions:

First, the contribution of biotic oxidation of Fe(II), Mn(II), As(III), and NH_4^+ to the filtration efficiency under varying groundwater geochemistry is poorly understood. The previous model-based study (Berg et al., 2006) indicated that co-precipitation of As with Fe(III) (oxyhydr)oxides underestimated the As removal by sand filters. The findings suggest that Fe, As, and Mn retention processes might be additionally catalyzed by microbial activities, which shed light on the role of microbial oxidations processes in sand filters. However, the microbial communities of sand filters can differ when fed by different groundwater varying in chemical composition. Other factors such as filter dimensions, the height of the sand layer, and irregularities during operation can also influence microbial activities in SFs, consequently controlling the removal efficiency of Fe(II), Mn(II), As(III), and NH_4^+.

Second, there need to be more studies monitoring Fe, As, and Mn effluent over time in unsaturated (fully oxic) and saturated (O_2-depleted) conditions to fully evaluate the stability of household sand filters. Most studies have examined As, Fe, and Mn removal by sampling at a specific time point to confirm their high efficiency. However, whether the high removal efficiency of sand filters remains stable over time, despite the flow changes from unsaturated (sand layer is fully oxic) to saturated conditions (sand layer forms oxic to anoxic zones along the filter depths) is unknown.

Previous studies indicated that the constant buildup of Mn oxides in sand filters under unsaturated conditions (Nitzsche et al., 2015a; Van Le et al., 2022b), followed by Mn reduction, might complement the heterogeneous oxidation of As(III) and Fe(II) under O_2-depleted conditions (saturated conditions) (Eq 1, 2).

$MnO_2 + AsO_3^{3-} + 2H^+ \rightarrow Mn^{2+} + AsO_4^{3-} + H_2O$ (Eq. 1)

$MnO_2 + 2Fe^{2+} + 4H^+ \rightarrow 2Fe^{3+} + Mn^{2+} + 2H_2O$ (Eq. 2)

However, there is no direct evidence that under O_2-depleted conditions the presence of Mn(IV) oxides can control the immobilization of As and Fe in the household sand

filters and the subsequent cleaning of water. Thus, monitoring of Fe, As, and Mn concentrations in the effluent at different time points (with varying saturation statuses and redox conditions) is crucial to answer the question whether As removal mechanisms change during redox fluctuations and can reveal the impact of Mn(III/IV) oxides on As and Fe retention in sand filters.

Third, despite the staggering amount of sand filter residues estimated as around 2.1 × 10^5 tons, openly deposed to the environment every six months, the extent of As mobilisation is still unknown and has yet to be investigated.

During the monsoon season, with frequent and heavy rainfall and potential flood events, the floodplain soil turns anoxic and releases suspended colloidal Fe(III) (oxyhydr)oxides to the stormwater. An increase of mobilized colloidal Fe(III) (oxyhydr)oxides can further facilitate As(V) transport (Montalvo et al., 2018; Yao et al., 2020) and promote solubilization of As-bearing colloidal Fe(III) minerals (Fan et al., 2018; Ma et al., 2018; Mansor and Xu, 2020). Thus, a mechanistic study following the mobilization and transformation of As in porewater, solid, and colloidal phases is essential to fully evaluate the risk of As mobilization from disposed sand materials.

1.5. Objectives of this study

This Ph.D. thesis aims to expand our understanding of different mechanisms controlling the retention of As in household sand filters and provide the first insights into potential environmental risks caused by using sand filters. Therefore, three main objectives were defined to address the knowledge gaps explained in the previous section. Each of main objectives, includes several side objectives to be followed.

i) To evaluate the core microbial community of household sand filters when being fed by varying groundwater composition and how the microorganisms contribute to the Fe(II), As(III), Mn(II), and NH_4^+ oxidation processes in household sand filters (paper 1 – chapter 2).

Side objectives are:

- To analyze operational conditions and contaminant removal efficiency of 20 household sand filters running under varying geochemical conditions in the Red River delta, Vietnam.

- To identify the microbial community composition focusing on potential Fe(II)-, Mn(II)-, As(III)- and NH_4^+-oxidizers among 7 households sand filters (selected based on differences in groundwater composition and depth of groundwater abstraction).
- To elucidate the influence of groundwater geochemistry on the microbial community structures in household sand filters.

ii) To monitor long-term performances and characterize spatiotemporal changes of solid-associated Fe, As, and Mn in sand columns mimicking household sand filters under unsaturated and saturated conditions (paper 2 – chapter 3).

Side objectives are:

- To monitor the performance of the sand columns applied to remove As, Fe, and Mn over time from unsaturated to saturated conditions.
- To quantify the distribution of total As, Fe, and Mn along the depth of sand columns.
- To identify the location and speciation of As, Fe, and Mn on the surface of sand particles under unsaturated and saturated conditions.

iii) To evaluate the environmental risk of As re-mobilization from disposed As-bearing filter materials to the soils, focusing on the fate of As in aqueous, solid, and colloidal phases (papers 3 & 4 – chapter 4 & 5).

Side objectives are:

- To characterize and interpret single particle inductively coupled plasma mass spectrometry (spICP-MS) data from disposed As-bearing sand filter materials samples to evaluate particle-facilitated mobilization of As under reducing conditions (paper 3 – chapter 4).
- To quantify dynamics of reactive Fe and As in microcosms incubating floodplain soil, disposed As-bearing filter materials and their mixture under reducing conditions (paper 4 – chapter 5).
- To evaluate the transformation of Fe minerals in microcosms (paper 4 – chapter 5).
- To identify As redox states, and coordination environments in the solid phase of microcosms (paper 4 – chapter 5).

- To quantify dynamics of colloidal Fe and As over time in microcosms (paper 4 – chapter 5).

The expected outcome of this work can enhance the water quality and help to minimize the mortality rate of using unsafe water for people living in As-affected areas in the Red River delta of Vietnam.

References

Ahmed, F., Minnatullah, K., Talbi, A., 2005. Arsenic mitigation technologies in South and East Asia. Towar. a more Eff. Oper. response 2, 166–207.

Ahmed, M.F., 2001. An overview of arsenic removal technologies in Bangladesh and India, in: Proceedings of BUET-UNU International Workshop on Technologies for Arsenic Removal from Drinking Water, Dhaka. Citeseer, pp. 5–7.

ATSDR, 2022. Priority list of hazardous substances. Public Heal. Serv.

Berg, M., Luzi, S., Trang, P.T.K., Viet, P.H., Giger, W., Stüben, D., 2006. Arsenic removal from groundwater by household sand filters: Comparative field study, model calculations, and health benefits. Environ. Sci. Technol. 40, 5567–5573. https://doi.org/10.1021/es060144z

Bundschuh, J., Niazi, N.K., Alam, M.A., Berg, M., Herath, I., Tomaszewska, B., Maity, J.P., Ok, Y.S., 2022. Global arsenic dilemma and sustainability. J. Hazard. Mater. 436, 129197. https://doi.org/https://doi.org/10.1016/j.jhazmat.2022.129197

Chappell, W.R., Abernathy, C.O., Calderon, R.L., 2001. Arsenic exposure and health effects IV. Elsevier.

Chowdhury, T.R., Basu, G.K., Mandal, B.K., Biswas, B.K., Samanta, G., Chowdhury, U.K., Chanda, C.R., Lodh, D., Roy, S.L., Saha, K.C., 1999. Arsenic poisoning in the Ganges delta. Nature 401, 545–546.

Das, D., Samanta, G., Mandal, B.K., Roy Chowdhury, T., Chanda, C.R., Chowdhury, P.P., Basu, G.K., Chakraborti, D., 1996. Arsenic in groundwater in six districts of West Bengal, India. Environ. Geochem. Health 18, 5–15.

Davies, S.H.R., Morgan, J.J., 1989. Manganese(II) oxidation kinetics on metal oxide surfaces. J. Colloid Interface Sci. 129, 63–77. https://doi.org/10.1016/0021-9797(89)90416-5

Dixit, S., Hering, J.G., 2003. Comparison of arsenic(V) and arsenic(III) sorption onto iron oxide minerals: Implications for arsenic mobility. Environ. Sci. Technol. 37, 4182–4189. https://doi.org/10.1021/es030309t

Fan, L., Zhao, F., Liu, J., Frost, R.L., 2018. The As behavior of natural arsenical-containing colloidal ferric oxyhydroxide reacted with sulfate reducing bacteria. Chem. Eng. J. 332, 183–191. https://doi.org/10.1016/j.cej.2017.09.078

Hanchett, S., Johnston, R., Khan, M.H., 2011. Arsenic removal filters in Bangladesh, in: UNC Water and Health Conference.

Hansel, C.M., 2017. Manganese in Marine Microbiology, 1st ed, Advances in microbial physiology. Elsevier Ltd. https://doi.org/10.1016/bs.ampbs.2017.01.005

Harvey, C.F., Swartz, C.H., Badruzzaman, A.B.M., Keon-Blute, N., Yu, W., Ali, M.A., Jay, J., Beckie, R., Niedan, V., Brabander, D., 2002. Arsenic mobility and groundwater extraction in Bangladesh. Science (80-.). 298, 1602–1606.

Hering, J.G., Katsoyiannis, I.A., Theoduloz, G.A., Berg, M., Hug, S.J., 2017. Arsenic removal from drinking water: Experiences with technologies and constraints in practice. J. Environ. Eng. 143, 03117002. https://doi.org/10.1061/(ASCE)EE.1943-7870.0001225

Hug, S.J., Leupin, O., 2003. Iron-catalyzed oxidation of Arsenic(III) by oxygen and by hydrogen peroxide: pH-dependent formation of oxidants in the Fenton reaction. Environ. Sci. Technol. 37, 2734–2742. https://doi.org/10.1021/es026208x

Hug, S.J., Leupin, O.X., Berg, M., 2008. Bangladesh and Vietnam: Different groundwater compositions require different approaches to arsenic mitigation. Environ. Sci. Technol. 42, 6318–6323. https://doi.org/10.1021/es7028284

Hussam, A., Munir, A.K.M., 2007. A simple and effective arsenic filter based on composite iron matrix: Development and deployment studies for groundwater of Bangladesh. J. Environ. Sci. Heal. - Part A Toxic/Hazardous Subst. Environ. Eng. 42, 1869–1878. https://doi.org/10.1080/10934520701567122

Islam, F.S., Gault, A.G., Boothman, C., Polya, D.A., Chamok, J.M., Chatterjee, D., Lloyd, J.R., 2004. Role of metal-reducing bacteria in arsenic release from Bengal delta sediments. Nature 430, 68–71. https://doi.org/10.1038/nature02638

Joshi, A., Chaudhuri, M., 1996. Removal of arsenic from ground water by iron oxide-coated sand. J. Environ. Eng. 122, 769–771.

Kabir, F., Chowdhury, S., 2017. Arsenic removal methods for drinking water in the developing countries: technological developments and research needs. Environ. Sci. Pollut. Res. 24, 24102–24120. https://doi.org/10.1007/s11356-017-0240-7

Koley, S., 2022. Future perspectives and mitigation strategies towards groundwater arsenic contamination in West Bengal, India. Environ. Qual. Manag. 31, 75–97. https://doi.org/10.1002/tqem.21784

Leupin, O.X., Hug, S.J., 2005. Oxidation and removal of arsenic (III) from aerated groundwater by filtration through sand and zero-valent iron. Water Res. 39, 1729–1740. https://doi.org/10.1016/j.watres.2005.02.012

Ma, J., Guo, H., Weng, L., Li, Y., Lei, M., Chen, Y., 2018. Distinct effect of humic acid on ferrihydrite colloid-facilitated transport of arsenic in saturated media at different pH. Chemosphere 212, 794–801. https://doi.org/10.1016/j.chemosphere.2018.08.131

Mandal, B.K., Chowdhury, T.R., Samanta, G., Basu, G.K., Chowdhury, P.P., Chanda, C.R., Lodh, D., Karan, N.K., Dhar, R.K., Tamili, D.K., 1996. Arsenic in groundwater in seven districts of West Bengal, India–the biggest arsenic calamity in the world. Curr. Sci. 976–986.

Mansor, M., Xu, J., 2020. Benefits at the nanoscale: a review of nanoparticle-enabled processes favoring microbial growth and functionality. Environ. Microbiol. 22, 3633–3649. https://doi.org/10.1111/1462-2920.15174

McArthur, J.M., Ravenscroft, P., Safiulla, S., Thirlwall, M.F., 2001. Arsenic in groundwater: testing pollution mechanisms for sedimentary aquifers in Bangladesh. Water Resour. Res. 37, 109–117.

Montalvo, D., Vanderschueren, R., Fritzsche, A., Meckenstock, R.U., Smolders, E., 2018. Efficient removal of arsenate from oxic contaminated water by colloidal humic acid-coated goethite: Batch and column experiments. J. Clean. Prod. 189, 510–518. https://doi.org/10.1016/j.jclepro.2018.04.055

Muehe, E.M., Kappler, A., 2014. Arsenic mobility and toxicity in South and South-east Asia–a review on biogeochemistry, health and socio-economic effects, remediation and risk predictions. Environ. Chem. 11, 483–495.

Mueller, B., Dangol, B., Ngai, T.K.K., Hug, S.J., 2021. Kanchan arsenic filters in the lowlands of Nepal: mode of operation, arsenic removal, and future improvements. Environ. Geochem. Health 43, 375–389.

Mukherjee, A., Gupta, S., Coomar, P., Fryar, A.E., Guillot, S., Verma, S., Bhattacharya, P., Bundschuh, J., Charlet, L., 2019. Plate tectonics influence on geogenic arsenic cycling: From primary sources to global groundwater enrichment. Sci. Total Environ. 683, 793–807. https://doi.org/10.1016/j.scitotenv.2019.04.255

Ngai, T.K.K., Shrestha, R.R., Dangol, B., Maharjan, M., Murcott, S.E., 2007. Design for sustainable development - Household drinking water filter for arsenic and pathogen treatment in Nepal. J. Environ. Sci. Heal. - Part A Toxic/Hazardous Subst. Environ. Eng. 42, 1879–1888. https://doi.org/10.1080/10934520701567148

Nitzsche, K.S., Lan, V.M., Trang, P.T.K., Viet, P.H., Berg, M., Voegelin, A., Planer-Friedrich, B., Zahoransky, J., Müller, S.K., Byrne, J.M., Schröder, C., Behrens, S., Kappler, A., 2015a. Arsenic removal from drinking water by a household sand filter in Vietnam - Effect of filter usage practices on arsenic removal efficiency and microbiological water quality. Sci. Total Environ. 502, 526–536. https://doi.org/10.1016/j.scitotenv.2014.09.055

Nitzsche, K.S., Weigold, P., Lösekann-Behrens, T., Kappler, A., Behrens, S., 2015b. Microbial community composition of a household sand filter used for arsenic, iron, and manganese removal from groundwater in Vietnam. Chemosphere 138, 47–59. https://doi.org/10.1016/j.chemosphere.2015.05.032

Oremland, R.S., Stolz, J.F., 2003. The ecology of arsenic. Science (80-.). 300, 939–944. https://doi.org/10.1126/science.1081903

Podgorski, J., Berg, M., 2020. Global threat of arsenic in groundwater. Science (80-.). 368, 845–850. https://doi.org/10.1126/science.aba1510

Polizzotto, M.L., Kocar, B.D., Benner, S.G., Sampson, M., Fendorf, S., 2008. Near-surface wetland sediments as a source of arsenic release to ground water in Asia. Nature 454, 505–508. https://doi.org/10.1038/nature07093

Ross, D.S., Bartlett, R.J., 1981. Evidence for nonmicrobial oxidation of manganese in soil. Soil Sci. 132, 153–160.

Smedley, P.L., Kinniburgh, D.G., 2002. A review of the source, behaviour and distribution of arsenic in natural waters. Appl. Geochemistry 17, 517–568. https://doi.org/10.1016/S0883-2927(02)00018-5

Sorlini, S., Gialdini, F., 2010. Conventional oxidation treatments for the removal of arsenic with chlorine dioxide, hypochlorite, potassium permanganate and monochloramine. Water Res. 44, 5653–5659.

Tebo, B.M., Johnson, H.A., McCarthy, J.K., Templeton, A.S., 2005. Geomicrobiology of manganese(II) oxidation. Trends Microbiol. 13, 421–428. https://doi.org/10.1016/j.tim.2005.07.009

UN, W., 2018. Sustainable Development Goal 6 Synthesis Report on Water and Sanitation. United Nations.

Van Le, A., Straub, D., Planer-Friedrich, B., Hug, S.J., Kleindienst, S., Kappler, A., 2022. Microbial communities contribute to the elimination of As, Fe, Mn, and NH4+ from groundwater in household sand filters. Sci. Total Environ. 838, 156496. https://doi.org/10.1016/j.scitotenv.2022.156496

Voegelin, A., Kaegi, R., Berg, M., Nitzsche, K.S., Kappler, A., Lan, V.M., Trang, P.T.K., Göttlicher, J., Steininger, R., 2014. Solid-phase characterisation of an effective household sand filter for As, Fe and Mn removal from groundwater in Vietnam. Environ. Chem. 11, 566–578.

WHO, 2011. Evaluating household water treatment options: Health-based targets and microbiological performance specifications. World Health Organization.

Winkel, L.H.E., Trang, P.T.K., Lan, V.M., Stengel, C., Amini, M., Ha, N.T., Viet, P.H., Berg, M., 2011. Arsenic pollution of groundwater in Vietnam exacerbated by deep aquifer exploitation for more than a century. Proc. Natl. Acad. Sci. U. S. A. 108, 1246–1251. https://doi.org/10.1073/pnas.1011915108

Yao, Y., Mi, N., He, C., Yin, L., Zhou, D., Zhang, Y., Sun, H., Yang, S., Li, S., He, H., 2020. Transport of arsenic loaded by ferric humate colloid in saturated porous media. Chemosphere 240. https://doi.org/10.1016/j.chemosphere.2019.124987

Zheng, Y., 2020. Global solutions to a silent poison. Science (80-.). 368, 818 LP – 819. https://doi.org/10.1126/science.abb9746

Chapter 2 _ Paper 1: Personal contribution

Anh Van Le: conceptualization, methodology, investigation, visualization, writing original draft. Daniel Straub: formal analysis, data curation, writing - review & editing. Britta Planer-Friedrich: resources, writing - review & editing. Stephan Hug: resources, supervision, writing - review & editing. Sara Kleindienst: resources, writing - review & editing. Andreas Kappler: conceptualization, resources, supervision, writing - review & editing, project administration, funding acquisition.

Chapter 2: Microbial communities contribute to the elimination of As, Fe, Mn, and NH_4^+ from groundwater in household sand filters

Anh Van Le[1], Daniel Straub[2], Britta Planer-Friedrich[3], Stephan J. Hug[4], Sara Kleindienst[5], Andreas Kappler[1,6]

[1]Geomicrobiology, Center for Applied Geoscience, University of Tuebingen, Germany
[2]Quantitative Biology Center (QBiC), University of Tuebingen, Germany
[3]Environmental Geochemistry, Bayreuth Center for Ecology and Environmental Research (BayCEER), University of Bayreuth
[4]Eawag, Swiss Federal Institute of Aquatic Science and Technology, Dübendorf, Switzerland
[5]Microbial Ecology, Center for Applied Geoscience, University of Tuebingen, Germany
[6]Cluster of Excellence: EXC 2124: Controlling Microbes to Fight Infection, Tuebingen, Germany

Published in: *Science of the Total Environment*

https://doi.org/10.1016/j.scitotenv.2022.156496

Abstract

Household sand filters (SFs) are widely applied to remove iron (Fe), manganese (Mn), arsenic (As), and ammonium (NH_4^+) from groundwater in the Red River delta, Vietnam. Processes in the filters probably include a combination of biotic and abiotic reactions. However, there is limited information on the microbial communities treating varied groundwater compositions and on whether biological oxidation of Fe(II), Mn(II), As(III), and NH_4^+ contributes to the overall performance of SFs. We therefore analyzed the removal efficiencies, as well as the microbial communities and their potential activities, of SFs fed by groundwater with varying compositions from low (3.3 µg L^{-1}) to high (600 µg L^{-1}) As concentrations. The results revealed that Fe(II)-, Mn(II)-, NH_4^+-, and NO_2^--oxidizing microorganisms were prevalent and contributed to the performance of SFs. Additionally, groundwater composition was responsible for the differences among the present microbial communities. We found i) microaerophilic Fe(II) oxidation by *Sideroxydans* in all SFs, with the highest abundance in SFs fed by low-As and high-Fe groundwater, ii) *Hyphomicropbiaceae* as the main Mn(II)-oxidizers in all SFs, iii) As sequestration on formed Fe and Mn (oxyhydr)oxide minerals, iv) nitrification by ammonium-oxidizing archaea (AOA) followed by nitrite-oxidizing bacteria (NOB), and v) unexpectedly, the presence of a substantial amount of methane monooxygenase genes (*pmoA*), suggesting microbial methane oxidation taking place in SFs. Overall, our study revealed diverse microbial communities in SFs used for purifying arsenic-contaminated groundwater and our data indicate an important contribution of microbial activities to the key functional processes in SFs.

2.1. Introduction

Household filters are recommended by the WHO as a solution to increase access to safe water for drinking purpose (WHO, 2011). Household filter technologies are modified depending on the sources and the identity of water contaminants, with the aim to eliminate contaminants such as pathogens, inorganic/organic compounds, and toxic metals (Freitas et al., 2022). Besides slow household sand filters (SHSFs) applied to remove particles and pathogens (Andreoli and Sabogal-Paz, 2020; Elliott et al., 2008; Medeiros et al., 2020), household filters to remove As have been widely implemented in developing countries such as Nepal (Kanchan filter) (Mueller et al., 2021; Ngai et al., 2007), Bangladesh (SONO filter) (Hussam and Munir, 2007; Neumann et al., 2013), and Vietnam (Berg et al., 2006).

In Vietnam, since the early 1990s until today, household sand filters (SFs) represent a conventional and popular treatment method to eliminate Fe and As from groundwater (Berg et al., 2006). Groundwater in Vietnam typically contains <0.01-48 mg L^{-1} Fe(II), 0.05-3.3 mg L^{-1} Mn(II), 10-382 µg L^{-1} As(III), and <0.25-96 mg-N L^{-1} NH_4^+ (Winkel et al., 2011). The groundwater is pumped intermittently into a top compartment meanwhile being mixed with atmospheric oxygen, bringing the DO of groundwater before entering the sand layer to 7-8 mg L^{-1} (VanLe et al., unpublished data). The aerated groundwater then trickles through the filter driven by gravity. The filtered water is drained out completely between each filtration, allowing oxygen to re-occupy into pore spaces in the sand layer. Outflow water is collected in a lower basin and used for drinking and cleaning purposes (Figure 1A) (Berg et al., 2006; Luzi et al., 2004; Nitzsche et al., 2015a). The As removal efficiency is dependent on the Fe:As:P ratios in the groundwater. After accounting the competition of P and As for sorption on Fe mineral surface, the mass ratio of (Fe-1.8P)/As has to be higher than 50 to ensure efficient As removal (Berg et al., 2006; Hug et al., 2008).

Fe(II), Mn(II), As(III), and NH_4^+ removal mechanisms in household SFs are governed by a complex interplay of biogeochemical processes. Abiotic Fe(II) oxidation by atmospheric oxygen (O_2) forms poorly crystalline Fe(III) (oxyhydr)oxide minerals coated on sand grains (Berg et al., 2006; Voegelin, Andreas; Kaegi, Ralf; Berg, Michael; Nitzsche, Katja Sonja; Kappler, Andreas; Lan, Vi Mai; Trang, Pham Thi Kim; Göttlicher, Jörg; Steininger, 2014). This process also mediates co-oxidation of arsenite to arsenate, which strongly adsorbs on Fe(III) (oxyhydr)oxide minerals (Hug and

Leupin, 2003; Voegelin, Andreas; Kaegi, Ralf; Berg, Michael; Nitzsche, Katja Sonja; Kappler, Andreas; Lan, Vi Mai; Trang, Pham Thi Kim; Göttlicher, Jörg; Steininger, 2014). Arsenic elimination in SFs predicted based on simple co-precipitation of As(III) with Fe(III) (oxyhydr)oxides was lower than observed for real household filters (Berg et al., 2006). Hence, it was suggested that As(III) oxidation might either be coupled to abiotic Mn(IV) reduction or is also catalyzed by bacteria. However, until now, there is only one study reporting the distribution of microbial communities in one household SF (Nitzsche et al., 2015b, 2015a). In this study, a black layer of MnO_2 coated on clean sand was observed in the bottom layer and an enrichment culture of manganese-oxidizing bacteria (MnOB) was obtained, suggesting the occurrence of biotic Mn oxidation in SFs (Nitzsche et al., 2015b; Voegelin, Andreas; Kaegi, Ralf; Berg, Michael; Nitzsche, Katja Sonja; Kappler, Andreas; Lan, Vi Mai; Trang, Pham Thi Kim; Göttlicher, Jörg; Steininger, 2014). Additionally, microbial ammonium oxidation forming nitrate (NO_3^-) was demonstrated in the same SF (Nitzsche et al., 2015b).

However, microbial communities of sand filters can differ when fed by groundwater with varying geochemical composition. Hence the contribution of biotic oxidation of Fe(II), Mn(II), As(III), and NH_4^+ in household SFs with varying groundwater geochemistry is still unrevealed. Additionally, other factors such as filter dimensions, height of the sand layer, and irregularities during operation (Figure S3) can influence microbial activities in SFs and control the removal efficiency of Fe(II), Mn(II), As(III), and NH_4^+. In order to evaluate the microbial composition of SFs when being fed by varying groundwater composition, and how the microorganisms contribute to the performance of the household SFs, a detailed study on microbial communities in household SFs running under different geochemical conditions is required.

Therefore, we investigated a series of household SFs in high to low-As areas in the Red River delta in Vietnam. The main objectives of this study were (i) to analyze operational conditions and contaminant removal efficiency of 20 household SFs running under varying geochemical conditions, (ii) to identify the microbial community composition focusing on potential Fe(II)-, Mn(II)-, As(III)- and NH_4^+-oxidizers among 7 households SFs (selected based on differences in groundwater composition and depth of groundwater abstraction), and (iii) to elucidate the influence of groundwater geochemistry on the microbial community structures in household SFs.

2.2. Materials and methods

2.2.1. Study areas and sample collection

To select suitable field sites to study the effect of varying groundwater composition on microbial communities in household sand filters, we created a GIS-based searchable map based on the Red River's groundwater database from Winkel et al.(Winkel et al., 2011) (ArcGIS Map, Esri, USA) (details are described in SI). The selected sampling sites are in 3 different villages, i.e., Van Phuc (20º 55' 08.63" N, 105 º 53' 47.61" E) called site A; Tu Nhien (20º 51' 30.05" N, 105 º 55' 33.34" E) called site B; and Dung Tien (20º 49' 01.21" N, 105 º 51' 13.59" E) called site C (Figure S1). Sand filter ID, coordinates, and the location at each field site are listed in Table S1.

All samples were collected during sampling campaigns in 2018 and 2020. Groundwater before flowing through the filter (termed inflow water), and water after filtration (termed outflow water) were filtered through 0.45 µm membrane filters and acidified on-site for later total element analysis with inductively coupled plasma mass spectrometry (ICP-MS, XSeries 2, Thermo-Fisher) and DOC analysis (High TOC II, Elementar). Non-acidified samples were used for NH_4^+, NO_3^-, NO_2^- quantification by continuous flow analysis (Seal Analytical AA3, Norderstedt, Germany). Water samples were collected in triplicate for each analysis, immediately cooled on ice during transport, and stored at 4^{o}C.

Water samples for DNA extraction were collected in sterile 5L PE bottles. The water was filtered through 0.22 µm pore size, sterile membrane filters (EMD Millipore) using a suction-type filter holder (Sartorius 16510) connected to a vacuum pump (Microsart®). Sand filter material was collected by a sterile spatula in different depth layers (every 1-5 cm) in SFs and stored in sterile Falcon tubes and zip bags. All sediment samples were collected in triplicates and stored on dry ice during transport. Sand for physical and chemical characterization was stored at 4°C. Samples for microbial community analysis were stored at -20°C.

2.2.2. DNA extraction

DNA of sand and water samples (collected biomass on membrane filters with 0.22 µm pore size) was extracted in triplicate by PowerWater® and PowerSoil® DNA Isolation Kits, respectively. 0.25 gram of sediment or ¼ of a membrane filter was used for

extraction based on the manufacturer‘s protocols. DNA concentrations were quantified by a Qubit® 2.0 Fluorometer with DNA HS kits (Life Technologies, Carlsbad, CA, USA).

2.2.3. 16S rRNA gene amplicon sequence analysis

Bacterial and archaeal 16S rRNA genes were amplified using universal primers 515f: GTGYCAGCMGCCGCGGTAA (Parada et al., 2016) and 806r: GGACTACNVGGGTWTCTAAT (Apprill et al., 2015) fused to Illumina adapters. Details of the PCR assay are mentioned in the SI.

Library preparation steps (Nextera, Illumina) and 250 bp paired-end sequencing with MiSeq (Illumina, San Diego, CA, USA) using v2 chemistry were performed by Microsynth AG (Switzerland), and between 19,219 and 259,470 read pairs were obtained for each sample. Raw sequencing data were analyzed with nf-core/ampliseq v1.2.0 (Straub et al., 2020) as detailed in the SI. Raw sequencing data can be found at the NCBI Sequence Read Archive (SRA); accession number PRJNA757982 (https://www.ncbi.nlm.nih.gov/bioproject/PRJNA757982)

2.2.4. Statical analysis

Spearman’s rank correlations and p-values were calculated using the Hmisc packages version 4.6-0 (Harrell Jr, 2021). Multiple testing corrected p-values (false discovery rate; fdr) were generated using the Benjamini-Hochberg method (Benjamini and Hochberg, 1995) in R version 4.1.2 (R Core Team, 2021) (Table S2).

Bray Curtis dissimilarity metrics, Principal Coordinates Analysis (PCoA) plot was generated with https://github.com/qiime2/q2-diversity in QIIME2 v2019.10 within the nf-core/ampliseq pipeline.

The ADONIS (Permutational Multivariate Analysis of Variance Using Distance Matrices) test (Anderson, 2001) was performed with QIIME2 v2019.10 on the previously calculated Bray Curtis dissimilarity metrics. ADONIS computes an R2 value (effect size) which shows the percentage of variation explained by a condition, as well as a p-value to determine the statistical significance. To determine the effect size of a specific condition, the variance of other factors was removed (statistically controlled for), see Table S3 for formula and test results.

2.2.5. Quantitative polymerase chain reaction (qPCR)

Quantitative PCR (qPCR) was used to quantify general 16S rRNA genes of bacteria and archaea, 16S rRNA genes of anaerobic ammonium-oxidizers (anammox), as well as functional genes, i.e., targeting the ammonium monooxidase (*amoA*) of bacterial and archaeal ammonia-oxidizers (AOB, AOA respectively), the nitrite oxidoreductase (*nxrB*) of bacterial nitrite-oxidizers (NOB), and methane monooxygenase genes (*pmoA*) of methanotrophs. The qPCR protocol was performed using an iQ5 real-time PCR system (iQ5 optical system software, version 2.0, Bio-Rad). qPCR primer sequences, gene-specific plasmid standards, and details of the thermal programs are given in the SI (Table S5).

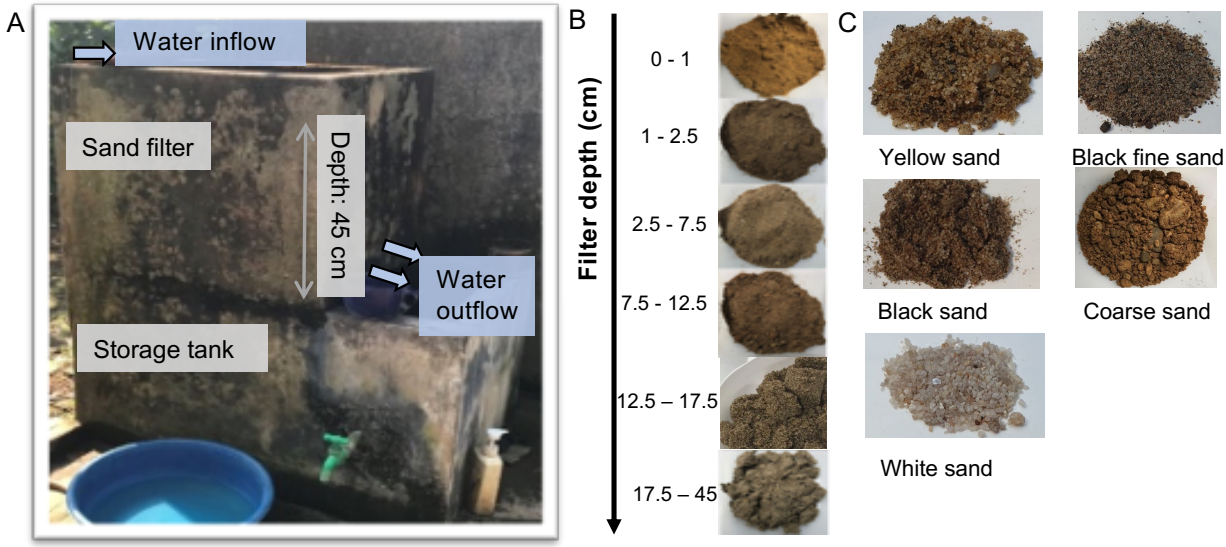

Figure 1. Example of a household SF (SF B5) applied to remove As and Fe from groundwater in the Red River delta (A), heterogeneous stratification of sand layers with depth of the sand filter (top compartment of the filter) (B), and different types of sands commonly used as filter materials in household SFs (C).

2.3. Results and discussion

2.3.1. Characterization and performance evaluation of household SFs

We first examined the design, performance, and solid-phase composition of 20 household SFs treating low (3.3 µg L^{-1}) to high (600 µg L^{-1}) As-containing groundwater in 3 villages located in the hotspots of As groundwater contamination in the Red River delta based on previous predictions (Figure S1) (Winkel et al., 2011).

SF design parameters and operational conditions

The sand filters are built as rectangular-shaped concrete boxes (open at the top), filled with sand (the height of the sand column ranged between 35 and 100 cm with a sand particle size of ca. 0.05-2.0 mm), and filter bed volumes varied from 0.2 to 1 m^3 depending on the demand of purified water (Table 1). The groundwater originated from an aquifer depth of ca. 15-55 m (Table 1) and was pumped intermittently on top of the sand surface (Figure 1). The water inflow and outflow pH values were 7.0±0.4 and 7.3±0.3, respectively, and the pH of the SF material was approximately 7.5. The filtration rate recorded in the field was between 1 to 4 $m^3m^{-2}h^{-1}$ with an estimated hydraulic retention time of ca. 30 min (Table 1). These parameters were confirmed in previous studies (Berg et al., 2006; Nitzsche et al., 2015a; Voegelin et al., 2014).

Table 1. Design parameters and operational conditions of selected household sand filters in the Red River delta in Vietnam. Data were collected in sampling campaigns in 2018 and 2020. The sand filters were collected at 3 field sites (A: Van Phuc, B: Tu Nhien and C: Dung Tien villages) along the Red River delta, coordinates of each filter ID and the location of the 3 field sites are listed in Table S1.

Filter ID	Surface area (m^2)	Sand layer volume (m^3)	Filtration rate ($m^3/m^2.h$)	Tube well depth (m)	Age of SF (years)	Design/ operational conditions		
						Filtration	Pre-aeration	Frequency changing sand (months)
(Voegelin et al., 2014)	0.47	0.2	2.5	45	8	1 step	NO	12
A1	0.28 0.73	0.2 0.53	4.2 1.64	35-45	1	2 steps	NO	6-7
B3	0.78	0.33	1.5	45-50	5	1 step	NO	12

B4	0.3	0.15	4	15-20	10	1 step	NO	24
B5	0.4	0.2	3	25-30	<1	1 step	NO	3-6
B8	1.15	0.7	1	35-40	>5	1 step	YES	6-12
C17	0.78	0.6	1.5	40-55	>5	1 step	YES	2-3
C18	0.65	0.52	1.8	40-50	< 3	1 step	YES	6

Performance of household SFs (Fe, Mn, As, and NH_4^+ removal efficiency)

The Fe, Mn, As, and NH_4^+ removal efficiency of SFs running with different groundwater compositions showed that independent from the filter design, size, and frequency of operation, SFs efficiently removed Fe, Mn, As, and partly oxidized NH_4^+ to NO_3^-. The groundwater pumped into the 20 studied SFs contained 11-30 mg L^{-1} Fe, 120-1300 µg L^{-1} Mn, 3.3-600 µg L^{-1} As, and <0.1 to 24 mg-N L^{-1} NH_4^+ with Fe/As ratios ranging from 23.4 to 190 (Figure 2A). After filtration, the removal efficiency of Fe, Mn, and As reached (on average) 96±3.8%, 92.2±13.9%, and 92.8±7.2%, respectively, and NH_4^+ was transformed to a large extent, but not completely, to NO_3^- (74.7±29.8%) (Figure 2B, S5). However, in some filters, the remaining As concentration after filtration (averaging 17±21 µg L^{-1}) was still higher than 10 µg L^{-1} (the drinking water standard provided by the WHO), thus requiring further treatment for being used as safe drinking water. Indeed, a Spearman correlation analysis revealed that the As concentration in the outflow was significantly positively correlated with As concentrations (correlation = 0.6; fdr = 0.02), but negatively correlated with $\frac{\text{Fe}}{\text{As}}$ ratios (correlation = -0.75, fdr = 0.004) and $\frac{\text{Fe-1.8P}}{\text{As}}$ ratios (correlation = -0.8; fdr = 0.0001) of the water inflow (Figure 3, Table S2). Additionally, the formation of NO_2^- and NO_3^- in the outflow was positively correlated to the amount of NH_4^+ in the inflow, suggesting nitrification during the filtration process (Figure 3, Table S2).

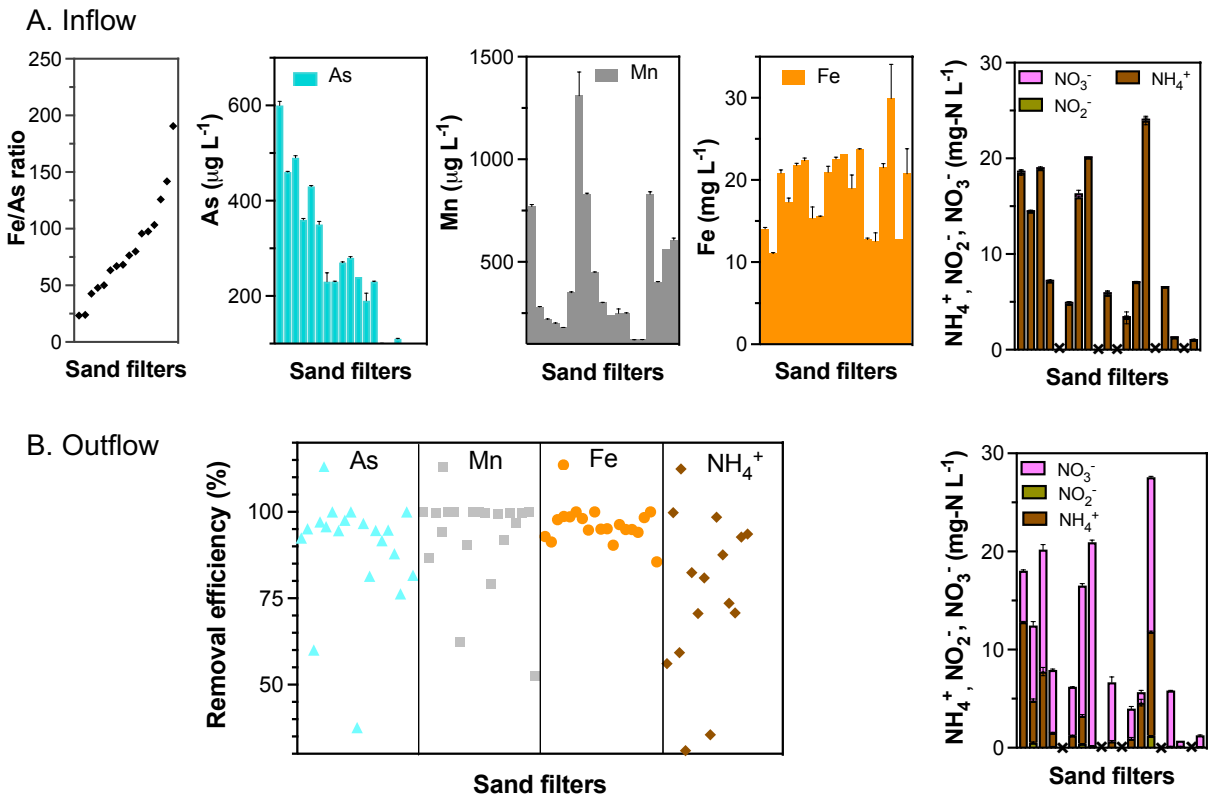

Figure 2. Groundwater composition of 20 studied SFs plotted in the order of increasing Fe/As ratios. From the left to the right: Fe/As ratio, As, Mn, Fe, NH_4^+, NO_2^-, and NO_3^- concentrations (indicated as inflow, panel A). Panel B shows the removal efficiency of As, Mn, Fe, and NH_4^+ of 20 studied SFs (B, left) and concentrations of NH_4^+, NO_2^-, and NO_3^- after filtration (B, right). All samples were analyzed in triplicate, and error bars indicate standard deviation.

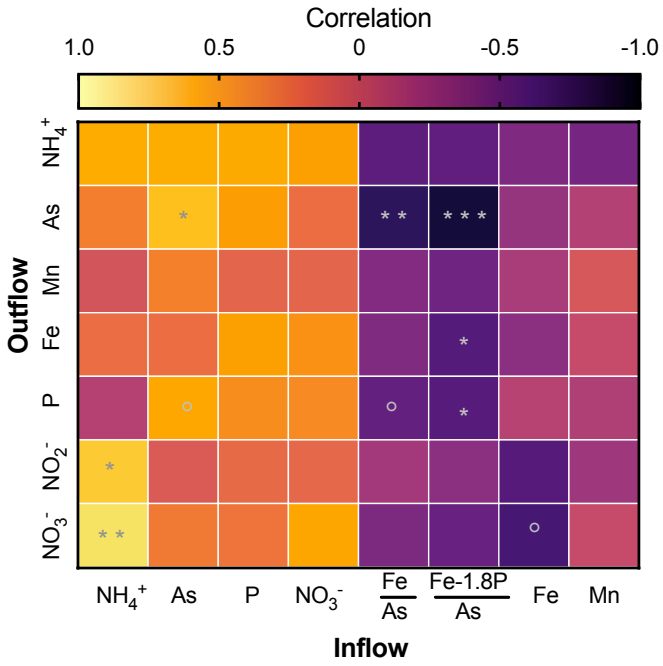

Figure 3. Relationship of water inflow and outflow based on Spearman correlation (0.05 < fdr > 0.1, fdr < 0.05, fdr < 0.01, fdr < 0.001).

Comparison of operational conditions and performance of household sand filters in Vietnam with other household sand filters

In this context, we compared the designs and performances of sand filters applied to remove As in Vietnam with i) original household slow sand filters (HSSFs), ii) SFs employing zero-valent iron (SONO, Kanchan, and NIS) and iii) delayed aeration sand filters. The relevant comparison parameters are shown in Table 2.

Overall, the designs, flow regimes, and maintenances of household SFs were similar in all filters. However, differences in performance were quite substantial. Firstly, the pathogen removal efficiency of As filters including the ones used in Vietnam, the elemental iron-based filters and the delayed aeration filters were insufficient compared to HSSFs, probably due to the absence of the “Schmutzdecke” as a biofilter layer. Secondly, the performance of iron-based filters applied to remove As, including SONO filters containing a layer of composite iron matrix (CIM) under a coarse sand layer (Hussam and Munir, 2007; Neumann et al., 2013), Kanchan filters containing an iron nail compartment above a sand layer (Mueller et al., 2021; Ngai et al., 2007), and NIS filters containing a layer of iron nails between two sand layers (Smith et al., 2017), were compared. Kanchan, and NIS did not effectively remove As when the groundwater simultaneously contained high P and low Fe (Bretzler et al., 2020a). So far, the SONO (Neumann et al., 2013) and NIS filters (Smith et al., 2017) have shown the best As removal efficiency (As outflow <50 µg L^{-1}, average As removal rate 92%). Lastly, filters that are based on delayed aeration, which means anoxic groundwater was stored in an anoxic container before aeration and a 2-steps sand filtration, were suggested as a promising solution for As elimination. However, the maintenance of these filters required backwashing, and their costs are slightly higher than for the other household SFs. Thus, delayed aeration filters might be more suitable for a small community rather than one family (Annaduzzaman et al., 2021).

Table 2. Comparison of operational conditions and performance of household sand filters in Vietnam with others household sand filters.

	SFs in Vietnam	Elemental iron-based filters			Delayed aeration	HSSFs
		SONO	Kanchan	NIS		
Aim	Remove As and Fe and Mn	Remove As, Mn and Fe	Remove As	Remove As	Remove As	Remove turbidity and pathogens
Area/ Country	Vietnam (Red River delta)	Bangladesh Burkina Faso	Nepal Cambodia	China	Bangladesh	
Flow regime	Intermittent	Intermittent	Intermittent	Intermittent	Intermittent	Intermittent
Flow rate ($L\ h^{-1}$)	n.a	20 - 30 8 - 12	10 – 15	n.a	9	1
Filtration rate ($m^3m^{-2}h^{-1}$)	1 - 4	0.1 - 0.15	n.a	n.a	1	0.06
Maintenance (When clogging	Remove top sand layers	Remove top sand layers	Stirring 5cm	Remove the top layer and slit up the nails	Backwashing	
Feeding volume (L)	30 - 100	40 - 80	18	80	n.a	48
Schmutzdecke	NO	NO	YES	YES		YES
Re.Eff. Fe (%)	96 ± 3.8	> 90	90 - 95	98	97	n.a
Re.Eff. Mn (%)	92.2 ± 13.9	n.a	n.a	- 800 (***)	n.a	n.a
Re.Eff. As (%)	92.8 ± 7.2 (*)	94-99 60-80 (*)	85-90 39-75 (*)	86 - 95	92	n.a
Re.Eff. NH_4^+(%)	74.7±29.8(**)	n.a	n.a	n.a	58 (**)	n.a
Re.Eff. Turbidity (%)	n.a	n.a	80-95	-44 (***)	n.a	64±9
Re.Eff. E. coli (log)	n.a	n.a	n.a	n.a	n.a	1.5-1.8
Re.Eff. Coliform	-10^3 (times) (***)	n.a	60-99 (%) 15-99 (%)	n.a	n.a	n.a
References	This study (Nitzsche et al., 2015a) (Berg et al., 2006)	(Bretzler et al., 2020a) (Hussam and Munir, 2007) (Neumann et al., 2013)	(Chiew et al., 2009) (Ngai et al., 2007) (Mueller et al., 2021)	(Smith et al., 2017)	(Annaduzzaman et al., 2021)	(Freitas et al., 2022; Medeiros et al., 2020)

(*) As effluent was higher than drinking standard (10 µg L^{-1})

(**) Incomplete nitrification

(***) Effluent value was higher than the influent.

2.3.2. Microbial community composition and shared core taxa in household SFs

To understand how microbial communities of SFs differ when running with varying groundwater composition, the microbial community composition from 7 selected households was analyzed and taxa that were identified among all SFs were defined as the core microbial community. Fe, Mn, As and NH_4^+ concentrations of groundwater feeding 7 selected filters ranged from 12.5-30 mg L^{-1} Fe, 120-830 µg L^{-1} Mn, 3.3-490 µg L^{-1} As, and 1.0-24 mg-N L^{-1} NH_4^+ (Figure S7). Microbial community analysis revealed the predominance of taxa potentially involved in Fe(II), Mn(II), NH_4^+ and, unexpectedly, CH_4 oxidation, suggesting their contribution to the excellent performances of the different SFs.

Microbial Fe, Mn, and As oxidation

In contrast to previous studies that suggested a minor contribution of Fe(II)-oxidizing bacteria in the filters (Berg et al., 2006; Nitzsche et al., 2015b; Voegelin, Andreas; Kaegi, Ralf; Berg, Michael; Nitzsche, Katja Sonja; Kappler, Andreas; Lan, Vi Mai; Trang, Pham Thi Kim; Göttlicher, Jörg; Steininger, 2014), we found the well-known Fe(II)-oxidizing genus *Sideroxydans* with a relative abundance of 0.1-13.2% predominantly in the top layer of all investigated SFs (Figure 4A). Additionally, since NO_3^- formed due to the nitrification processes, it became a dominant electron acceptor in the deeper layers of the filters where O_2 is depleted. We also suggest that *Gallionellaceae* (3.0±3.0%) belonged to the core microbial community that was shared in all studied SFs (Figure 4B) to be involved in nitrate reduction coupled to Fe(II) oxidation (NRFeOx) because recently several novel species of NRFeOx bacteria (*Candidatus* Ferrigenium) (Huang et al., 2022) belonging to the *Gallionellacea* family were enriched under similar conditions as present in the sand filters (poor in organic carbon and enriched in NO_3^- and Fe) (Huang et al., 2021; Jakus et al., 2021). Therefore, the high Fe removal efficiency in the SFs (on average 96±3.8%) might be achieved by a combination of heterogeneous abiotic Fe(II) oxidation and microbial Fe(II) oxidation. The formation of extra Fe(III) phases via microbial Fe(II) oxidation then provides additional minerals with binding sites for As removal, ultimately enhancing As removal efficiency of the SF.

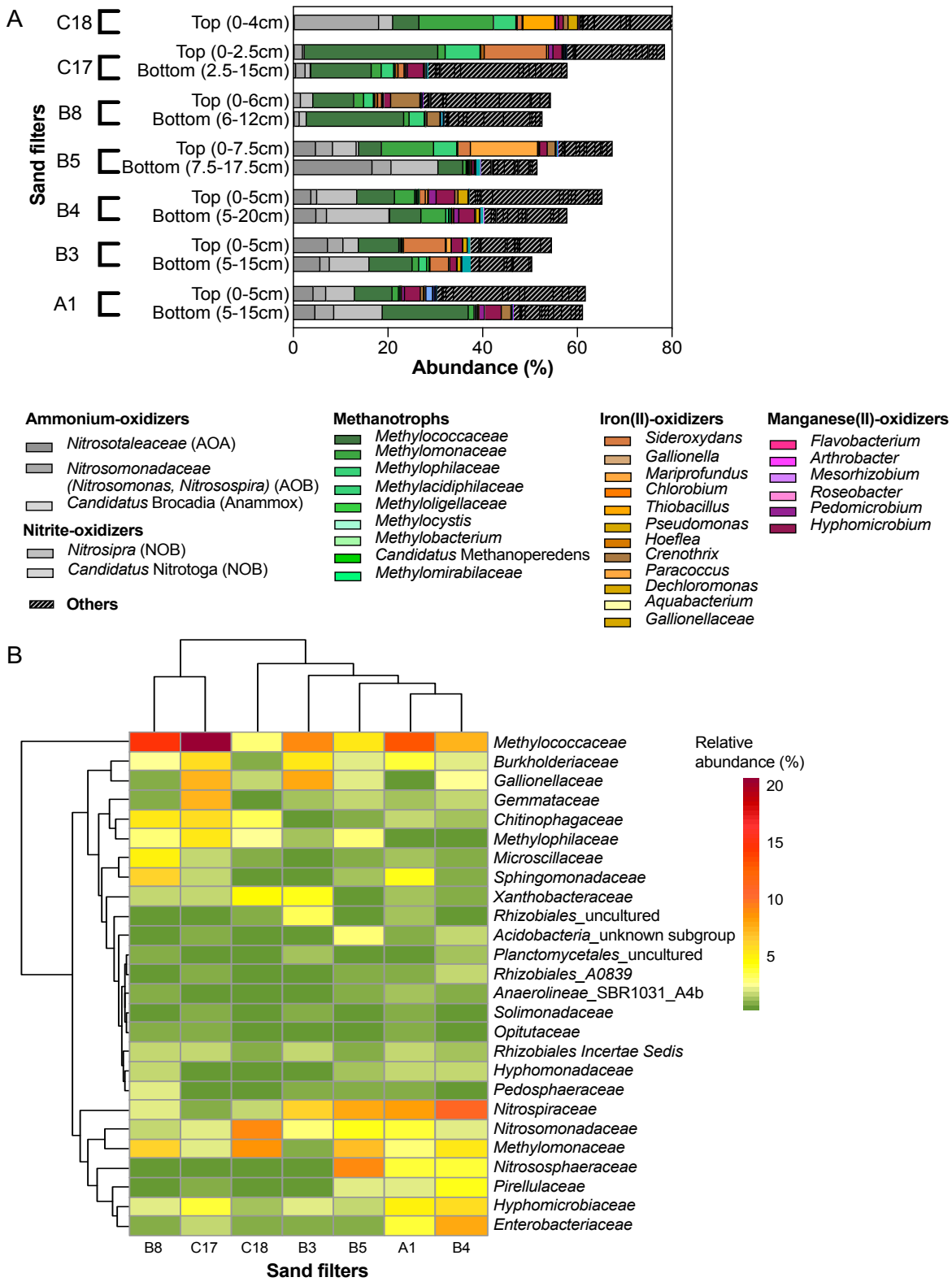

Figure 4. Microbial composition in 7 selected household sand filters based on 16S rRNA gene amplicon sequencing. Relative abundance of selected taxa (including potential function) in two distinct layers in sand filters: the top layer is considered to be oxic and Fe(III)-rich, while the bottom layer is considered to be oxygen-poor (A). Relative abundances of core microbial communities (at the family level) that were shared across all selected sand filters (B).

The genera *Hyphomicrobium* and *Pedomicrobium,* belonging to the core microbial community affiliating with *Hyphomicrobiaceae* (2.8±1.8%) (Figure 4B) were likely the key MnOB in the SFs. They contain the Mn(II)-oxidizing gene *moxA* and were used as model organisms for studying Mn(II) oxidation (Larsen et al., 1999; Ridge et al., 2007). Microbial Mn(II) oxidation is considered a predominant process over abiotic Mn(II) oxidation in SFs, due to the much slower abiotic Mn(II) oxidation rate (half-live times of Mn(II) controlled by abiotic oxidation on mineral surfaces are between 5-2800 days) (Davies and Morgan, 1989; Diem and Stumm, 1984; Morgan, 2005). In comparison to abiotic Mn(II) oxidation, the presence of MnOB can accelerate the process up to several orders of magnitude (Hansel, 2017; Nealson, 2006; Tebo et al., 2005). The formation of Mn oxides via biotic Mn(II) oxidation provides a second possibility for As(III) oxidation in SFs (by the reactive Mn oxides). Therefore, SFs show a very stable As removal efficiency under different geochemical conditions.

In contrast to the evidence for microbial Fe(II)- and Mn(II)-oxidizers in the SFs, we did not see extensive evidence for biological As oxidation. This suggests that As(III) as predominant As species in the groundwater was abiotically oxidized to As(V) and immobilized in the filter bed (Voegelin et al., 2014). The As(III) oxidation processes are mainly governed by Fe(II,III)-mediated abiotic surface-catalyzed As(III) oxidation (Amstaetter et al., 2010; Hug and Leupin, 2003) or coupled to Mn(III, IV) reduction (Bai et al., 2016b; Gude et al., 2017; Katsoyiannis et al., 2004).

Nitrification in sand filters

Geochemical data indicated NH_4^+ oxidation and NO_3^- formation during filtration processes with conversion rates (on average) of 74.7±29.8% (Figure 2B). Additionally, we found sequences affiliating with typical nitrifiers, such as *Nitrosomonadaceae* (AOB), *Nitrososphaeraceae* (AOA), and *Nitrospiraceae* (NOB) accounting for 13.5±8.4% relative abundances of the microbial community (Figure 4A). We thus conclude that nitrification likely plays a crucial role in nitrogen species transformation in the SFs.

We further investigated the vertical distribution of ammonium- and nitrite-oxidizers in different depths by qPCR. Bacterial and archaeal *amoA* genes (targeting AOA and AOB), the *nxrB* gene (targeting NOB), and the 16S rRNA gene targeting anammox taxa as well as total bacteria and total archaea were analyzed from selected SFs.

These SFs were selected due to their highest (SF-A1, B5) and lowest (SF-B4) NH_4^+ removal efficiency (Figure 5). Our results showed that AOA was predominant over AOB in 3 selected filters with an (qPCR-based) relative abundance of archaeal *amoA* genes ranging from 0.5-2.5%. In contrast, the bacterial *amoA* gene targeting AOB was less than 0.3% (Figure 5), and its copy number was reduced along the filter depths by the factor from 2 to 10 (Figure S9). A relative abundance of *nxrB* genes of NOB was also detected between 2-4% in selected filters (Figure 5). The presence of AOB (*Nitrosomonas*) and NOB (*Nitrospira*) was commonly found in other full-scale water treatment SFs (Albers et al., 2015; Hu et al., 2020; Palomo et al., 2016; Poghosyan et al., 2020), but the remarkable occurrence of AOA is a unique finding for the household SFs of our study. Quantification of functional genes of AOA and NOB along the filter depths suggested their widespread abundance along the sand filters, even in deeper sand layer (below 15 cm) (Figure S9) where we observed a depletion of AOB. Both AOA and *Nitrospira*-NOB were found to have a better tolerance to low DO level (Mehrani et al., 2020; You et al., 2009). Some studies showed that they can be active and enriched even at a DO concentration below 1.0 mg O_2/L (Erguder et al., 2009; Mehrani et al., 2020). Finally, a small fraction of anaerobic ammonium-oxidizing bacteria (anammox) was also detected below 5 cm depth in our sand filters (<0.3%) (Figure 5). However, their functional role needs to be confirmed in future studies.

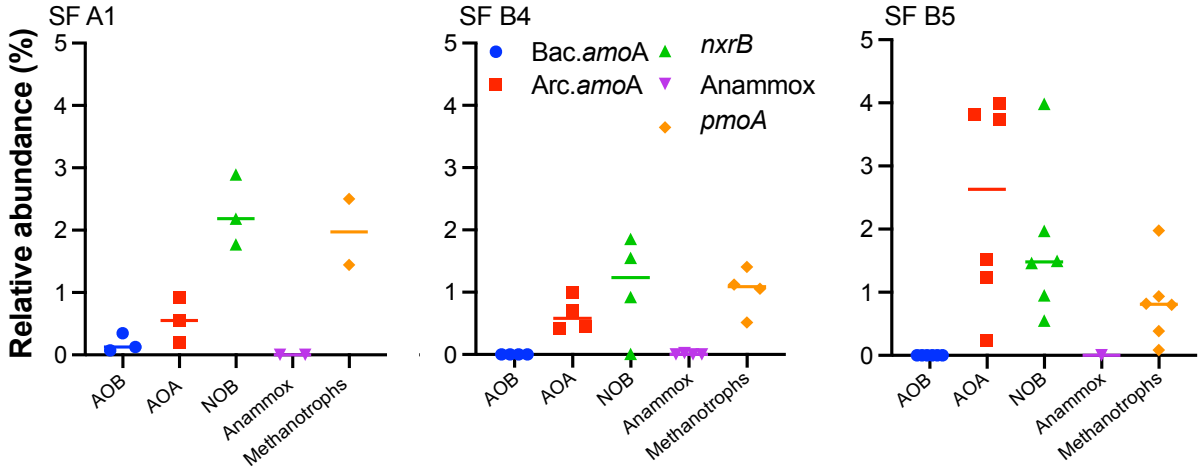

Figure 5. Relative abundance of AOA, AOB, NOB, anammox, and methanotrophs was calculated from quantitative PCR results targeting 16S rRNA genes of total bacteria, archaea, anammox taxa, and functional genes such as archaeal and bacterial *amoA* affiliated to AOA and AOB, respectively, *nxrB* genes of NOB, and *pmoA* genes of methanotrophs. Samples were analyzed in three different filters, representing the highest (SF A1 and B5) and lowest (SF B4) performances of NH_4^+ oxidation. Error bars represent the standard deviation of triplicates.

Potential methane oxidation in sand filters

Unexpectedly, a high relative abundance of putative methanotrophs was detected in all SFs, such as *Methylococcaceae* (10.3±6.1%) and *Methylomonaceae* (4.5±2.8%) (Figure 4B). Since an elevated concentration of CH_4 (up to 45 mg L^{-1}) was detected in the groundwater at the same field sites (Martyna Glodowska et al., 2020; Stopelli et al., 2020), we speculated that the microbial communities in the household sand filters might be capable of oxidizing methane. We therefore performed qPCR targeting the particulate methane monooxygenase genes (*pmoA*) for 3 selected sand filters (SF A1, B4, B5) and the results are presented as (qPCR) relative abundance (proportion of this specific gene in relation to total bacterial and archaeal 16S rRNA genes) in Figure 5. The results confirmed the presence of methanotrophs in all 3 sand filters, with the abundance of *pmoA* genes accounting up to 2.5% (Figure 5). Most of the recognized methanotrophs belonged to type I aerobic methanotrophic bacteria that oxidize methane to CO_2 using O_2 as electron acceptor (Stein et al., 2012). Recent studies about methane oxidation in the same As-contaminated aquifer revealed anaerobic methane oxidation coupled to the reduction of Fe(III) minerals (by *Candidatus* Methanoperedens) (Martyna Glodowska et al., 2020; Pienkowska et al., 2021), suggesting a similar process might take place in the O_2-depleted zone in household SFs.

2.3.3. Influence of groundwater geochemistry on the microbial community structures in household sand filters

The groundwater chemistry is the primary factor affecting the structure of microbial communities in sand filters (Hu et al., 2020). Indeed, the Bray Curtis dissimilarity analysis also indicated that microbial community composition differed considerably among filters running under various groundwater compositions, whereas minor differences were observed between microbial composition in the top (2.5-7.5 cm) and bottom layer (between 2.5-17.5 cm) from the same SF fed by the same groundwater (Figure 6A). Additionally, we used the ADONIS test to analyze the relative influence of groundwater composition on microbial communities. The results indicated that each factor of Fe, Mn, As, and NH_4^+ inflow concentrations can influence microbial communities in sand filters between 15-20% (Figure 6B, Table S3). This finding is also in line with Hu et al., 2020, which revealed that Fe, Mn, NH_4^+ and PO_4^{3-} were strongly influencing the microbial community variation in rapid sand filters. We noticed that in

SFs B3 and C17, fed by groundwater enriched with Fe(II) (Fe concentration of 21 and 30 mg L^{-1} respectively) and depleted in As(III) (As concentrations of 3.3 and 16.97 µg L^{-1}, respectively), *Sideroxydans* was present as the most dominant potential Fe(II)-oxidizer, with a relative abundance of up to 8.8 and 13.2%, respectively (Figure 4A). Additionally, we also found that SF B4 had the lowest NH_4^+ removal rate (12%), probably due to the lower abundance of ammonium-oxidizers as indicated by the ca. 10-100 times lower *amoA* gene copy number in comparison to SFs which possessed a high NH_4^+ conversion rate such as SFs A1 and B5 (Figure S8).

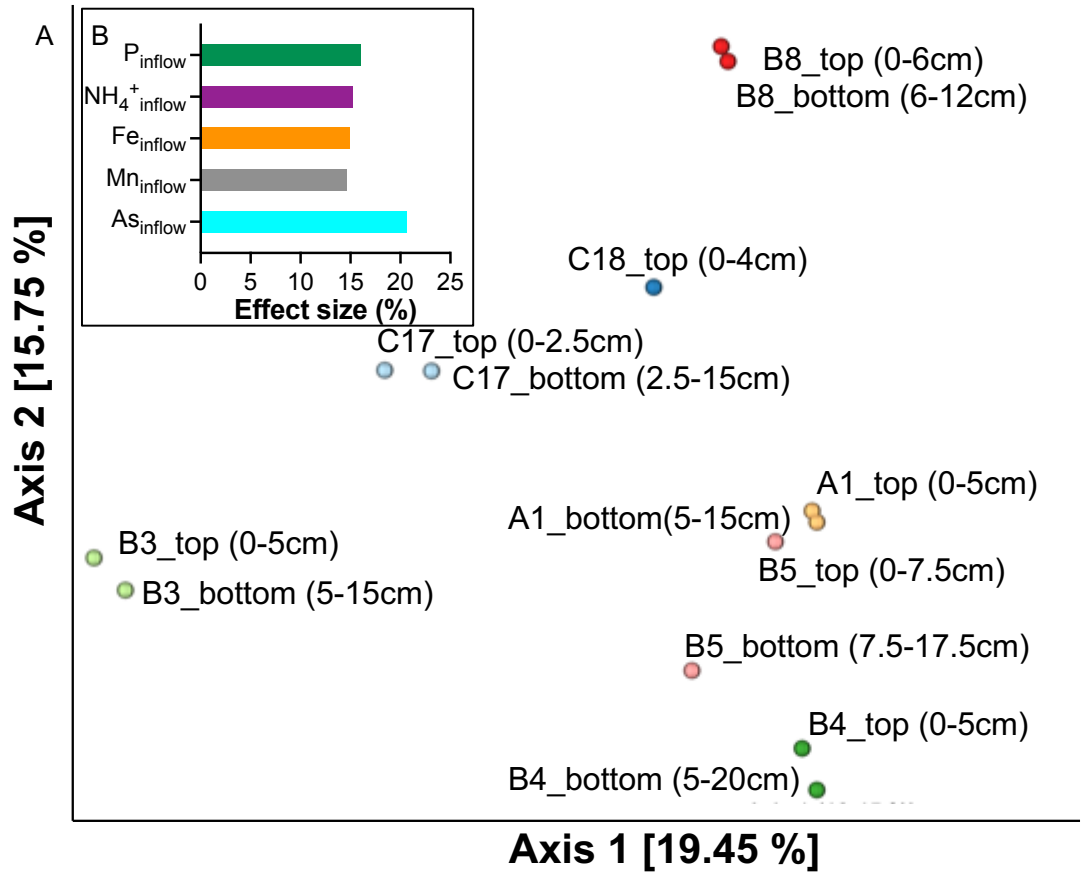

Figure 6. Principal Coordinate Analysis (PCoA) plot based on Bray Curtis dissimilarity to compare the differences of microbial community composition based on 16S rRNA gene amplicon sequencing between samples (A). The effect of groundwater components (Fe, Mn, As, and NH_4^+ inflow) on microbial communities of SFs analyzed by ADONIS test, with Pr (>F) = 0.001 for all results (B).

2.4. Conclusions

We conducted a comprehensive study on overall sand filter performance, microbial community composition, and the contribution of biological processes to the elimination of metal(loid)s (As, Mn, Fe) and nutrients (NH_4^+, NO_2^-, NO_3^-) from groundwater. Our findings suggest that Fe(II)- and Mn(II)-oxidizers probably complement abiotic oxidation in household SFs, thus contributing to the excellent Fe, Mn, and As removal efficiencies. Our data also indicated a role of AOA and NOB for NH_4^+ and NO_2^- oxidation and thus ammonium removal. Although, formed NO_3^- in filtered water did not exceed EU limits of 50 mg/L, it still raises a potential concern for the water quality when being used as drinking water. Finally, a high abundance of methanotrophs was detected in the sand filters, suggesting that SFs might also simultaneously oxidize CH_4 during the filtration processes. Overall, Fe(II)-, Mn(II)-, NH_4^+- and NO_2^--oxidizers belong to the core microbial communities in household SFs and their presence correlates with key functional processes in SFs.

2.5. Acknowledgement

This work was funded by the German Research Foundation (DFG, KA1736/41-1). AK and DS acknowledge infrastructural support by the Deutsche Forschungsgemeinschaft (DFG) under Germany's Excellence Strategy, cluster of Excellence EXC2124, project ID 390838134. Daniel Straub was funded by the Institutional Strategy of the University of Tuebingen (DFG, ZUK63). Sara Kleindienst is funded by an Emmy-Noether fellowship from the DFG (grant number 326028733). AVL acknowledge support by Pham Vy Anh, Pham Hung Viet, Pham Thi Kim Trang, Vu Thi Duyen, and The Anh (KLATEFOS) during the sampling campaigns. We thank Ellen Röhm, Franziska Schädler, Caroline Schlaiss for helping with FIA and qPCR analysis.

2.6. References

Albers, C.N., Ellegaard-Jensen, L., Harder, C.B., Rosendahl, S., Knudsen, B.E., Ekelund, F., Aamand, J., 2015. Groundwater chemistry determines the prokaryotic community structure of waterworks sand filters. Environ. Sci. Technol. 49, 839–846. https://doi.org/10.1021/es5046452

Amstaetter, K., Borch, T., Larese-Casanova, P., Kappler, A., 2010. Redox transformation of arsenic by Fe (II)-activated goethite (α-FeOOH). Environ. Sci. Technol. 44, 102–108.

Anderson, M.J., 2001. A new method for non-parametric multivariate analysis of variance. Austral Ecol. 26, 32–46.

Andreoli, F.C., Sabogal-Paz, L.P., 2020. Household slow sand filter to treat groundwater with microbiological risks in rural communities. Water Res. 186. https://doi.org/10.1016/j.watres.2020.116352

Annaduzzaman, M., Rietveld, L.C., Hoque, B.A., Bari, M.N., van Halem, D., 2021. Arsenic removal from iron-containing groundwater by delayed aeration in dual-media sand filters. J. Hazard. Mater. 411, 124823. https://doi.org/10.1016/j.jhazmat.2020.124823

Apprill, A., McNally, S., Parsons, R., Weber, L., 2015. Minor revision to V4 region SSU rRNA 806R gene primer greatly increases detection of SAR11 bacterioplankton. Aquat. Microb. Ecol. 75, 129–137.

Bai, Y., Yang, T., Liang, J., Qu, J., 2016. The role of biogenic Fe-Mn oxides formed in situ for arsenic oxidation and adsorption in aquatic ecosystems. Water Res. 98, 119–127. https://doi.org/10.1016/j.watres.2016.03.068

Benjamini, Y., Hochberg, Y., 1995. Controlling the false discovery rate: a practical and powerful approach to multiple testing. J. R. Stat. Soc. Ser. B 57, 289–300.

Berg, M., Luzi, S., Trang, P.T.K., Viet, P.H., Giger, W., Stüben, D., 2006. Arsenic removal from groundwater by household sand filters: Comparative field study, model calculations, and health benefits. Environ. Sci. Technol. 40, 5567–5573. https://doi.org/10.1021/es060144z

Bretzler, A., Nikiema, J., Lalanne, F., Hoffmann, L., Biswakarma, J., Siebenaller, L., Demange, D., Schirmer, M., Hug, S.J., 2020. Arsenic removal with zero-valent iron

filters in Burkina Faso: Field and laboratory insights. Sci. Total Environ. 737, 139466. https://doi.org/10.1016/j.scitotenv.2020.139466

Chiew, H., Sampson, M.L., Huch, S., Ken, S., Bostick, B.C., 2009. Effect of groundwater iron and phosphate on the efficacy of arsenic removal by iron-amended biosand filters. Environ. Sci. Technol. 43, 6295–6300.

Davies, S.H.R., Morgan, J.J., 1989. Manganese(II) oxidation kinetics on metal oxide surfaces. J. Colloid Interface Sci. 129, 63–77. https://doi.org/10.1016/0021-9797(89)90416-5

Diem, D., Stumm, W., 1984. Is dissolved Mn2+ being oxidized by O2 in absence of Mn-bacteria or surface catalysts? Geochim. Cosmochim. Acta 48, 1571–1573.

Elliott, M.A., Stauber, C.E., Koksal, F., DiGiano, F.A., Sobsey, M.D., 2008. Reductions of E. coli, echovirus type 12 and bacteriophages in an intermittently operated household-scale slow sand filter. Water Res. 42, 2662–2670. https://doi.org/10.1016/j.watres.2008.01.016

Erguder, T.H., Boon, N., Wittebolle, L., Marzorati, M., Verstraete, W., 2009. Environmental factors shaping the ecological niches of ammonia-oxidizing archaea. FEMS Microbiol. Rev. 33, 855–869.

Freitas, B.L.S., Terin, U.C., Fava, N.M.N., Maciel, P.M.F., Garcia, L.A.T., Medeiros, R.C., Oliveira, M., Fernandez-Ibañez, P., Byrne, J.A., Sabogal-Paz, L.P., 2022. A critical overview of household slow sand filters for water treatment. Water Res. 208. https://doi.org/10.1016/j.watres.2021.117870

Glodowska, M., Stopelli, E., Schneider, M., Rathi, B., Straub, D., Lightfoot, A., Kipfer, R., Berg, M., Jetten, M., Kleindienst, S., 2020. Arsenic mobilization by anaerobic iron-dependent methane oxidation. Commun. Earth Environ. 1, 1–7.

Gude, J.C.J., Rietveld, L.C., van Halem, D., 2017. As(III) oxidation by MnO2during groundwater treatment. Water Res. 111, 41–51. https://doi.org/10.1016/j.watres.2016.12.041

Hansel, C.M., 2017. Manganese in Marine Microbiology, 1st ed, Advances in Microbial Physiology. Elsevier Ltd. https://doi.org/10.1016/bs.ampbs.2017.01.005

Hu, W., Liang, J., Ju, F., Wang, Q., Liu, R., Bai, Y., Liu, H., Qu, J., 2020. Metagenomics Unravels Differential Microbiome Composition and Metabolic Potential in Rapid

Sand Filters Purifying Surface Water Versus Groundwater. Environ. Sci. Technol. 54, 5197–5206. https://doi.org/10.1021/acs.est.9b07143

Huang, Y.-M., Jakus, N., Straub, D., Konstantinidis, K.T., Blackwell, N., Kappler, A., Kleindienst, S., 2022. 'Candidatus ferrigenium straubiae'sp. nov.,'Candidatus ferrigenium bremense'sp. nov.,'Candidatus ferrigenium altingense'sp. nov., are autotrophic Fe (II)-oxidizing bacteria of the family Gallionellaceae. Syst. Appl. Microbiol. 126306.

Huang, Y.-M., Straub, D., Kappler, A., Smith, N., Blackwell, N., Kleindienst, S., 2021. A novel enrichment culture highlights core features of microbial networks contributing to autotrophic Fe(II) oxidation coupled to nitrate reduction. Microb. Physiol. In press, 1–16.

Hug, S.J., Leupin, O., 2003. Iron-catalyzed oxidation of Arsenic(III) by oxygen and by hydrogen peroxide: pH-dependent formation of oxidants in the Fenton reaction. Environ. Sci. Technol. 37, 2734–2742. https://doi.org/10.1021/es026208x

Hug, S.J., Leupin, O.X., Berg, M., 2008. Bangladesh and Vietnam: Different groundwater compositions require different approaches to arsenic mitigation. Environ. Sci. Technol. 42, 6318–6323. https://doi.org/10.1021/es7028284

Hussam, A., Munir, A.K.M., 2007. A simple and effective arsenic filter based on composite iron matrix: Development and deployment studies for groundwater of Bangladesh. J. Environ. Sci. Heal. - Part A Toxic/Hazardous Subst. Environ. Eng. 42, 1869–1878. https://doi.org/10.1080/10934520701567122

Jakus, N., Blackwell, N., Osenbrück, K., Straub, D., Byrne, J.M., Wang, Z., Glöckler, D., Elsner, M., Lueders, T., Grathwohl, P., Kleindienst, S., Kappler, A., 2021. Nitrate removal by a novel lithoautotrophic nitrate-reducing iron(II)-oxidizing culture enriched from a pyrite-rich limestone aquifer. Appl. Environ. Microbiol. AEM-00460. https://doi.org/10.1128/aem.00460-21

Katsoyiannis, I.A., Zouboulis, A.I., Jekel, M., 2004. Kinetics of Bacterial As(III) Oxidation and Subsequent As(V) Removal by Sorption onto Biogenic Manganese Oxides during Groundwater Treatment. Ind. Eng. Chem. Res. 43, 486–493. https://doi.org/10.1021/ie030525a

Larsen, E.I., Sly, L.I., McEwan, A.G., 1999. Manganese (II) adsorption and oxidation by whole cells and a membrane fraction of Pedomicrobium sp. ACM 3067. Arch. Microbiol. 171, 257–264.

Luzi, S., Berg, M., Trang, P.T.K., Viet, P.H., Schertenleib, R., 2004. Household sand filters for arsenic removal: An option to mitigate arsenic from iron-rich groundwater.

Medeiros, R.C., de, N., Freitas, B.L.S., Sabogal-Paz, L.P., Hoffmann, M.T., Davis, J., Fernandez-Ibañez, P., Byrne, J.A., 2020. Drinking water treatment by multistage filtration on a household scale: Efficiency and challenges. Water Res. 178. https://doi.org/10.1016/j.watres.2020.115816

Mehrani, M.-J., Sobotka, D., Kowal, P., Ciesielski, S., Makinia, J., 2020. The occurrence and role of Nitrospira in nitrogen removal systems. Bioresour. Technol. 303, 122936.

Morgan, J.J., 2005. Kinetics of reaction between O2 and Mn (II) species in aqueous solutions. Geochim. Cosmochim. Acta 69, 35–48.

Mueller, B., Dangol, B., Ngai, T.K.K., Hug, S.J., 2021. Kanchan arsenic filters in the lowlands of Nepal: mode of operation, arsenic removal, and future improvements. Environ. Geochem. Health 43, 375–389.

Nealson, K.H., 2006. The Manganese-Oxidizing Bacteria. The Prokaryotes 222–231. https://doi.org/10.1007/0-387-30745-1_11

Neumann, A., Kaegi, R., Voegelin, A., Hussam, A., Munir, A.K.M., Hug, S.J., 2013. Arsenic removal with composite iron matrix filters in Bangladesh: A field and laboratory study. Environ. Sci. Technol. 47, 4544–4554.

Ngai, T.K.K., Shrestha, R.R., Dangol, B., Maharjan, M., Murcott, S.E., 2007. Design for sustainable development - Household drinking water filter for arsenic and pathogen treatment in Nepal. J. Environ. Sci. Heal. - Part A Toxic/Hazardous Subst. Environ. Eng. 42, 1879–1888. https://doi.org/10.1080/10934520701567148

Nitzsche, K.S., Lan, V.M., Trang, P.T.K., Viet, P.H., Berg, M., Voegelin, A., Planer-Friedrich, B., Zahoransky, J., Müller, S.K., Byrne, J.M., Schröder, C., Behrens, S., Kappler, A., 2015a. Arsenic removal from drinking water by a household sand filter in Vietnam - Effect of filter usage practices on arsenic removal efficiency and

microbiological water quality. Sci. Total Environ. 502, 526–536. https://doi.org/10.1016/j.scitotenv.2014.09.055

Nitzsche, K.S., Weigold, P., Lösekann-Behrens, T., Kappler, A., Behrens, S., 2015b. Microbial community composition of a household sand filter used for arsenic, iron, and manganese removal from groundwater in Vietnam. Chemosphere 138, 47–59. https://doi.org/10.1016/j.chemosphere.2015.05.032

Palomo, A., Jane Fowler, S., Gülay, A., Rasmussen, S., Sicheritz-Ponten, T., Smets, B.F., 2016. Metagenomic analysis of rapid gravity sand filter microbial communities suggests novel physiology of Nitrospira spp. ISME J. 10, 2569–2581. https://doi.org/10.1038/ismej.2016.63

Parada, A.E., Needham, D.M., Fuhrman, J.A., 2016. Every base matters: assessing small subunit rRNA primers for marine microbiomes with mock communities, time series and global field samples. Environ. Microbiol. 18, 1403–1414.

Pienkowska, A., Glodowska, M., Mansor, M., Buchner, D., Straub, D., Kleindienst, S., Kappler, A., 2021. Isotopic Labeling Reveals Microbial Methane Oxidation Coupled to Fe (III) Mineral Reduction in Sediments from an As-Contaminated Aquifer. Environ. Sci. Technol. Lett.

Poghosyan, L., Koch, H., Frank, J., van Kessel, M.A.H.J., Cremers, G., van Alen, T., Jetten, M.S.M., Op den Camp, H.J.M., Lücker, S., 2020. Metagenomic profiling of ammonia- and methane-oxidizing microorganisms in two sequential rapid sand filters. Water Res. 185, 116288. https://doi.org/10.1016/j.watres.2020.116288

Ridge, J.P., Lin, M., Larsen, E.I., Fegan, M., McEwan, A.G., Sly, L.I., 2007. A multicopper oxidase is essential for manganese oxidation and laccase-like activity in Pedomicrobium sp. ACM 3067. Environ. Microbiol. 9, 944–953.

Smith, K., Li, Zhenyu, Chen, B., Liang, H., Zhang, X., Xu, R., Li, Zhilin, Dai, H., Wei, C., Liu, S., 2017. Comparison of sand-based water filters for point-of-use arsenic removal in China. Chemosphere 168, 155–162. https://doi.org/10.1016/j.chemosphere.2016.10.021

Stein, L.Y., Roy, R., Dunfield, P.F., 2012. Aerobic Methanotrophy and Nitrification: Processes and Connections. eLS. https://doi.org/10.1002/9780470015902.a0022213

Stopelli, E., Duyen, V.T., Mai, T.T., Trang, P.T.K., Viet, P.H., Lightfoot, A., Kipfer, R., Schneider, M., Eiche, E., Kontny, A., 2020. Spatial and temporal evolution of groundwater arsenic contamination in the Red River delta, Vietnam: Interplay of mobilisation and retardation processes. Sci. Total Environ. 717, 137143.

Straub, D., Blackwell, N., Langarica-Fuentes, A., Peltzer, A., Nahnsen, S., Kleindienst, S., 2020. Interpretations of Environmental Microbial Community Studies Are Biased by the Selected 16S rRNA (Gene) Amplicon Sequencing Pipeline. Front. Microbiol. 11, 1–18. https://doi.org/10.3389/fmicb.2020.550420

Tebo, B.M., Johnson, H.A., McCarthy, J.K., Templeton, A.S., 2005. Geomicrobiology of manganese(II) oxidation. Trends Microbiol. 13, 421–428. https://doi.org/10.1016/j.tim.2005.07.009

Voegelin, Andreas; Kaegi, Ralf; Berg, Michael; Nitzsche, Katja Sonja; Kappler, Andreas; Lan, Vi Mai; Trang, Pham Thi Kim; Göttlicher, Jörg; Steininger, R., 2014. Solid-phase characterisation of an effective household sand filter for As, Fe and Mn removal from groundwater in Vietnam. Environ. Chem. 11, 566–578. https://doi.org/10.1071/EN14011

Voegelin, A., Kaegi, R., Berg, M., Nitzsche, K.S., Kappler, A., Lan, V.M., Trang, P.T.K., Göttlicher, J., Steininger, R., 2014. Solid-phase characterisation of an effective household sand filter for As, Fe and Mn removal from groundwater in Vietnam. Environ. Chem. 11, 566–578.

WHO, 2011. Evaluating household water treatment options: Health-based targets and microbiological performance specifications. World Health Organization.

Winkel, L.H.E., Trang, P.T.K., Lan, V.M., Stengel, C., Amini, M., Ha, N.T., Viet, P.H., Berg, M., 2011. Arsenic pollution of groundwater in Vietnam exacerbated by deep aquifer exploitation for more than a century. Proc. Natl. Acad. Sci. U. S. A. 108, 1246–1251. https://doi.org/10.1073/pnas.1011915108

You, J., Das, A., Dolan, E.M., Hu, Z., 2009. Ammonia-oxidizing archaea involved in nitrogen removal. Water Res. 43, 1801–1809.

SUPPLEMENTARY INFORMATION

GIS-based searchable map

To identify suitable field sites, we created a GIS-based searchable map (ArcGIS Map, Esri, USA) by adding spatial information of measured groundwater data, followed by overlapping a layer of arsenic risk areas derived from a modeled map of the Red River Delta which allowed us to identify locations of low to high risk of As contamination. The map and its groundwater database have been published before (Winkel et al., 2011).

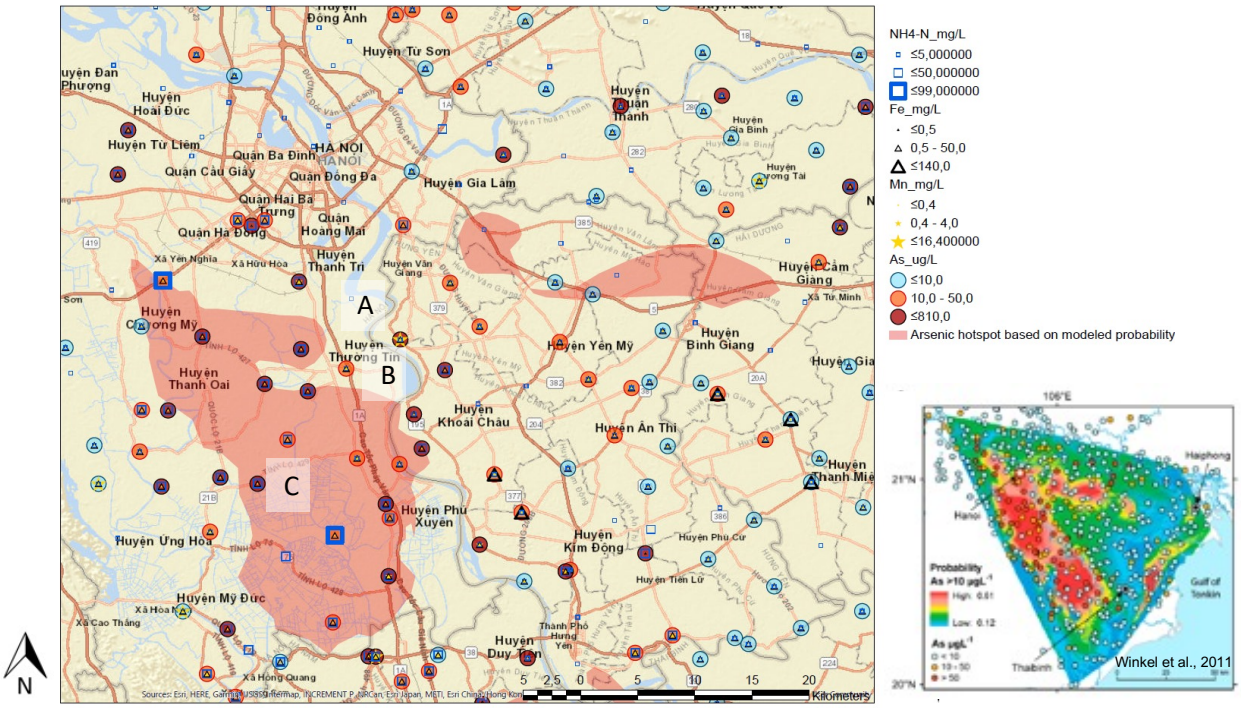

Figure S1. Searchable Arc GIS Map with sampling wells' locations added to the map based on the database in Winkel et al., 2011. The groundwater composition based on As, Mn, Fe and NH_4^+ concentrations was divided into 3 concentration ranges: low level concentrations which are below the WHO standard for drinking water (As: <10 µg/L; Mn: <0.4 mg/L; Fe: <0.5 mg/L and NH_4^+: <5 mg-N/L), medium level (As: 10-50 µg/L; Mn: 0.4-4.0 mg/L; Fe: 0.5-50 mg/L and NH_4^+: 5-50 mg-N/L), and high level (As: 50 810 µg/L; Mn: 4.0-16.4 mg/L; Fe: 50-140 mg/L and NH_4^+: 50-99.0 mg-N/L). As hotspots were identified based on results from Winkel et al. (2011). The location of the three field sites Van Phuc (A), Tu Nhien (B), and Dung Tien (C) are shown on the map.

Sand filter solid phase characterization

Total element contents of sand filter materials were analyzed by energy-dispersive X-ray fluorescence spectrometry (XRF) (XEPOS┼, SPECTRO Analytical Instruments GmbH, Kleve, Germany) as described before (Voegelin, Andreas; Kaegi, Ralf; Berg, Michael; Nitzsche, Katja Sonja; Kappler, Andreas; Lan, Vi Mai; Trang, Pham Thi Kim; Göttlicher, Jörg; Steininger, 2014). The sand was dried at 60˚C, 8 g of dry sample were ground in a mixer mill using a 25 mL ZrO2 grinding jar (Retsch MM400). Four g of sample were mixed with 0.9 g of Licowax C (Clariant, Switzerland) and pressed into 32-mm diameter pellets for analysis by X-ray fluorescence spectrometry (Spectro Xepos+, Spectro GmbH, Kleve, Germany; calibration from the manufacturer validated with certified reference materials). Quantification was based on a built-in calibration for geological samples.

For total organic carbon (TOC) quantification, samples were dried at 60˚C, then ground and acidified with 16% HCl to remove inorganic carbon. After washing with DI water and drying, the TOC content was analyzed in triplicate by a TOC analyzer (Elementar Analysensysteme GmbH, Germany).

PCR assay using universal primers 515f and 806r for 16S rRNA gene amplicon Illumia sequencing

PCR mixtures for amplification contained (per 25 µL reaction): 0.5 µl of each primer (515f and 806r with Illumina tags; 10 µM stock concentration), 12.5 µL of 2× KAPA HiFi Hotstart Readymix (Kapa Biosystems, Inc., Wilmington, MA, United States), 10.5 µL of RNAse/DNAse-free water and 1 µL of the template. The thermal profile used was: 3 min at 95˚C, and subsequent 22 or 25 cycles of 95˚C for 30 s, 55˚C for 30 s, 72˚C for 30 s, followed by 5 min at 72˚C.

16S rRNA gene amplicon sequencing analysis

Sequencing data were analyzed with nf-core/ampliseq v1.2.0, which includes all analysis steps and software and is publicly available (Ewels et al., 2019; Straub et al., 2020) with Nextflow v20.10.0 (Di Tommaso et al., 2017) using containerized software with singularity v3.4.2 (Kurtzer et al., 2017). Data from two sequencing runs were treated initially separately by the pipeline using the option “--mulipleSequencingRuns” and ASV tables were merged. Primers were trimmed, and untrimmed sequences were

discarded (<15% per sample) with Cutadapt version 2.8 (Martin, 2011). Adapter and primer-free sequences were imported into QIIME2 version 2019.10 (Bolyen et al., 2019), processed with DADA2 version 1.10.0 (Callahan et al., 2016) to eliminate PhiX contamination, trim reads (before median quality drops below 35; forward reads were trimmed at 230 bp and reverse reads at 229 bp), correct errors, merge read pairs, and remove PCR chimeras; ultimately, 10,831 amplicon sequencing variants (ASVs) were obtained across all samples. Alpha rarefaction curves were produced with the QIIME2 diversity alpha-rarefaction plugin, which indicated that the richness of the samples had been fully observed. A Naive Bayes classifier was fitted with 16S rRNA gene sequences extracted with the PCR primer sequences from the QIIME compatible, 99%-identity clustered SILVA v132 database (Pruesse et al., 2007). ASVs were classified by taxon using the fitted classifier (https://github.com/qiime2/q2-feature-classifier). ASVs classified as chloroplasts or mitochondria were removed. The number of removed ASVs was 100, totaling <1% relative abundance per sample, and the remaining 10,731 ASVs had their abundances extracted by feature-table (Pruesse et al., 2007).

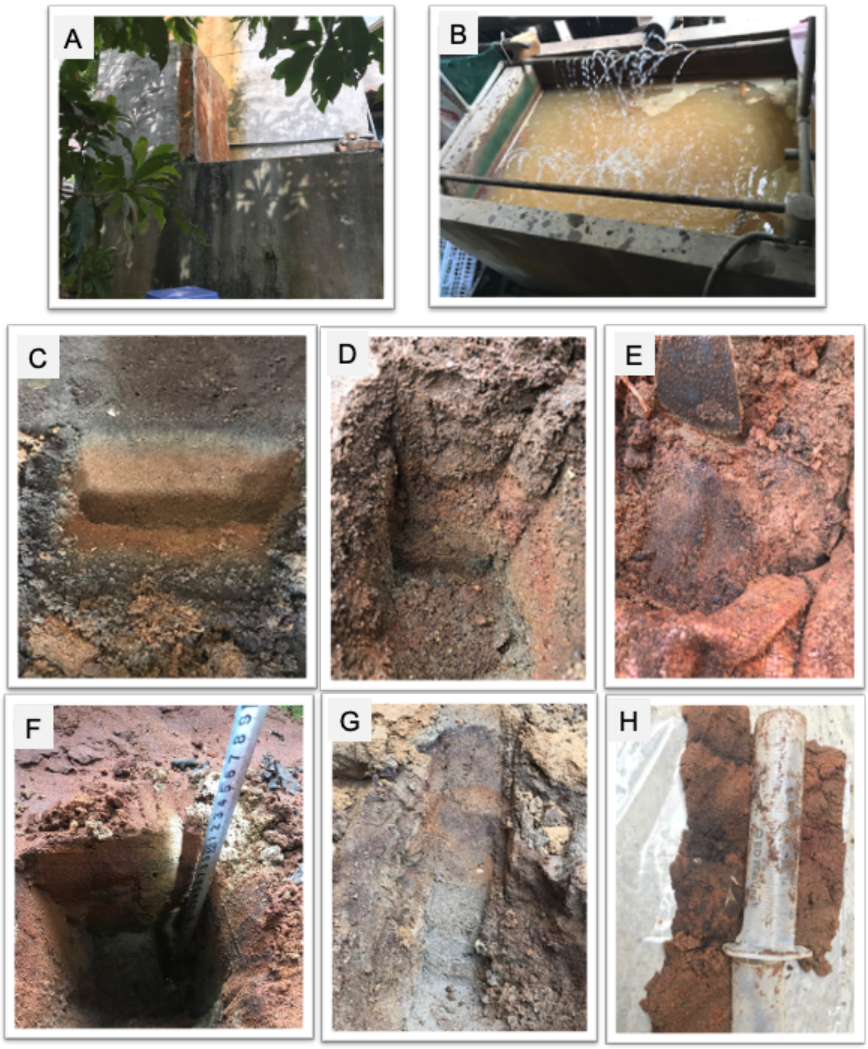

Figure S2. Typical household sand filter (A) where the groundwater was pre-aerated before filtration to enhance abiotic Fe(II) oxidation (B). Figures C-H indicate the heterogenous stratification of sand layers inside the filters with combinations of red/orange, grey, and black layers or patches. The black MnO_2 was found in most of the cases as black patches along the sand column, such as shown in figures E, F, H or as a distinct layer under the (red/orange) Fe(III) (oxyhydr)oxide layer (see figures D, G).

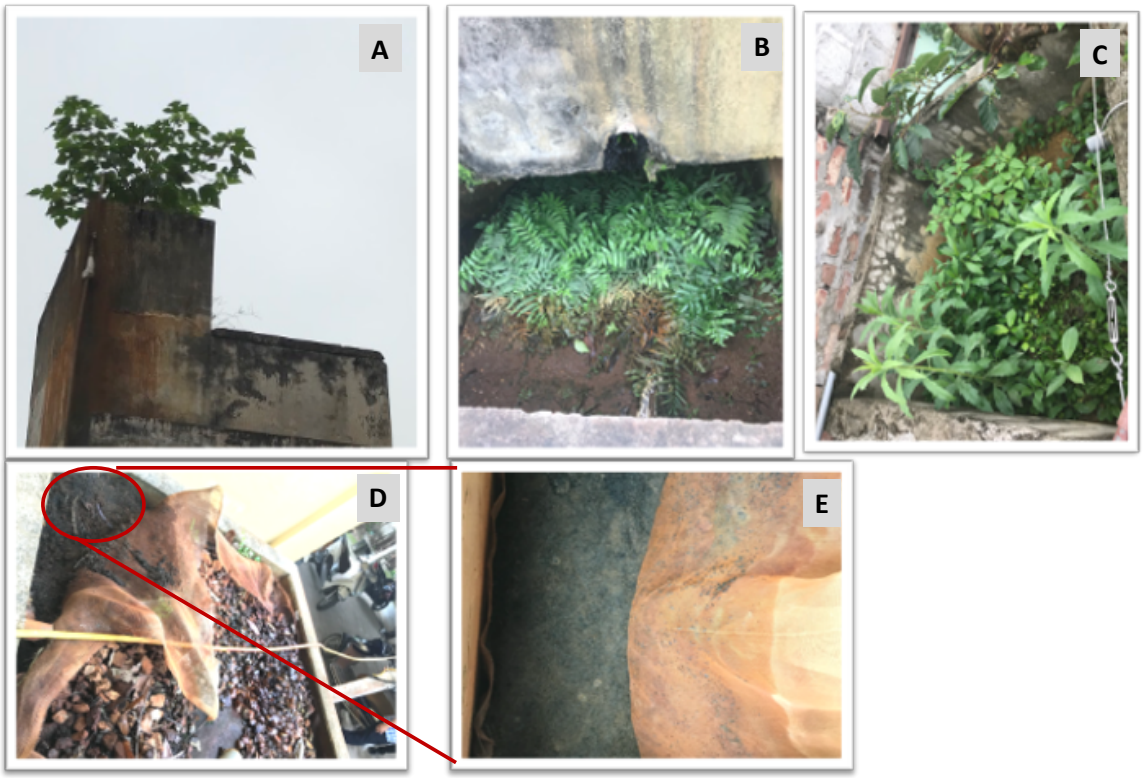

Figure S3. Irregularities during operation and maintainance of household SFs. Photos show plants growing in SFs which are not covered on top (A, B, C) and layers of burnt rice hulls that were added on top of the sand layer in SFs (D, E).

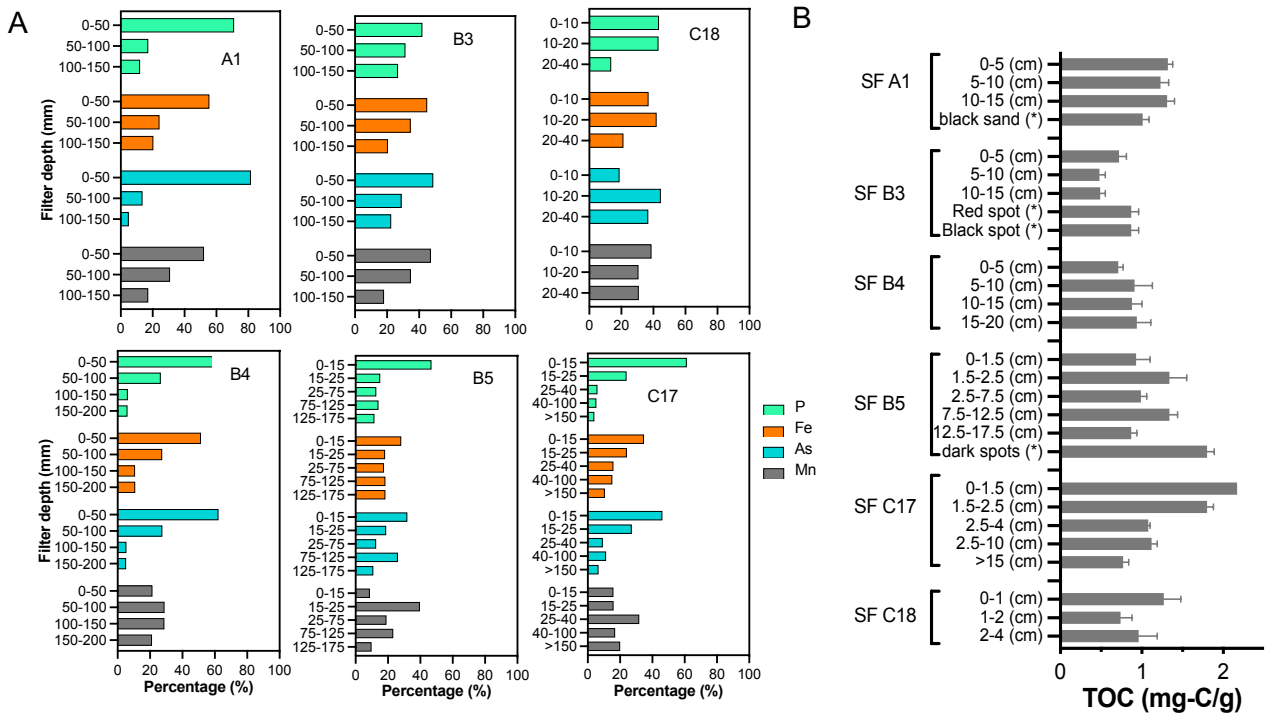

Figure S4. Total P, Fe, As, and Mn (A) and total organic carbon (B) distribution in different layers along the filter depth of studied sand filters.

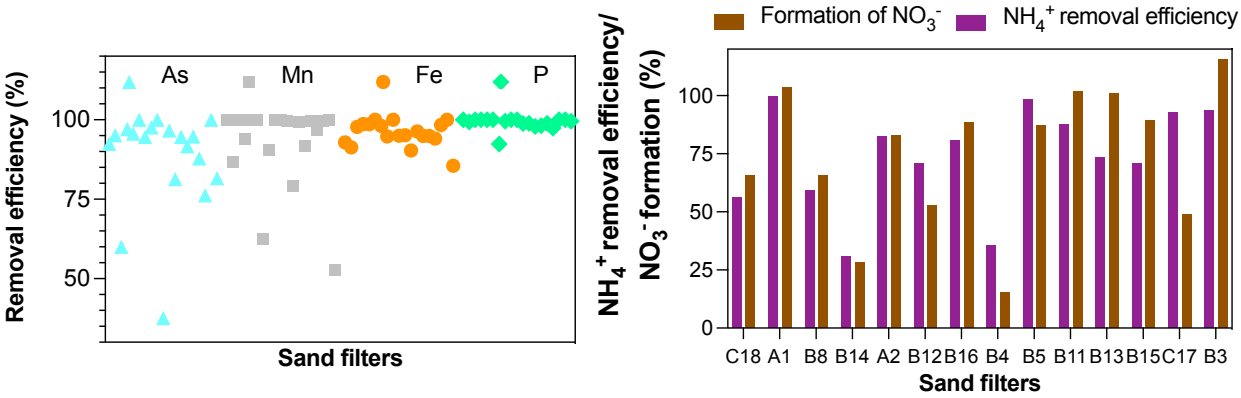

Figure S5. Contaminant removal efficiency of 20 studied sand filters across 3 field sites. Fe, Mn, As, and P removal efficiency is shown on the left, and NH_4^+ removal efficiency and percentage of NO_3^- formation detected in the outflow due to nitrification processes are shown on the right.

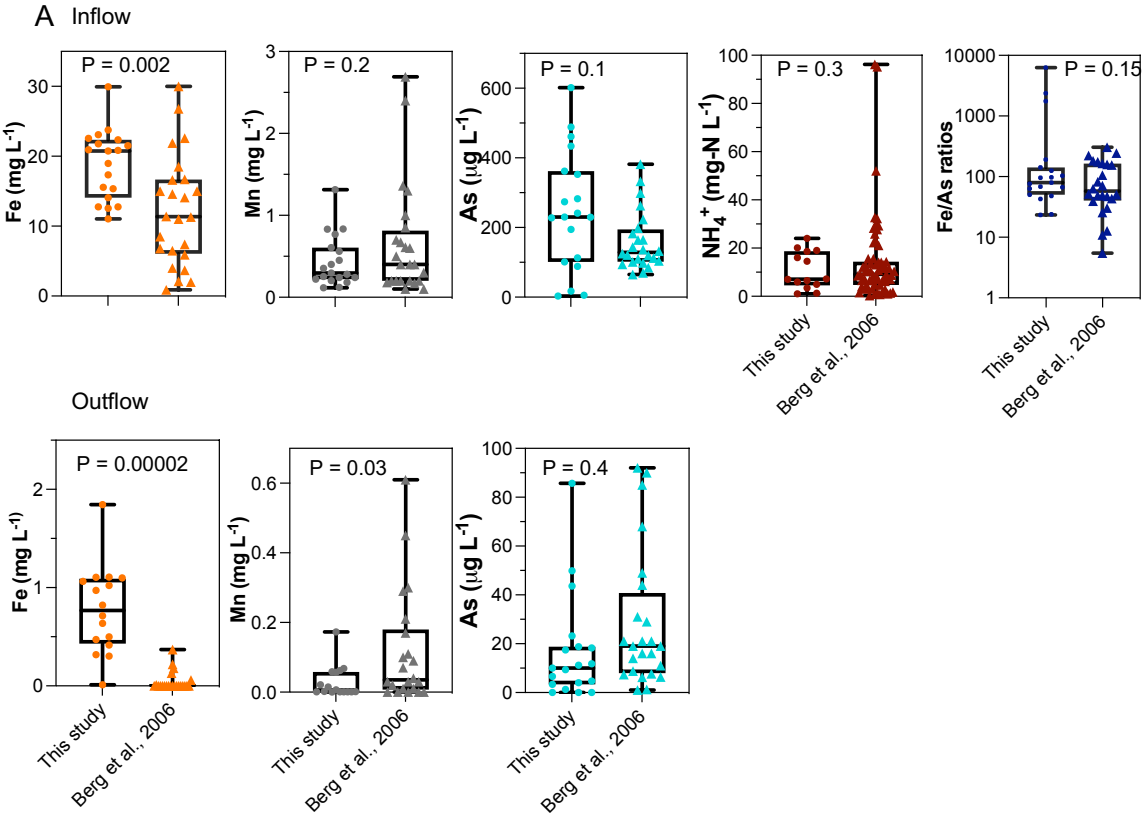

Figure S6: Fe, Mn, As, NH_4^+ concentrations of water inflow (top) and outflow (bottom) from household SFs based on our study (20 SFs from sampling campaigns in 2018 and 2020) and the database derived from (Berg et al., 2006) (Welch's t-test was used to compare the differences between the two groups in which p >0.05 means there is no significant difference between the two data sets.

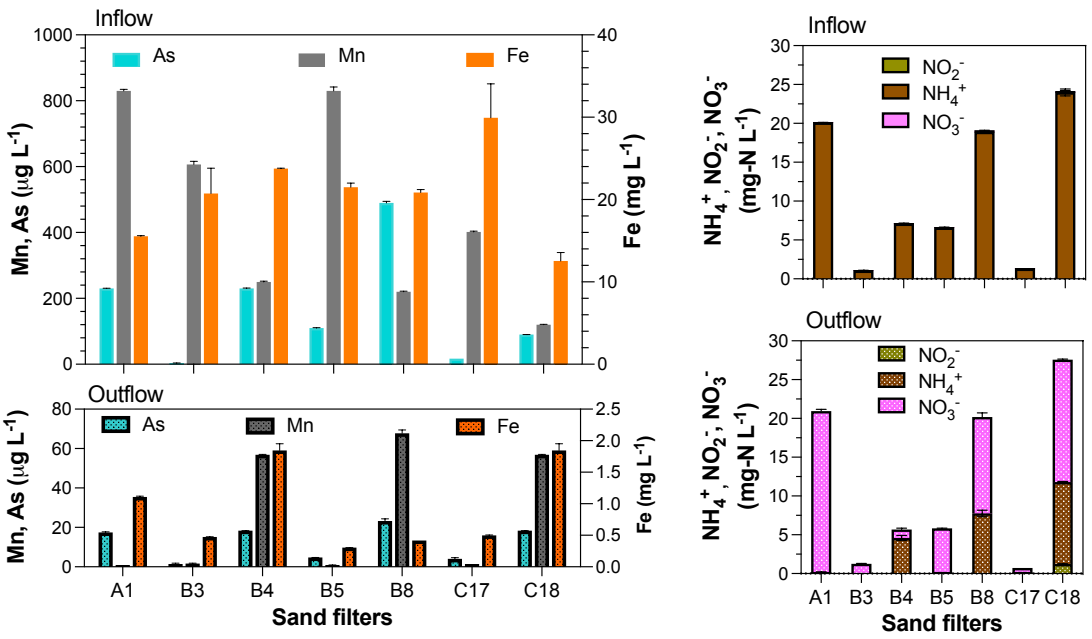

Figure S7. Performance (Fe, Mn, As, NH_4^+ concentration before and after filtration) of 7 selected SFs for microbial community analysis at 3 different field sites (A-Van Phuc, B-Tu Nhien, C-Dung Tien village). Dissolved concentrations of As, Mn, Fe (left) and NH_4^+, NO_2^-, NO_3^- (right) before (shown as inflow) and after (shown as outflow) sand filtration. All samples were analyzed in triplicate. Error bars indicate standard deviations.

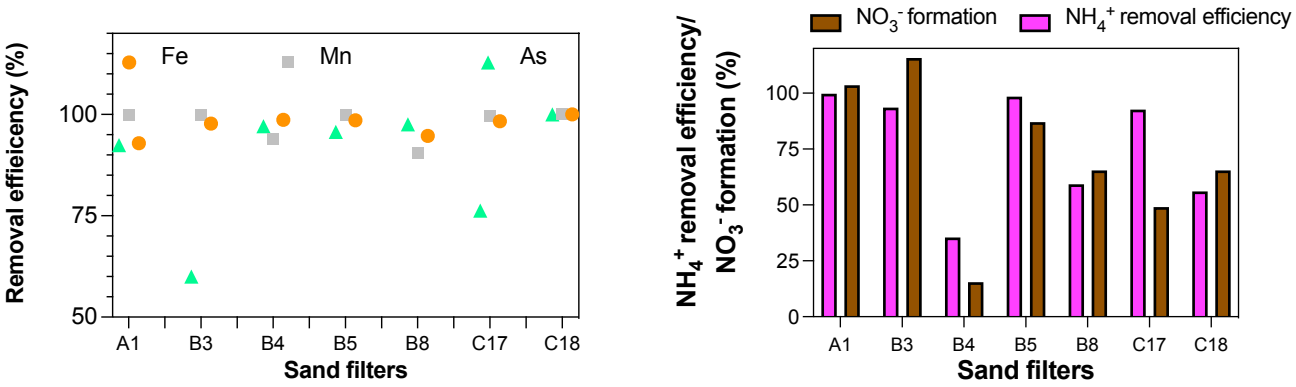

Figure S8. Contaminant removal efficiency of 7 sand filters that were selected for microbial community analysis. Fe, Mn, and As removal efficiency is shown on the left, and NH_4^+ removal efficiency and percentage of NO_3^- formation detected in the outflow due to nitrification processes are shown on the right.

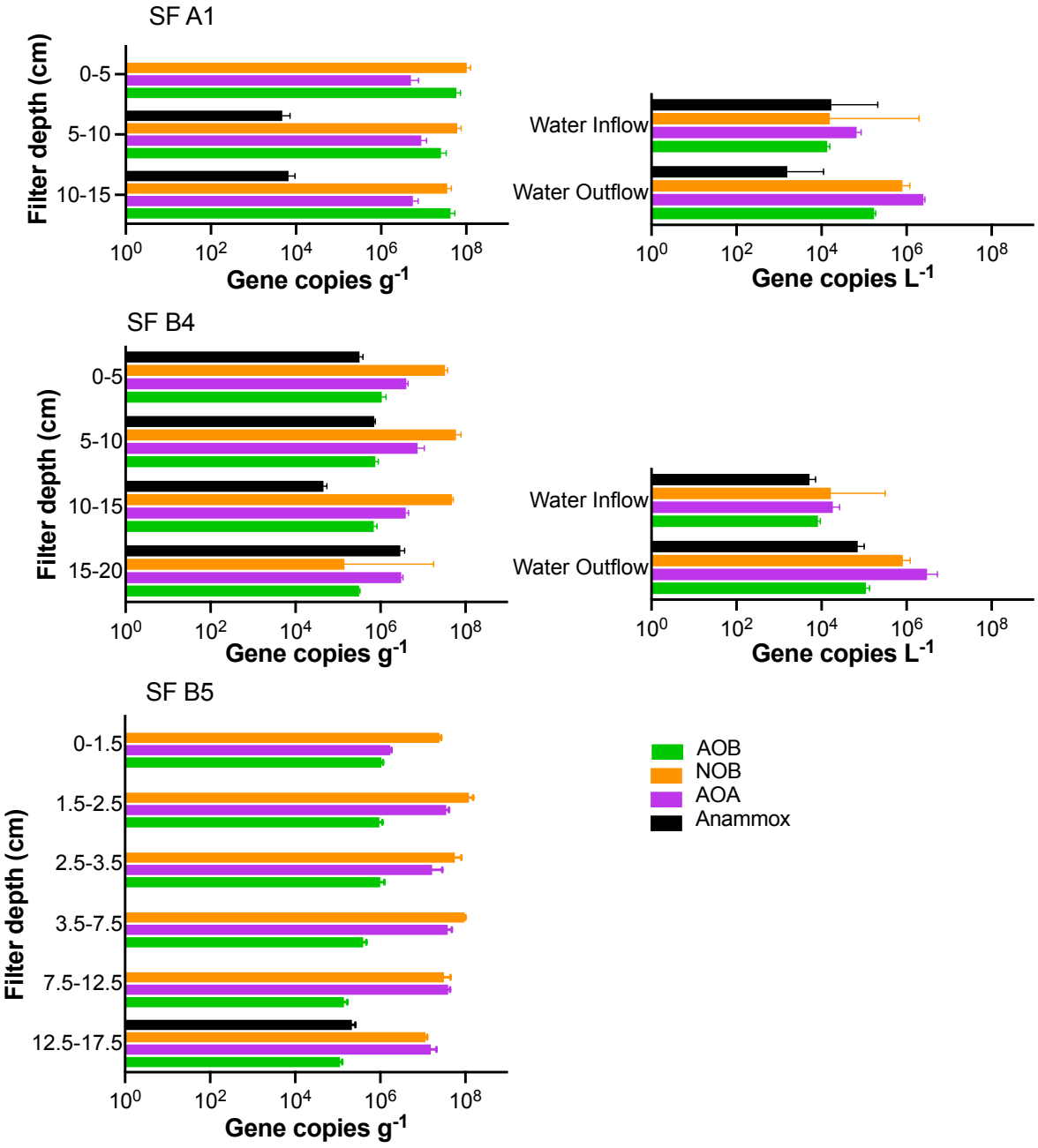

Figure S9. Quantitative PCR analysis of archaeal and bacterial *amoA* genes affiliating with ammonium-oxidizing bacteria (AOB) and archaea (AOA) respectively; bacterial *nxrB* genes belonging to nitrite-oxidizing bacteria (NOB), and 16S rRNA genes of anaerobic ammonium-oxidizing bacteria (anammox) in SFs and in the inflow and outflow water. Samples were analyzed from three different filters, representing the highest (SF A1, B5) (SF A1 with an increased content of 20.0 mg NH_4^+-N/L inflow and B5 with a low content of 7.0 mg NH_4^+-N/L inflow) and lowest (SF B4) performances of NH_4^+ oxidation. Error bars represent the standard deviation of triplicates.

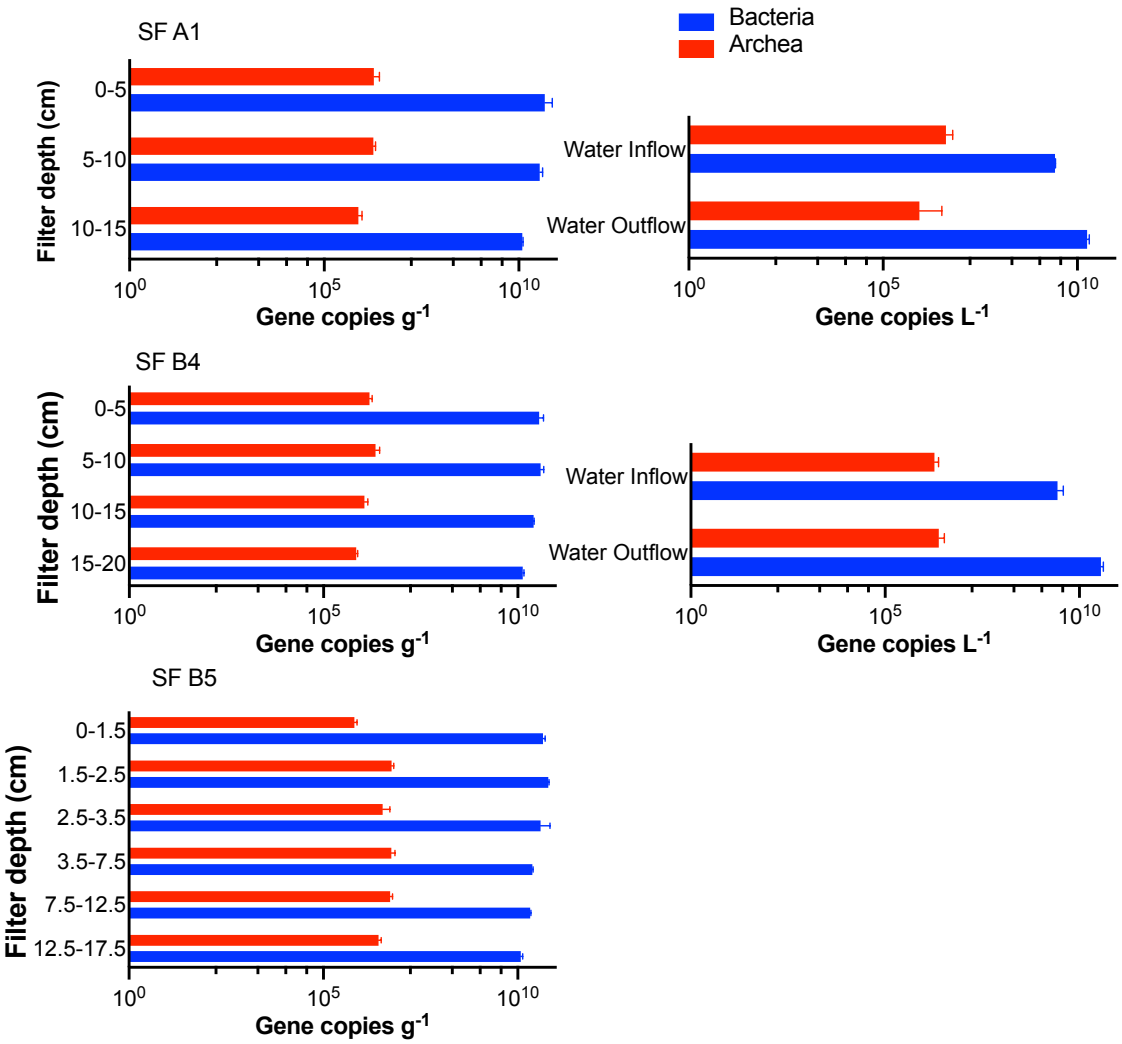

Figure S10. Quantitative PCR analysis of 16S rRNA genes of bacteria and archaea in sand filters and in the inflow and outflow water. Samples were analyzed from three different filters representing the highest (SF A1, B5) (SF A1 with an increased content of 20.0 mg NH_4^+-N/L inflow and B5 with a low content of 7.0 mg NH_4^+-N/ L inflow) and lowest (SF B4) performances of NH_4^+ oxidation. Error bars represent the standard deviation of triplicates.

Table S1. GPS coordinates of 20 studied SFs across 3 field sites and information about the depth of the sampling wells from which groundwater was abstracted.

SFs ID	Field site	Field site ID	Coordination	Depth of the well (m)
A1	Van Phuc	A	20.919444 N; 105.897778 E	35-45
A2	Van Phuc	A	20.919444 N; 105.897778 E	35-45
B3	Tu Nhien	B	20.864167 N; 105.918056 E	45-50
B4	Tu Nhien	B	20.84836 N; 105.91988 E	15-20
B5	Tu Nhien	B	20.847709 N; 105.916562 E	25-30

B6	Tu Nhien	B	20.8480194 N; 105.91931945 E	(N/A)
B7	Tu Nhien	B	20.848518 N; 105.919483 E	(N/A)
B8	Tu Nhien	B	20.848518 N; 105.919483 E	35-40
B9	Tu Nhien	B	20.8473417N; 105.91944723 E	(N/A)
B10	Tu Nhien	B	(N/A)	(N/A)
B11	Tu Nhien	B	20.847775N; 105.91904723 E	38
B12	Tu Nhien	B	20.8473417N; 105.91944723 E	62
B13	Tu Nhien	B	20.8464056 N; 105.91878612 E	33
B14	Tu Nhien	B	20.8687111 N; 105.91810834 E	24
B15	Tu Nhien	B	20.8513667 N; 105.92188056 E	60
B16	Tu Nhien	B	20.8520444 N; 105.92115001 E	57
C17	Dung Tien	C	20.816106 N; 105.851549 E	40-50
C18	Dung Tien	C	20.815656 N; 105.853192 E	40-50
C19	Dung Tien	C	20.815656 N; 105.853192 E	40-50
A20	Van Phuc	A	20.9188889 N; 105.9022222 E	45

Table S2. Relationship of groundwater (inflow) and filtered water (outflow) geochemistry during filtration processes in household SFs by Spearman correlation analysis.

Inflow	**Outflow**	**Cor**	**fdr**	**Inflow**	**Outflow**	**Cor**	**fdr**
(Fe-1.8P)/As	As	-0.8434	0.0002	As	Mn	0.3454	0.2546
Fe/As	As	-0.7500	0.0039	Fe	Fe	-0.3449	0.2546
NH_4^+	NO_3^-	0.8330	0.0040	NO_3^-	P	0.3944	0.2609
As	As	0.6621	0.0206	Fe	NH_4^+	-0.4066	0.2609
NH_4^+	NO_2^-	0.7114	0.0431	NH_4^+	As	0.3393	0.3562
(Fe-1.8P)/As	Fe	-0.6060	0.0431	Fe	As	-0.2892	0.3562
(Fe-1.8P)/As	P	-0.5912	0.0484	(Fe-1.8P)/As	NO_2^-	-0.3408	0.3729
Fe	NO_3^-	-0.6571	0.0746	As	NO_3^-	0.3024	0.4562
As	P	0.5463	0.0790	As	Fe	0.2404	0.4652
Fe/As	P	-0.5360	0.0831	P	NO_3^-	0.2747	0.5037
Fe	NO_2^-	-0.5993	0.1111	NO_3^-	As	0.2426	0.5509
P	Fe	0.4996	0.1111	NH_4^+	Fe	0.2377	0.5510
P	As	0.4970	0.1111	Mn	NO_2^-	-0.2405	0.5568
(Fe-1.8P)/As	Mn	-0.4880	0.1163	Fe	Mn	-0.1852	0.5674
NH_4^+	NH_4^+	0.5692	0.1212	P	Mn	0.1837	0.5674
As	NH_4^+	0.5629	0.1212	Fe/As	NO_2^-	-0.2219	0.5674
Fe/As	NH_4^+	-0.5604	0.1212	P	NO_2^-	0.2127	0.5790
P	NH_4^+	0.5560	0.1212	NO_3^-	NO_2^-	0.1925	0.6086
(Fe-1.8P)/As	NH_4^+	-0.5429	0.1322	NO_3^-	Mn	0.1797	0.6086

NO_3^-	NO_3^-	0.5360	0.1349	Mn	P	-0.1523	0.6086
(Fe-1.8P)/As	NO_3^-	-0.5077	0.1702	Mn	As	-0.1274	0.6773
NO_3^-	NH_4^+	0.5006	0.1738	Fe	P	-0.1119	0.7151
P	P	0.4052	0.1808	NH_4^+	P	-0.1162	0.7467
Fe/As	Fe	-0.4038	0.1808	As	NO_2^-	0.1103	0.7544
Fe/As	Mn	-0.3886	0.2026	Mn	Mn	0.0874	0.7544
Mn	NH_4^+	-0.4532	0.2192	NH_4^+	Mn	0.0679	0.8401
NO_3^-	Fe	0.4344	0.2192	Mn	Fe	-0.0253	0.9286
Fe/As	NO_3^-	-0.4198	0.2546	Mn	NO_3^-	-0.0264	0.9286

Table S3. Relative influence of groundwater composition (Fe, Mn, As, and NH_4^+ inflow) on sand filters microbial communities in household SF by ADONIS test.

Formula	Factor	Df	Sums Of Sqs	Mean Sqs	F.Model	Effect size R2	significance Pr(>F)	Effect size (%) R2
"Fe+P+Mn+NH4+As"	As	1	0.940	0.940	5.834	0.206	0.001	20.628
"Fe+As+NH4+P+Mn"	Mn	1	0.669	0.669	4.151	0.147	0.001	14.677
"As+NH4+P+Mn+Fe"	Fe	1	0.679	0.679	4.214	0.149	0.001	14.900
"As+Fe+P+Mn+NH4"	NH4	1	0.694	0.694	4.304	0.152	0.001	15.219
"Mn+Fe+As+NH4+P"	P	1	0.733	0.733	4.546	0.161	0.001	16.074

Table S4. t-Test performance for water inflow outflow composition including Fe, As, Mn, NH_4^+ concentrations of the present study in comparison to the values provided in (Berg et al., 2006)

	t-Test: Two-Sample Assuming Unequal Variances														
	Fe (inflow)		**Mn (Inflow)**		**As (Inflow)**		**NH_4^+ (Inflow)**		**Fe/As ratios (Inflow)**		**Fe (Outflow)**		**Mn (Outflow)**		**As (Outflow)**	
	This study	(Berg et al., 2006)	This study	(Berg et al., 2006)	This study	(Berg et al., 2006)	This study	(Berg et al., 2006)	This study	(Berg et al., 2006)	This study	(Berg et al., 2006)	This study	(Berg et al., 2006)	This study	(Berg et al., 2006)
Mean	18.83	12.2	0.44	0.66	247.7	159.5	10.7	7.69	616.8	97.9	0.78	0.04	0.029	0.11	38.84	28.5
Variance	24.53	63.07	0.10	0.47	29444.3	7104.6	59.58	61.80	2289695.9	6900.5	0.20	0.01	0.002	0.02	742.88	789.3
Observations	19	24	19.00	24.00	19	24	14	24	19	24	16	23	16	22	6	24
P (T<=t) two-tail	0.002		0.17		0.06		0.26		0.15		0.00002		0.025		0.43	
t Critical two-tail	2.023		2.03		2.06		2.05		2.10		2.12		2.06		2.31	

Table S5. Standards, primers, and thermal profiles used in qPCR assay for different target genes.

Specificity	Primer	Primer sequence (5´ → 3´)	Thermal program	References
16S rRNA gene	341F	CCT ACG GGA GGC AGC AG	98ºC - 2';	(Muyzer et al., 1993)
Bacteria	534R	ATT ACC GCG GCT GCT GG	(98ºC - 5''; 60ºC - 12''; 95ºC - 1'; 60ºC - 1') x 40;	
			60 - 95ºC - 10''	
16S rRNA gene	Ar 109F	ACK GCT GAG TAA CAC GT	98ºC - 3';	(Großkopf et al., 1998)
Archaea	Ar 915R	GTG CTC CCC CGC CAA TTC CT	(98ºC - 5''; 52ºC - 12''; 95ºC - 1'; 72ºC - 15') x 40;	(Stahl, 1991)
			98ºC - 1'; 52ºC - 1'; 52 - 95ºC - 10''	
amoA	amoA1F	GGGGTTTCTACTGGTGGT	(98ºC - 45''; 60ºC - 45''; 72ºC - 45'') x 40;	(Rotthauwe et al., 1997)
AOB	amoA2R	CCCCTCKGSAAAGCCTTCTTC	60 - 95ºC - 10''	
amoA	Amo10F	ATGGTCTGGCTWAGACG	98ºC - 2';	(Leininger et al., 2006)
AOA	Crenamo	GCCATCCABCKRTANGTCCA	(98ºC - 30''; 55ºC - 30''; 72ºC - 45'') x 40;	(Schauss et al., 2009)
	A616r48x		98ºC - 1'; 55ºC - 1'; 55 - 95ºC - 10''	(Treusch et al., 2005)
nxrB bacterial	nxrB169F	TACATGTGGTGGAACA	95ºC - 5';	(Pester et al., 2014)
Nitrospira	nxrB638R	CGGTTCTGGTCRATCA	(95ºC - 15''; 60ºC - 80''; 72ºC - 90'') x 40;	
			65 - 95ºC - 10''	
16S rRNA	Amx368F	TTCGCAATGCCCGAAAGG	94ºC - 4';	(Schmid et al., 2000)
genes bacterial	Amx 820R	AAACCCCTCTACTTAGTGCCC	(94ºC - 30''; 56ºC - 30''; 72ºC - 1';') x 40;	(Kartal et al., 2007,
anammox			60 - 95ºC - 10''	2006)
pmoA	A189f	GGNGACTGGGACTTCTGG	96°C - 5´;	(Holmes et al., 1995)
Methanotrophs	A682r	GAASGCNGAGAAGAASGC	(94°C - 1´; 56°C - 1´; 72°C - 1´) x 38; 72°C - 5´	

References

Berg, M., Luzi, S., Trang, P.T.K., Viet, P.H., Giger, W., Stüben, D., 2006. Arsenic removal from groundwater by household sand filters: Comparative field study, model calculations, and health benefits. Environ. Sci. Technol. 40, 5567–5573. https://doi.org/10.1021/es060144z

Bolyen, E., Rideout, J.R., Dillon, M.R., Bokulich, N.A., Abnet, C.C., Al-Ghalith, G.A., Alexander, H., Alm, E.J., Arumugam, M., Asnicar, F., 2019. Reproducible, interactive, scalable and extensible microbiome data science using QIIME 2. Nat. Biotechnol. 37, 852–857.

Callahan, B.J., McMurdie, P.J., Rosen, M.J., Han, A.W., Johnson, A.J.A., Holmes, S.P., 2016. DADA2: high-resolution sample inference from Illumina amplicon data. Nat. Methods 13, 581–583.

Di Tommaso, P., Chatzou, M., Floden, E.W., Barja, P.P., Palumbo, E., Notredame, C., 2017. Nextflow enables reproducible computational workflows. Nat. Biotechnol. 35, 316–319.

Ewels, P.A., Peltzer, A., Fillinger, S., Alneberg, J., Patel, H., Wilm, A., Garcia, M.U., Di Tommaso, P., Nahnsen, S., 2019. nf-core: Community curated bioinformatics pipelines. BioRxiv 610741.

Großkopf, R., Janssen, P.H., Liesack, W., 1998. Diversity and structure of the methanogenic community in anoxic rice paddy soil microcosms as examined by cultivation and direct 16S rRNA gene sequence retrieval. Appl. Environ. Microbiol. 64, 960–969.

Holmes, A.J., Costello, A., Lidstrom, M.E., Murrell, J.C., 1995. Evidence that participate methane monooxygenase and ammonia monooxygenase may be evolutionarily related. FEMS Microbiol. Lett. 132, 203–208.

Kartal, B., Koleva, M., Arsov, R., van der Star, W., Jetten, M.S.M., Strous, M., 2006. Adaptation of a freshwater anammox population to high salinity wastewater. J. Biotechnol. 126, 546–553.

Kartal, B., Kuypers, M.M.M., Lavik, G., Schalk, J., Op den Camp, H.J.M., Jetten, M.S.M., Strous, M., 2007. Anammox bacteria disguised as denitrifiers: nitrate reduction to dinitrogen gas via nitrite and ammonium. Environ. Microbiol. 9, 635–

642.

Kurtzer, G.M., Sochat, V., Bauer, M.W., 2017. Singularity: Scientific containers for mobility of compute. PLoS One 12, e0177459.

Leininger, S., Urich, T., Schloter, M., Schwark, L., Qi, J., Nicol, G.W., Prosser, J.I., Schuster, S.C., Schleper, C., 2006. Archaea predominate among ammonia-oxidizing prokaryotes in soils. Nature 442, 806–809.

Martin, M., 2011. Cutadapt removes adapter sequences from high-throughput sequencing reads. EMBnet. J. 17, 10–12.

Muyzer, G., De Waal, E.C., Uitterlinden, A.G., 1993. Profiling of complex microbial populations by denaturing gradient gel electrophoresis analysis of polymerase chain reaction-amplified genes coding for 16S rRNA. Appl. Environ. Microbiol. 59, 695–700.

Pester, M., Maixner, F., Berry, D., Rattei, T., Koch, H., Lücker, S., Nowka, B., Richter, A., Spieck, E., Lebedeva, E., Loy, A., Wagner, M., Daims, H., 2014. NxrB encoding the beta subunit of nitrite oxidoreductase as functional and phylogenetic marker for nitrite-oxidizing Nitrospira. Environ. Microbiol. 16, 3055–3071. https://doi.org/10.1111/1462-2920.12300

Pruesse, E., Quast, C., Knittel, K., Fuchs, B.M., Ludwig, W., Peplies, J., Glöckner, F.O., 2007. SILVA: a comprehensive online resource for quality checked and aligned ribosomal RNA sequence data compatible with ARB. Nucleic Acids Res. 35, 7188–7196.

Rotthauwe, J.-H., Witzel, K.-P., Liesack, W., 1997. The ammonia monooxygenase structural gene amoA as a functional marker: molecular fine-scale analysis of natural ammonia-oxidizing populations. Appl. Environ. Microbiol. 63, 4704–4712.

Schauss, K., Focks, A., Leininger, S., Kotzerke, A., Heuer, H., Thiele-Bruhn, S., Sharma, S., Wilke, B., Matthies, M., Smalla, K., 2009. Dynamics and functional relevance of ammonia-oxidizing archaea in two agricultural soils. Environ. Microbiol. 11, 446–456.

Schmid, M., Twachtmann, U., Klein, M., Strous, M., Juretschko, S., Jetten, M., Metzger, J.W., Schleifer, K.-H., Wagner, M., 2000. Molecular evidence for genus level diversity of bacteria capable of catalyzing anaerobic ammonium oxidation.

Syst. Appl. Microbiol. 23, 93–106.

Stahl, D.A., 1991. Development and application of nucleic acid probes. Nucleic acid Tech. Bact. Syst. 205–248.

Straub, D., Blackwell, N., Langarica-Fuentes, A., Peltzer, A., Nahnsen, S., Kleindienst, S., 2020. Interpretations of Environmental Microbial Community Studies Are Biased by the Selected 16S rRNA (Gene) Amplicon Sequencing Pipeline. Front. Microbiol. 11, 1–18. https://doi.org/10.3389/fmicb.2020.550420

Treusch, A.H., Leininger, S., Kletzin, A., Schuster, S.C., Klenk, H., Schleper, C., 2005. Novel genes for nitrite reductase and Amo-related proteins indicate a role of uncultivated mesophilic crenarchaeota in nitrogen cycling. Environ. Microbiol. 7, 1985–1995.

Voegelin, Andreas; Kaegi, Ralf; Berg, Michael; Nitzsche, Katja Sonja; Kappler, Andreas; Lan, Vi Mai; Trang, Pham Thi Kim; Göttlicher, Jörg; Steininger, R., 2014. Solid-phase characterisation of an effective household sand filter for As, Fe and Mn removal from groundwater in Vietnam. Environ. Chem. 11, 566–578. https://doi.org/10.1071/EN14011

Winkel, L.H.E., Trang, P.T.K., Lan, V.M., Stengel, C., Amini, M., Ha, N.T., Viet, P.H., Berg, M., 2011. Arsenic pollution of groundwater in Vietnam exacerbated by deep aquifer exploitation for more than a century. Proc. Natl. Acad. Sci. U. S. A. 108, 1246–1251. https://doi.org/10.1073/pnas.1011915108

Chapter 3_Paper 2: Personal contribution

Anh Van Le contributed to concept of the study, sampling campaigns, lab work, and manuscript writing with support and feedback from Andreas Kappler and Eva Marie Muehe. Andreas Kappler obtained funding and conceptualized the study. Sample preparation, measurement, and data analysis for μXRF were done by Saron Bone, Eva Marie Muehe. The ICP-MS analysis was conducted by Sören Drabesch. The SEM/EDS was conducted by Stefan Fischer. The manuscript was revised by all co-authors.

Chapter 3: Field and laboratory evidence for manganese redox cycling controlling Fe and As retention in household sand filters

Anh Van Le[1], E. Marie Muehe [2,3], Sharon Bone[4], Sören Drabesch[1,2], Stefan Fischer[5], Andreas Kappler[1,6]

[1]Geomicrobiology, Department of Geosciences, University of Tuebingen, 72076 Tuebingen, Germany

[2]Plant Biogeochemistry, Department of Environmental Microbiology, Helmholtz Centre for Environmental Research - UFZ, 04318 Leipzig, Germany

[3]Plant Biogeochemistry, Department of Geosciences, University of Tuebingen, 72076 Tuebingen, Germany

[4]SLAC National Accelerator Laboratory, 2575 Sand Hill Rd Menlo Park, CA-94025, US

[5]Tuebingen Structural Microscopy Core Facility, University of Tuebingen, 72076 Tuebingen, Germany

[6]Cluster of Excellence: EXC 2124: Controlling Microbes to Fight Infection, 72076 Tuebingen, Germany

For submission to *ES&T Water*

Abstract

In the Red River delta, Vietnam, operation of household sand filters that are applied to remove Fe, Mn and As from groundwater, starts with (oxic) unsaturated conditions followed by saturated conditions, which semi-oxic to anoxic zones are formed along sand layers. Most studies evaluated filtration efficiency and solid-phase composition at a specific time point. Therefore, long-term filter performances and spatiotemporal changes of solid-associated Fe, As, and Mn in unsaturated and saturated conditions remain unknown. We therefore established column experiments following Fe, As, and Mn removal over time and their distribution and speciation on sand grain surfaces under unsaturated and saturated conditions. Averagely 99±0.2, 93±0.7, and 91±8% of $Fe(II)_{aq}$, $As(III)_{aq}$, and $Mn(II)_{aq}$ were removed by filtration under unsaturated conditions. Under saturated conditions, Fe and As removal remained the same (99±0.4 and 95±1.7%), while $Mn(II)_{aq}$ was leached (up to 5 mg/L) from columns to the effluent. Micro-X-ray absorption near-edge structure (μXANES) analysis showed that solid-associated Fe(III), As(V), and Mn(III)/(IV) dominated in unsaturated sand. Under saturated conditions, up to 46% and 15% of Fe(III) and As(V) were reduced in the anoxic zone (5-10 cm) and the Mn adsorption maximum position shifted towards lower energy with a shoulder at 6554 eV, indicating the presence of Mn(II). Therefore, the high retention of Fe and As under reducing conditions can be explained by i) re-adsorption of reduced Fe(II) and desorbed As(III)/(V) to remaining Fe(III)(oxyhydr)oxide and Mn oxides minerals and ii) abiotic oxidation of Fe(II) by Mn(IV) oxides forming new Fe(III) phases that sequester As(III)/(V).

3.1. Introduction

Water filtration by household sand filters (SFs) is one the oldest point-of-use water treatment techniques that has been recommended by the World Health Organization (WHO) to provide safe drinking water for people living in rural areas (Freitas et al., 2022; WHO, 2011). In the Red River delta, Vietnam, groundwater is acutely contaminated by As; up to 3000 μg/L of As was detected in some places (Berg et al., 2001). Household SFs have been used in this area to eliminate As(III) and other contaminants such as Fe(II) and Mn(II) from groundwater for more than 30 years (Berg et al., 2006; Luzi et al., 2004). Groundwater is pumped intermittently onto the top of the sand surface followed by gravitational trickling through the sand layer. Filtered water is collected in a lower compartment and can be used for drinking and cleaning (Berg et al., 2006; Nitzsche et al., 2015a). As(III), Fe(II) and Mn(II) are co-oxidized in the filter, followed by the precipitation of As(V)-bearing Fe(III) (oxyhydr)oxides and Mn(III/IV) oxides on sand particle surfaces (Hug and Leupin, 2003; Voegelin et al., 2014).

The operation of sand filter starts with unsaturated flow when sand layers maintain oxic conditions and is followed by saturated flow when an oxygen gradient is formed along the sand column creating a semi-oxic (top layer) and anoxic zone (bottom layer). When the filters get clogged (every 3-6 months), 10-20 cm of the top sand is scraped off for unclogging. Thus, sand filters are usually operated under alternating unsaturated and saturated flow for many years.

Under unsaturated conditions, Fe-, Mn- and As-species in the groundwater are almost completely oxidized (Fe(III), Mn(IV) and As(V)). Mn oxides are therefore constantly formed in sand filters, forming distinguished black patches or layers in the sand filters (Nitzsche et al., 2015a; Van Le et al., 2022b). The formation of Mn(IV) oxides is due to i) microbial activity of Mn(II)-oxidizing bacteria (MnOB) (Hansel, 2017; Tebo et al., 2005) and ii) abiotic oxidation of Mn(II) by O_2 catalyzed at Fe(III) (oxyhydr)oxides surfaces (Davies and Morgan, 1989; Morgan, 2005; Ross and Bartlett, 1981). Since Mn(IV) oxides are strong oxidants they can directly oxidize dissolved As(III) and Fe(II) in the groundwater (Eq 1, 2),

$MnO_2 + AsO_3^{3-} + 2H^+ \rightarrow Mn^{2+} + AsO_4^{3-} + H_2O$ (Eq. 1)

$2MnO_2 + Fe^{2+} + 5H^+ \rightarrow Fe(OH)_3 + 2Mn^{2+} + H_2O$ (Eq. 2)

Over a long operational time (several months to years), the filter surface is getting blocked by precipitation of carbonate minerals and metal (oxyhydr)oxides, thus inhibiting the abiotic oxidation of Fe(II) and As(III) by O_2 (Petitjean et al., 2016). Under such conditions, Mn oxides might complement the heterogeneous oxidation of As(III) and Fe(II) (Eq 1, 2) to enhance As and Fe retention in sand filters. Indeed, under O_2-depleted conditions, Mn(IV) oxides (either as abiotic or biogenic birnessite) prevented As mobilization in soil and sand columns (Bai et al., 2016a; Ehlert et al., 2016; Liu et al., 2022). However, until now, there is no direct evidence that under O_2-depleted conditions the presence of Mn(IV) oxides can control the immobilization of As and Fe) in household sand filters. One of the issues is that most studies have examined As, Fe, and Mn removal by sampling at specific timepoints to confirm the high removal efficiency. There is inadequate data regarding long-time monitoring of Fe, As, and Mn effluent over unsaturated (fully oxic) to saturated (O_2-depleted) operational phases in sand filters. Obtaining such analyses at different timepoints (with different saturation status and different redox conditions) is essential as it will reveal whether As removal mechanisms change during redox fluctuations and can reveal the impact of Mn(III/IV) oxides on As and Fe retention in sand filters.

Therefore, in this study, we conducted column experiments in the lab and in the field in which sand columns were fed by sterile artificial and local native groundwater, respectively. We aimed at i) monitoring the performance of the sand filter applied to remove As, Fe, and Mn over time from unsaturated to saturated conditions, ii) quantifying the distribution of total As, Fe, and Mn along the depth of sand columns, and iii) identifying the location and speciation of As, Fe, and Mn on the surface of sand particles under unsaturated and saturated conditions.

3.2. Materials and methods

3.2.1. Column setup

The glass columns (inner diameter 4.5 cm, length 25 cm) consisted of support layers filled with 2 cm gravel (particles size: 6-8 mm, Flairstone, Germany) and 3 cm sterilized quartz sand (particle size: 0.4-0.8 mm, Carl Roth GmbH, Germany) at the bottom, followed by a reactive layer filled with 10 cm of sand filter materials. Columns were intermittently operated in gravitational down-flow mode 2-3 times per day. Two similar

column setups were running in the field (20°55′08.63” N, 105°53′47.61″ E, Van Phuc village in the Red River delta, Vietnam) (field site description see SI, section S1) and in the lab.

3.2.2. Column flow experiment

Columns in the field

In the field, the biotic columns contained the reactive layer (top 10 cm) filled with sand collected from the local sand supplier. 250 ml of natural groundwater was pumped directly on top of the sand columns each time. The inflow water contained 16.1 mg/L of Fe(II), 1.4 mg/L of Mn(II), and 240 μg/L of As(III). The filtration rate, and the concentrations of Fe, Mn, As in the effluent were recorded at every feeding batches. The experiment ran over 1.5 months, equaling 169 pore volumes.

Columns in the lab

In the lab, the duplicate biotic columns contained a reactive layer (top 10 cm) filled with sand collected from a frequently running household filter (sample collection is described in SI, section S1). Additionally, an abiotic control column was setup in the lab, with the reactive layer (top 10 cm) filled with sterile quartz sand (particle size: 0.4-0.8 mm, Carl Roth GmbH, Germany). To follow the dissolved oxygen (DO) in the sand columns (biotic and abiotic setups), six pieces of oxygen optode foil (PreSens, Germany) were glued inside at different depths along the columns. Sterile artificial groundwater (AGW) was freshly prepared every week and contained 20.9±1.5 mg/L of Fe(II), 1.8±0.6 mg/L of Mn(II), and 307.0±24.4 μg/L of As(III). The preparation of AGW is described in SI section S2 and Table S1. The pH of AGW was adjusted to 7.3 which is the average pH value of groundwater in the Red River delta (Berg et al., 2006). Every time, up to 150 ml of ARW was fed to the columns. In total, the experiment was operated over two months equaling 141 pore volumes and we experienced two clogging events at pore volumes 93 and 141. After the first clogging event, 3 cm of top sand was scraped off the column to unclog the sand column, and the experiment was continuously running until the second clogging.

3.2.3. Aqueous analysis

At every filtration time, inflow and outflow water was collected. To quantify dissolved As, Fe and Mn, 2 ml of inflow and outflow water were filtered (0.22 μm cellulose filter,

EMD Millipore) and diluted with 1% HNO_3 before analysis by inductively coupled plasma mass spectrometry (ICP-MS) (Agilent 7900, Agilent Technologies)

3.2.4. Solid phase analysis

The column experiments were performed at a temperature ranging from 20-25^{o}C. After the experiments, to prevent further oxidation of solid-associated Fe(II), As(III) and Mn(II), filter materials were collected from 2-5 cm depth in the glovebox (100% N_2, <30 ppm O_2, MBRAUN UNIlab).

Elemental composition analysis

12 ml of aqua-regia solution (9 ml of 37% HCl and 3 mL of 65% HNO_3) were added slowly to the Xpress Plus Teflon vessels containing 0.5 gram of dried sand materials. The samples were digested in the Microwave Accelerated Reaction System, MARS 6 (CEM, USA) (details in SI section S3). Afterwards, the digested samples were adjusted to a final volume of 50 ml by adding milliQ H_2O under the fume hood. The samples were centrifuged at 16,873 g for 15 min (Thermo Scientific Sorvall LYNX6000). 100 µl of the supernatant were collected and diluted 100-fold in 1% HNO_3. Samples were stored at 4°C in the dark until analysis via the Agilent 7900 ICP-MS.

X-ray fluorescence imaging

The distribution of As, Fe, and Mn on the surface of sand particles was visualized with X-ray fluorescence (XRF) mapping using beamline 7-2 at Stanford Synchrotron Radiation Lightsource (SSRL). Samples were freeze-dried and transferred to wells with 5 mm diameter on multi-well sample holders. Samples were embedded in Epotek 301-1 resin (Epoxy Technology). All preparatory steps were performed in a glovebox (100% N_2, <30 ppm O_2). Epoxied samples were polished to 5 mm thickness under oxic (ambient) conditions.

Beam line 7-2 is equipped with a bend magnet, capillary optics, and a double crystal (Si 111) monochromator. Samples were placed at a 45° to the incoming focused beam with a 50 µm spot size and a 100 ms dwell time per pixel. Samples were imaged at two energies 12,000 eV for obtaining As and total elemental maps, and 8000 eV for obtaining accurate Fe and Mn maps. Fluorescence intensities of aimed at elements were monitored with a four-element Vortex Silicon Drift Detector.

As, Fe and Mn maps were visualized in SMAK (Webb, 2011), deadtime corrected, normalized to the incoming beam and back-calculated to image-averaged counts at each point of the map. Fluorescent count maps were converted to elemental concentration per unit area based on quantification of elemental references provided by the beamline scientists. Four areas of interest with differences in the amounts of coinciding Fe, As, and Mn were identified for each map and used to visualize elemental correlations of Fe, As, and Mn. The areas were selected if the fluorescence count of at least one element (Fe, As and Mn) was at high intensity.

Areas with a simultaneous presence of high counts of As, Fe and Mn were identified and selected for spot μ-X-ray Absorption Near Edge Structure (μ-XANES) spectroscopy. Mn K-edge, Fe K-edge, and last As K-edge μXANES data were obtained in this order at the same spot, starting with the lowest energy to prevent beam redox changes. Three to six spectra were obtained per spot, depending on spectra quality. In Athena (Ravel and Newville, 2005), spectra were aligned, merged, calibrated, and normalized. To evaluate speciation shifts in As and Fe, spectra were linear combination fitted between -35 and 50 eV using our reference library of As(III) and As(V) adsorbed onto ferrihydrite for As (Van Le et al., 2022a), and for Fe we used ferrihydrite, goethite, pyrite, and siderite (Tufano and Fendorf, 2008). For Mn, we used reference materials MnO_2, $MnSO_4$, and birnessite (synthesis of birnessite is mentioned in SI, section S4). Unfortunately, spectra quality of all samples was not good enough for fitting so that we rely on spectra descriptions and comparisons as means of assessing redox changes.

Scanning electron microscopy (SEM)

The morphology of precipitates coated on the sand particles surface was analyzed by SEM using a Zeiss Crossbeam 550L Scanning Electron Microscope (Zeiss, Germany). Filter materials collected from saturated and unsaturated columns were dried in oven at 30°C, then placed on aluminum SEM sample holders onto carbon adhesive tabs. The samples were sputter-coated with 8 nm platinum with a BALTEC SCD 500 sputter coater. SEM micrographs were collected using the Secondary Electrons Secondary Ions (SESI) detector with an accelerating voltage of 5 kV

3.3. Results and discussion

3.3.1. Long-term monitoring of As, Mn and Fe in the effluent

Field column experiment

Column experiments in the field were performed over 169 pore volumes in 1.5 months under unsaturated conditions (flow rate ranged from 0.3-0.15 ml/s) (Figure 1A). The columns were fed twice per day by natural groundwater containing 16.1 mg/L of Fe(II), 1.4 mg/L of Mn(II), and 240 μg/L of As(III) (Table S2). Low concentrations of Fe, Mn, and As in the outflow indicated high and stable removal efficiencies by the sand filters. The relative effluent values (C/C_0, where C and C_0 are effluent and influent concentration, respectively) for Fe, Mn, and As were 0.002, 0.08, and 0.07 (Figure 1) which corresponded to effluent concentrations of 38, 117, and 17.5 µg/L, respectively (Figure S3). The residual As concentration in the water after filtration was higher than the WHO drinking water standard (10 µg/L). Our observation is consistent with other studies investigating full-scale household filters in the Red River delta (Nitzsche et al., 2015a; Van Le et al., 2022b; Voegelin et al., 2014), suggesting further As treatment steps are required for drinking purposes.

Lab column experiment

To further investigate the effect of saturated versus unsaturated conditions on the filter performance, we conducted a similar column experiment in the lab. The aim of the lab experiment was to investigate the filter performance at slower flow regime than in the field experiment (the flow rate in the field ranged from 0.3-0.15 ml/s) (Figure 1A). Therefore, we set the initial flowrate of the lab experiment to 0.14 ml/s. The abiotic control was performed with sterile quartz sand added the column instead of native sand materials collected from household filters in Vietnam. Both abiotic and biotic setups were fed by sterile, anoxic, artificial groundwater containing 20.9±1.5 mg/L of Fe(II), 1.8±0.6 mg/L of Mn(II) and 307.0±24.4 μg/L of As(III) (Table S2).

The performance of the biotic sand column was divided into two phases (Figure 1B). In the first phase (93 pore volumes, before the first clogging), the sand column remained oxic with a DO in the porewater ranging between 4-6 ppm (Figure S4). Fe, Mn, and As were effectively removed with relative effluent concentrations (C/C_0) of 0.0004, 0.13 and 0.04, respectively (Figure 1B). We noticed that the Fe and As removal efficiency in the lab setup was higher than in the field probably due to the

absence of Si and higher Ca in the AGW relative to natural groundwater. Silicate has a weaker adsorption affinity to Fe(III) (oxyhydr)oxides compared to As(III) and As(V) (Roberts et al., 2004), therefore Si is only a weak competitor of As regarding adsorption on Fe(III) phases during filtration. In contrast, Ca was shown to enhance As retention by forming Ca-As(V) bonds on the sand particle surface (van Genuchten et al., 2014; Voegelin et al., 2010).

During the second phase between the 1st and 2nd clogging (pore volumes 93-141) the column was operated under semi-oxic conditions (DO of porewater <0.5 ppm) (Figure S4). After the 1st clogging, 3 cm of the top sand was scraped off, then the column was continuously run until the second clogging event. Fe removal efficiency was comparable to phase 1 ($C/C_{0\ (Fe)}$: 0.009), while Mn breakthrough occurred throughout this phase as the Mn concentration in the effluent was constantly higher than in the influent with C/C_0 ranging between 1 and 3.5 (Figure 1B). Arsenic removal slightly changed from 8.9 to 12.6 μg/L in the effluent (Figure S3). The drop in DO along the sand column in the second phase compared to the first phase suggests an incomplete oxidation of Fe(II) and As(III) by O_2. Therefore, MnO_2 could be involved in the oxidation of aqueous As(III) and Fe(II) to varying extents (Ep 1, 2), forming mobile Mn(II) but maintaining the high retention of Fe and As in the sand column, consequently increasing Mn(II) concentrations in the effluent. The abiotic control column indicated that 99% of the Fe(II) was removed by abiotic oxidation with O_2, albeit As and Mn removal were limited to 70 and 66%, respectively (Figure 1C). These findings clearly show the important roles of microbial oxidation of Fe(II), As(III) and Mn(II) in order to complement the abiotic processes to maintain high removal rates of Fe, As and Fe in the sand column as shown before by (Van Le et al., 2022b).

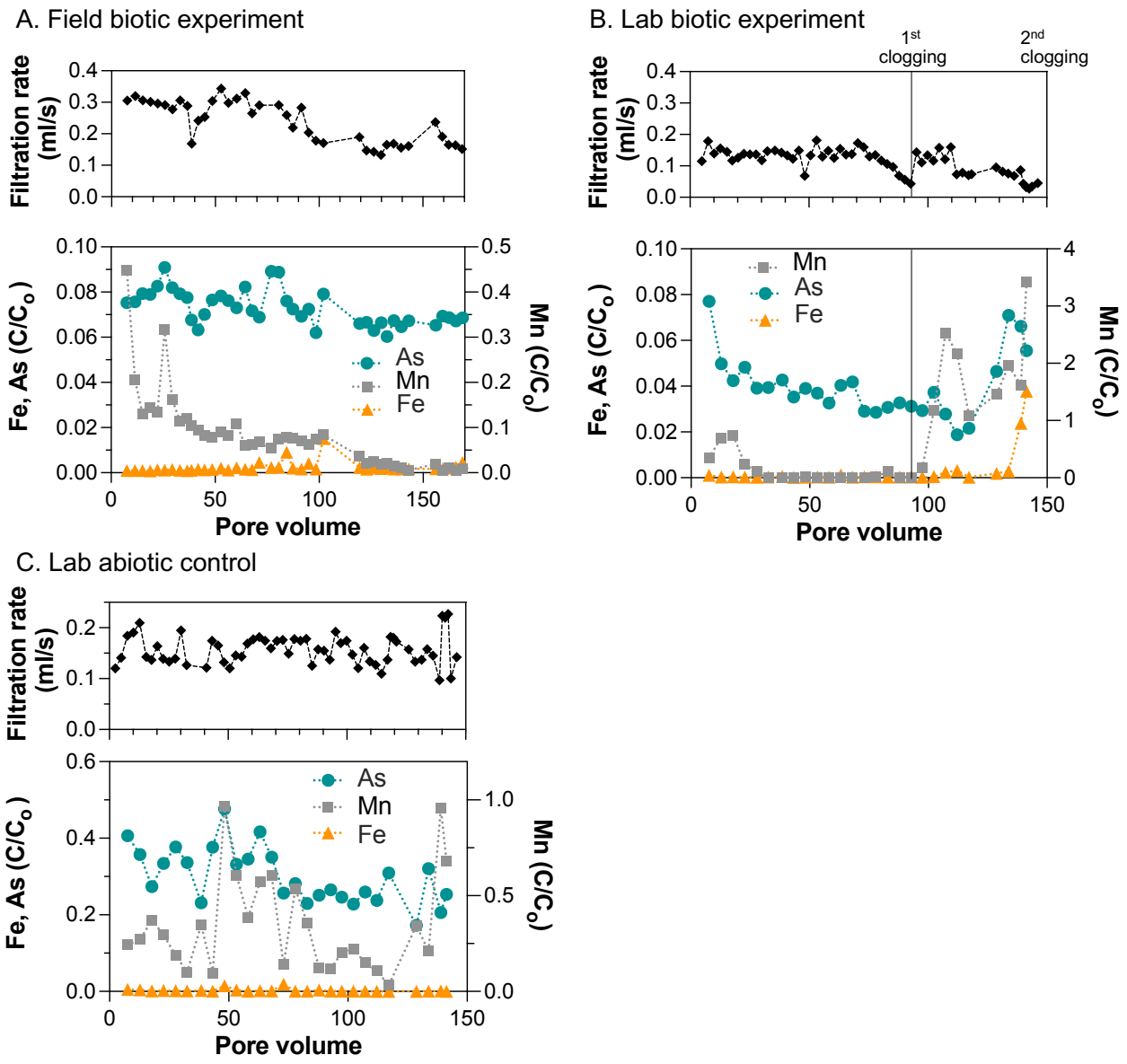

Figure 1. Filtration rate (upper panel) and relative effluent concentration (C/C_0, where C and C_0 are effluent and influent concentration, respectively) of Fe, Mn and As (lower panel) in the field-based biotic setups (A), lab-based biotic setups (B) and the abiotic control (C). The filtration rate as well as the concentrations of Fe, Mn, As in the influent and effluent were recorded at every feeding batches.

3.3.2. Distribution of solid Fe, As and Mn in unsaturated and saturated columns

To understand changes in Fe, As, and Mn distribution in different depth layers in the unsaturated column (field setup) and saturated column (lab setup), total Fe, As, and Mn associated with sand materials at every 2-5 cm depths were analyzed by ICP-MS after microwave digestion.

Fe, As, and Mn accumulated in the top 2-3 cm of the sand columns and their concentrations decreased with filter depth. Since the groundwater in the Red River delta is enriched with Fe(II), Fe showed the highest abundance in the sand column. Up to 18.5-22.0 g/kg and 26.5-28.8 g/kg were found in unsaturated and saturated columns, respectively (Figure 2A). Manganese in the solid phase of the saturated sand column was between 744-991 mg/kg, twice as much as in the unsaturated column (Figure 2B). Arsenic enriched in the saturated column with a concentration between 159 and 178 mg/kg, which was three times as high as As in the unsaturated column (Figure 2C). Since the removal efficiency of the abiotic columns was lower than in the biotic ones, the Fe, As, and Mn retained in the sand was up to 10 times less than in the biotic setups.

At the macro scale, we found that both As and Mn linearly correlated with Fe with correlation factors R^2 of 0.99 and 0.92, respectively (Figure S5, S6), suggesting that As adsorbed on Fe(III) (oxyhydr)oxides on the sand particles as reported before (Nitzsche et al., 2015; Voegelin et al., 2014). The element's distribution in unsaturated and saturated columns followed the same pattern. Thus, we hypothesize that the changes of Fe, As, and Mn concentrations might occur due to changes in speciation and binding environment. It has to be noted that new sand material was used for the field experiment (unsaturated conditions). In contrast, sand material collected from existing household filters was used for the lab experiment (saturated conditions) to utilize the microbial activities in the sand. Therefore, filter materials in the saturated column already contained higher amounts of Fe, As, and Mn than the unsaturated column, which could lead to catalytic effects (Hug and Leupin, 2003; Leupin and Hug, 2005)).

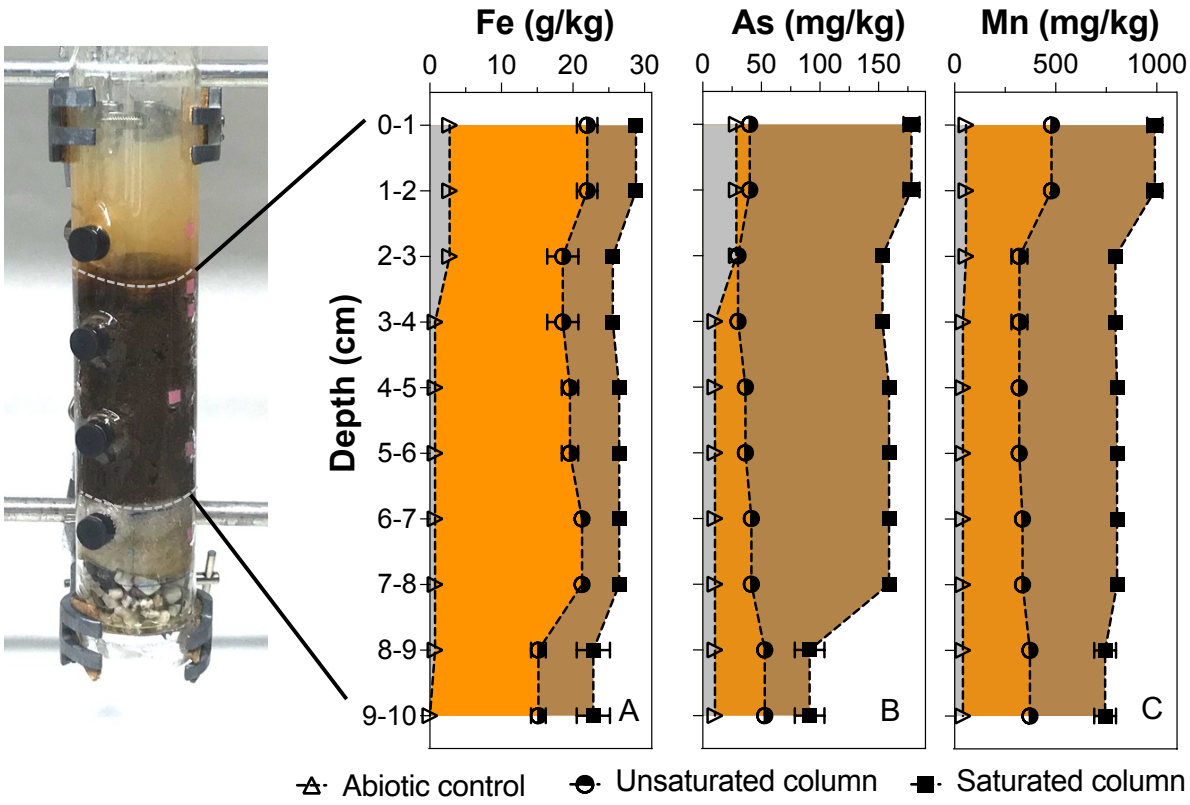

Figure 2. Vertical distribution of Fe (A), As (B), and Mn (C) in abiotic control (black), unsaturated (orange) and saturated (brown) columns. All samples were analyzed in triplicate, and error bars indicate the standard deviation.

3.3.3. Morphology of precipitates and elemental distribution on sand particle surface

We combined scanning electron microscopy (SEM) and micro-X-ray fluorescence (μXRF) mapping to assess the sand particle size (Figures 3A and S7), the morphology of minerals (Figure 3 B, C, D), and the elemental distribution on the sand particle surfaces (Figures 4, S8, and S9). Our results indicated a heterogenous elemental distribution and micro- to nano-sized mineral structures coating sand particle surfaces. We found three mineral structures: micro-platelets associated with nano-globular-aggregates (Figure 3C, D) and nano-flower shaped structures (Figure 3E, F). The nano-globules had a similar structure to Fe nano-aggregates found on the surface of sand particles in other Fe-Mn-based sand filtration systems (Gülay et al., 2014; Han et al., 2022). We suggest that the flower-like nano morphology is similar to the birnessite structure reported in previous studies (Han et al., 2022; Ying et al., 2020). Pixel fluorescence counts of Fe, As, and Mn collected from μXRF maps indicated a

strong correlation of Fe and Mn with correlation co-efficiency (R^2) in some spots >0.9 (Figure 4E), while the correlation factor of As and Fe was lower (Figure 4F). This is probably caused by the fluorescence yield difference between Fe and As (Root et al., 2013), since As concentrations were two orders of magnitude lower than for Fe in the solid phase. We also observed that Mn was associated with Fe(III) (oxyhydr)oxides in the unsaturated sample (R^2 = 0.73) (Figure S8), while in the saturated sample, Fe-Mn-rich spots were detected in fewer locations indicated by a lower correlation factor (R^2 = 0.6) (Figure 4B). Arsenic possessed a lower fluorescence count than Mn and Fe and enriched as rims at the mineral's surface-water (solid-water) interface (Figure 4C), that is also in line with previous studies (Root et al., 2013; Voegelin et al., 2014; Wielinski et al., 2022).

Additionally, other elements such as P, Ca, and Si also showed a strong partitioning into the Fe(III) (oxyhydr)oxide phase (Figure S10), probably influencing As removal in the sand filter. Iron was well co-located with P in all samples as phosphate is preferentially adsorbed to Fe(III) (oxyhydr)oxide compared to As(V), As(III) and silicate (Hug et al., 2008; Roberts et al., 2004). Thus, low Fe/P ratios (0.05-1) of the groundwater were an asset for high As retention. Tricolor maps of Si, Ca, and Fe indicated a lower amount of Si and Ca associated with Fe (Figure S10). Most detected Si fluorescence counts stemmed from the sample holder (made from quartz). Ca-rich sand crusts were found separately from the Fe signal, probably precipitated as calcite in the filters.

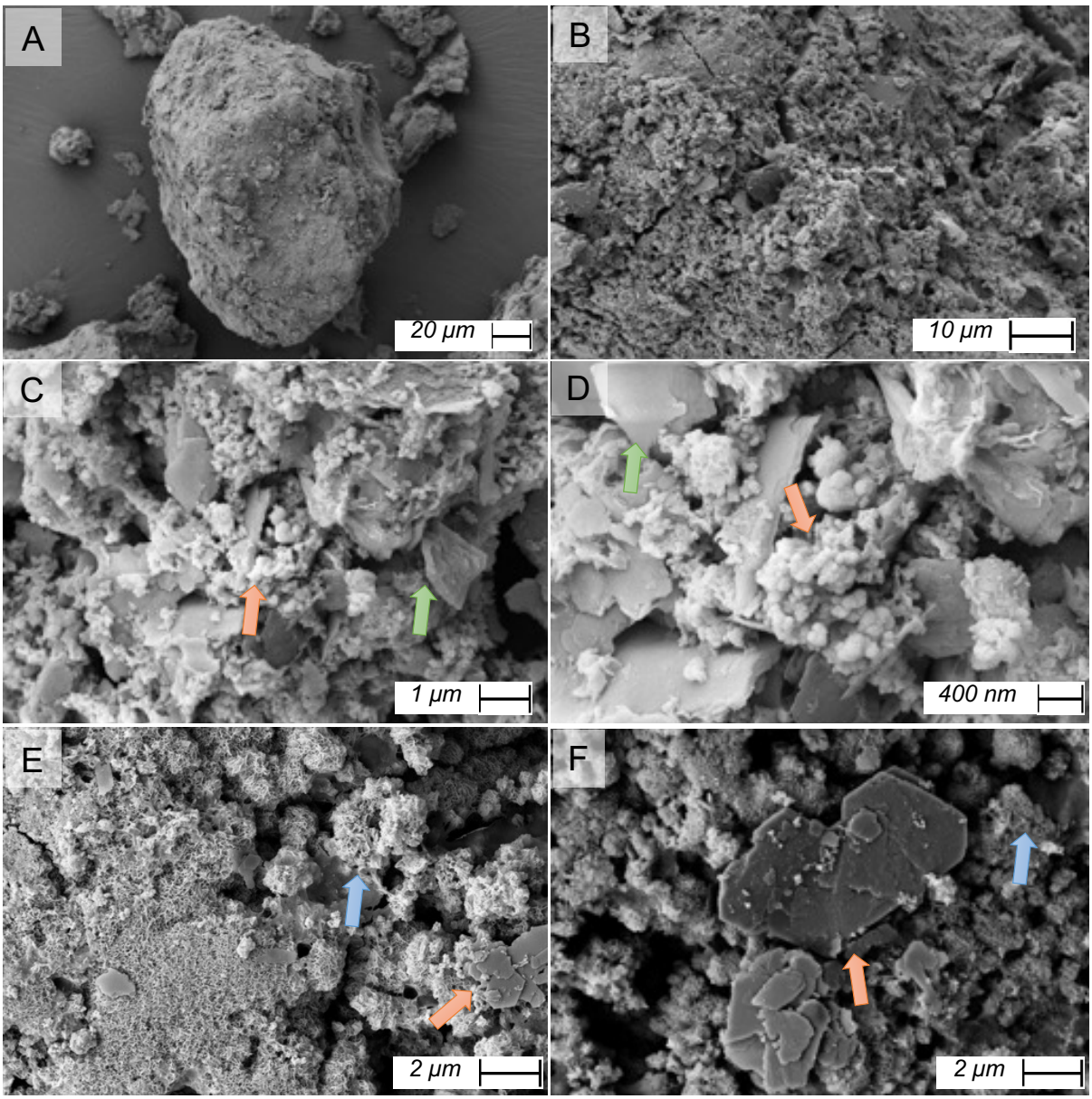

Figure 3. Scanning electron micrographs showing the distribution of precipitates on the sand particle surface (A, B). The most dominant mineral structures were micro-platelets (green arrows) associated with nano-globular-aggregates (orange arrows) (C, D) and nano-flower shapes (blue arrows) (E, F).

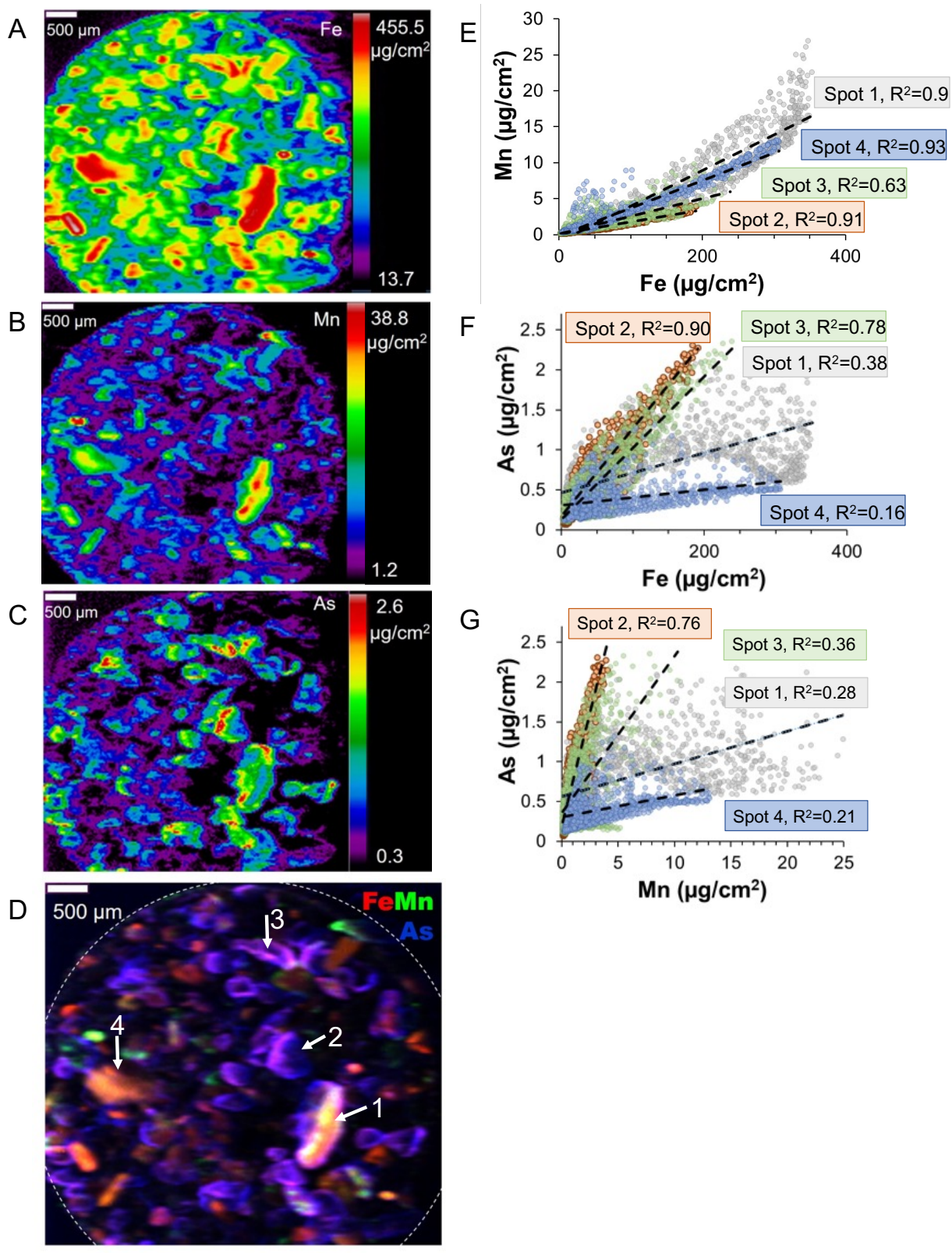

Figure 4: Multiple energy μ-XRF maps of sand filter materials from saturated columns operated in the lab. μ-XRF maps of Fe (A), Mn (B), As (C) distributed on sand surfaces and their tricolor map (D). Correlations of Mn vs Fe (E), As vs Fe (F), As vs Mn (G) and their correlation co-efficiency (R^2) were displayed for 4 selected spots from tricolor map.

3.3.4. Fe, As and Mn speciation in saturated and unsaturated sand columns

Filter materials were collected from different depth layers (2-5 cm) in unsaturated and saturated columns. Redox states of Mn, Fe and As on selected spots from μXRF maps were analyzed by X-ray absorption near edge structure (μXANES) spectroscopy using linear combination fitting (LCF) (Figure 5 A,B,C). μXANES spectra of different spots on the same sample were almost identical indicating the speciation distribution was homogenous and representative for that sample. The proportions of Fe(II) and As(III) in each sample were converted to concentrations for a better quantitative comparison between unsaturated and saturated columns (Figure 5D,E). We found that oxidized species such as Mn(III)/(IV), Fe(III), and As(V) dominated in unsaturated columns while reduced Mn(II), Fe(II), and As(III) were identified at a higher relative contribution in saturated column.

Under the unsaturated flow conditions, adsorption maximum positions of Mn, Fe and As were near 6563, 7134, and 11875 eV, respectively (Figure 5 A,B,C), indicating the presence of Mn(III)/(IV), Fe(III), As(V) and in the sand columns (Manning et al., 1998; Tournassat, 2002). LCF fitting results of Fe showed a mixture of ferrihydrite and goethite contributed between 61 and 80% along the unsaturated column except in the sample collected at 6-8 cm depth that contained only 36% of Fe(III) (Figure 5B, Table S4). Additionally, up to 87-93% of As(V) were detected along the unsaturated columns (Figure 5C, Table S3). The speciation contribution of Mn, Fe and As in unsaturated columns is comparable to the solid phase analysis results obtained from a series of household filters in Vietnam (Van Le et al., 2022b; Voegelin et al., 2014).

Under the saturated conditions, Mn K-edge XANES spectra of samples taken from top (0-2 cm) and bottom (5-10 cm) layers showed an adsorption maximum at 6563 eV representing Mn(IV) and indicating a more diffused distribution than in the unsaturated sample (black arrow, Figure 5D). A shift of the edge position toward lower energy and a concomitant appearance of a shoulder at 6554 eV indicated the presence of Mn(II). Similarly, we also observed an energy shift toward the positions of Fe(II) (7125 eV) from the Fe k-edge XANES spectra of 5-10 cm sand samples (arrow, Figure 5A). LCF fitting results confirmed that Fe(II) was contributing up to 44% to the total Fe pool equaling 11.6 g/kg (Figure 5D). This finding revealed an expansion of the Fe(III) reduction zone from 6-8 cm (in the unsaturated column) to 5-10 cm under saturated conditions. As(III) increased to 15% in the saturated sand column equaling 26-22 mg As(III)/kg which is 10 times more than the amount of As(III) in the unsaturated column.

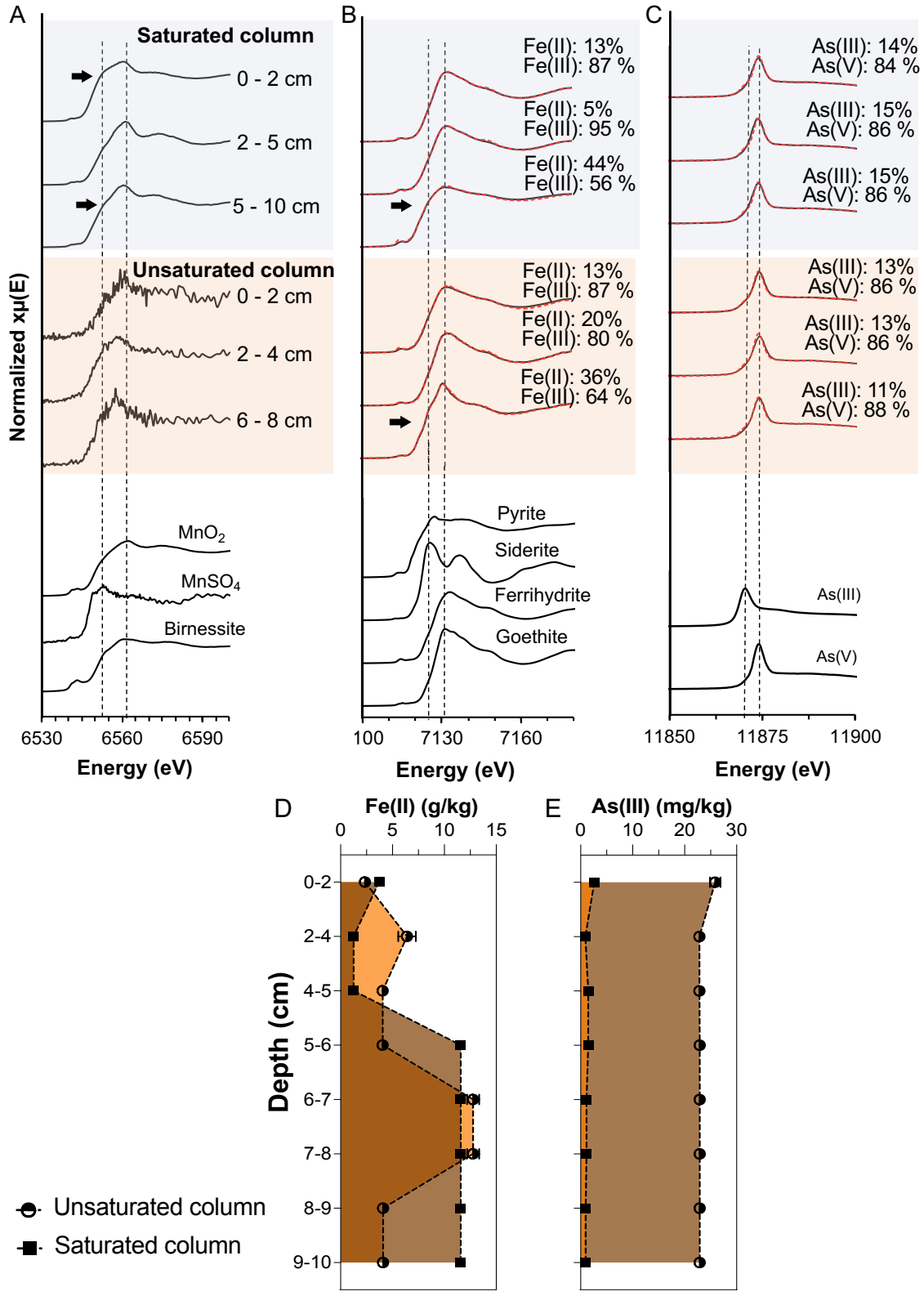

Figure 5. Normalized K-edge μXANES spectra of Mn (A), Fe (B) and As (C) in filter materials at different depths in the saturated and unsaturated columns. Experimental and linear combination fit curves are plotted as black and red lines, respectively. The concentrations of solid-phase Fe(II) (D) and As(III) (E) in saturated and unsaturated columns were calculated by combining μXANES data and extraction data.

3.3.5. MnO_2 controlling the Fe and As retention under semi-oxic and anoxic zones in the saturated sand columns

Under unsaturated conditions, Fe, As, and Mn were primarily present as As(V) adsorbed on Fe(III) (oxyhydr)oxide and Mn(III)/(IV) oxide minerals. Under saturated flow conditions, we found evidence that microbial Fe(III) and As(V) reduction led to elevated Fe(II) and As(III) in the solid phase that might be oxidized by and/or associated with Mn(IV) oxides to different extents. The mechanisms of As(III) and Fe(II) oxidation in the presence of Mn(III)(IV) oxides and Fe(III) (oxyhydr)oxide are complex, involving many simultaneously occurring reactions. Based on our observations, the following mechanistic reaction network is proposed to explain Fe-, As- and Mn-redox speciation in the top and bottom layers of sand columns.

Under saturated conditions, Mn(II) and As(III) accumulated at the top layer (0-2 cm), indicating limited oxidation of these species. It suggests that Mn(II) and As(III) adsorbed to the surfaces of Fe(III) (oxyhydr)oxide and previously formed Mn oxide minerals. Since the artificial groundwater contained high concentrations of bicarbonate, solid-associated Mn(II) also could be present as $MnCO_3$ (rhodochrosite) as previously reported (Schaefer et al., 2020).

The oxidation of As(III) by Mn(IV) oxides in the top layer of the sand column was limited due to i) the high amount of Fe(II) of 21 mg/L as well as high Fe/As ratio of 68 in the groundwater so that Fe(II) outcompeted As(III) for adsorption and oxidation on Mn(IV) oxides surface (Gude et al., 2017; Wu et al., 2018) and ii) the formation of Fe(III) (oxyhydr)oxide minerals with adsorbed Mn(II) might cause a surface passivation of Mn oxides thus slowing down As(III) and Fe(II) oxidation (Ehlert et al., 2014; Lan et al., 2018; Wu et al., 2018). Even though Mn(IV) oxides might not directly oxidize As(III) (Ehlert et al., 2016, 2014; Han et al., 2011; Wu et al., 2018, 2015), these studies confirmed that the presence of Mn oxides maintain high As(V)/As(III) ratios in the solid phase, thus enhancing As immobilization. Additionally, the intermittent feeding of oxygenated water into the sand columns allowed O_2 re-penetration into the pore spaces to enhance oxidation processes in the top layers of the sand filters. (Bretzler et al., 2020b; Wielinski et al., 2022).

In contrast, under saturated flow, almost no dissolved oxygen was detected at the bottom layer (5-10 cm) (Figure S3, leading to an increase of Fe(III) reduction (up to

44% of Fe(II) detected in the sand column). The main reason is the microbial reduction of As-bearing Fe(III) (oxyhydr)oxides, as demonstrated in our previous study (Van Le et al., 2022a). The mobilized Fe(II) and desorbed As(V)/(III) likely re-adsorbed to the remaining Fe(III) (oxyhydr)oxide and Mn(III)/(IV) oxide minerals. While at the sand filter surface constantly new Fe(III) (oxyhydr)oxides formed, there was a reduction of available binding sites for Fe(II) and As(III)/(V) on the Fe(III) minerals at the bottom layer. These differences highlight the role of Mn(III)/(IV) oxides on the one hand as secondary hosting phase and on the other hand as oxidant for Fe(II) and As(III). Based on the stronger correlation of Mn with Fe compared to As at the sand surfaces, we conclude that Fe(II) adsorbed on Mn oxides was instantaneously oxidized to Fe(III) sequestering As(V) and As(III) into the solid phase. This finding is in line with previous studies on the role of Mn(IV) oxides controlling As mobilization in floodplain soils (Dong et al., 2021; Ehlert et al., 2016) and paddy soils (Xu et al., 2017). In addition to the abiotic reduction of Mn(IV) oxides by Fe(II), microbial reduction pathways (Cerrato et al., 2010) were probably involved in the elevated Mn(II) concentrations in the effluent in our columns. Nevertheless, bulk XAS for Fe, Mn, and As should be done in the future to obtain better insights into Fe, Mn and As binding environment under unsaturated and saturated conditions.

3.4. Conclusions

The operation of household sand filters for removal of Fe, Mn and As from water is divided into two phases, it starts with unsaturated flow when the sand column maintains oxic conditions and is followed by saturated flow when an oxygen gradient is formed along the sand column creating a semi-oxic (top) and anoxic zone (bottom). By conducting lab and field-based column experiments, this study showed an increased reduction of Fe and As concentrations in the water under saturated flow conditions. Mn(IV) oxides that formed during the oxic flow were acting as a secondary hosting phase and oxidant for Fe(II) and As(III)/(V). Consequently, As(III) and Fe(II) were effectively removed from sand columns with removal rates of 95 and 99% respectively, while Mn(II) was leached from the sand column, and up to 5.5 mg/L was detected in the effluent. Based on our findings, we therefore provide a few suggestions to improve the performance of household/ small-scale sand filters applied to remove Mn(II), As(III) and Fe(II) from groundwater as follows. First, we recommend intermittent

feeding with water rather than continuous flow. The intermittent feeding allows the sand filters to completely drain between filtration periods, pulling new air into the pore spaces and reducing the hydraulic conductivity, thus prolong the time until filter clogging (Wielinski et al., 2022). Second, we advise backwashing rather than scrapping off the top sand layer. The scrapping removes a substantial amount of microorganisms accumulated at the top layer, which contribute to Fe, As and Mn oxidation (Bai et al., 2016a; Hu et al., 2020; Van Le et al., 2022b) while backwashing can preserve better the sand filter microbial community (de Souza et al., 2021). Third, the risk of Mn contamination in the effluent should we reduced. In the household filters without backwashing, the top layer of the sand filter will be removed once sand filter is clogged leading to prolonged saturated conditions in the sand filters, consequently, Mn remobilization from the filter. Even though Mn(II) is not as toxic as As(III) or As(V), long-term chronic exposure to elevated Mn levels can lead to several adverse health effects (Ljung and Vahter, 2007; Oulhote et al., 2015; Rahman et al., 2017).

3.5. Acknowledgement

This work was funded by the German Research Foundation (DFG, KA1736/41-1). The authors acknowledge infrastructural support by the Deutsche Forschungsgemeinschaft (DFG) under Germany's Excellence Strategy, cluster of Excellence EXC2124, project ID 390838134. We appreciate Tübingen Structural Microscopy Core Facility (Funded by the Federal Ministry of Education and Research (BMBF) and the Baden-Württemberg Ministry of Science as part of the Excellence Strategy of the German Federal and State Governments) for their support and thank the DFG (INST 37/1027-1 FUGG) for the financial support. We thank Sam Webb at SSRL for beamline support (proposal number 5587). Use of the Stanford Synchrotron Radiation Lightsource, SLAC National Accelerator Laboratory, is supported by the U.S. Department of Energy, Office of Science, Office of Basic Energy Sciences under Contract No. DE-AC02-76SF00515. The SSRL Structural Molecular Biology Program is supported by the DOE Office of Biological and Environmental Research, and by the National Institutes of Health, National Institute of General Medical Sciences (including P41GM103393). The contents of this publication are solely the responsibility of the authors and do not necessarily represent the official views of NIGMS or NIH. We appreciate the help of our Vietnamese collaborators (P.H. Viet, P. T. K. Trang, V.T. Duyen, The Anh and P. Tutiyasarn) during the sampling campaigns.

3.6. References

Bai, Y., Chang, Y., Liang, J., Chen, C., Qu, J., 2016. Treatment of groundwater containing Mn(II), Fe(II), As(III) and Sb(III) by bioaugmented quartz-sand filters. Water Res. 106, 126–134. https://doi.org/10.1016/j.watres.2016.09.040

Berg, M., Luzi, S., Trang, P.T.K., Viet, P.H., Giger, W., Stüben, D., 2006. Arsenic removal from groundwater by household sand filters: Comparative field study, model calculations, and health benefits. Environ. Sci. Technol. 40, 5567–5573. https://doi.org/10.1021/es060144z

Berg, M., Tran, H.C., Nguyen, T.C., Pham, H.V., Schertenleib, R., Giger, W., 2001. Arsenic contamination of groundwater and drinking water in Vietnam: A human health threat. Environ. Sci. Technol. 35, 2621–2626. https://doi.org/10.1021/es010027y

Borch, T., Kretzschmar, R., Kappler, A., Cappellen, P. Van, Ginder-Vogel, M., Voegelin, A., Campbell, K., 2010. Biogeochemical redox processes and their impact on contaminant dynamics. Environ. Sci. Technol. 44, 15–23. https://doi.org/10.1021/es9026248

Bretzler, A., Nikiema, J., Lalanne, F., Hoffmann, L., Biswakarma, J., Siebenaller, L., Demange, D., Schirmer, M., Hug, S.J., 2020. Arsenic removal with zero-valent iron filters in Burkina Faso: Field and laboratory insights. Sci. Total Environ. 737, 139466. https://doi.org/10.1016/j.scitotenv.2020.139466

Cerrato, J.M., Falkinham, J.O., Dietrich, A.M., Knocke, W.R., McKinney, C.W., Pruden, A., 2010. Manganese-oxidizing and -reducing microorganisms isolated from biofilms in chlorinated drinking water systems. Water Res. 44, 3935–3945. https://doi.org/10.1016/j.watres.2010.04.037

Davies, S.H.R., Morgan, J.J., 1989. Manganese(II) oxidation kinetics on metal oxide surfaces. J. Colloid Interface Sci. 129, 63–77. https://doi.org/10.1016/0021-9797(89)90416-5

de Souza, F.H., Roecker, P.B., Silveira, D.D., Sens, M.L., Campos, L.C., 2021. Influence of slow sand filter cleaning process type on filter media biomass: backwashing versus scraping. Water Res. 189. https://doi.org/10.1016/j.watres.2020.116581

Dong, G., Han, R., Pan, Y., Zhang, C., Liu, Y., Wang, H., Ji, X., Dahlgren, R.A., Shang, X., Chen, Z., Zhang, M., 2021. Role of MnO2 in controlling iron and arsenic mobilization from illuminated flooded arsenic-enriched soils. J. Hazard. Mater. 401, 123362. https://doi.org/10.1016/j.jhazmat.2020.123362

Ehlert, K., Mikutta, C., Kretzschmar, R., 2016. Effects of manganese oxide on arsenic reduction and leaching from contaminated floodplain soil. Environ. Sci. Technol. 50, 9251–9261. https://doi.org/10.1021/acs.est.6b01767

Ehlert, K., Mikutta, C., Kretzschmar, R., 2014. Impact of birnessite on arsenic and iron speciation during microbial reduction of arsenic-bearing ferrihydrite. Environ. Sci. Technol. 48, 11320–11329. https://doi.org/10.1021/es5031323

Freitas, B.L.S., Terin, U.C., Fava, N.M.N., Maciel, P.M.F., Garcia, L.A.T., Medeiros, R.C., Oliveira, M., Fernandez-Ibañez, P., Byrne, J.A., Sabogal-Paz, L.P., 2022. A critical overview of household slow sand filters for water treatment. Water Res. 208. https://doi.org/10.1016/j.watres.2021.117870

Gude, J.C.J., Rietveld, L.C., van Halem, D., 2017. As(III) oxidation by MnO2 during groundwater treatment. Water Res. 111, 41–51. https://doi.org/10.1016/j.watres.2016.12.041

Gülay, A., Tatari, K., Musovic, S., Mateiu, R. V., Albrechtsen, H.J., Smets, B.F., 2014. Internal porosity of mineral coating supports microbial activity in rapid sand filters for groundwater treatment. Appl. Environ. Microbiol. 80, 7010–7020. https://doi.org/10.1128/AEM.01959-14

Han, X., Li, Y.-L., Gu, J.-D., 2011. Oxidation of As(III) by MnO2 in the absence and presence of Fe(II) under acidic conditions. Geochim. Cosmochim. Acta 75, 368–379. https://doi.org/https://doi.org/10.1016/j.gca.2010.10.010

Han, Y.S., Kim, S.H., Jang, J.Y., Ji, S., 2022. Arsenic removal characteristics of natural Mn-Fe binary coating on waste filter sand from a water treatment facility. Environ. Sci. Pollut. Res. 29, 2136–2145. https://doi.org/10.1007/s11356-021-15580-0

Hansel, C.M., 2017. Manganese in Marine Microbiology, 1st ed, Advances in Microbial Physiology. Elsevier Ltd. https://doi.org/10.1016/bs.ampbs.2017.01.005

Hu, W., Liang, J., Ju, F., Wang, Q., Liu, R., Bai, Y., Liu, H., Qu, J., 2020. Metagenomics unravels differential microbiome composition and metabolic potential in rapid sand

filters purifying surface water versus groundwater. Environ. Sci. Technol. 54, 5197–5206. https://doi.org/10.1021/acs.est.9b07143

Hug, S.J., Leupin, O., 2003. Iron-catalyzed oxidation of Arsenic(III) by oxygen and by hydrogen peroxide: pH-dependent formation of oxidants in the Fenton reaction. Environ. Sci. Technol. 37, 2734–2742. https://doi.org/10.1021/es026208x

Hug, S.J., Leupin, O.X., Berg, M., 2008. Bangladesh and Vietnam: Different groundwater compositions require different approaches to arsenic mitigation. Environ. Sci. Technol. 42, 6318–6323. https://doi.org/10.1021/es7028284

Lan, S., Ying, H., Wang, X., Liu, F., Tan, W., Huang, Q., Zhang, J., Feng, X., 2018. Efficient catalytic As (III) oxidation on the surface of ferrihydrite in the presence of aqueous Mn (II). Water Res. 128, 92–101.

Leupin, O.X., Hug, S.J., 2005. Oxidation and removal of arsenic (III) from aerated groundwater by filtration through sand and zero-valent iron. Water Res. 39, 1729–1740. https://doi.org/10.1016/j.watres.2005.02.012

Liu, H., Xu, R., Zhang, J., Sun, X., Gao, Peng, Li, J., Yan, W., Gao, W., Gao, Pin, Liu, G., Zhang, H., Sun, W., 2022. Immobile iron-rich particles promote arsenic retention and regulate arsenic biotransformation in treatment wetlands. https://doi.org/10.1021/acs.est.2c04421

Ljung, K., Vahter, M., 2007. Time to re-evaluate the guideline value for manganese in drinking water? Environ. Health Perspect. 115, 1533–1538.

Luzi, S., Berg, M., Trang, P.T.K., Viet, P.H., Schertenleib, R., 2004. Household sand filters for arsenic removal: An option to mitigate arsenic from iron-rich groundwater.

Manning, B.A., Fendorf, S.E., Goldberg, S., 1998. Surface structures and stability of arsenic(III) on goethite: Spectroscopic evidence for inner-sphere complexes. Environ. Sci. Technol. 32, 2383–2388. https://doi.org/10.1021/es9802201

Morgan, J.J., 2005. Kinetics of reaction between O2 and Mn(II) species in aqueous solutions. Geochim. Cosmochim. Acta 69, 35–48.

Nitzsche, K.S., Lan, V.M., Trang, P.T.K., Viet, P.H., Berg, M., Voegelin, A., Planer-Friedrich, B., Zahoransky, J., Müller, S.K., Byrne, J.M., Schröder, C., Behrens, S., Kappler, A., 2015. Arsenic removal from drinking water by a household sand filter in Vietnam - Effect of filter usage practices on arsenic removal efficiency and

microbiological water quality. Sci. Total Environ. 502, 526–536. https://doi.org/10.1016/j.scitotenv.2014.09.055

Oulhote, Y., Mergler, D., Barbeau, B., Bellinger, D.C., Bouffard, T., Brodeur, M.È., Saint-Amour, D., Legrand, M., Sauvé, S., Bouchard, M.F., 2015. Neurobehavioral function in school-age children exposed to manganese in drinking water. Environ. Health Perspect. 122, 1343–1350. https://doi.org/10.1289/ehp.1307918

Petitjean, A., Forquet, N., Boutin, C., 2016. Oxygen profile and clogging in vertical flow sand filters for on-site wastewater treatment. J. Environ. Manage. 170, 15–20. https://doi.org/https://doi.org/10.1016/j.jenvman.2015.12.033

Rahman, S.M., Kippler, M., Tofail, F., Bölte, S., Derakhshani Hamadani, J., Vahter, M., 2017. Manganese in drinking water and cognitive abilities and behavior at 10 years of age: a prospective cohort study. Environ. Health Perspect. 125, 57003.

Ravel, B., Newville, M., 2005. ATHENA, ARTEMIS, HEPHAESTUS: data analysis for X-ray absorption spectroscopy using IFEFFIT. J. Synchrotron Radiat. 12, 537–541.

Roberts, L.C., Hug, S.J., Ruettimann, T., Billah, M.M., Khan, A.W., Rahman, M.T., 2004. Arsenic removal with iron(II) and iron(III) in waters with high silicate and phosphate concentrations. Environ. Sci. Technol. 38, 307–315.

Root, R.A., Fathordoobadi, S., Alday, F., Ela, W., Chorover, J., 2013. Microscale speciation of arsenic and iron in ferric-based sorbents subjected to simulated landfill conditions. Environ. Sci. Technol. 47, 12992–13000. https://doi.org/10.1021/es402083h

Ross, D.S., Bartlett, R.J., 1981. Evidence for nonmicrobial oxidation of manganese in soil. Soil Sci. 132, 153–160.

Schaefer, M. V., Plaganas, M., Abernathy, M.J., Aiken, M.L., Garniwan, A., Lee, I., Ying, S.C., 2020. Manganese, arsenic, and carbonate interactions in model oxic groundwater systems. Environ. Sci. Technol. https://doi.org/10.1021/acs.est.0c02084

Tebo, B.M., Johnson, H.A., McCarthy, J.K., Templeton, A.S., 2005. Geomicrobiology of manganese(II) oxidation. Trends Microbiol. 13, 421–428. https://doi.org/10.1016/j.tim.2005.07.009

Tournassat, C., 2002. Arsenic(III) oxidation by birnessite and precipitation of manganese(II) arsenate 493–500.

Tufano, K.J., Fendorf, S., 2008. Confounding impacts of iron reduction on arsenic retention. Environ. Sci. Technol. 42, 4777–4783. https://doi.org/10.1021/es702625e

van Genuchten, C.M., Gadgil, A.J., Peña, J., 2014. Fe (III) nucleation in the presence of bivalent cations and oxyanions leads to subnanoscale 7 Å polymers. Environ. Sci. Technol. 48, 11828–11836.

Van Le, A., Marie Muehe, E., Drabesch, S., Lezama Pacheco, J., Bayer, T., Joshi, P., Kappler, A., Mansor, M., 2022a. Environmental risk of arsenic mobilization from disposed sand filter materials. Environ. Sci. & Technol. 0. https://doi.org/10.1021/acs.est.2c04915

Van Le, A., Straub, D., Planer-Friedrich, B., Hug, S.J., Kleindienst, S., Kappler, A., 2022b. Microbial communities contribute to the elimination of As, Fe, Mn, and NH4+ from groundwater in household sand filters. Sci. Total Environ. 838, 156496. https://doi.org/10.1016/j.scitotenv.2022.156496

Voegelin, A., Kaegi, R., Berg, M., Nitzsche, K.S., Kappler, A., Lan, V.M., Trang, P.T.K., Göttlicher, J., Steininger, R., 2014. Solid-phase characterisation of an effective household sand filter for As, Fe and Mn removal from groundwater in Vietnam. Environ. Chem. 11, 566–578.

Voegelin, A., Kaegi, R., Frommer, J., Vantelon, D., Hug, S.J., 2010. Effect of phosphate, silicate, and Ca on Fe (III)-precipitates formed in aerated Fe (II)-and As (III)-containing water studied by X-ray absorption spectroscopy. Geochim. Cosmochim. Acta 74, 164–186.

Webb, S.M., 2011. The MicroAnalysis Toolkit: X-ray fluorescence image processing software. AIP Conf. Proc. 1365, 196–199. https://doi.org/10.1063/1.3625338

WHO, 2011. Evaluating household water treatment options: Health-based targets and microbiological performance specifications. World Health Organization.

Wielinski, J., Jimenez-Martinez, J., Göttlicher, J., Steininger, R., Mangold, S., Hug, S.J., Berg, M., Voegelin, A., 2022. Spatiotemporal mineral phase evolution and

arsenic retention in microfluidic models of zerovalent iron-based water treatment. Environ. Sci. Technol. https://doi.org/10.1021/acs.est.2c02189

Wu, Y., Kukkadapu, R.K., Livi, K.J.T., Xu, W., Li, W., Sparks, D.L., 2018. Iron and arsenic speciation during As(III) oxidation by manganese oxides in the presence of Fe(II): Molecular-level characterization using XAFS, Mössbauer, and TEM analysis. ACS Earth Sp. Chem. 2, 256–2684. https://doi.org/10.1021/acsearthspacechem.7b00119

Wu, Y., Li, W., Sparks, D.L., 2015. The effects of iron (II) on the kinetics of arsenic oxidation and sorption on manganese oxides. J. Colloid Interface Sci. 457, 319–328.

Xu, X., Chen, C., Wang, P., Kretzschmar, R., Zhao, F.J., 2017. Control of arsenic mobilization in paddy soils by manganese and iron oxides. Environ. Pollut. 231, 37–47. https://doi.org/10.1016/j.envpol.2017.07.084

Ying, C., Lanson, B., Wang, C., Wang, X., Yin, H., Yan, Y., Tan, W., Liu, F., Feng, X., 2020. Highly enhanced oxidation of arsenite at the surface of birnessite in the presence of pyrophosphate and the underlying reaction mechanisms. Water Res. 187. https://doi.org/10.1016/j.watres.2020.116420

SUPPLEMENTARY INFORMATION

S1. Field site and sample collection

We collected sand filter materials in several households in the villages Tu Nhien (20°51′30.05” N, 105°55′33.34″ E) and Van Phuc (20°55′08.63” N, 105°53′47.61″ E), located 25-35 km Southeast of Hanoi, Vietnam, inside the meander of the Red River. Sand filter materials were collected using sterile spatula at different depth (every 1-5 cm), then immediately cooled on ice during transport and stored at 4°C. In the laboratory, filter materials collected at different layers were mixed into one homogenous sample with a ratio of 1:1 before being used for the column experiment.

S2. Preparation of artificial groundwater

Artificial groundwater (ARW) was prepared based on (Nitzsche et al., 2015a) (Table S1). Five liters of ARW (without Fe and As) were prepared anoxically every week. Afterwards, the anoxic ARW was sterilized by autoclaving at 121°C for 40 minutes. Fe(II) and As(III) stock solutions (x1000) were prepared separately and spiked to the ARW bottle right before each filtration round.

Table S1. Composition of artificial groundwater (ARW) medium, designed based on (Nitzsche et al., 2015a).

Chemical	Concentration/ Value
$CaCl_2.2H_2O$ (mg/L)	130
$MgSO_4.7H_2O$ (mg/L)	46
KH_2PO_4 (mg/L)	0.97
$MnCl_2.4H_2O$ (mg/L)	0.8
NH_4Cl (mg/L)	20
$FeCl_2.4H_2O$ (mg/L)	71
$NaAsO_2$ (mg/L)	0.5
pH	7.3

Table S2. Artificial and native groundwater composition fed to the lab and field column experiments. Fe, As and Mn were spiked into the artificial groundwater bottle fresh at each filtration round.

	Artificial groundwater	Native groundwater
Fe(II) (mg/L)	20.9±1.5	16.1±0.1
As(III) (μg/L)	307±24.4	240±0.6
Mn(II) (mg/L)	1.8±0.6	1.4±0.04
NH_4^+ (mg-N/L)	20.1±0.03	16±0.1
NO_3^- (mg-N/L)	0.07±0	0.4±0.3
Mg (mg/L)	46	-
Cl (mg/L)	432	-
P (mg/L)	0.97	2.5
pH	7.3	7.2

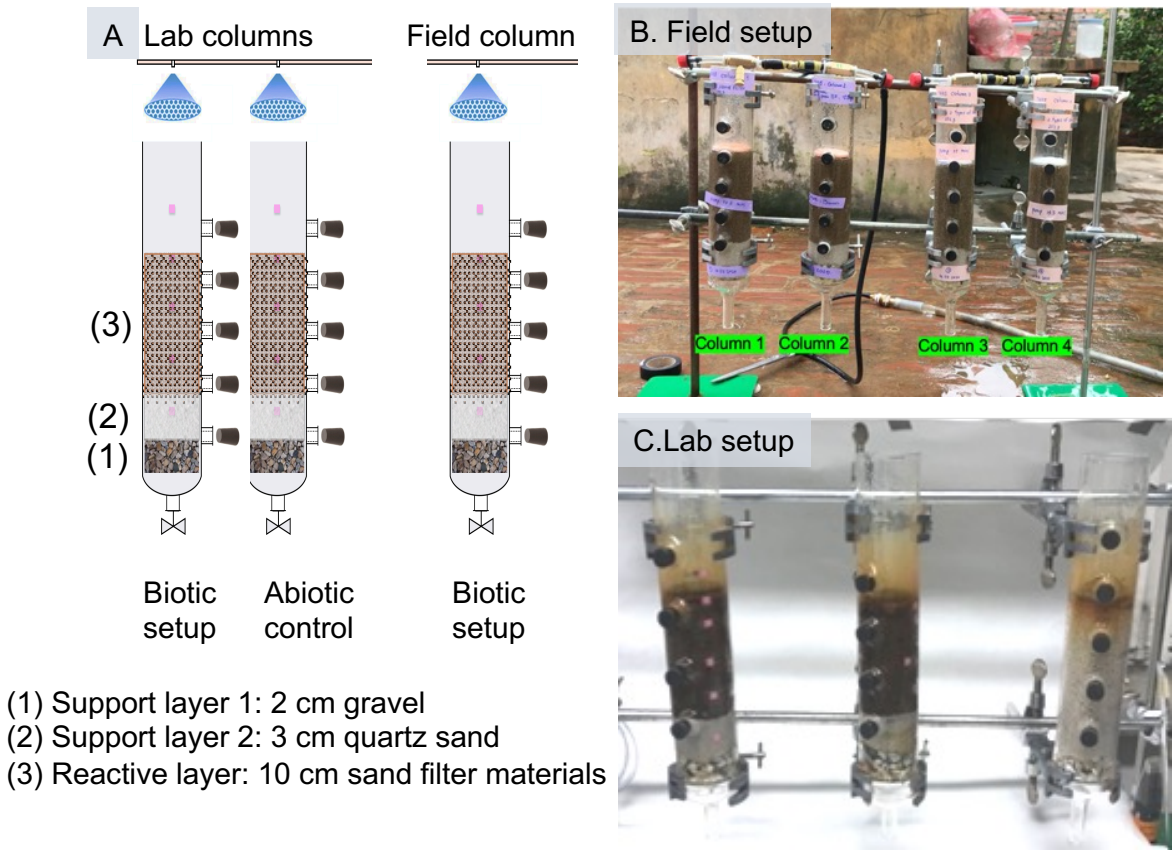

Figure S1. Design of column experiments in the lab and in the field (A), picture of column experiment in the field (B) and in the lab (C).

S3. Quantification of the elemental composition of samples by microwave digestion

Samples were digested in a Microwave Accelerated Reaction System, MARS 6 (CEM, USA) with 20 minutes of ramp time and 30 minutes of holding time at 180°C. Afterward, the digested samples were transferred into a 50 ml Falcon tube and adjusted to a total volume of 50 ml by adding milliQ water. Samples were centrifuged at 16,873 g for 15 minutes (Thermo Scientific Sorvall LYNX6000), then 100 µl of the supernatant was collected and diluted 100-fold in 1% HNO_3. Samples were stored at 4°C in the dark until analysis via the Agilent 7900 ICP-MS (Agilent Technologies, Santa Clara, CA).

S4. Synthesis and characterization of birnessite

Birnessite was synthesized following McKenzie's protocal (McKenzie, 1971). 6.3 gram $KMnO_4$ was dissolved in 100 mL milliQ water and heated to 90°C. The solution was then combined with 6.6 mL of concentrated HCl (37%) in a 2 L Erlenmeyer flask. The reaction took place at 90°C for 10 minutes, then the mineral suspension was cooled to room temperature for 30 min. Afterwards the suspension was filtered through 50 µm filter paper. The filtered solids were washed several times with milliQ water to remove excess salts. The process was repeated until the filtrate solution was clear. The solids were then air-dried and crushed with a mortar and pestle. Birnessite structure was confirmed using X-ray diffraction (Figure S1).

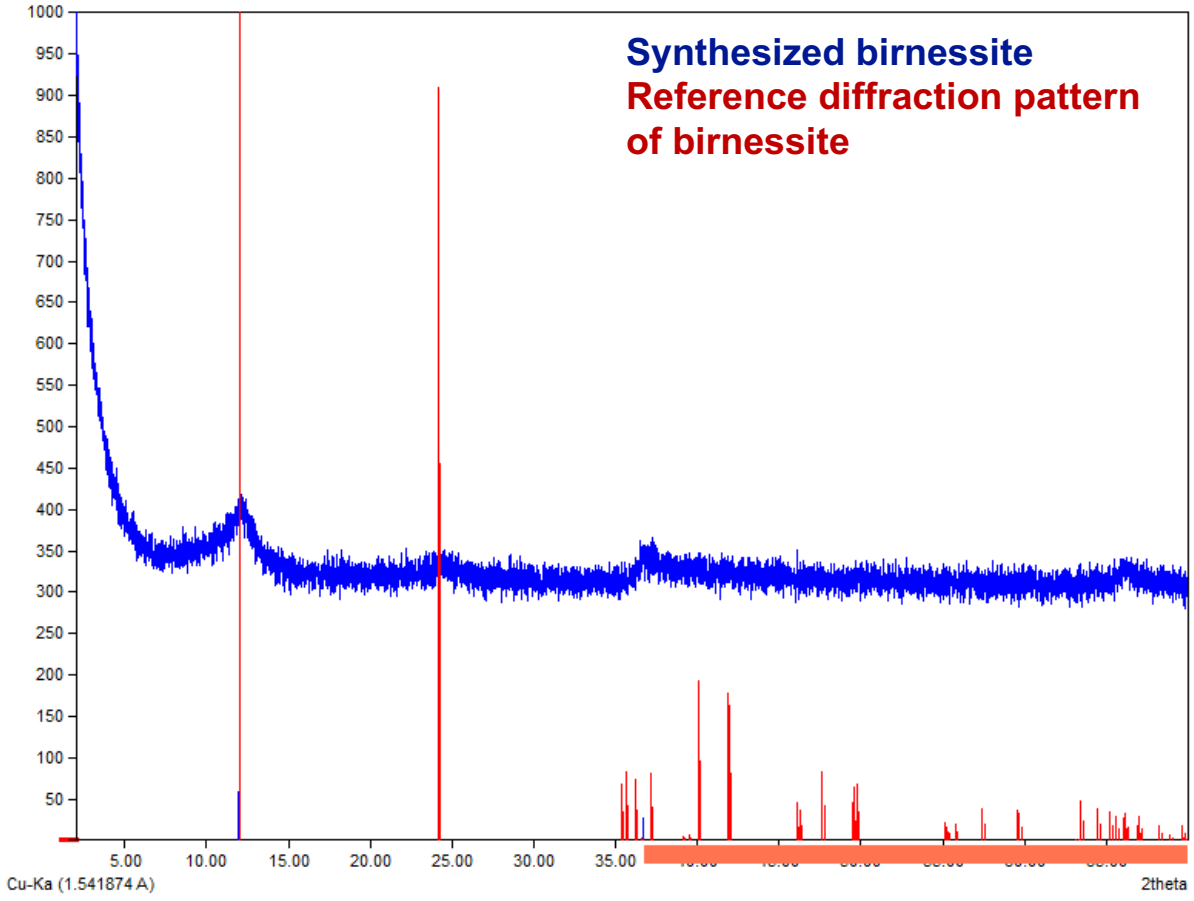

Figure S2. X-ray diffraction pattern of synthesized birnessite in comparison to the referenced birnessite.

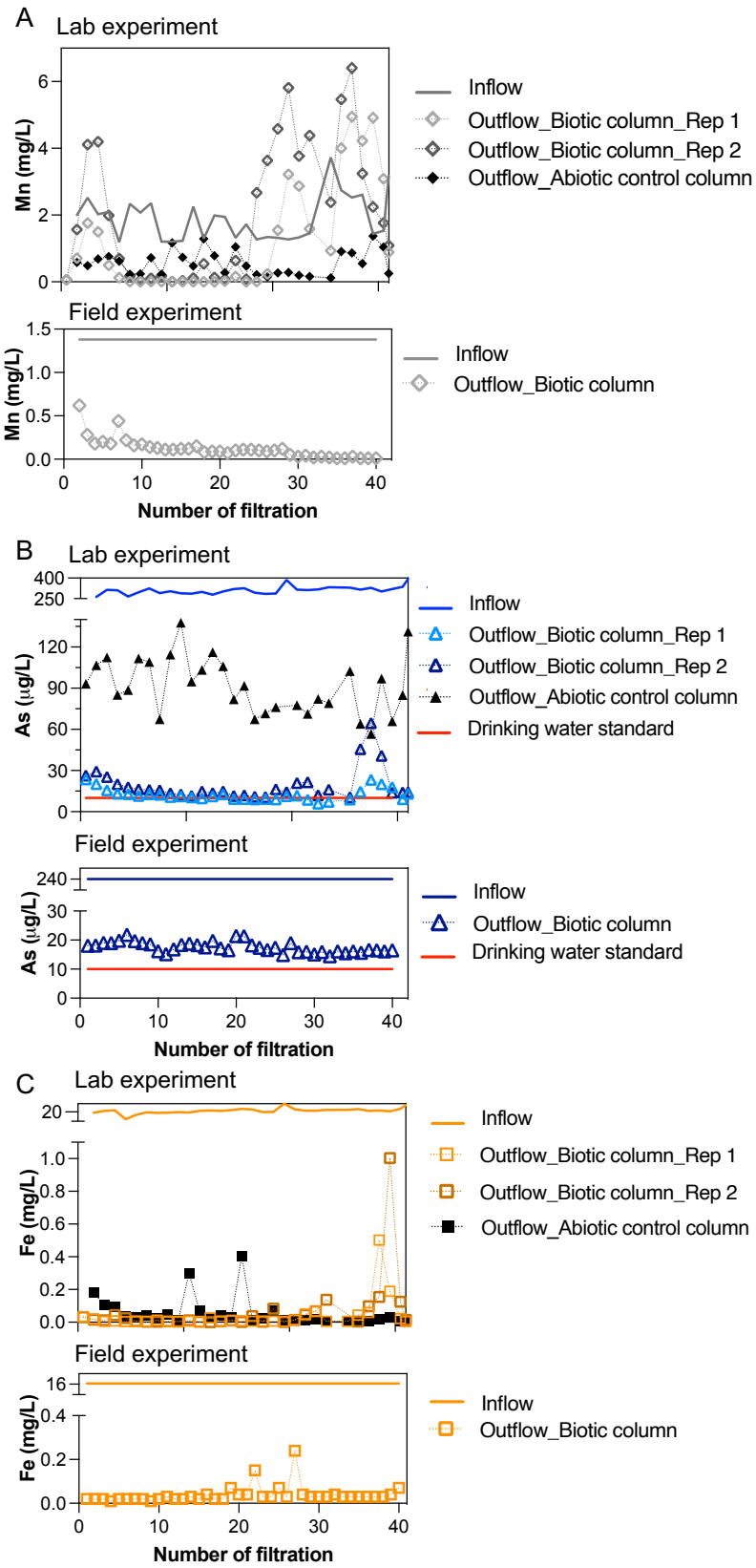

Figure S3: Results of column experiment in the lab (biotic and abiotic control (AC)) (upper panel) and in the field (biotic column) (lower panel) including inflow, outflow concentration of Mn (A), As (B) and Fe (C). The concentrations of Fe, Mn, As in the influent and effluent were recorded at every feeding batches.

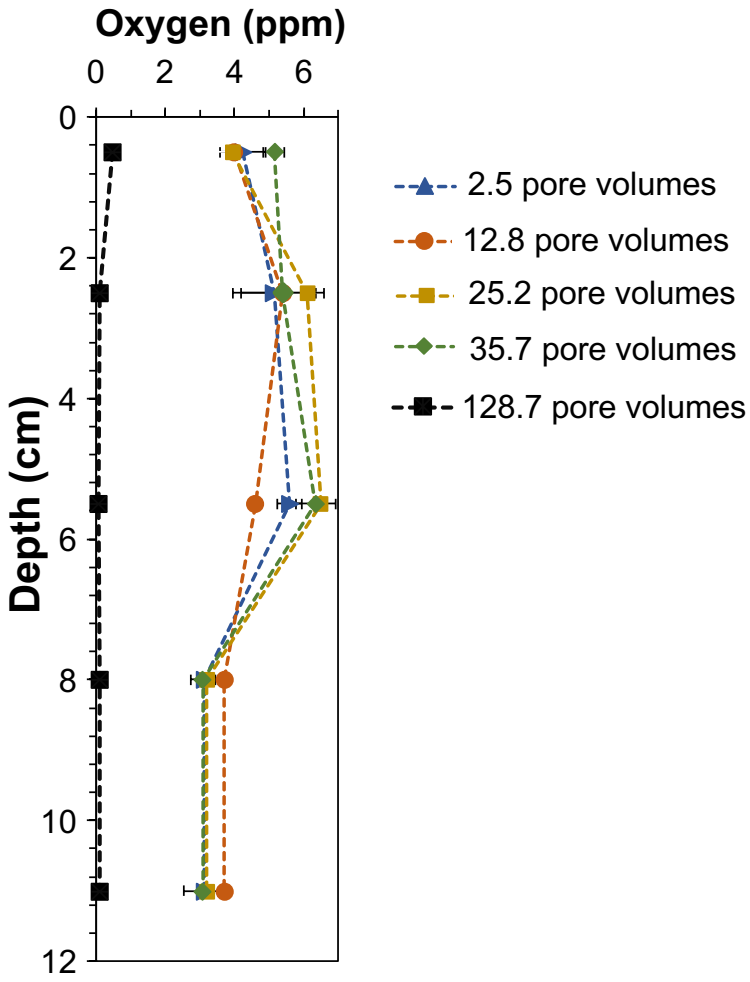

Figure S4. Dissolved oxygen concentration of pore water at different depth levels along the sand column measured under unsaturated conditions (colored data points) and saturated conditions (black data points). All samples were analyzed in triplicate, and error bars indicate the standard deviation.

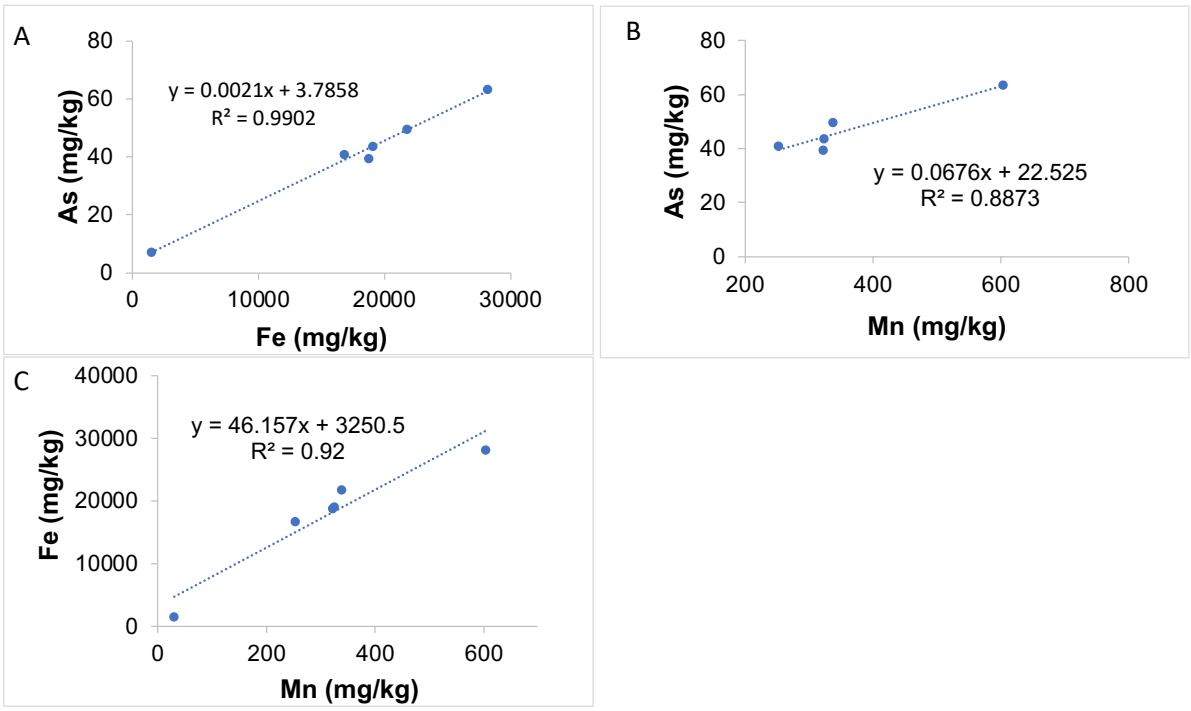

Figure S5. Linear correlation of total Fe, As, and Mn contents measured by ICP-MS after microwave digestion by aqua-regia solution. Correlations of As vs Fe (A), As vs Mn (B), and Fe vs Mn (C) of sand filter materials collected after the column experiment in the field.

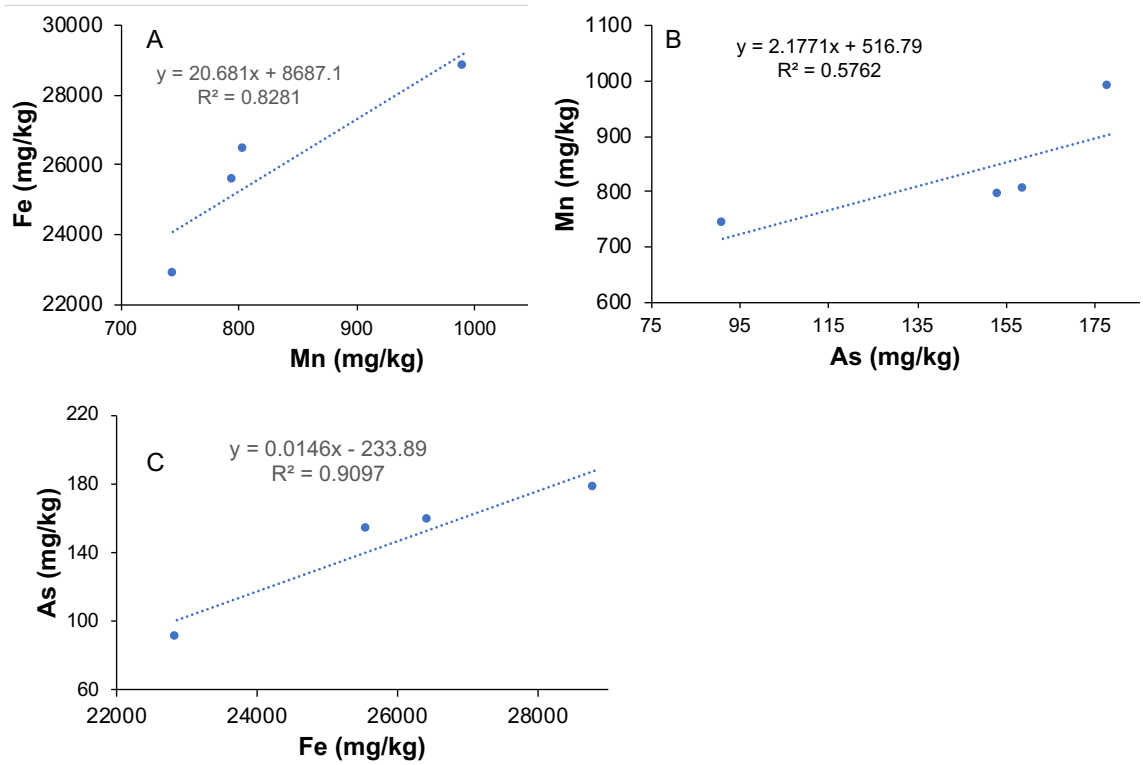

Figure S6 Linear correlation of total Fe, As, and Mn contents measured by ICP-MS after microwave digestion by aqua-regia solution. Correlations of As vs Fe (A), As vs Mn (B), and Fe vs Mn (C) of sand filter materials collected after the column experiment in the lab.

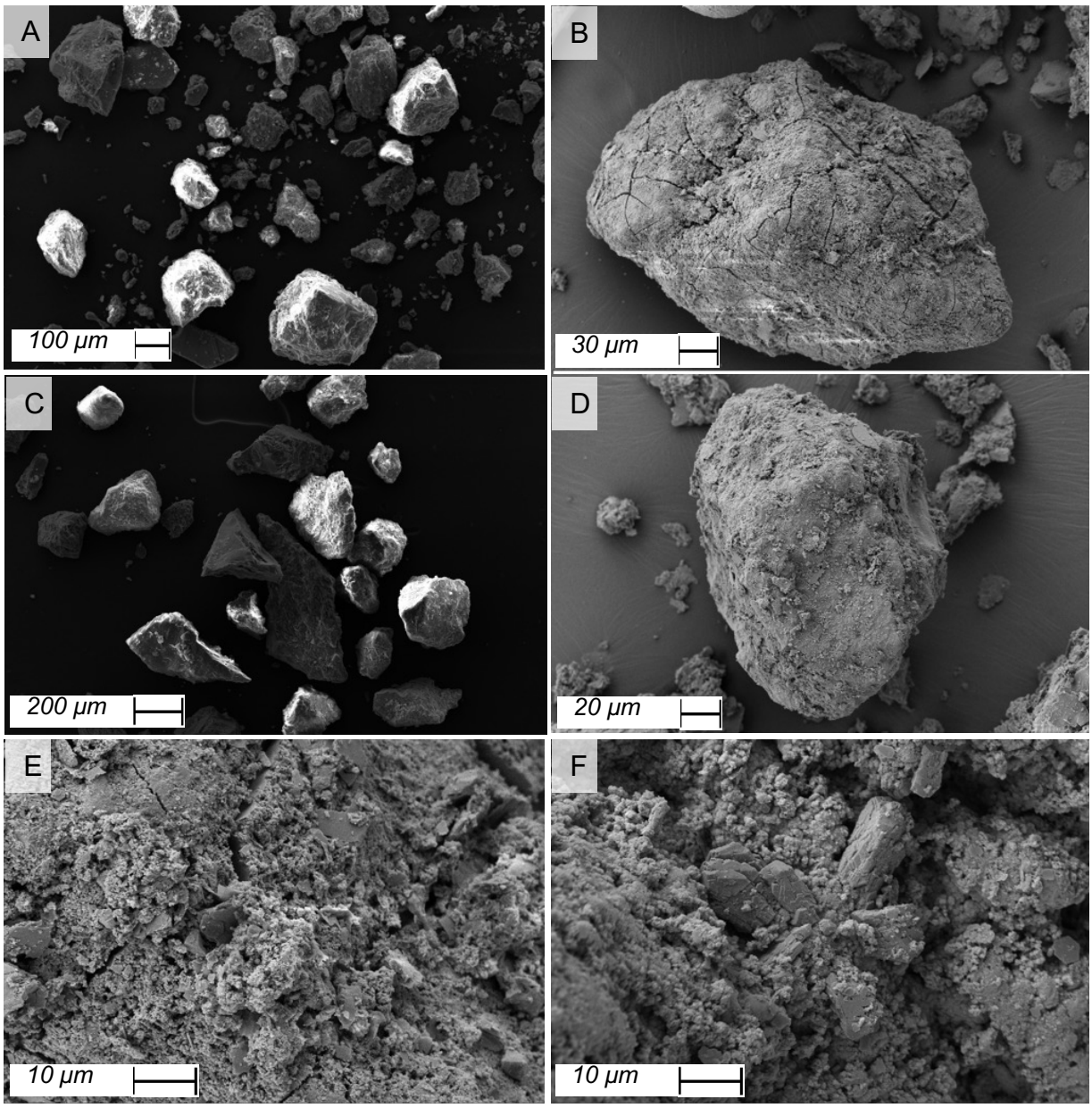

Figure S7. Scanning electron micrographs of sand filter materials. Different sand grain sizes used as filter materials (A-D) and morphology of precipitates coated on sand grains in sand columns (E-F).

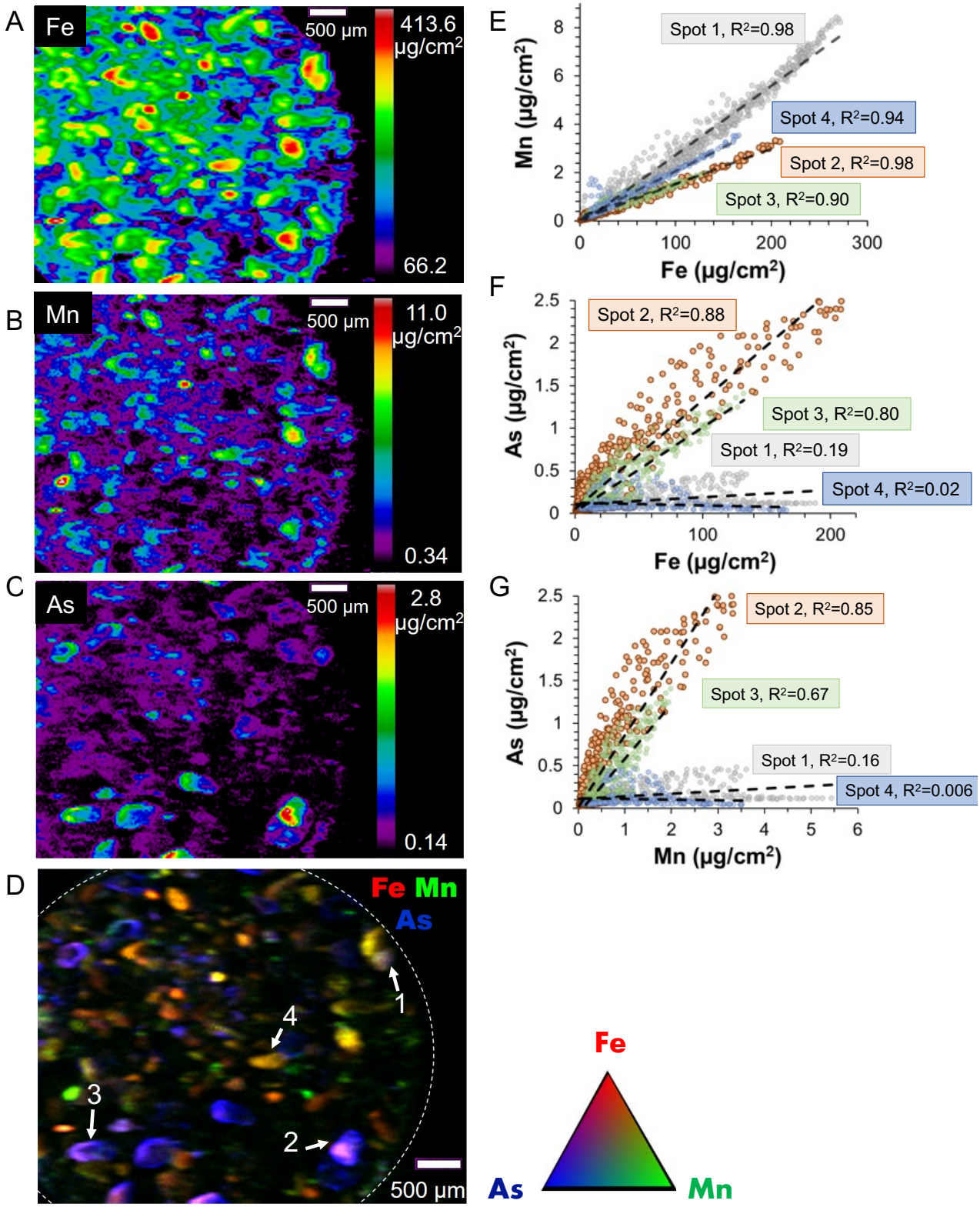

Figure S8. Multiple energy µ-XRF maps of sand filter material in unsaturated columns operated in the field including the distribution of Fe (A), Mn (B), As (C) and tricolor maps of Fe, Mn, As (D) and correlations of Mn vs Fe (E), As vs Fe (F), As vs Mn (G) in 4 selected spots displayed in the tricolor map (D).

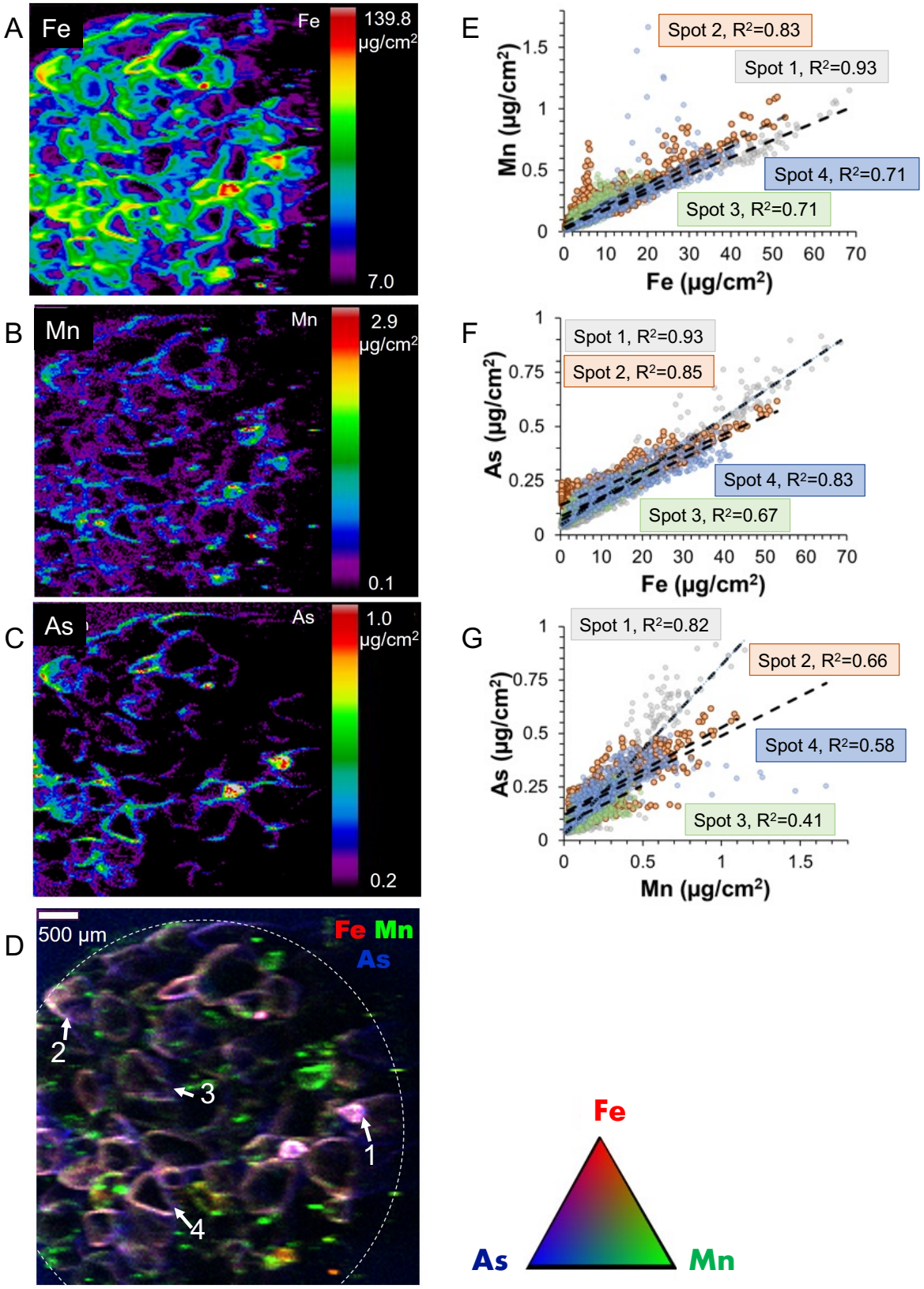

Figure S9. Multiple energy µ-XRF maps of sand filter material in abiotic control columns operated in the lab including distribution of Fe (A), Mn (B), As (C) and tricolor maps of Fe, Mn, As (D) and correlations of Mn vs Fe (E), As vs Fe (F), As vs Mn (G) in 4 selected spots displayed in the tricolor map (D).

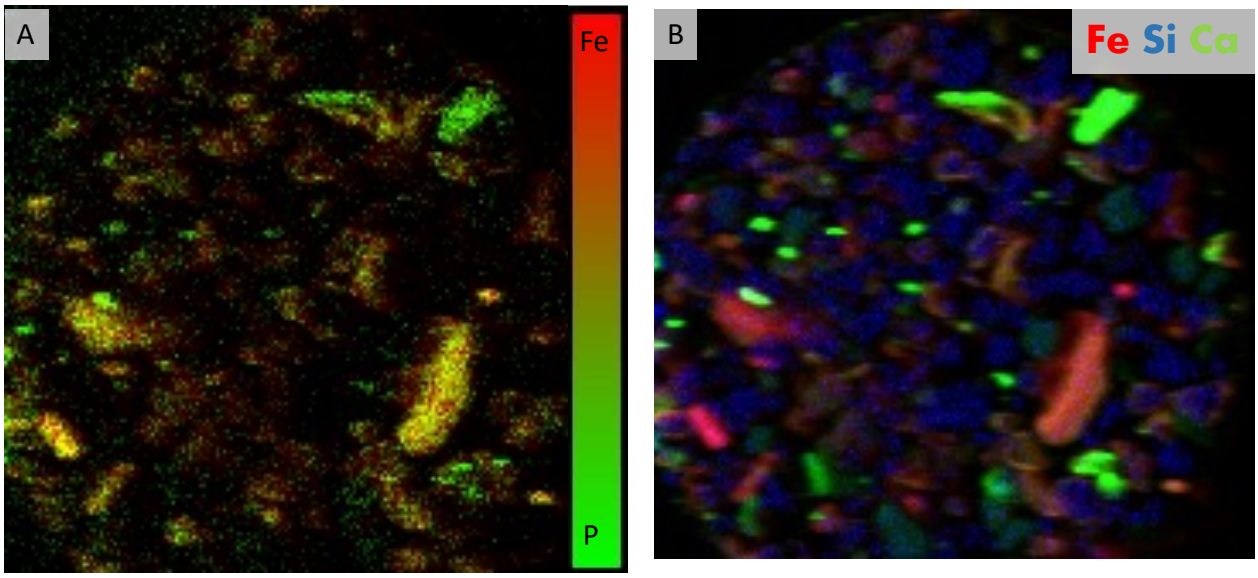

Figure S10: Multiple energy μ-XRF maps displaying Fe and P (A) and tricolor maps of Fe, Si and Ca (B) distribution on the surface of sand particles collected from saturated sand materials (lab experiment).

Table S3: Relative contribution of As redox species in sand materials obtained by linear combination fitting of As K-edge XANES spectra. The samples were collected at different depths in unsaturated and saturated columns conducted in the field and in the lab respectively.

Sample	Unsaturated columns			Saturated columns		
Depth (cm)	6-8	2-4	0-2	5-10	2-5	0-2
As(III)~FHY (%)	11.4	12.8	12.6	14.5	15.0	14.3
As(V)-FHY (%)	87.7	86.3	85.8	86.1	86.0	84.2
Total	99.1	99.1	98.4	100.6	101	98.5
R-factor	0.002097	0.003550	0.003653	0.00412	0.008574	0.004125
Reduced Chi Squared	1.9519	3.2492	3.3011	3.8897	8.1866	3.7072

Table S4: Relative contribution of different Fe minerals in sand materials obtained by linear combination fitting of Fe K-edge XANES spectra. The samples were collected at different depths in unsaturated and saturated columns conducted in the field and in the lab respectively.

Sample	Unsaturated columns			Saturated columns		
Depth (cm)	6-8	2-4	0-2	5-10	2-5	0-2
Goethite (%)	58	40.6			17.3	7.6
Pyrite (%)	20.6		13.2	52.8	4.6	14.8
Ferrihydrite (%)		57.3	84.4	45	77.5	77.3
Siderite (%)	21.4	2.0	01.2			
Total	1	0.999	0.988	0.978	0.994	0.997
R-factor	0.01034	0.000442	0.001446	0.000989	0.000202	0.000309
Reduced Chi Squared	0.02686	0.001201	0.003575	0.074617	0.00053	0.000774

References

McKenzie, R.M., 1971. The synthesis of birnessite, cryptomelane, and some other oxides and hydroxides of manganese. Mineral. Mag. 38, 493–502. https://doi.org/10.1180/minmag.1971.038.296.12

Nitzsche, K.S., Lan, V.M., Trang, P.T.K., Viet, P.H., Berg, M., Voegelin, A., Planer-Friedrich, B., Zahoransky, J., Müller, S.K., Byrne, J.M., Schröder, C., Behrens, S., Kappler, A., 2015. Arsenic removal from drinking water by a household sand filter in Vietnam - Effect of filter usage practices on arsenic removal efficiency and microbiological water quality. Sci. Total Environ. 502, 526–536. https://doi.org/10.1016/j.scitotenv.2014.09.055

Chapter 4 _ Paper 3: Personal contribution

Muammar Mansor adapted the spICP-MS technique with a focus on environmental applications, supported and encouraged by Andreas Kappler. Sören Drabesch, Ankita Chauhan, **Anh Van Le**, Johanna Schmidtmann, and Timm Bayer prepared samples. All authors contributed to data interpretation and manuscript revisions.

Chapter 4: Application of single-particle ICP-MS to determine the mass distribution and number concentrations of environmental nanoparticles and colloids

Muammar Mansor[1], Sören Drabesch[1], Timm Bayer[1], **Anh Van Le[1]**, Ankita Chauhan[1], Johanna Schmidtmann[2], Stefan Peiffer[2], Andreas Kappler[1]

[1]Geomicrobiology, Department of Geosciences, University of Tuebingen, 72076 Tuebingen, Germany

[2] Department of Hydrology, University of Bayreuth, 95447 Bayreuth, Germany

Published in: Environmental Science & Technology letters

https://doi.org/10.1021/acs.estlett.1c00314

Abstract

Analyzing the elemental compositions and size distributions of nanoparticles, colloids, and their aggregates in environmental samples represents a key task in understanding contaminant, substrate, and nutrient cycling. Single-particle ICP- MS (spICP-MS) is a high-throughput method that is capable of providing the elemental mass of thousands of particles within minutes. The challenge, however, lies in data analysis and interpretation, especially for complex environmental samples. Here we present successful applications of spICP-MS for environmental samples. We first analyzed the homoaggregation behavior of synthetic microplastic and magnetite (abiogenic and biogenic) nanoparticles. The measured distribution of aggregate mass was described as a function of the number of primary particles/aggregate (N_{pp}). In tandem with dynamic light scattering data, differences in aggregates' compactness (primary particles per nanometer) between samples can be determined. Second, we showed how sequential elemental analysis allows evaluation of the mobility of a toxic arsenic metalloid and its inferred association with colloidal Fe(III) (oxyhydr)oxides. Finally, we investigated the composition of heterogeneous iron−carbon-rich colloidal flocs, highlighting distinct colloidal Fe and C distributions and C/Fe ratios between samples from different permafrost thawing stages. On the basis of our results, we provide guidelines for successful sample preparation and promising future spICP-MS opportunities and applications with environmental samples.

4.1. Introduction

Nanoparticles (NPs, ≤100 nm in diameter) and colloids (≤1000 nm) constitute a highly dynamic environmental pool of elements with a wide continuum of size, reactivity, aggregation, and transport properties. Natural NPs have always been part of the Earth's biogeochemical cycling, while engineered and incidental NPs are increasingly being released to the environment due to anthropogenic activities (Hochella Jr et al., 2019). Our understanding of particle-driven processes is limited by the analytical techniques at our disposal. Electron microscopy is the standard technique for providing mineralogical and elemental information at the single-particle level but suffers from the high cost, time, and effort needed to translate this information to the whole particle population, as well as artifacts during sample preparation. In contrast, sequential filtration (coupled to subsequent elemental/mineralogical analyses) provides population-level information about particles separated into discrete size classes but fails to treat them as a continuum of size and reactivity. Field-flow fractionation can also separate particles on the basis of their properties (e.g., size), but separation parameters are highly sample-specific (Moens et al., 2019). A combination of all of these techniques is ideal for characterizing NPs and colloids, but a gap in our understanding of how to combine the information gained from single particle up to the population level remains. Single-particle inductively coupled plasma mass spectrometry (spICP-MS) has the potential to become the method of choice to fill this technical gap. In spICP-MS, single particles are channeled to the instrument and detected as separate pulses in a time-resolved mode (Degueldre and Favarger, 2003; Montaño et al., 2016). The intensity of each pulse is proportional to the element mass per particle and can be converted to particle size given prior knowledge on the particle's density, shape, and element mass fraction (Figure 1). Sample preparation is comparatively simple, often requiring only dilutions, and thousands of particles can be analyzed within minutes. Simultaneous information is obtained at the single-particle level (particle mass distribution) as well as the population level (particle number and mass concentration). However, the use of spICP-MS for characterization of natural colloids has lagged behind its use for engineered NPs (Flores et al., 2021; Mozhayeva and Engelhard, 2020; Peters et al., 2015), largely due to the inherent complexity of the former. spICP- MS is also limited to the analysis of one element per particle, but elemental association can be inferred by sequential elemental analysis of the same

sample. The lack of element- and size-specific reference materials is another challenge, although so far commonly used calibration techniques are suitable for most particles (Laborda et al., 2021; Montaño et al., 2016; Mozhayeva and Engelhard, 2020) (except for selenium NPs (Jiménez-Lamana et al., 2018)). Here we detail approaches to characterizing and interpreting spICP-MS data from environmental samples to facilitate the adoption of this technique. We present examples ranging from relatively simple aggregation of lab-synthesized particles (microplastics and abiogenic vs biogenic magnetite nano- particles) to particle-facilitated mobilization of the toxic metalloid arsenic and characterization of iron−carbon-rich colloids from a thawing permafrost.

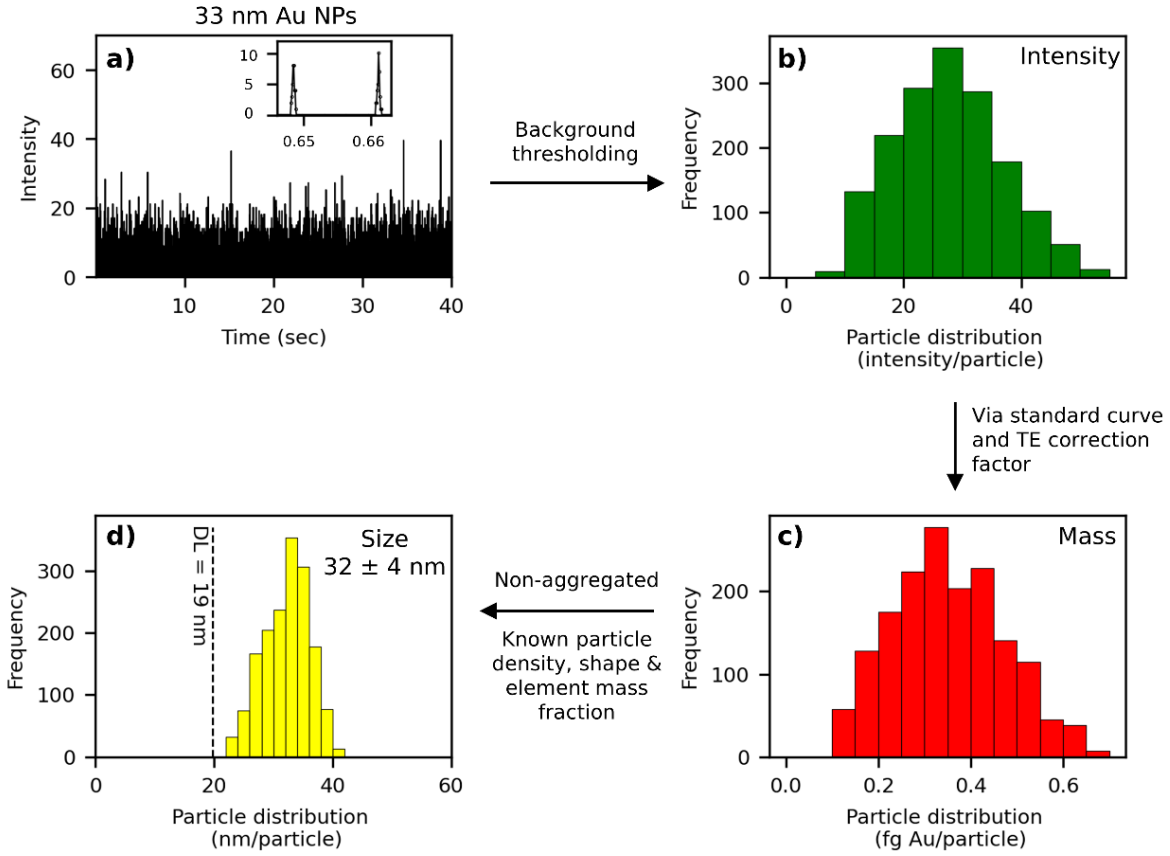

Figure 1: Illustration of data processing steps for spICP-MS. (a) An Au nanoparticle (NP) standard is analyzed in single-particle mode, yielding a time-series consisting of pulses corresponding to particle detection events. Inset shows two adjoining pulses within a timeframe of ~0.02 sec, with a background intensity of 0. (b) After applying background thresholding (typically mean + 3 standard deviations), intensities corresponding to particle pulses are collected to generate a histogram. (c) Particle intensities are converted to the element mass per particle using a standard curve (from dissolved elements) and a transport efficiency (TE) correction factor (to account for different efficiency for the detection of dissolved

elements versus particles). The masses can be summed to obtain the total mass or concentration in a sample. (d) Mass distribution can be converted to particle size distribution if the particles are non-aggregated and if the particle density, shape and metal mass fraction are known.

4.2. Materials and methods

All samples were analyzed in time-resolved analysis mode on an Agilent 7900 ICP-MS instrument (Agilent Technologies, Santa Clara, CA) with a RF power of 1550 V and a sampling depth of 8 mm. Samples and standards were prepared and measured as detailed in Tables S1 and S2, with results from standards listed in Table S3. Acid and water rinses were monitored between samples to ensure no carryover. The transport efficiency (TE) was determined daily by comparing the median intensity of 50 nm Au NPs to that of dissolved Au standards using the particle mass method, which is less susceptible to dilution errors compared to the particle number method (Montaño et al., 2016; Heather E. Pace et al., 2011). Over six separate days, the TE was comparable and

averaged 0.037 ± 0.001. Masses of 12C, 27Al, 56Fe, 75As, or 197Au were monitored using an integration time of 0.1 ms, an acquisition time of 40−60 s, and a sample flow rate of 0.466 mL/min in either NoGas (argon only) or Gas mode (helium flow of 1 mL/min). Sequential analysis with a time gap of 10 s between elements was employed for multielement analysis of the same sample. Data analysis was performed via a custom Python script following the approaches of (Heather E Pace et al., 2011) and as described in detail in SI Data Analysis. Lower detection limits with increasing element mass were observed (Table S2), consistent with previous studies (Laborda et al., 2021; Lee et al., 2014).

4.3. Results and discussion

4.3.1 Example 1: Aggregation of microplastic beads and magnetite nanoparticles. Aggregation of nanoparticles and colloids greatly affects their reactivity (surface area loss) and mobility (settling velocity) (Hotze et al., 2010). With spICP-MS, particle mass distribution can be directly measured as a parameter to quantify the state of aggregation. An example is presented for the aggregation of

synthetic polystyrene microplastic beads, which affects the sedimentation and mobilization of micro-plastics in aquatic systems (Li et al., 2019; Michels et al., 2018). Here we introduce the term Npp (number of primary particles per aggregate), which can be obtained by dividing the mass of the measured aggregate (determined via spICP-MS) to the mass of the primary particle (calculable for particles of known size and composition (SI Data Analysis)). Figure 2a shows that particle signals consisting of isolated microplastic beads (N_{pp} = 1) and aggregates composed of five beads (N_{pp} = 5) were readily distinguished on the basis of their relative masses. Furthermore, the number frequency of each aggregate can be summed and compared to yield their relative frequencies and aggregation pattern. The combination of spICP-MS with ongoing work on microplastic aggregation holds promise for providing new insights on their fate in the environment (Alimi et al., 2018; Bolea-Fernandez et al., 2020; Laborda et al., 2021; Oriekhova and Stoll, 2018). This approach was further developed through the analysis of ~13 nm NPs of abiogenic and biogenic magnetite (Byrne et al., 2011; C I Pearce et al., 2012; Sundman et al., 2020). The detection limit for spICP-MS is 0.9 fg of Fe/particle, which means that only aggregates larger than 140 N_{pp} can be detected. Panels b and c of Figure 2 show that magnetite aggregates with up to 30000 N_{pp} were detectable. Due to the smaller sizes, the separation of signals for nanoparticle aggregates was not as clear as for the larger microplastics, but differences in aggregation patterns were still distinguish- able. Analyzing the same samples at higher particle concentrations led to the formation of larger aggregates and a more positively skewed particle distribution, because the level of aggregation increases with the total number of primary particles in the suspension (Baalousha, 2009; Vikesland et al., 2016). Between samples, biogenic magnetite was observed to form larger aggregates compared to abiogenic magnetite at the same concentration. This result was consistent with measurements of the hydrodynamic diameter (D_H) via dynamic light scattering; biogenic magnetite displayed a D_H of 3671 ± 670 nm (n = 9) compared to a smaller D_H of 1567 ± 192 nm (n = 8) for abiogenic magnetite.

By combining measurements of N_{pp} from spICP-MS and D_H from DLS (Li et al., 2020), we can calculate the compaction factor (CF, number of primary particles per nanometer) of a sample:

$$CF = N_{pp} / D_H \quad (1)$$

We determined the CF for biogenic magnetite to be 2−6 times smaller than that of abiogenic magnetite, depending on the measurement dilutions and statistics used to describe skewed particle distributions (Table S4). The lower CF values indicated that biogenic magnetite formed less compact aggregates than abiogenic magnetite. Overall, the data suggest that biogenic magnetite aggregation was enhanced via bridging by associated organic matter, but they were not packed as tightly as in the case of abiogenic magnetite. This in turn would affect the particle reactivity, which depends on the degree of reactive sites lost due to the decrease in surface area (as well as organic matter coverage) upon aggregation. Note, however, that CF values are dependent on the sample concentrations used for both DLS (parts per million level required due to lower sensitivity) and spICP-MS (parts per billion level) but can be applied to compare different samples as long as the same concentrations are used.

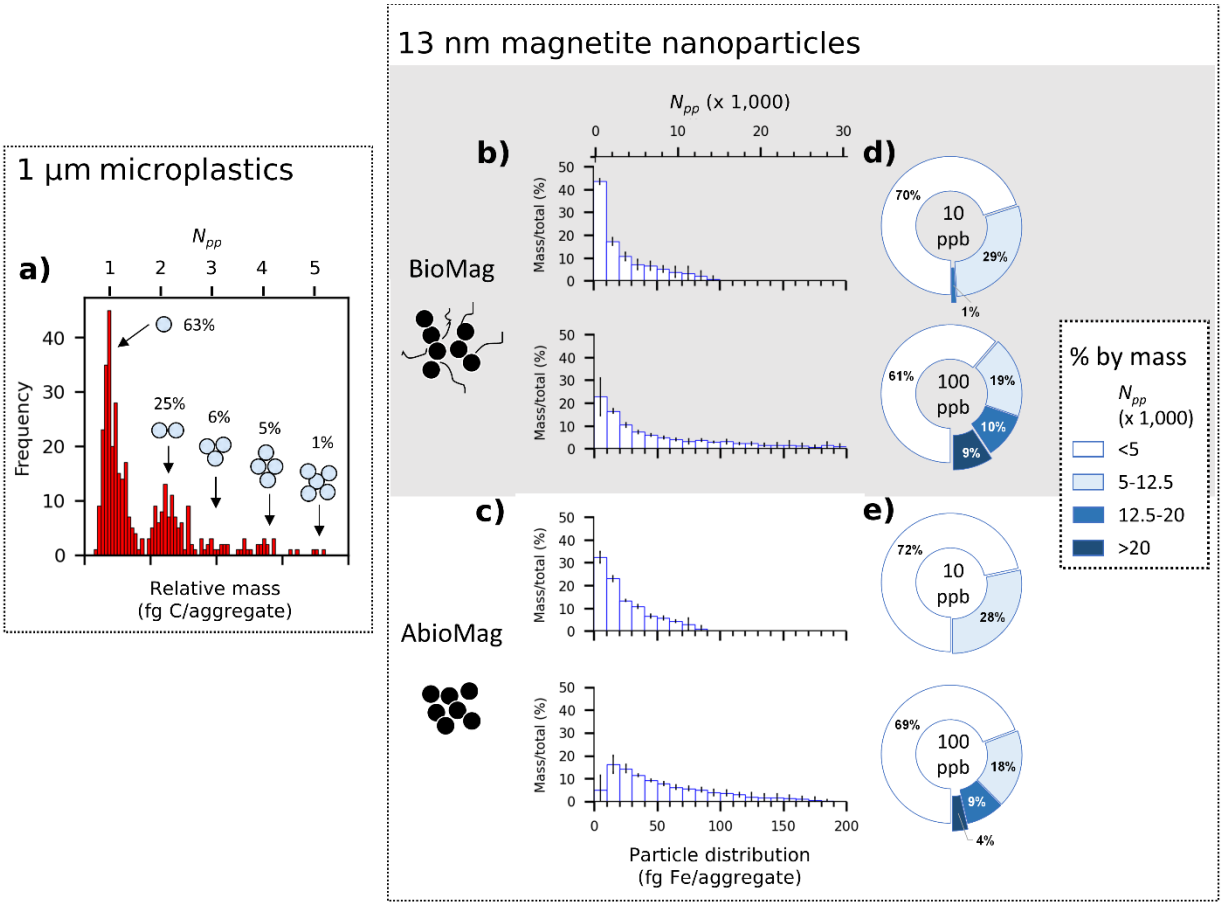

Figure 2: Examples on the usage of spICP-MS to quantify particle aggregation. (a) Frequency-based particle distribution (femtogram of C per aggregate) of unsonicated 1 µm microplastic beads. The detected particles cluster based on their relative masses, which varies according to their corresponding N_{pp} (number of primary particles per aggregate, (formula in SI Data analysis)). The use of the term N_{pp} allows for the description of the particle distribution

based on their masses, remaining true to the parameter actually measured by spICP-MS. The percentages of each aggregate can be quantified on the basis of their relative detection frequencies with a typical reproducibility of <1%. Mass-based particle distribution of (b) biogenic (BioMag) and (c) abiogenic (AbioMag) magnetite NPs at 10 and 100 ppb total Fe. The y-axis is converted from frequency to mass (percent mass within a histogram bin relative to total particle mass in the sample). Error bars correspond to standard deviations from triplicate measurements. (d and e) Mass-based percentages of the magnetite aggregates. Most of the particle masses are contributed by aggregates with N_{pp} < 5,000 (these include mass of particles smaller than spICP-MS's detection limit, assuming no dissolved Fe in the samples). The mass distribution changes depending on the total NP concentration (10 vs 100 ppb) and the sample type (BioMag vs AbioMag).

4.3.2. Example 2: Colloid-facilitated mobilization of arsenic contaminant from used sand filters.

In Asia, household sand-based filters are used regularly to treat arsenic- contaminated groundwater for drinking. Oxidation of dissolved Fe(II) in the sand filter results in the formation of solid-phase Fe(III) (oxyhydr)oxides that sequester toxic As and remove it from solution (Nitzsche et al., 2015b). After being used up, the contaminated sand filter material is often dumped in the backyard garden, thus potentially acting as a point source that will channel As back into the pore water or enter the human food chain. Our ongoing research has shown limited release of dissolved As from the used sand even as Fe(III) reduction occurs extensively in anoxic microcosms (Table S1). However, we noticed that the microcosms also produced colloids that remain stably suspended in solution for weeks. We therefore investigated through spICP-MS if colloid-facilitated mobilization of As could be an important mechanism for As release, similar to the case in acid mine drainage (Gomez-Gonzalez et al., 2016).

Colloids from three microcosm samples were analyzed: As-rich used sand, uncontaminated garden soil, and a 1:1 mixture of the two. The results were stark. As-containing colloids were detectable and most abundant from the used sand (∼50), followed by the sand/soil mix (∼10), while very low As- containing colloids were detected in uncontaminated soil (≤2; comparable to the H_2O blank) (Figure 3a−c). After accounting for dilution, colloids from used sand were found to contain ∼10^5 As-containing particles per milliliter with a collective mass of ∼10 μg/L As, close to the

World Health Organization's drinking water limit for dissolved As (Figure 3d-e). The bioavailability of these colloids is an open question. Nonetheless, this result indicated that colloid-facilitated mobilization of As from used sand could indeed be an important source of contamination.

We sought to understand the particle association of As by monitoring colloidal Fe and Al (Figure 3e-f). The used sand contained a higher level of colloidal Fe but a lower level of colloidal Al than soil and the sand/soil mix. This trend was consistent regardless of whether the particle number or particle mass concentration was used as a comparison metric. Given the concurrent increased Fe and As levels, we hypothesize that As was mobilized in the form of colloidal Fe(III) (oxyhydr)oxides, consistent with their known associations (Wallis et al., 2020). Future work using (sub)micrometer visualization of the elemental distribution will help in the evaluation of this hypothesis.

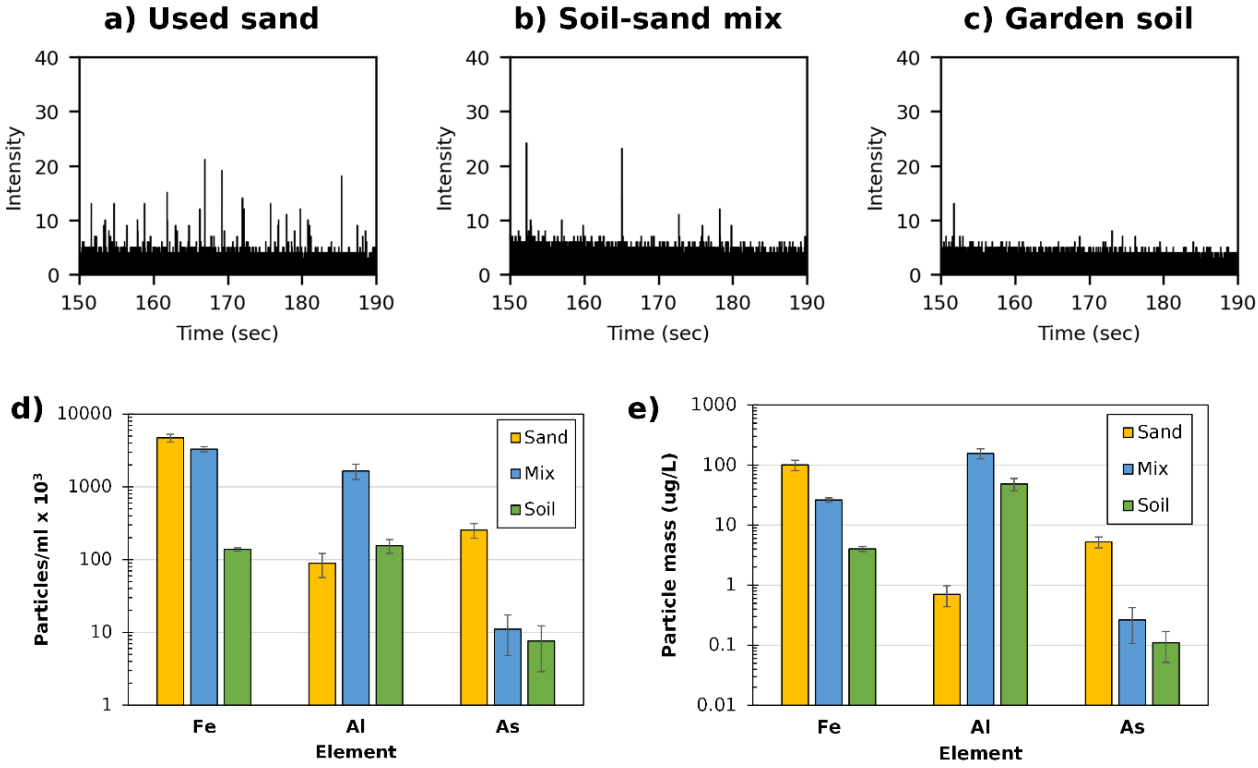

Figure 3: Example of spICP-MS usage to quantify colloidal contaminant mobilization. (a-c) Raw spICP-MS time series for arsenic (As) in used As-rich sand filters (left), a sand/soil mix (middle), and uncontaminated garden soil (right). The used sand filters show elevated levels of colloidal As. (d and e) Particle number concentrations (left) or particle mass concentrations (right) of Fe, Al, and As-containing colloids. The two parameters show the same trend between samples but with different relative values depending on the particle number frequency in each

mass histogram bin, highlighting the need to compare both number and mass concentrations side by side. Error bars represent standard deviations from measurements of three separate microcosm bottles.

4.3.3. Example 3: Colloidal Fe−carbon flocs released from thawing permafrost.

Permafrost regions store a significant amount of organic carbon that is becoming increasingly bioavailable due to an increasing global temperature (Estop-Aragonés et al., 2018). Thawing of permafrost leads to the release of organic carbon that interacts with iron to form Fe−organic-rich aggregates (flocs). These flocs are composed of heterogeneous mixtures of amorphous Fe (oxyhydr)oxides with humic acids, microbial cells, and plant detritus that are likely to be highly reactive and mobile (Pokrovsky et al., 2011; Zak and Gelbrecht, 2007). Characterizing these flocs is vital for understanding the role that they will play in greenhouse gas formation and climate change. We analyzed the flocs collected from an intermediately thawed bog and a fully thawed fen from the Stordalen Mire (Abisko, Sweden). Bog and fen represent two distinct stages of thawing permafrost with different biogeochemical character- istics (e.g., E_h−pH, microbial communities) (Patzner et al., 2020). Figure 4 illustrates the colloidal C and Fe distribution. A significant difference was apparent between the two samples. Flocs from the bog were characterized by high colloidal C and low colloidal Fe concentrations, while flocs from the fen were characterized by low colloidal C (∼1.5-fold lower) and high colloidal Fe (∼15-fold higher) concentrations. Correspondingly, the total colloidal C/Fe ratio (mass/mass) decreased from 14.3 ± 3.7 (n = 8) to 0.7 ± 0.5 (n = 7; replicates including different treatments in Figure S1) from bog to fen. The increase in the colloidal Fe concentration may be explained by microbial Fe cycling that weathers large particles to form smaller colloidal particles that could be detected by spICP-MS, while the decrease in the colloidal C concentration was consistent with inferred organic C degradation during the bog-to-fen transition (Patzner et al., 2020). Lower colloidal Fe and C concentrations were also likely present but not detectable due to the detection limit of spICP-MS (Table S2).

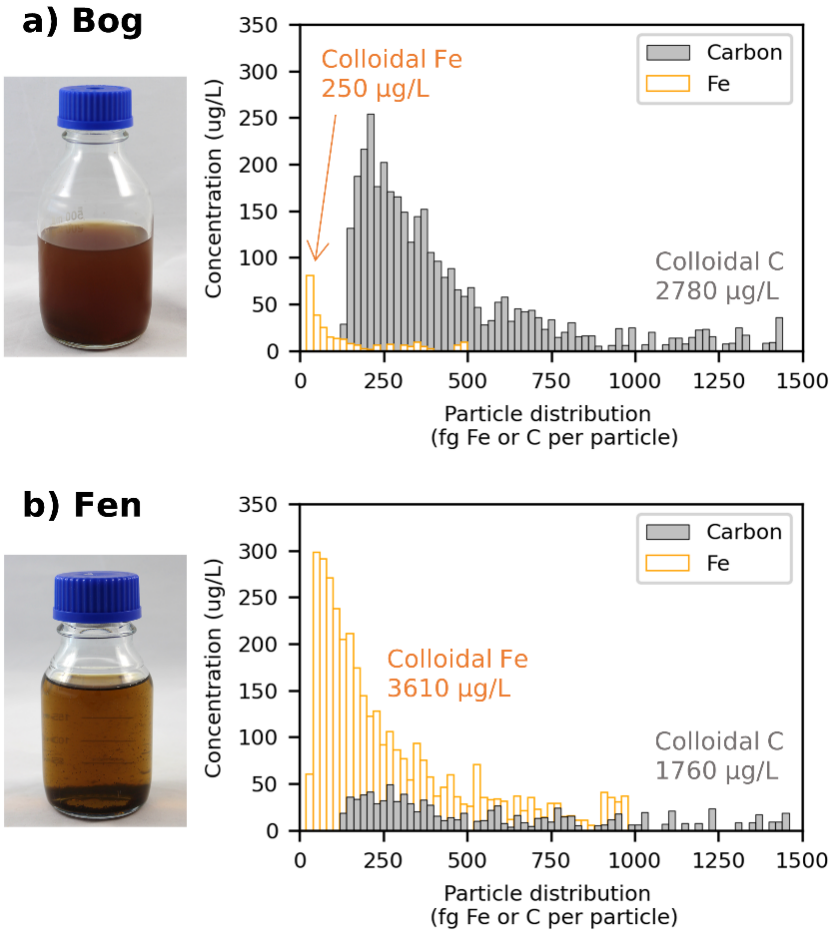

Figure 4: Results of spICP-MS analysis from colloidal Fe-C flocs from site (a) bog and (b) fen samples. The y-axis shows the colloid concentration (µg/L) by converting from frequency to mass to concentration after correcting for the sample volume analyzed (see **SI section S1 Data Analysis)**. The lack of smaller colloidal Fe (<20 fg of Fe/particle) and C particles (<140 fg of C/particles) is not due to their absence but is rather due to the detection limit of spICP-MS. Replicate samples show the same trend even after different treatments (**Figure S1**).

4.4. Guidelines and future opportunities.

The presented examples highlight the utility of spICP-MS in providing new insights into particle aggregation, adsorption, and mobilization of toxic elements and their mass distributions in environmental samples. The given examples are only snapshots, and further analysis will undoubtedly provide more information about particle-driven biogeochemical cycling as a function of time or reaction progress. Sample preparation and interpretation are vital for spICP-MS, and here we present several guidelines.

Remove large particles (>5 µm) by filtration, centrifugation, or gravitational settling to avoid clogging in the tubings. When using gravitational settling, always

report the container type, sample volume and height, settling time, and sampling depth.

Dilute samples to a particle number concentration of $\leq 10^6$ particles/mL or to low parts per billion levels to reduce coincidence (two particles reaching the plasma at the same time) and particle carryover effects (Montaño et al., 2016). Optimal dilution for unknown environmental samples can be determined via trial and error. The diluent choice is a compromise between ease of use and minimization of background and elemental interference (MQ H_2O) to maintain an environmentally relevant pH and ionic strength (e.g., filtered environmental water).

Consciously select your mixing methods. Sonication for 5−10 min followed by brief mixing by inversion is recommended for analysis of irreversibly bonded aggregates. Weaker mixing methods such as hand shaking, and gas bubbling can be used to analyze weakly bonded agglomerates.

Choose the appropriate sample container, tubing, and reagents to minimize background and adsorptive losses. Reagents can be filtered beforehand to remove colloids. Fe and Al colloids are especially common in blank reagents, but they can be statistically removed by conservative background thresholding.

Variants of spICP-MS are increasingly finding environmental applications (Flores et al., 2021). Single-cell ICP-MS has been used successfully to quantify the metal content of single cells (Amor et al., 2020; Gomez-Gomez et al., 2020). Recent development of dual-element spICP-MS and time-of-flight (TOF) spICP-MS can identify elemental association at the single-particle level (Bevers et al., 2020; Montaño et al., 2014; Naasz et al., 2018; Praetorius et al., 2017). We expect spICP-MS to be an essential tool in environmental research in upcoming years.

4.5. Acknowledgment

M.M. thanks Jie Xu for initial support in encouraging him to learn new techniques, Jim Ranville and Manuel Montaño for teaching him spICP-MS, Saurav Kumar for building the original Python framework for data analysis, Weinan Leng and Frank Wackenhut for supplying Au NPs, Peter Kühn for supplying noble metal standards, and Christoph Glotzbach for easy access to the ICP-MS instrument. A.C. acknowledges Monique Patzner and Erik Lundin (Abisko Research Station, Abisko, Sweden) for their help in

sampling and providing floc samples. The authors acknowledge infrastructural support by the Deutsche Forschungsgemeinschaft (DFG, German Re- search Foundation) under Germany's Excellence Strategy, cluster of Excellence EXC2124, Project 390838134. This work was supported by the DFG Project 391977956 (SFB 1357) as well as DFG funding provided to AK (KA 1736/66-1, KA 1736/51-1, and KA 1736/48-1 and Cluster of Excellence: EXC 2124: Controlling Microbes to Fight Infection, Tübingen, Germany).

4.6. References

Alimi, O.S., Farner Budarz, J., Hernandez, L.M., Tufenkji, N., 2018. Microplastics and Nanoplastics in Aquatic Environments: Aggregation, Deposition, and Enhanced Contaminant Transport. Environ. Sci. Technol. 52, 1704–1724. https://doi.org/10.1021/acs.est.7b05559

Amor, M., Tharaud, M., Gélabert, A., Komeili, A., 2020. Single-cell determination of iron content in magnetotactic bacteria: implications for the iron biogeochemical cycle. Environ. Microbiol. 22, 823–831. https://doi.org/https://doi.org/10.1111/1462-2920.14708

Baalousha, M., 2009. Aggregation and disaggregation of iron oxide nanoparticles: Influence of particle concentration, pH and natural organic matter. Sci. Total Environ. 407, 2093–2101. https://doi.org/10.1016/j.scitotenv.2008.11.022

Bevers, S., Montaño, M.D., Rybicki, L., Hofmann, T., von der Kammer, F., Ranville, J.F., 2020. Quantification and Characterization of Nanoparticulate Zinc in an Urban Watershed. Front. Environ. Sci. 8. https://doi.org/10.3389/fenvs.2020.00084

Bolea-Fernandez, E., Rua-Ibarz, A., Velimirovic, M., Tirez, K., Vanhaecke, F., 2020. Detection of microplastics using inductively coupled plasma-mass spectrometry (ICP-MS) operated in single-event mode. J. Anal. At. Spectrom. 35, 455–460. https://doi.org/10.1039/C9JA00379G

Byrne, J.M., Telling, N.D., Coker, V.S., Pattrick, R.A.D., van der Laan, G., Arenholz, E., Tuna, F., Lloyd, J.R., 2011. Control of nanoparticle size, reactivity and magnetic properties during the bioproduction of magnetite by Geobacter sulfurreducens. Nanotechnology 22, 455709. https://doi.org/10.1088/0957-4484/22/45/455709

Degueldre, C., Favarger, P.-Y., 2003. Colloid analysis by single particle inductively coupled plasma-mass spectroscopy: a feasibility study. Colloids Surfaces A Physicochem. Eng. Asp. 217, 137–142. https://doi.org/https://doi.org/10.1016/S0927-7757(02)00568-X

Estop-Aragonés, C., Cooper, M.D.A., Fisher, J.P., Thierry, A., Garnett, M.H., Charman, D.J., Murton, J.B., Phoenix, G.K., Treharne, R., Sanderson, N.K., Burn, C.R., Kokelj, S. V, Wolfe, S.A., Lewkowicz, A.G., Williams, M., Hartley, I.P., 2018. Limited release of previously-frozen C and increased new peat formation after thaw

in permafrost peatlands. Soil Biol. Biochem. 118, 115–129. https://doi.org/https://doi.org/10.1016/j.soilbio.2017.12.010

Flores, K., Turley, R.S., Valdes, C., Ye, Y., Cantu, J., Hernandez-Viezcas, J.A., Parsons, J.G., Gardea-Torresdey, J.L., 2021. Environmental applications and recent innovations in single particle inductively coupled plasma mass spectrometry (SP-ICP-MS). Appl. Spectrosc. Rev. 56, 1–26. https://doi.org/10.1080/05704928.2019.1694937

Gomez-Gomez, B., Corte-Rodríguez, M., Perez-Corona, M.T., Bettmer, J., Montes-Bayón, M., Madrid, Y., 2020. Combined single cell and single particle ICP-TQ-MS analysis to quantitatively evaluate the uptake and biotransformation of tellurium nanoparticles in bacteria. Anal. Chim. Acta 1128, 116–128. https://doi.org/https://doi.org/10.1016/j.aca.2020.06.058

Gomez-Gonzalez, M.A., Bolea, E., O'Day, P.A., Garcia-Guinea, J., Garrido, F., Laborda, F., 2016. Combining single-particle inductively coupled plasma mass spectrometry and X-ray absorption spectroscopy to evaluate the release of colloidal arsenic from environmental samples. Anal. Bioanal. Chem. 408, 5125–5135.

Hochella Jr, M.F., Mogk, D.W., Ranville, J., Allen, I.C., Luther, G.W., Marr, L.C., McGrail, B.P., Murayama, M., Qafoku, N.P., Rosso, K.M., 2019. Natural, incidental, and engineered nanomaterials and their impacts on the Earth system. Science (80-.). 363, eaau8299.

Hotze, E.M., Phenrat, T., Lowry, G. V, 2010. Nanoparticle Aggregation: Challenges to Understanding Transport and Reactivity in the Environment. J. Environ. Qual. 39, 1909–1924. https://doi.org/https://doi.org/10.2134/jeq2009.0462

Jiménez-Lamana, J., Abad-Álvaro, I., Bierla, K., Laborda, F., Szpunar, J., Lobinski, R., 2018. Detection and characterization of biogenic selenium nanoparticles in selenium-rich yeast by single particle ICPMS. J. Anal. At. Spectrom. 33, 452–460.

Laborda, F., Trujillo, C., Lobinski, R., 2021. Analysis of microplastics in consumer products by single particle-inductively coupled plasma mass spectrometry using the carbon-13 isotope. Talanta 221, 121486. https://doi.org/https://doi.org/10.1016/j.talanta.2020.121486

Lee, S., Bi, X., Reed, R.B., Ranville, J.F., Herckes, P., Westerhoff, P., 2014. Nanoparticle Size Detection Limits by Single Particle ICP-MS for 40 Elements. Environ. Sci. Technol. 48, 10291–10300. https://doi.org/10.1021/es502422v

Li, Y., Wang, X., Fu, W., Xia, X., Liu, C., Min, J., Zhang, W., Crittenden, J.C., 2019. Interactions between nano/micro plastics and suspended sediment in water: Implications on aggregation and settling. Water Res. 161, 486–495. https://doi.org/https://doi.org/10.1016/j.watres.2019.06.018

Li, Z., Shakiba, S., Deng, N., Chen, J., Louie, S.M., Hu, Y., 2020. Natural Organic Matter (NOM) Imparts Molecular-Weight-Dependent Steric Stabilization or Electrostatic Destabilization to Ferrihydrite Nanoparticles. Environ. Sci. Technol. 54, 6761–6770. https://doi.org/10.1021/acs.est.0c01189

Michels, J., Stippkugel, A., Lenz, M., Wirtz, K., Engel, A., 2018. Rapid aggregation of biofilm-covered microplastics with marine biogenic particles. Proc. R. Soc. B Biol. Sci. 285, 20181203. https://doi.org/10.1098/rspb.2018.1203

Moens, C., Waegeneers, N., Fritzsche, A., Nobels, P., Smolders, E., 2019. A systematic evaluation of Flow Field Flow Fractionation and single-particle ICP-MS to obtain the size distribution of organo-mineral iron oxyhydroxide colloids. J. Chromatogr. A 1599, 203–214.

Montaño, M.D., Badiei, H.R., Bazargan, S., Ranville, J.F., 2014. Improvements in the detection and characterization of engineered nanoparticles using spICP-MS with microsecond dwell times. Environ. Sci. Nano 1, 338–346. https://doi.org/10.1039/C4EN00058G

Montaño, M.D., Olesik, J.W., Barber, A.G., Challis, K., Ranville, J.F., 2016. Single Particle ICP-MS: Advances toward routine analysis of nanomaterials. Anal. Bioanal. Chem. 408, 5053–5074. https://doi.org/10.1007/s00216-016-9676-8

Mozhayeva, D., Engelhard, C., 2020. A critical review of single particle inductively coupled plasma mass spectrometry – A step towards an ideal method for nanomaterial characterization. J. Anal. At. Spectrom. 35, 1740–1783. https://doi.org/10.1039/C9JA00206E

Naasz, S., Weigel, S., Borovinskaya, O., Serva, A., Cascio, C., Undas, A.K., Simeone, F.C., Marvin, H.J.P., Peters, R.J.B., 2018. Multi-element analysis of single

nanoparticles by ICP-MS using quadrupole and time-of-flight technologies. J. Anal. At. Spectrom. 33, 835–845. https://doi.org/10.1039/C7JA00399D

Nitzsche, K.S., Weigold, P., Lösekann-Behrens, T., Kappler, A., Behrens, S., 2015. Microbial community composition of a household sand filter used for arsenic, iron, and manganese removal from groundwater in Vietnam. Chemosphere 138, 47–59. https://doi.org/10.1016/j.chemosphere.2015.05.032

Oriekhova, O., Stoll, S., 2018. Heteroaggregation of nanoplastic particles in the presence of inorganic colloids and natural organic matter. Environ. Sci. Nano 5, 792–799. https://doi.org/10.1039/C7EN01119A

Pace, H.E., Rogers, N.J., Jarolimek, C., Coleman, V.A., Higgins, C.P., Ranville, J.F., 2011. Determining transport efficiency for the purpose of counting and sizing nanoparticles via single particle inductively coupled plasma mass spectrometry. Anal. Chem. 83, 9361–9369. https://doi.org/10.1021/ac201952t

Patzner, M.S., Mueller, C.W., Malusova, M., Baur, M., Nikeleit, V., Scholten, T., Hoeschen, C., Byrne, J.M., Borch, T., Kappler, A., 2020. Iron mineral dissolution releases iron and associated organic carbon during permafrost thaw. Nat. Commun. 11, 1–11.

Pearce, C.I., Qafoku, O., Liu, J., Arenholz, E., Heald, S.M., Kukkadapu, R.K., Gorski, C.A., Henderson, C.M.B., Rosso, K.M., 2012. Synthesis and properties of titanomagnetite (Fe3−xTixO4) nanoparticles: A tunable solid-state Fe(II/III) redox system. J. Colloid Interface Sci. 387, 24–38. https://doi.org/https://doi.org/10.1016/j.jcis.2012.06.092

Peters, R., Herrera-Rivera, Z., Undas, A., van der Lee, M., Marvin, H., Bouwmeester, H., Weigel, S., 2015. Single particle ICP-MS combined with a data evaluation tool as a routine technique for the analysis of nanoparticles in complex matrices. J. Anal. At. Spectrom. 30, 1274–1285. https://doi.org/10.1039/C4JA00357H

Pokrovsky, O.S., Shirokova, L.S., Kirpotin, S.N., Audry, S., Viers, J., Dupré, B., 2011. Effect of permafrost thawing on organic carbon and trace element colloidal speciation in the thermokarst lakes of western Siberia. Biogeosciences 8, 565–583. https://doi.org/10.5194/bg-8-565-2011

Praetorius, A., Gundlach-Graham, A., Goldberg, E., Fabienke, W., Navratilova, J., Gondikas, A., Kaegi, R., Günther, D., Hofmann, T., von der Kammer, F., 2017. Single-particle multi-element fingerprinting (spMEF) using inductively-coupled plasma time-of-flight mass spectrometry (ICP-TOFMS) to identify engineered nanoparticles against the elevated natural background in soils. Environ. Sci. Nano 4, 307–314. https://doi.org/10.1039/C6EN00455E

Sundman, A., Vitzthum, A.-L., Adaktylos-Surber, K., Figueroa, A.I., van der Laan, G., Daus, B., Kappler, A., Byrne, J.M., 2020. Effect of Fe-metabolizing bacteria and humic substances on magnetite nanoparticle reactivity towards arsenic and chromium. J. Hazard. Mater. 384, 121450. https://doi.org/https://doi.org/10.1016/j.jhazmat.2019.121450

Vikesland, P.J., Rebodos, R.L., Bottero, J.Y., Rose, J., Masion, A., 2016. Aggregation and sedimentation of magnetite nanoparticle clusters. Environ. Sci. Nano 3, 567–577. https://doi.org/10.1039/C5EN00155B

Wallis, I., Prommer, H., Berg, M., Siade, A.J., Sun, J., Kipfer, R., 2020. The river–groundwater interface as a hotspot for arsenic release. Nat. Geosci. 13, 288–295. https://doi.org/10.1038/s41561-020-0557-6

Zak, D., Gelbrecht, J., 2007. The mobilisation of phosphorus, organic carbon and ammonium in the initial stage of fen rewetting (a case study from NE Germany). Biogeochemistry 85, 141–151. https://doi.org/10.1007/s10533-007-9122-2

SUPPLEMENTARY INFORMATION

S1. Data Analysis

S1.1 First, determine the average background intensity (σ_{diss}) by an iterative approach.

- Average the whole dataset.
- Remove datapoints that are higher than σ_{diss} + x standard deviation (SD). See step 2 for discussions on the appropriate value of x.
- Repeat the first two steps until there is no significant change in σ_{diss}.
- The dissolved element concentration in the sample can be calculated by using σ_{diss} and the slope and intercept of the standard curve of the dissolved element. However, one must keep in mind that the determined value includes contribution from particles that are below the particle detection limit (see step 4 on how to determine detection limit).

S1.2 Collect all the datapoints corresponding to particle events (i.e. datapoints higher than σ_{diss} + xSD) and subtract the background.

- The appropriate value of x can be anywhere from 3 to 8 (references compiled in Laborda et al., 2020), depending on the element and the noisiness of the background signal.
- Optimal value of x aims to minimize false positives i.e., the signals detected as “particles” from rinse acids or dissolved element standards compared to real particle-containing samples. Aim to achieve a false positive value of < 3% by trial and error.
- Proper tuning of the instrument to maximize stability and reduction of background signals (from contamination/residues) will help in improving particle detection limit.
- After collecting the datapoints, subtract each one with the average background value determined in step 1.

S1.3 Sum up the intensity of all datapoints that constitute a particle event.

- Depending on the signal integration time, each particle event may consist of several consecutive datapoints. For example, a particle event with 5 datapoints has a transit time of 500 µs with an integration time of 100 µs. Longer transit times

are observed for larger particles and with measurements using He in Gas mode (Bolea-Fernandez et al., 2019).

- To reduce false positives, we can further implement a minimum consecutive point (MCP) threshold, in which a particle event must contain a minimum number of consecutive datapoints to be considered as real. We found that MCP implementation significantly decreased the number of false positives, likely due to the statistical elimination of short-lived instrument shot noise.
- We advise using MCP = 1 to 3 with SD = 3 to 5.
- For each particle event, sum up the intensity of the consecutive datapoints. The summed intensity of each particle can be tabulated and used to generate a frequency-based particle intensity distribution.

S1.4 Convert intensity to element mass per particle and subsequently to other derived parameters (particle mass, particle size, number of primary particles per aggregate).

- First, calculate the slope of the standard curve of element mass per particle (m_p) based on the pre-determined transport efficiency (TE) (Heather E Pace et al., 2011) and the slope of the standard curve of the dissolved element (m_{diss}):

$$m_p = m_{diss} / \text{TE} / \text{flow rate} / \text{integration time} \quad (1)$$

- Determine the detection limit (DL) of element mass per particle:

$$\text{DL} = \frac{(\sigma_{diss} + x\text{SD}) * \text{MCP}}{\text{IE} * m_p} \quad (2)$$

where IE = ionization efficiency (often assumed to be equal to 1, but can be less than 1 especially for elements with low ionization efficiencies such as selenium and carbon (Jiménez-Lamana et al., 2018; this study)).

- Then, calculate the element mass per particle (M_E) for each detected particle event:

$$M_E = \frac{I_{sum}}{\text{IE} * m_p} \quad (3)$$

where I_{sum} = summed particle intensity from step 3.
Data for all particles can be tabulated and used to generate a frequency-based particle distribution with element mass per particle on the x-axis.

- If the element mass fraction (f) of the particle is known, the whole mass of the particle (M_p) can be calculated as following:

$$M_p = M_E / f \quad (4)$$

- If the particle is not aggregated, is spherical in shape and has a known density (ρ), particle size (D) can be calculated as following:

$$D = \sqrt[3]{\frac{6 * M_p}{\rho * \pi}} \quad (5)$$

- For the analysis of aggregates, if the size (D_{pp}), density (ρ) and mass fraction (f) of the primary particle are known, then the number of primary particles per aggregate (N_{pp}) can be calculated:

$$M_{pp} = \frac{{D_{pp}}^3 * \rho * \pi}{6} \quad (6)$$

$$N_{pp} = M_E / M_{pp} \quad (7)$$

where M_{pp} = element mass per primary particle. Due to analytical error and natural size variation, the determined N_{pp} values are usually non-integers but can be rounded for simplicity.

- Particle distribution data can then be expressed in terms of element mass per particle, particle mass, particle size or N_{pp}. We recommend always reporting element mass per particle on the primary x-axis as this parameter is directly measured by spICP-MS. Other derivative parameters can be reported on the secondary axis depending on the information of interest.

S1.5 Population-level information – particle number and mass concentration.

- Particle number concentration (PNC) and particle element mass concentration (PMC) can be calculated with the following:

$$\text{PNC} = F_{event} / \text{acquisition time} / \text{flow rate} / \text{TE} / \text{IE} \quad (8)$$

$$\text{PMC} = \Sigma M_E / \text{acquisition time} / \text{flow rate} / \text{TE} \quad (9)$$

where F_{event} = frequency of the particle event over the period of the acquisition time and ΣM_E = sum of the element mass per particle for all particles.

S2. Tables and figures

Table S1. Details for sample and standard preparation methods

Material	Source	Sample preparation
Dissolved Fe, Al & As standards	Agilent Environmental Calibration Standard, product #5183-4688	Diluted in 1% HCl to 0-1,000 ppb
Dissolved Au standards	LGC noble metal standard, product #SM40-100	Diluted in 1% HCl to 0-50 ppb
Dissolved C standards	Potassium hydrogen phthalate	Diluted in 1% HCl to 0-20 ppm
30 nm Au NPs	NanoPartz, product # A11-30-Cit	Sonication for 10 minutes, diluted to ~10^5 particles/ml in H_2O
33 nm Au NPs	In-house standard from NanoEarth*, confirmed by TEM	Sonication for 10 minutes, diluted to ~10^5 particles/ml in H_2O
50 nm Au NPs	Sigma Aldrich, product #742007	Sonication for 10 minutes, diluted to ~10^5 particles/ml in H_2O
1 µm polystyrene microplastic beads	microParticles GmbH, product # PS-F-KM392-2	Unsonicated/sonication for 10 minutes, diluted to 1 ppm in H_2O or 1% HCl
2.5 µm polystyrene microplastic beads	Fluidigm, product #201078	Vortexed vigorously for 1 minute and analyzed immediately undiluted
13 nm biogenic (BioMag) and abiogenic (AbioMag) magnetite NPs	BioMag synthesized via microbial reduction of ferrihydrite by *Geobacter sulfurreducens* (Byrne et al., 2011) and washed 3 times with H_2O. AbioMag synthesized abiotically via co-precipitation of Fe(II) and Fe(III) (C. I. Pearce et al., 2012). Size and shape were previously characterized (Sundman et al., 2020).	Total Fe concentration first determined via spectrophotometric ferrozine assay (Hegler et al., 2008). Samples then serially diluted in H_2O with 5-10 seconds of vortexing in-between dilutions
As-containing colloids from	Household sand filter and garden soils were collected from Hanoi,	Microcosms were shaken and large particles were

microcosm experiments	Vietnam (20.848518 N; 105.919483 E). Sand, soil or 1:1 mixture of the two (2.5 g) was then incubated at 28°C in the dark in the presence of 125 ml of anoxic artificial rainwater (in 225 cm^3 serum bottles).	allowed to settle for 24 hrs while standing. About 1 ml of suspensions were sampled directly from the top and diluted 100-fold in anoxic H_2O. All sampling performed in an anoxic glovebox.
Fe-C-rich flocs	Flocs were collected from bog and fen in Stordalen Mire, Abisko, Sweden. The flocs were collected in a sterilized HPDE 1L bottle, immediately put in dry ice, transported to the station, and stored at 4°C in the dark. (	1 L Schott bottles containing ~1 L of samples were briefly shaken by inversion and then left standing for 30 minutes. About 10 ml of suspensions were sampled directly from the top and diluted 100-fold in MQ H_2O. Samples were then analyzed untreated, with 5 minutes of N_2 degassing or with 5 minutes of sonication

*Virginia Tech National Center for Earth and Environmental Nanotechnology Infrastructure

Table S2. Measurement details and detection limits for the measured elements

Mass	Measurement mode	DL element mass per particle (fg)	DL size (nm)	Assumptions for size calculation
^{12}C	NoGas	91	564	Polystyrene microplastic, f_C = 0.923, ρ = 1.05 g/cm^3
^{27}Al	He = 1 ml/min	1.4	109	Al_2O_3, f_{Al} = 0.529, ρ = 3.95 g/cm^3
^{56}Fe	He = 1 ml/min	0.9	66	Magnetite, f_{Fe} = 0.724, ρ = 7.87 g/cm^3
			94	Ferrihydrite, f_{Fe} = 0.523, ρ = 3.8 g/cm^3
^{75}As	He = 1 ml/min	0.4	-	-
^{197}Au	He = 1 ml/min	0.06	18	Au NPs, f_{Au} = 1 , ρ = 19.3 g/cm^3

Values shown correspond to ideal condition determined from blanks (rinse acids or MQ H_2O). Background thresholding was applied using SD = 3 and MCP = 3 for all elements. For ^{12}C, an additional correction factor for ionization efficiency (IE = 0.1) was applied, following

determination via analysis of microplastic standards. DL = detection limit; *f* = element mass fraction; ρ = particle density.

Table S3. Size and particle number concentration of particle standards

Material	Measured size (nm)	Particle number concentration (particles/ml)	
		Measured	**Expected[a]**
33 nm Au NPs	32 ± 4	1×10^5	10^5
30 nm Au NPs	32 ± 5	8×10^5	10^6
	31 ± 5	8×10^5	
	29 ± 3	8×10^4	10^5
	30 ± 3	9×10^4	
50 nm Au NPs	50 ± 10	6×10^4	10^5
	50 ± 10	2×10^5	
	49 ± 10	4×10^4	
1 µm polystyrene	992 ± 167	4×10^6	5×10^6
microplastic beads[b]	1,068 ± 200	4×10^6	5×10^6
	1,008 ± 136	2×10^6	2×10^6
2.5 µm polystyrene	2,707 ± 470	3×10^5	3×10^5
microplastic beads	2,460 ± 691	6×10^4	3×10^5

[a]Expected values calculated assuming no errors in dilution.

[b]Different stocks of diluted standards are prepared for each analysis day. All samples were dispersed via 10 minutes of sonication or vigorous vortexing for 1 minute.

Table S4: Compaction factor and associated parameters for magnetite aggregates

Sample	D_H (nm)[a]	spICP-MS concentration (ppb Fe)	Number-weighted mean		Number-weighted median		Mass-weighted mean	
			N_{pp}	CF[b]	N_{pp}	CF[b]	N_{pp}	CF[b]
BioMag	3671 ± 670	10	1230 ± 6	0.34	580 ± 17	0.16	3840 ± 91	1.0 5
AbioMag	1567 ± 192	10	1540 ± 70	0.98	832 ± 11	0.53	3797 ± 324	2.4 2
BioMag	3671 ± 670	100	2251 ± 479	0.61	978 ± 216	0.27	8101 ± 1650	2.2 1
AbioMag	1567 ± 192	100	4477 ± 1177	2.86	2691 ± 887	1.72	8263 ± 1674	5.2 7

[a]Z-average hydrodynamic diameters (D_H) obtained from DLS measurements at 100 ppm Fe.

[b]CF = Compaction Factor = N_{pp}/D_H

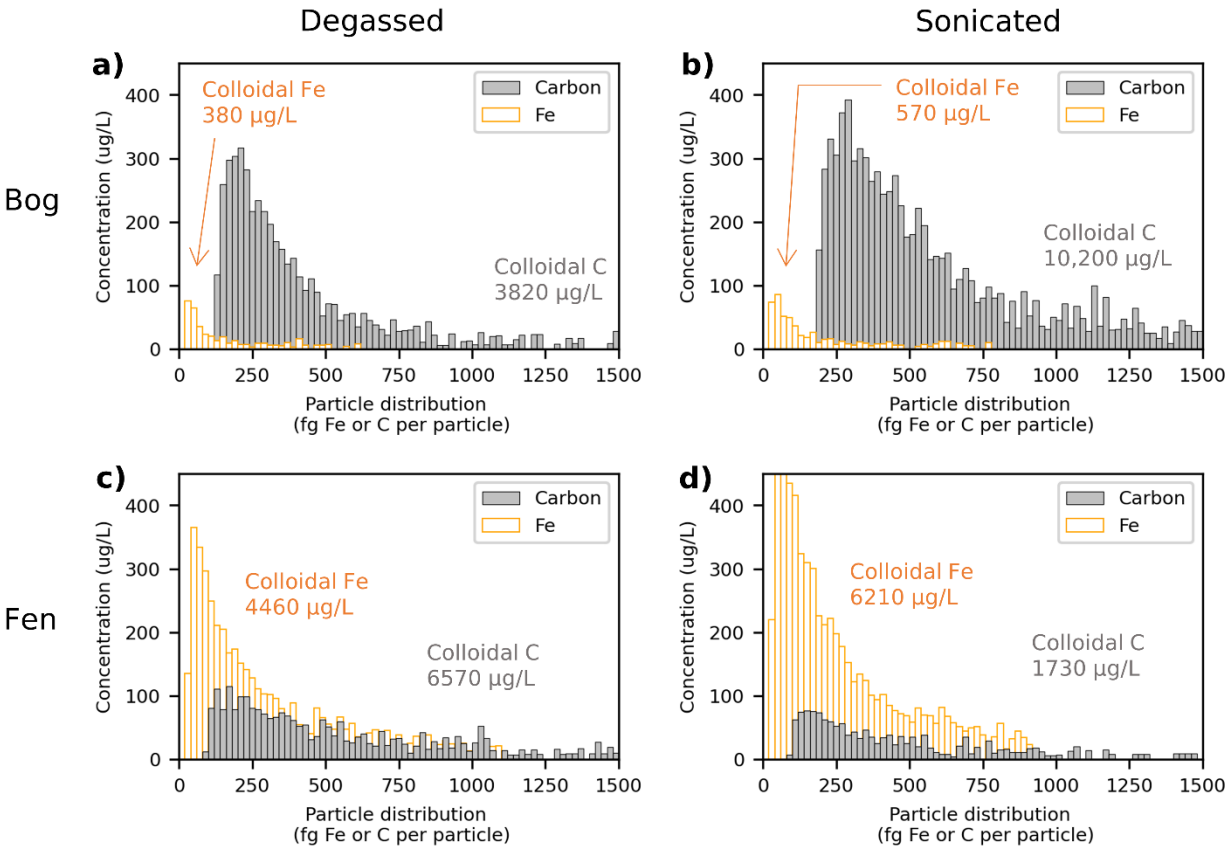

Figure S1. Selected replicate analysis of colloidal flocs. The samples came from either (a-b) bog or (c-d) fen. They were treated by degassing for 5 minutes with N_2 (to remove CO_2) or sonicated to break weakly-bonded agglomerates. Compared to untreated samples (Figure 4 in the main text), degassed and sonicated samples had a lower C detection limit, more detection of smaller colloids, and overall higher concentrations of colloidal C and Fe. Irrespective of treatments, the particle distribution trends are similar and bog samples always have higher C/Fe than fen.

References

Bolea-Fernandez, E., Leite, D., Rua-Ibarz, A., Liu, T., Woods, G., Aramendia, M., Resano, M., Vanhaecke, F., 2019. On the effect of using collision/reaction cell (CRC) technology in single-particle ICP-mass spectrometry (SP-ICP-MS). Anal. Chim. Acta 1077, 95–106. https://doi.org/10.1016/j.aca.2019.05.077

Byrne, J.M., Telling, N.D., Coker, V.S., Pattrick, R.A.D., van der Laan, G., Arenholz, E., Tuna, F., Lloyd, J.R., 2011. Control of nanoparticle size, reactivity and magnetic properties during the bioproduction of magnetite by Geobacter sulfurreducens. Nanotechnology 22, 455709. https://doi.org/10.1088/0957-4484/22/45/455709

Hegler, F., Posth, N.R., Jiang, J., Kappler, A., 2008. Physiology of phototrophic iron(II)-oxidizing bacteria: Implications for modern and ancient environments. FEMS Microbiol. Ecol. 66, 250–260. https://doi.org/10.1111/j.1574-6941.2008.00592.x

Jiménez-Lamana, J., Abad-Álvaro, I., Bierla, K., Laborda, F., Szpunar, J., Lobinski, R., 2018. Detection and characterization of biogenic selenium nanoparticles in selenium-rich yeast by single particle ICPMS. J. Anal. At. Spectrom. 33, 452–460.

Laborda, F., Gimenez-Ingalaturre, A.C., Bolea, E., Castillo, J.R., 2020. About detectability and limits of detection in single particle inductively coupled plasma mass spectrometry. Spectrochim. Acta Part B At. Spectrosc. 169, 105883. https://doi.org/https://doi.org/10.1016/j.sab.2020.105883

Pace, H.E., Rogers, N.J., Jarolimek, C., Coleman, V.A., Higgins, C.P., Ranville, J.F., 2011. Determining Transport Efficiency for the Purpose of Counting and Sizing Nanoparticles via Single Particle Inductively Coupled Plasma Mass Spectrometry. Anal. Chem. 83, 9361–9369. https://doi.org/10.1021/ac201952t

Patzner, M. S.; Mueller, C. W.; Malusova, M.; Baur, M.; Nikeleit, V.; Scholten, T.; Hoeschen, C.; Byrne, J. M.; Borch, T.; Kappler, A.; Bryce, C. Iron Mineral Dissolution Releases Iron and Associated Organic Carbon during Permafrost Thaw. *Nat. Commun.* **2020**, *11* (1), 1–11. https://doi.org/10.1038/s41467-020-20102-6.

Pearce, C.I., Qafoku, O., Liu, J., Arenholz, E., Heald, S.M., Kukkadapu, R.K., Gorski, C.A., Henderson, C.M.B., Rosso, K.M., 2012. Synthesis and properties of titanomagnetite (Fe3-xTixO4) nanoparticles: A tunable solid-state Fe(II/III) redox system. J. Colloid Interface Sci. 387, 24–38. https://doi.org/10.1016/j.jcis.2012.06.092

Sundman, A., Vitzthum, A.-L., Adaktylos-Surber, K., Figueroa, A.I., van der Laan, G., Daus, B., Kappler, A., Byrne, J.M., 2020. Effect of Fe-metabolizing bacteria and humic substances on magnetite nanoparticle reactivity towards arsenic and chromium. J. Hazard. Mater. 384, 121450. https://doi.org/https://doi.org/10.1016/j.jhazmat.2019.121450

Chapter 5 _ Paper 4: Personal contribution

Sampling campaigns, lab work, and manuscript writing were done by **Anh Van Le** with the support and feedback of Muammar Mansor and Andreas Kappler. Andreas Kappler obtained funding and conceptualized the study. Sample preparation, measurement, and data analysis for XAS were done by Juan Lezama Pacheco, Eva Marie M and Sören Drabesch. The Moessbauer spectra were collected by and analyzed by Timm Bayer. and Prachi Joshi. The manuscript was revised by all co-authors.

Chapter 5: Environmental risk of arsenic mobilization from disposed sand filter materials

Anh Van Le[1], E. Marie Muehe[2,3], Soeren Drabesch[1], Juan Lezama Pacheco[4], Timm Bayer[1], Prachi Joshi[1], Andreas Kappler[1,5], Muammar Mansor[1*]

[1]Geomicrobiology, Department of Geosciences, University of Tuebingen, 72076 Tuebingen, Germany
[2]Plant Biogeochemistry, Department of Geosciences, University of Tuebingen, 72076 Tuebingen, Germany
[3]Plant Biogeochemistry, Department of Environmental Microbiology, Helmholtz Centre for Environmental Research - UFZ, 04318 Leipzig, Germany
[4]Department of Earth System Science, Stanford University, Stanford, California 94305, United States
[5]Cluster of Excellence: EXC 2124: Controlling Microbes to Fight Infection, University of Tuebingen, 72076 Tuebingen, Germany

Published in: Environmental Science & Technology

https://doi.org/10.1021/acs.est.2c04915

Abstract

Arsenic (As)-bearing water treatment residuals (WTRs) from household sand filters is usually disposed on top of floodplain soils and may act as a secondary As contamination source. We hypothesized that open disposal of these filter-sand to soils will facilitate As release under reducing conditions. To quantify the mobilization risk of As, we incubated filter-sand, soil, and a mixture of filter-sand and soil in anoxic artificial rainwater and followed the dynamics of reactive Fe and As in aqueous, solid, and colloidal phases. Microbially-mediated Fe(III)/As(V) reduction led to the mobilization of 0.1-4% of total As into solution, with the highest As released from the mixture microcosms equaling 210 µg/L. Due to filter-sand and soil interaction, Moessbauer and X-ray absorption spectroscopies indicated that up to 10% Fe(III) and 32% As(V) was reduced in the mixture microcosm. Additionally, the mass concentration of colloidal Fe, and As analyzed by single-particle ICP-MS, decreased by 77-100% compared to the onset of reducing conditions, with the highest decrease observed in the mixture setups (>95%). Overall, our study suggests that (i) soil provides bioavailable components (e.g., organic matter) that promote As mobilization via microbial reduction of As-bearing Fe(III) (oxyhydr)oxides and (ii) As mobilization as colloids is important especially right after the onset of reducing conditions, but its importance decreases over time.

5.1. Introduction

Drinking water treatment facilities generate vast quantities of residuals that are enriched in contaminants (Ippolito et al., 2011; Turner et al., 2019). These water treatment residuals (WTRs) are commonly discharged in landfills in regions with sufficient space and resources (Clancy et al., 2013; Sullivan et al., 2010). However, in As-affected areas in rural South Asia, management of As-bearing WTRs is poor, leading to the open disposal of As-bearing WTRs to ponds, rivers, and soils without any site preparation (Genuchten et al., 2022; Koley, 2022). A challenge in the management of As-bearing WTRs is inadequate testing procedures that are not representative of actual conditions in the disposal sites, thus leading to over- or underprediction of As remobilization (Clancy et al., 2013). Common leach test, such as the toxicity characteristic leaching procedure (TCLP) have been shown to underpredict As mobilization from WTRs in landfills (Ghosh et al., 2004; Islam et al., 2011), since the test do not account for microbial activities that change over long periods and redox fluctuations (Clancy et al., 2013; Sullivan et al., 2010). A recent study (Genuchten et al., 2022) indicated that open disposal strategies especially pose the highest potential risk to environment and human health.

In the Red River delta in Vietnam, household sand filters are regularly used to remove toxic As from groundwater for drinking purposes. The groundwater is filtered through a reactive sand layer by gravity, in which Fe and As co-oxidize and precipitate on the sand matrix (Nitzsche et al., 2015a; Van Le et al., 2022b; Voegelin et al., 2014). Eleven million people rely on household sand filters in Vietnam (data in 2007) (Berg et al., 2007; Winkel et al., 2011). With an average 3.5 people per (reported in 2009) (General Statistics Office of Vietnam, 2011), this means that around 3.1 million household with sand filters. The implication of this is that around 2.1×10^5 tons of sand filter residues is openly disposed to the environment every 6 months (assuming 0.47 m^2 surface area, 1470 kg/m^3 density, 35% porosity, 10 cm of sand layer disposed every 6 months) (Voegelin et al., 2014). The As mobilization risk from these staggering amount of materials has yet to be investigated. Other As contaminated sources from mining waste were previously reported to cause pollution to soil and crops around the disposal area (Ha et al., 2019; Hoang et al., 2021).

The mobilization risk of As from filter-sand is susceptible to redox alteration. Under oxic conditions, arsenic primarily exists as oxidized As(V) adsorbed to

Fe(III) (oxyhydr)oxides (Voegelin et al., 2014). During the monsoon season, with frequent and heavy rainfall and potential flood events, the disposed filter-sand turns anoxic and reducing, leading to a high risk of As release to the porewater. The general accepted mechanisms of As mobilization are via microbial reduction of As-bearing Fe(III) (oxyhydr)oxides (Connolly et al., 2022; Stuckey et al., 2016a), as well as the direct reduction of As(V) to As(III) by As-reducing bacteria (AsRB) (Oremland and Stolz, 2003). As(III) has a lower adsorption affinity to Fe(III) (oxyhydr)oxides than As(V), and is thus more amenable to mobilization (Dixit and Hering, 2003).

Open disposal of As-contaminated filter-sand material to the topsoil leads to mixing with complex soil matrix that contains diverse microbial communities, organic matter (OM), and minerals (e.g., Fe-Al-Mn (oxyhydr)oxides). The interaction between disposed filter-sand (enriched with As) and soil, therefore potentially plays a crucial but poorly understood role in the fate of As. Another factor to consider is whether disposed filter-sand is mobilized in the form of colloids, similar to the transport mechanism of other toxic contaminants in natural waters (Hassellov and von der Kammer, 2008). We define colloids as small particles subject to suspension and mobilization; this definition encompasses particles with size ranges that are beyond the traditionally considered 1-µm size cutoff (Noël et al., 2020). An increase of mobilized colloidal Fe(III) (oxyhydr)oxides can further facilitate As(V) transport (Montalvo et al., 2018; Yao et al., 2020). At the same time, colloidal Fe(III) (oxyhydr)oxides are known to be more susceptible to microbial reduction than larger mineral aggregates, therefore possibly promoting solubilization of As-bearing colloidal Fe(III) minerals (Fan et al., 2018; Ma et al., 2018; Mansor and Xu, 2020). Thus, it is crucial to also consider colloid-facilitated transport of As to fully evaluate the risk of As mobilization (Bauer and Blodau, 2009; Gomez-Gonzalez et al., 2016; Mansor et al., 2021).

In this study, we performed microcosm experiments in which As-bearing WTRs from filter-sand, soil, and a mixture of filter-sand and soil were incubated under reducing conditions over 130 days. We followed changes in reactive Fe(II), Fe minerals, As redox states and coordination environment in the solid phase, and the dynamics of dissolved and colloidal Fe and As over time. The results allowed us to assess the mobilization risk of As from open disposal of sand filter material

5.2. Materials and methods

5.2.1 Field site and sample collection.

We collected disposed filter-sand materials from several household filters in Tu Nhien village (20.848518 N; 105.919483 E), around 25 km Southeast of Hanoi, Vietnam, inside the meander of the Red River. Soil samples (top 20 cm) were collected from several gardens in the same village – we collected soils that were not in contact before with disposed filter material. Filter-sand and floodplain soils were collected in 5 independent replicates immediately cooled on ice during transport, and stored at 4°C. In the laboratory, filter-sand or floodplain soils were used alone (100%) or mixed at a ratio of 1:1 before being used for incubation experiments.

5.2.2 Filter-sand and soil samples characterization.

The elemental composition (Fe, Al, P, As, Mn) of disposed filter-sand, floodplain soil, and the mixture of filter-sand and soil were analyzed by microwave digestion followed by inductively coupled plasma mass spectrometry analysis (ICP-MS) (Agilent 7900, Agilent Technologies). After drying in the oven (105°C), 0.5 grams of the sample was added to 12 ml of aqua-regia solution (9 ml of 37% HCl and 3 ml of 65% HNO_3) in Xpress Plus Teflon vessels. The samples were digested in the Microwave Accelerated Reaction System, MARS 6 (CEM, USA), with further details in SI section S1.

For total organic carbon (TOC) quantification, samples were dried at 60°C, grounded, and analyzed in triplicates with a soliTOC cube (Elementar Analysensysteme GmbH, Germany)

5.2.3 Microcosm experiments.

Microcosms were set up by adding 12.5 grams of disposed filter-sand, or soil, or pre-mixed 1:1 filter-sand and soil into 125 ml of sterile anoxic artificial rainwater (ARW; Table S1, section S2) within 250 ml serum bottles. Thus, the solid: liquid ratio is 1:10 in all bottles. The initial pH of all microcosms ranged from 6.8 to 7.3 (Table 1). Additionally, abiotic controls were amended with 160 mM sodium azide (NaN_3) to inhibit microbial respiration. All microcosms were prepared in triplicate in an anoxic glovebox (100% N_2, <30 ppm O_2, MBRAUN UNIlab). The microcosms were kept standing vertically at 28°C in the dark without shaking until analysis.

5.2.4 Solution chemistry analysis.

Immediately before sampling, the microcosms were homogenized by shaking. Aliquot suspensions (3 ml) were collected in two 2 ml Eppendorf tubes (1.5 ml in each) and centrifuged for 15 min at 12,100 g in the glovebox. The supernatants was filtered (0.22 µm cellulose filter, EMD Millipore) and diluted with 1% HNO_3 for quantification of dissolved Fe and As by ICP-MS. Sediment pellets remaining after centrifugation were either extracted with (a) 1 ml 0.5 M HCl for 2 hours (to quantify bioavailable/ poorly crystalline Fe) or (b) 1 ml 6 M HCl for 24 hours (to quantify crystalline Fe) (Schaedler et al., 2018). Afterwards, all samples were centrifuged at 15 min at 12100g, and 100 µl of the supernatant was collected and diluted 10-folds with 1 M HCl before analysis. HCl-extractable Fe(II) and Fe(total) were quantified spectrophotometrically using the ferrozine assay (Stookey, 1970; Viollier et al., 2000).

5.2.5 Iron mineral analysis using Moessbauer spectroscopy.

Moessbauer spectroscopy was used to identify Fe minerals. Pre-incubation samples were loaded as dried powders into 1 cm^2 Plexiglas holders. Solids from the microcosms collected by filtration (0.45 µm nitrocellulose filter, Millipore) were fixed between two pieces of Kapton tape in the glovebox and kept frozen and anoxically at -20°C in a sealed bottle until measurement. Spectra were collected at 77 K and 5 K using a constant acceleration drive system (WissEL) in transmission mode with a $^{57}Co/Rh$ source. Analyses were carried out using Recoil (University of Ottawa) and the Voigt Based Fitting (VBF) routine (Lagarec and Rancourt, 1997).

5.2.6 X-ray absorption spectroscopy (XAS).

To identity As redox states and binding environments, samples were collected prior to incubation and from the microcosms, then freeze-dried, ground, and stored anoxically until measurement.

Reference model compounds were synthesized in an anoxic glovebox by adsorbing arsenate ($Na_2HAsO_4x7H_2O$, Sigma-Aldrich) and arsenite ($AsNaO_2$, Sigma-Aldrich) onto ~30 mg of freshly prepared 500 mM ferrihydrite (Muehe et al., 2013) in a molar ratio of 30:1 for 10 hours with gentle overhead-mixing. Model compounds were washed twice in anoxic MQ water, freeze-dried, ground and diluted with approximately 26 mg of boron nitride and stored anoxically until measurement. Samples and standards were placed in aluminum sample holders (window 3 mm by 13 mm) and

sealed with 0.5 mil Kapton tape from both sides. Arsenic K-edge extended X-ray absorption fine structure (EXAFS) data were obtained at beamline 7-3 at Stanford Synchrotron Radiation Lightsource (SSRL), Menlo Park, USA. Spectra were collected in fluorescence detection mode using a 30-element germanium detector array, using a reference gold foil in transmission detection mode and calibrating to 11919 eV. More details on beamline settings are given in SI section S3. Data was deadtime-corrected and averaged with Sixpack (Webb, 2005) and repetitive scans aligned, merged, truncated, deglitched, normalized to an edge step of one, and background-subtracted in Athena (Ravel and Newville, 2005). To verify data, XANES (extracted from EXAFS) and EXAFS were analyzed for As speciation differences. Principle components (PCA) and target transforms were analyzed for merged scans, followed by least-square fitting by linear combination (LCF) of synthesized model compound spectra(Muehe et al., 2016). EXAFS were analyzed to a k of 12. The LCF components are estimated to be accurate at 10% and the detection limit of contributing components is set to 10% (Cancès et al., 2005; O'Day et al., 2004). Shell-by-shell fitting was performed to support LCF fits, given in SI section S3.

5.2.7 Quantification of Fe and As in colloidal fraction.

Microcosms were shaken, and large particles were allowed to settle for 24 hours while standing in the glove box. Afterward, about 0.1 ml of suspension was carefully sampled directly from the top and stored anoxically at 4°C. The suspensions were diluted 1000-fold in anoxic H_2O in a Falcon tube in the glove box and taken out right before the analysis. All samples were analyzed in time-resolved analysis mode on an Agilent 7900 ICP-MS instrument (Mansor et al., 2021). More details are provided in SI section S4.

5.3. Results and discussion

5.3.1 Characterization of disposed filter-sand and floodplain soil prior to incubation experiments.

Microwave digestion and TOC analyses were performed to quantify elemental (Fe, Al, P, As, Mn) and organic carbon contents. The samples contained 50-100 g/kg of Fe, 22-80 g/kg of Al, 1-5 g/kg of P, 29-1440 mg/kg of As, 540-1166 mg/kg of Mn, and 2-12 g/kg of TOC (Table 1). The filter-sand material was enriched in Fe, P, and As relative to the soil, with an enrichment factor of approximately 2, 5, and 50, respectively. The soil was enriched in Al, Mn, and organic carbon, with an approximate enrichment factor of 4, 2, and 6, respectively. Aqua regia extraction followed by microwave digestion most likely underestimated soil's total Fe and Al content due to poor extractability of Fe phyllosilicates (Raiswell et al., 1994). In contrast, Fe in disposed filter-sand material primarily exists as short-range ordered (SRO) Fe(III) (oxyhydr)oxides (Voegelin et al., 2014) that are easily extractable with aqua regia.

Table 1. Elemental compositions of floodplain soil, disposed filter-sand material, and the mixture of filter-sand and soil prior to incubation. All samples were analyzed in triplicates.

	Floodplain soil	Disposed filter-sand material	Mixture of filter-sand and soil
Fe (g/kg)	50±4	97±6	76±8
Al (g/kg)	79±6	22±2	55±6
P (g/kg)	1±0.1	5±0.5	3±0.3
As (mg/kg)	29±3	1441±81	725±64
Mn (mg/kg)	1166±92	539±52	911±153
Fe/Mn ratio	42.5±0.1	182.4±28.3	84.3±6.3
Fe/As ratio	1723±39	67.5±0.6	105±3
TOC (g/kg)	11.7±0.4	3.2±0.2	7.2±0.2
Initial pH*	6.8	7.3	7.2

(*) Initial pH values of the microcosms

5.3.2 Dynamics of reactive Fe and As in floodplain soil and disposed filter-sand microcosms.

As- and Fe-rich sand filter materials are usually disposed onto the floodplain soil or along the riverbank. To evaluate the potential for As mobilization from the filter-sand

after disposal, we first incubated filter-sand and soil samples separately with ARW under reducing conditions. Within 130 days of incubation, the color changed from orange/gray to a darker black in the biotic microcosms, indicative of Fe(III) reduction (Figure S1). The highest Fe(III) reduction took place in the soil microcosms, in which 0.5 M HCl-extractable Fe(II) increased from 0.008 to 4.6 g/kg sediment (Figure 1A). This equals to near-complete Fe(III) reduction from the 0.5 M HCl-extractable fraction (93±8%) (Figure S2A). In comparison, microcosms with filter-sand only displayed a limited extent of Fe(III) reduction, in which the 0.5 M HCl-extractable Fe(II) increased from 0.15 to 1.1 g/kg sediment (Figure 1A). This equals a reduction of only 6±1% of the poorly crystalline Fe pool (Figure S2A). Similar trends were observed in the 6 M-extractable Fe(II) and Fe(II)/Fe(total) ratios (Figure S2, S3 respectively), albeit with a lower magnitude of changes compared to the 0.5 M HCl-extractable fractions.

Dissolved total Fe was detected in small amounts in all microcosms; it increased from 2 to 4.2 mg/L in filter-sand microcosms. In contrast, the concentration remained around 0.7-0.9 mg/L in soil microcosms throughout the incubation (Figure 1B). Interestingly, even though total As in the soil was lower relative to the disposed filter-sand, we detected the constant release of As from soil to the aqueous phase from 3 to 115 µg/L over 130 days (Figure 1C). In comparison, dissolved As in filter-sand microcosms increased sharply during the first 40 days to around 150 µg/L, which then leveled off until the end of the experiment (Figure 1C). Abiotic controls for both microcosms showed low levels of Fe(III) reduction and As mobilization, possibly due to abiotic processes or incomplete inhibition of microbial activity by NaN_3(Bore et al., 2017) . 0.5 M HCl-extractable Fe(II) and dissolved As were <0.5 g/kg and <60 µg/L, respectively, which were lower than the values observed in the experimental setups without microbial inhibition (Figure 1C).

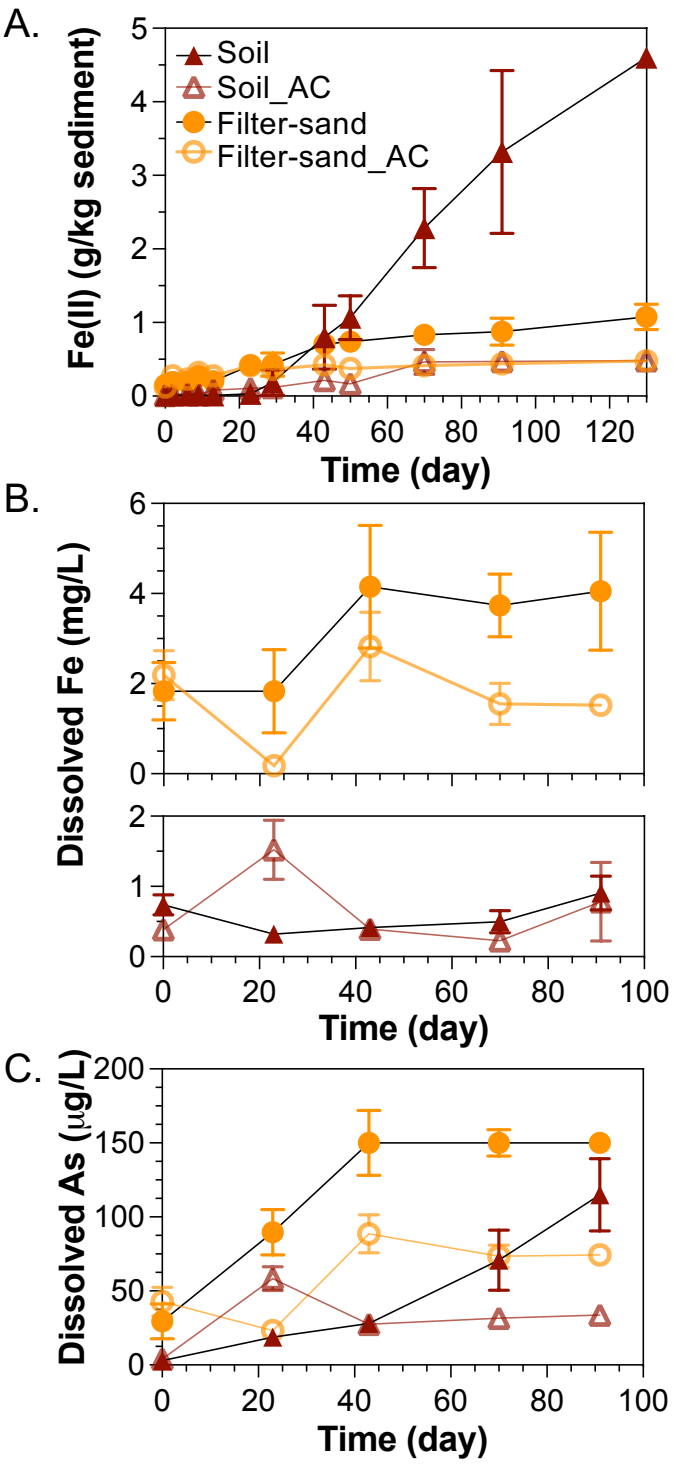

Figure 1. Changes in the concentration of 0.5 M HCl-extractable Fe(II) (A), dissolved Fe (B), and dissolved As (C) in floodplain soil, disposed filter-sand and their abiotic control (AC) microcosms. All samples were analyzed in triplicate, and error bars indicate standard deviation.

5.3.3 Dynamics of reactive Fe and As in the microcosm containing the mixture of filter-sand and soil.

We hypothesized that when disposed filter-sand is mixed with soil, the microbial community and/or organic matter from the soil matrix may promote As mobilization from the disposed filter-sand by stimulating microbial Fe(III) and As(V) reduction. Therefore, we followed changes of reactive Fe and As in the mixture of filter-sand and soil microcosms (termed “sand-soil interaction”) and compared them to a “no-interaction” scenario. The values for the “no interaction” scenario were calculated by averaging the data obtained in soil-only and filter-sand only microcosms as a method of applying mass correction. This scenario, therefore, represents a hypothetical case that accounts for the mass of Fe and As in both soil and filter-sand and implicitly assumes the soil matrix plays no role in promoting or inhibiting Fe and As reduction.

By comparing the experimental sand-soil interaction case with the hypothetical “no interaction” case, we were able to clearly observe a promotive effect of sand-soil interaction to Fe(III) and As(V) reduction, which overall led to about twice more As being mobilized compared to “no interaction”. The content of 0.5 M HCl-extractable Fe(II) increased significantly in the mixture of filter-sand and soil from 0.07 to 3.5 g/kg, which is 1.2 times higher than the “no interaction” case (Figure 2A). Similar trends were observed in the 6 M HCl-extractable Fe(II) and Fe(II)/Fe(total) ratios (Figure S2, S3), albeit with a lower magnitude of changes compared to the 0.5 M HCl-extractable fractions.

The dissolved Fe concentration of the mixture microcosm was slightly lower than in the “no interaction” case. Dissolved Fe in the mixture of filter-sand and soil microcosms and abiotic control at day 0 (immediately after setup of the microcosm) was higher than on other days. – We consider this to be an outlier, possibly due to short-term mixing effects between the soil and filter-sand materials. Disregarding these data points, dissolved Fe gradually increased from 0.7 mg/L on day 23 to 2.1 mg/L, but remained lower than the “no interaction” case throughout the incubation period (Figure 2B).

Lastly, dissolved As showed a marked increase in the mixture setup (up to 210 µg/L) relative to abiotic controls (maximum 90 µg/L) and the “no interaction” scenario (maximum 120 µg/L) (Figure 2C). It means that As mobilization was promoted 1.8

times higher due to the sand-soil interaction than the “no-interaction” case. Abiotic controls for the mixture microcosms showed lower levels of Fe(III) reduction and As mobilization overall (Figure 2).

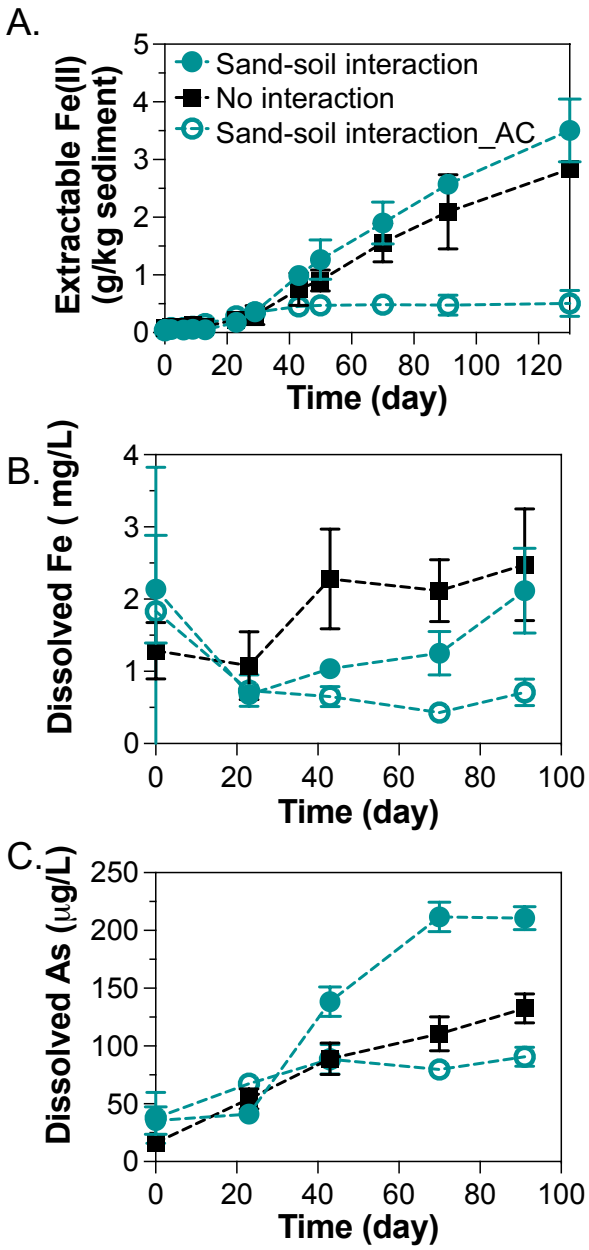

Figure 2. Comparison of Fe and As dynamics in the presence or absence of sand-soil interactions. Changes of poorly crystalline Fe (0.5M HCl-extractable Fe), dissolved Fe and As of the sand-soil interaction (mixture of filter-sand and soil) microcosms and their abiotic control (AC) microcosms are shown in figure A, B, C respectively. The data is compared with corresponding value in the no-interaction case. The no-interaction value is calculated with values obtained from soil only and filter-sand only microcosms, assuming 1:1 mixture and no promotion or inhibition effects. All samples were analyzed in triplicate, and error bars indicate standard deviation.

5.3.4 Transformation of Fe minerals in the microcosms.

Changes in Fe mineralogy can affect the fate of As and were therefore followed by Moessbauer spectroscopy. Fitting results and Moessbauer spectra collected at 5 K and 77 K are shown in Table S2 and Figures S5-S7, respectively. The disposed filter-sand material prior to incubation consisted of 100% short-range-order (SRO) Fe(III) (oxyhydr)oxides (Figure 3A, Table S2), consistent with previous studies on sand filters (Nitzsche et al., 2015a; Voegelin et al., 2014). After 100 days of incubation, there was up to 14% of Fe(II) in the filter-sand matrix (Figure 3A), equaling a Fe(II)/Fe(III) ratio of 0.17 (Figure 3B), indicative of microbial Fe(III) reduction. In comparison, the soil initially contained a mixture of goethite (50%), low amounts of hematite (11%), Fe(III) phyllosilicates (25%), and Fe(II) (14%) (Figure 3A). The Fe(II) in the pre-incubation soil was likely in the form of phyllosilicates and not adsorbed Fe(II), as the soil had been sampled under oxic conditions. We observed a ~6.3% increase in Fe(II) after 100 days in the soil incubations, equaling a Fe(II)/Fe(III) ratio of 0.25 (Figure 3B). Note that the increased Fe(II) observed based on spectra collected at 5K may be slightly underestimated as the Fe(II) doublet can partially split at lower temperatures(Notini et al., 2018). Based on the spectra collected at 77K, the Fe(II) increased by 11% (Table S2). The mixture of filter-sand and soil microcosm showed Fe mineral distributions that reflect the end-member sand and soil, with detectable levels of goethite, SRO Fe(III) (oxyhydr)oxides, and Fe(II) and Fe(III) phyllosilicates. We observed an increase of around 3.4% Fe(II) in the mixture setup after 100 days (Figure 3) based on the Mössbauer spectra at 5K and 10% based on spectra collected at 77K. We did not observe the formation of distinct Fe(II)-containing minerals such as magnetite or siderite.

In summary, we confirmed Fe(III) reduction in all microcosms. The filter-sand microcosm exhibited the highest relative increase in solid-phase Fe(II) over 100 days of incubation. This is because filter-sand material consisted of nearly 100% (SRO) Fe(III) (oxyhydr)oxides in the form of two-line ferrihydrite (Voegelin et al., 2014), which is more thermodynamically available for microbial reduction than hematite and goethite (Kappler et al., 2021) found in soils.

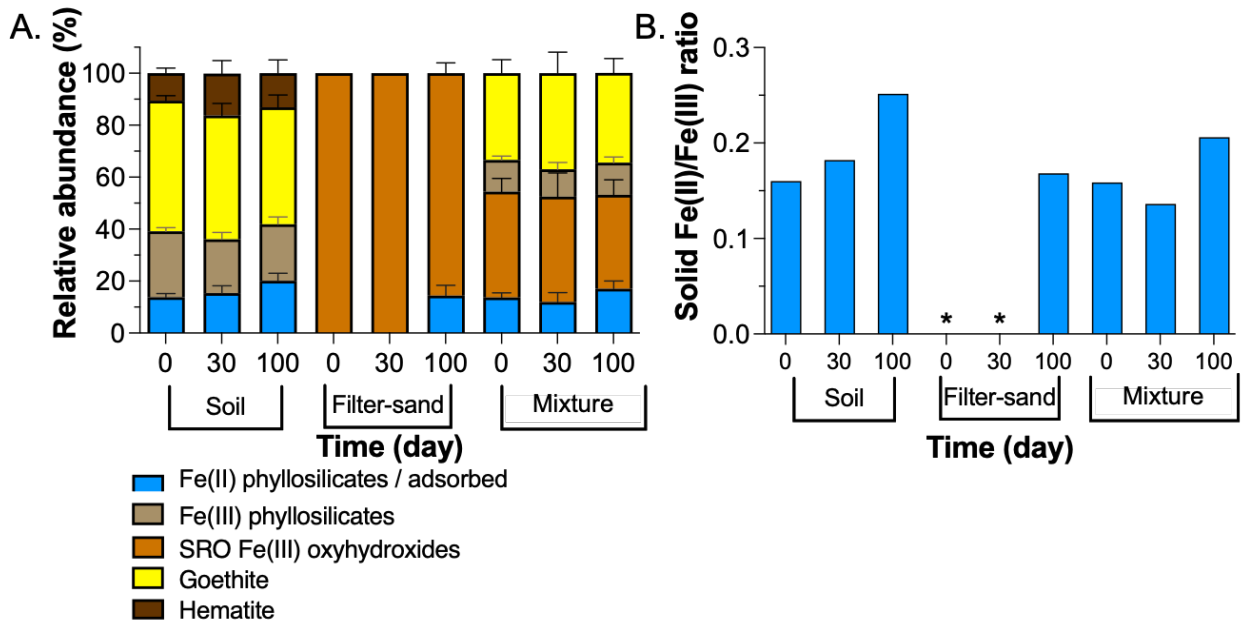

Figure 3. Fe mineralogy based on Moessbauer spectroscopy. Changes of relative abundance of Fe minerals, measured temperature at 5 K (A) and ratios difference of Fe(II)/Fe(III) phases (B) over time in 3 different microcosms (soil, filter-sand, and the mixture of filter-sand and soil). (*) No Fe(II) detected in sand microcosms at days 0 and 30.

5.3.5 Changes in solid phase As redox state and implications for As binding environment in the microcosms.

To determine changes in As redox states in the solid matrix, samples were analyzed at days 0, 30, and 84 by XANES and EXAFS at the As K-edge using a linear combination fitting (LCF) approach (Figures 4, S8, S9). XANES and EXAFS As speciation analyses showed comparable trends with minor differences in percentage contributions (Table S3). Arsenic redox distribution indicated that the disposed filter-sand and soil samples initially contained up to 90% As(V) and less than 10% As (III) (Figure 4A). After incubation, the As(III) contribution in sand microcosms increased by 23.6% of total As (Figure 4A). In the mixtures of filter-sand and soil, As(III) was increased by 32% of the total As pool (Figure 4A), corresponding to an increase of As(III) from 41.3 to 273 mg/kg (Figure 4B).

Analysis of As EXAFS data suggested As-Fe complex in all microcosms (at a distance of 2.88Å radial structure function equal to 3.3Å in real distances) (Figure 4C), corresponding to As-Fe inner-sphere complexes dominated by a bidentate-mononuclear edge-sharing (^{2}E) formation on the surface of Fe(III) (oxyhydr)oxides (Fendorf et al., 1997; Ona-Nguema et al., 2005). This type of complex might result

from As-O-O-As multiple scattering (Manning et al., 1998; Ona-Nguema et al., 2005; Sherman and Randall, 2003). Overall, As K-edge EXAFS to the k of 12 were not able to resolve outer-sphere As binding beyond 3.5Å, which were more typically found above 5Å (Catalano et al., 2008). Shell-by-shell fits did not show any clear trend for As coordination differences between sand, soil and sand-soil mixture (SI Table S4). On a more descriptive note, in the mixture samples at day 30 and 84 and not in the filter-sand only or soil only microcosms, a shift from 2.88Å (= 3.3Å in real distances) to lower Å was observed compared to day 0. This shift caused the 2.88Å peak to be more diffuse suggesting that an outer-sphere As binding contribution possibly stemming of As mobilized from disposed filter-sand material now re-adsorbed in a slightly tighter coordination onto soils (arrows in Figure 4C).

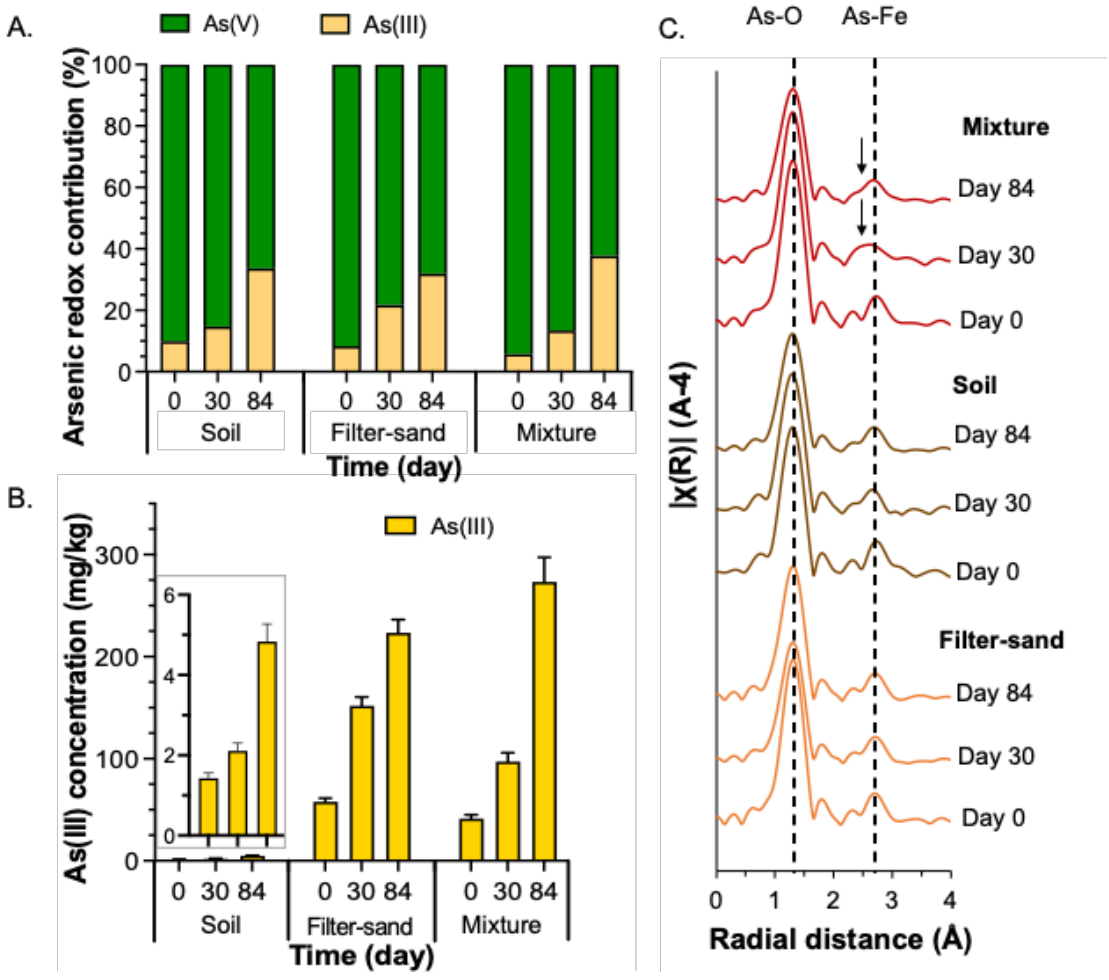

Figure 4. Changes of As redox contribution obtained by LC fitting of XANES data (A) calculated solid phase As(III) concentration combing XANES data and extraction data (B) and As K-edge EXAFS Fourier transform magnitude (C) over time in 3 different microcosms (soil, filter-sand, and the mixture of filter-sand and soil). Arsenic EXAFS *k*3 graphs of samples are shown in the supplement Figure S8.

5.3.6 Dynamics of colloidal Fe and As in the microcosms.

In our microcosms, we observed colloids that regularly remained suspended near the top of the solution. This led us to investigate changes in Fe and As contents in the colloidal fraction, as they can also be potentially mobilized and are reactive. We investigated the changes of Fe and As in the colloidal fraction at 3-time points (days 0, 30, and 100) by single particle ICP-MS (spICP-MS). Our previous work already showed a strong correlation between colloidal Fe and As but not with Al, suggesting that colloidal Fe is the main carrier of As instead of Al (Mansor et al., 2021).

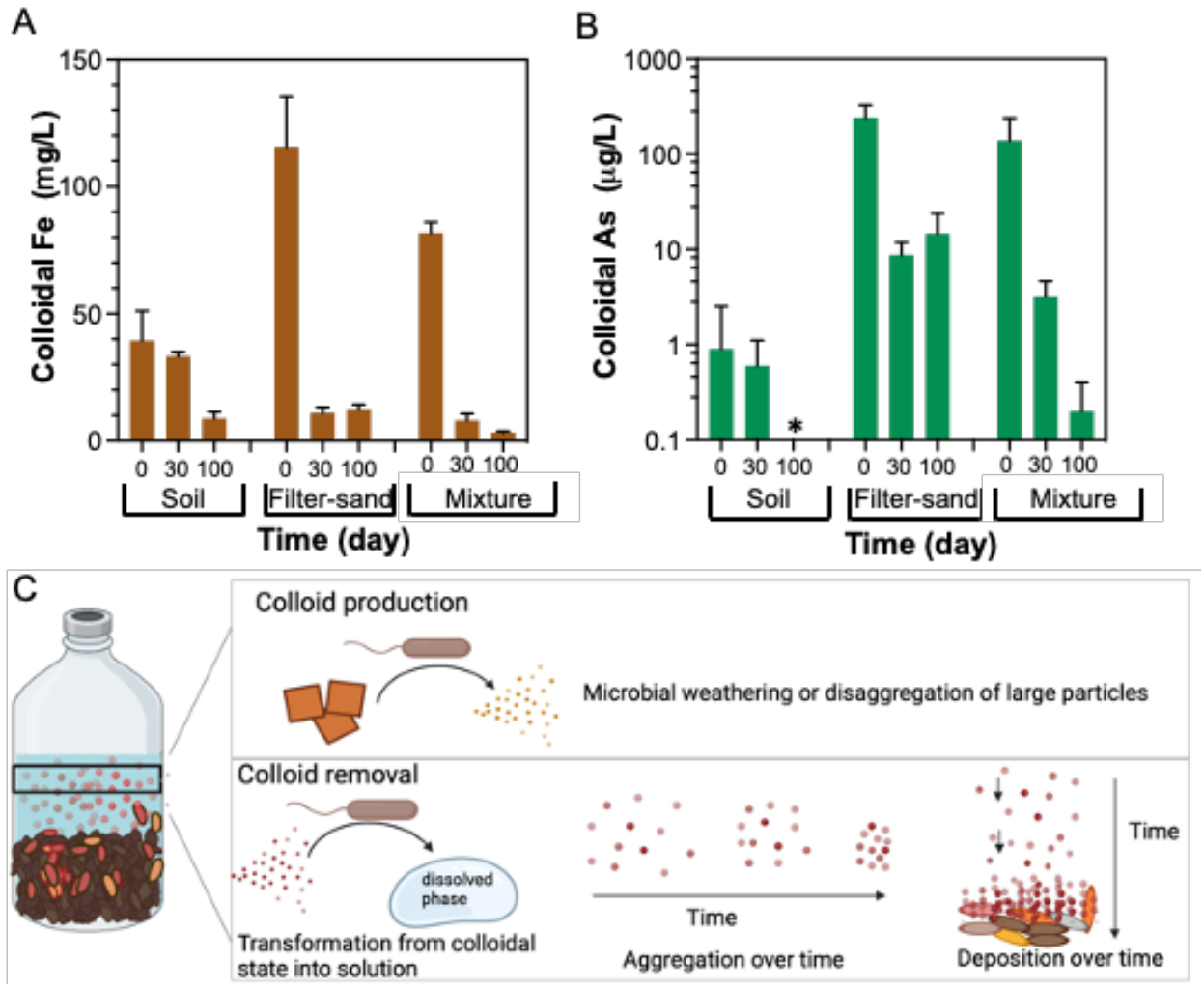

Figure 5. Changes in colloidal mass concentration of Fe and As in microcosms (A and B, respectively) containing either soil, disposed filter-sand or the mixture of filter-sand and soil over time. All samples were analyzed in triplicate and error bars indicate standard deviation. (*) No colloidal As detected in soil microcosms at day 100. Schematic conceptualization of colloid production and removal in the microcosms is shown in figure C.

Consistent with our expectation, the results indicated that the filter-sand material was the main source of colloidal Fe and As at day 0, with mass concentrations of 115 mg/L Fe and 240 µg/L As, respectively (Figure 5). These concentrations are much higher than dissolved Fe and As measured in the microcosms. In comparison, lower amounts of colloidal Fe and As were detectable in soil microcosms. The mixture of filter-sand and soil had intermediate amounts of colloidal Fe and As, in-between the unmixed filter-sand and soil microcosms. The colloidal Fe/As ratios were elevated by a factor of 5 to 141 compared to the microwave digestion-extractable fraction. This is likely due to the presence of small (but detectable) Fe-rich particles with As contents below the detection limit of spICP-MS (0.81 fg As/particle; Table S5), thus causing elevated colloidal Fe/As ratios. Over 100 days of incubation, we observed colloidal Fe and As decreased over time. The most pronounced decrease was observed in the mixture microcosms, in which over 90% of the colloidal mass was removed by the end (Figure 5).

5.3.7 Sand-soil interactions promote Fe and As reduction, leading to As mobilization.

Our results indicated that open disposal of filter-sand to soils and mixing between the two can promote microbial reduction and mobilization of As-bearing Fe(III) (oxyhydr)oxides. We propose three non-exclusive mechanisms that can explain this observation. First, sand materials provide Fe(III) minerals that are more reactive (e.g., ferrihydrite) compared to those found in soils (e.g., goethite, hematite). Microbial reduction rates of ferrihydrite are generally up to 2 orders of magnitude faster than for goethite and hematite that were in the soil samples (Cutting et al., 2009; Kappler et al., 2021). Second, soil-associated organic carbon is likely to be more reactive than organic carbon associated with sand materials. During the flood season (June to October), massive amounts of organic-rich fluvial sediment are deposited in floodplain soils (Connolly et al., 2022; Smedley and Kinniburgh, 2002). The soil organic carbon in the Red River delta was previously identified to be derived predominantly from C_3/C_4 plant (Eiche et al., 2017). The water extractable fraction of this organic matter was shown to trigger microbial reduction of As-bearing Fe(III) (oxyhydr)oxides in the same sediments (M. Glodowska et al., 2020). Last but not least, microbial input from the soil to the filter-sand can promote the activities of iron(III)- and arsenic(V)-reducing

bacteria in the mixture of filter-sand and soil. Iron-reducing bacteria such as *Shewanella* and *Geobacter* are common bacterial groups that are responsible for microbial reductive dissolution of As-bearing Fe(III) (oxyhydr)oxides in flooded soil (Corsini et al., 2011; Huang, 2014). Additionally, arsenate reducers are phylogenetically diverse and frequently present in paddy soils. They can directly reduce As(V) to toxic As(III) via dissimilation (ArrAB gene) or detoxification (*ars* gene) mechanisms (Huang, 2014; Vaxevanidou et al., 2015, 2012; Zhu et al., 2017).

Colloidal Fe and As were observed in our system, suggesting that As mobilization in the form of colloids could be substantial. Colloids can form in the environment due to seasonal water table changes and physical perturbation such as caused by heavy precipitation (Kretzschmar et al., 1999; Ma et al., 2018; Zhao et al., 2017). The production and removal mechanisms of colloids in the microcosms are schematized in Figure 5C. In our microcosms, colloids are produced by partial dissolution or disaggregation (weathering) of larger particles (Hochella Jr et al., 2019). Conversely, colloids can be removed by i) complete dissolution of colloidal particles and ii) aggregation or deposition over time to form larger particles (Kretzschmar et al., 1999; Noël et al., 2020). Despite high concentrations of colloids at the initial stages of our experiments, we observed a strong decrease in colloidal As and Fe over time. This indicates a lower risk of colloidal As mobilization over time, and the removal of colloids is faster than their production in our experiments.

There are two possible reasons for this observation. First, since colloids are highly reactive and bioavailable, anaerobic bacteria might prefer Fe(III) and As(V) in the colloidal fraction to obtain energy for growth. Indeed, the reduction rate of Fe(III)-reducers such as *Geobacter* and *Shewanella* species are faster when supplied with small-sized Fe(III) (oxyhydr)oxides (Mansor and Xu, 2020). Since the amount of colloidal Fe and As made up <1.2 % of the total Fe and As extractable by aqua regia, a significant amount of colloids can be reduced without impacting the mass balance of the system.

Alternatively, since our microcosms were incubated standing with brief shaking only before sampling, there was ample time over the 100 days incubation period for aggregation and deposition of colloids to proceed. The stability of Fe colloids can be considered in terms of the C/Fe ratio of the systems. At low organic C/Fe ratios, as found in our experiments (C/Fe < 0.2), colloidal Fe is not stabilized by organic

matter(Liao et al., 2017). Therefore, the colloids were more susceptible to forming larger aggregates (Amstaetter et al., 2012; Liao et al., 2017). This was followed by the deposition of the colloids by gravitational sedimentation over time, with larger aggregates leading to faster deposition (Liao et al., 2017).

5.4. Environmental implications

Our results indicated that a combined total of 116-390 µg/L of aqueous and colloidal As (0.3-4% of total As) was released from the solid phase. The remaining 96.0-99.7% of As was retained in the solid phases. In comparison, a recent estimate suggests that 100% of the As from open disposal will be mobilized to either soils or water over 100 years (Genuchten et al., 2022). The comparison between our experiments and this model estimation is not direct, but our results would at least suggest that As can be retained in the original solid phases over a period of a few months. Therefore, we anticipate different implications of As remobilization from filter-sand materials. First, short-distance transport (centimeters to meters) can lead to As being retained primarily in the surrounding soils. This is not an immediate concern unless the soil is then used for agricultural purposes, in which case this can lead to increased As contents in consumable plants. Second, frequent flooding and anoxic conditions can lead to enhanced long-distance transport (e.g., kilometers) of As in the form of colloids and aqueous phases, entering water sources such as aquifers and rivers. This is especially bad if As is released into groundwater aquifers, wells or rivers that are used for drinking water consumption and which were previously tested to have low As concentrations below the drinking water threshold. Thus, continuous testing is recommended for areas that utilize the open disposal method. The ultimate fate of remobilized As will need to be constrained in the context of flooding events (Connolly et al., 2022) and the heterogenous distribution of As in soils (Fakhreddine et al., 2021), and these will have varying influence from site-to-site.

Redox fluctuations are particularly important in the field due to changes in precipitation frequency throughout the year. Redox fluctuations can influence the crystallinity of Fe(III) (oxyhydr)oxides (Thompson et al., 2006). Ferrihydrite – the main host of As – can be transformed into more crystalline phases such as goethite or hematite as a result of redox fluctuations (Kocar and Fendorf, 2009). Additionally, redox fluctuations

can promote organic carbon degradation in the aerobic zones near the surface, thus limiting the availability of organic carbon for anaerobic metabolisms at depth (Stuckey et al., 2016b). Incubation under cycled redox conditions is required in future experiments to understand changes in Fe mineralogy, organic carbon availability, and how these affect the release of colloidal and aqueous As.

5.5. Acknowledgements

This work was funded by the German Research Foundation (DFG, KA1736/41-1). We thank M. Latimer for beamline support (proposal number 5587). Use of the Stanford Synchrotron Radiation Lightsource, SLAC National Accelerator Laboratory, is supported by the U.S. Department of Energy, Office of Science, Office of Basic Energy Sciences under Contract No. DE-AC02-76SF00515. The SSRL Structural Molecular Biology Program is supported by the DOE Office of Biological and Environmental Research, and by the National Institutes of Health, National Institute of General Medical Sciences (including P41GM103393). The contents of this publication are solely the responsibility of the authors and do not necessarily represent the official views of NIGMS or NIH. AVL acknowledges the feedbacks from S.J.Hug for the manuscript and the help of P.Tutiyasarn and T.Schlereth for sampling and experiment setup. AK acknowledges infrastructural support by the DFG under Germany's Excellence Strategy, cluster of Excellence EXC2124, project ID 390838134. Graphical abstract created with BioRender.com.

5.6. References

Amstaetter, K., Borch, T., Kappler, A., 2012. Influence of humic acid imposed changes of ferrihydrite aggregation on microbial Fe(III) reduction. Geochim. Cosmochim. Acta 85, 326–341. https://doi.org/10.1016/j.gca.2012.02.003

Bauer, M., Blodau, C., 2009. Arsenic distribution in the dissolved, colloidal and particulate size fraction of experimental solutions rich in dissolved organic matter and ferric iron. Geochim. Cosmochim. Acta 73, 529–542. https://doi.org/10.1016/j.gca.2008.10.030

Berg, M., Stengel, C., Trang, P.T.K., Hung Viet, P., Sampson, M.L., Leng, M., Samreth, S., Fredericks, D., 2007. Magnitude of arsenic pollution in the Mekong and Red River Deltas - Cambodia and Vietnam. Sci. Total Environ. 372, 413–425. https://doi.org/10.1016/j.scitotenv.2006.09.010

Bore, E.K., Apostel, C., Halicki, S., Kuzyakov, Y., Dippold, M.A., 2017. Soil microorganisms can overcome respiration inhibition by coupling intra-and extracellular metabolism: 13C metabolic tracing reveals the mechanisms. ISME J. 11, 1423–1433. https://doi.org/10.1038/ismej.2017.3

Cancès, B., Juillot, F., Morin, G., Laperche, V., Alvarez, L., Proux, O., Hazemann, J.-L., Brown, G.E., Calas, G., 2005. XAS evidence of As (V) association with iron oxyhydroxides in a contaminated soil at a former arsenical pesticide processing plant. Environ. Sci. Technol. 39, 9398–9405.

Catalano, J.G., Park, C., Fenter, P., Zhang, Z., 2008. Simultaneous inner-and outer-sphere arsenate adsorption on corundum and hematite. Geochim. Cosmochim. Acta 72, 1986–2004.

Clancy, T.M., Hayes, K.F., Raskin, L., 2013. Arsenic waste management: A critical review of testing and disposal of arsenic-bearing solid wastes generated during arsenic removal from drinking water. Environ. Sci. Technol. 47, 10799–10812. https://doi.org/10.1021/es401749b

Connolly, C.T., Stahl, M.O., DeYoung, B.A., Bostick, B.C., 2022. Surface Flooding as a Key Driver of Groundwater Arsenic Contamination in Southeast Asia. Environ. Sci. Technol. 56, 928–937. https://doi.org/10.1021/acs.est.1c05955

Corsini, A., Cavalca, L., Zaccheo, P., Crippa, L., Andreoni, V., 2011. Influence of microorganisms on arsenic mobilization and speciation in a submerged contaminated soil: Effects of citrate. Appl. Soil Ecol. 49, 99–106. https://doi.org/10.1016/j.apsoil.2011.06.010

Cutting, R.S., Coker, V.S., Fellowes, J.W., Lloyd, J.R., Vaughan, D.J., 2009. Mineralogical and morphological constraints on the reduction of Fe (III) minerals by Geobacter sulfurreducens. Geochim. Cosmochim. Acta 73, 4004–4022.

Dixit, S., Hering, J.G., 2003. Comparison of arsenic(V) and arsenic(III) sorption onto iron oxide minerals: Implications for arsenic mobility. Environ. Sci. Technol. 37, 4182–4189. https://doi.org/10.1021/es030309t

Eiche, E., Berg, M., Hönig, S.M., Neumann, T., Lan, V.M., Pham, T.K.T., Pham, H.V., 2017. Origin and availability of organic matter leading to arsenic mobilisation in aquifers of the Red River Delta, Vietnam. Appl. Geochemistry 77, 184–193. https://doi.org/10.1016/j.apgeochem.2016.01.006

Fakhreddine, S., Prommer, H., Scanlon, B.R., Ying, S.C., Nicot, J.P., 2021. Mobilization of arsenic and other naturally occurring contaminants during managed aquifer recharge: A critical review. Environ. Sci. Technol. 55, 2208–2223. https://doi.org/10.1021/acs.est.0c07492

Fan, L., Zhao, F., Liu, J., Frost, R.L., 2018. The As behavior of natural arsenical-containing colloidal ferric oxyhydroxide reacted with sulfate reducing bacteria. Chem. Eng. J. 332, 183–191. https://doi.org/10.1016/j.cej.2017.09.078

Fendorf, S., Eick, M.J., Grossl, P., Sparks, D.L., 1997. Arsenate and chromate retention mechanisms on goethite. 1. Surface structure. Environ. Sci. Technol. 31, 315–320. https://doi.org/10.1021/es950653t

General Statistics Office of Vietnam, 2011. The Vietnam Population and Housing Census 2009—Age-sex structure and marital status of the population in Vietnam.

Genuchten, C.M. Van, Etmannski, T.R., Jessen, S., Breunig, H.M., 2022. LCA of Disposal Practices for Arsenic-Bearing Iron Oxides Reveals the. https://doi.org/10.1021/acs.est.2c05417

Ghosh, A., Mukiibi, M., Ela, W., 2004. TCLP underestimates leaching of arsenic from solid residuals under landfill conditions. Environ. Sci. Technol. 38, 4677–4682. https://doi.org/10.1021/es030707w

Glodowska, M., Stopelli, E., Schneider, M., Lightfoot, A., Rathi, B., Straub, D., Patzner, M., Duyen, V.T., Berg, M., Kleindienst, S., Kappler, A., 2020. Role of in Situ Natural Organic Matter in Mobilizing As during Microbial Reduction of FeIII-Mineral-Bearing Aquifer Sediments from Hanoi (Vietnam). Environ. Sci. Technol. 54, 4149–4159. https://doi.org/10.1021/acs.est.9b07183

Gomez-Gonzalez, M.A., Bolea, E., O'Day, P.A., Garcia-Guinea, J., Garrido, F., Laborda, F., 2016. Combining single-particle inductively coupled plasma mass spectrometry and X-ray absorption spectroscopy to evaluate the release of colloidal arsenic from environmental samples. Anal. Bioanal. Chem. 408, 5125–5135.

Ha, N.T.H., Ha, N.T., Nga, T.T.H., Minh, N.N., Anh, B.T.K., Hang, N.T.A., Duc, N.A., Nhuan, M.T., Kim, K.W., 2019. Uptake of arsenic and heavy metals by native plants growing near Nui Phao multi-metal mine, northern Vietnam. Appl. Geochemistry 108. https://doi.org/10.1016/j.apgeochem.2019.104368

Hassellov, M., von der Kammer, F., 2008. Iron oxides as geochemical nanovectors for metal transport in soil-river systems. Elements 4, 401–406.

Hoang, A.T.P., Prinpreecha, N., Kim, K.W., 2021. Influence of mining activities on arsenic concentration in rice in asia: A review. Minerals 11, 1–14. https://doi.org/10.3390/min11050472

Hochella Jr, M.F., Mogk, D.W., Ranville, J., Allen, I.C., Luther, G.W., Marr, L.C., McGrail, B.P., Murayama, M., Qafoku, N.P., Rosso, K.M., 2019. Natural, incidental, and engineered nanomaterials and their impacts on the Earth system. Science (80-.). 363, eaau8299.

Huang, J.H., 2014. Impact of microorganisms on arsenic biogeochemistry: A review. Water. Air. Soil Pollut. 225. https://doi.org/10.1007/s11270-013-1848-y

Ippolito, J.A., Barbarick, K.A., Elliott, H.A., 2011. Drinking Water Treatment Residuals : A Review of Recent Uses 2, 1–12. https://doi.org/10.2134/jeq2010.0242

Islam, M.S., Al Mamun, M.A., Islam, M.N., 2011. Leachability Of Arsenic From Wastes Of Arsenic Removal Units Using Modified Toxicity Characteristic Leaching Procedure. J. Life Earth Sci. 6, 19–26. https://doi.org/10.3329/jles.v6i0.9716

Kappler, A., Bryce, C., Mansor, M., Lueder, U., Byrne, J.M., Swanner, E.D., 2021. An evolving view on biogeochemical cycling of iron. Nat. Rev. Microbiol. 19, 360–374. https://doi.org/10.1038/s41579-020-00502-7

Kocar, B.D., Fendorf, S., 2009. Thermodynamic constraints on reductive reactions influencing the biogeochemistry of arsenic in soils and sediments. Environ. Sci. Technol. 43, 4871–4877. https://doi.org/10.1021/es8035384

Koley, S., 2022. Future perspectives and mitigation strategies towards groundwater arsenic contamination in West Bengal, India. Environ. Qual. Manag. 31, 75–97. https://doi.org/10.1002/tqem.21784

Kretzschmar, R., Borkovec, M., Grolimund, D., Elimelech, M., 1999. Mobile Subsurface Colloids and Their Role in Contaminant Transport. Adv. Agron. 66, 121–193. https://doi.org/10.1016/S0065-2113(08)60427-7

Lagarec, K., Rancourt, D.G., 1997. Extended Voigt-based analytic lineshape method for determining N-dimensional correlated hyperfine parameter distributions in Mössbauer spectroscopy. Nucl. Instruments Methods Phys. Res. Sect. B Beam Interact. with Mater. Atoms 129, 266–280.

Liao, P., Li, W., Jiang, Y., Wu, J., Yuan, S., Fortner, J.D., Giammar, D.E., 2017. Formation, aggregation, and deposition dynamics of nom-iron colloids at anoxic-oxic interfaces. Environ. Sci. Technol. 51, 12235–12245. https://doi.org/10.1021/acs.est.7b02356

Ma, J., Guo, H., Weng, L., Li, Y., Lei, M., Chen, Y., 2018. Distinct effect of humic acid on ferrihydrite colloid-facilitated transport of arsenic in saturated media at different pH. Chemosphere 212, 794–801. https://doi.org/10.1016/j.chemosphere.2018.08.131

Manning, B.A., Fendorf, S.E., Goldberg, S., 1998. Surface structures and stability of arsenic(III) on goethite: Spectroscopic evidence for inner-sphere complexes. Environ. Sci. Technol. 32, 2383–2388. https://doi.org/10.1021/es9802201

Mansor, M., Drabesch, S., Bayer, T., Van Le, A., Chauhan, A., Schmidtmann, J., Peiffer, S., Kappler, A., 2021. Application of Single-Particle ICP-MS to Determine the Mass Distribution and Number Concentrations of Environmental Nanoparticles and Colloids. Environ. Sci. Technol. Lett. https://doi.org/10.1021/acs.estlett.1c00314

Mansor, M., Xu, J., 2020. Benefits at the nanoscale: a review of nanoparticle-enabled processes favouring microbial growth and functionality. Environ. Microbiol. 22, 3633–3649. https://doi.org/10.1111/1462-2920.15174

Montalvo, D., Vanderschueren, R., Fritzsche, A., Meckenstock, R.U., Smolders, E., 2018. Efficient removal of arsenate from oxic contaminated water by colloidal humic acid-coated goethite: Batch and column experiments. J. Clean. Prod. 189, 510–518. https://doi.org/10.1016/j.jclepro.2018.04.055

Muehe, E.M., Morin, G., Scheer, L., Le Pape, P., Esteve, I., Daus, B., Kappler, A., 2016. Arsenic(V) Incorporation in Vivianite during Microbial Reduction of Arsenic(V)-Bearing Biogenic Fe(III) (Oxyhydr)oxides. Environ. Sci. Technol. 50, 2281–2291. https://doi.org/10.1021/acs.est.5b04625

Muehe, E.M., Obst, M., Hitchcock, A., Tyliszczak, T., Behrens, S., Schröder, C., Byrne, J.M., Michel, F.M., Krämer, U., Kappler, A., 2013. Fate of Cd during microbial Fe (III) mineral reduction by a novel and Cd-tolerant Geobacter species. Environ. Sci. Technol. 47, 14099–14109.

Nitzsche, K.S., Lan, V.M., Trang, P.T.K., Viet, P.H., Berg, M., Voegelin, A., Planer-Friedrich, B., Zahoransky, J., Müller, S.K., Byrne, J.M., Schröder, C., Behrens, S., Kappler, A., 2015. Arsenic removal from drinking water by a household sand filter in Vietnam - Effect of filter usage practices on arsenic removal efficiency and microbiological water quality. Sci. Total Environ. 502, 526–536. https://doi.org/10.1016/j.scitotenv.2014.09.055

Noël, V., Kumar, N., Boye, K., Barragan, L., Lezama-Pacheco, J.S., Chu, R., Tolic, N., Brown, G.E., Bargar, J.R., 2020. FeS colloids–formation and mobilization pathways in natural waters. Environ. Sci. Nano 7, 2102–2116.

Notini, L., Latta, D.E., Neumann, A., Pearce, C.I., Sassi, M., N'Diaye, A.T., Rosso, K.M., Scherer, M.M., 2018. The role of defects in Fe (II)–goethite electron transfer. Environ. Sci. Technol. 52, 2751–2759.

O'Day, P.A., Rivera Jr, N., Root, R., Carroll, S.A., 2004. X-ray absorption spectroscopic study of Fe reference compounds for the analysis of natural sediments. Am. Mineral. 89, 572–585.

Ona-Nguema, G., Morin, G., Juillot, F., Calas, G., Brown, G.E., 2005. EXAFS analysis of arsenite adsorption onto two-line ferrihydrite, hematite, goethite, and lepidocrocite. Environ. Sci. Technol. 39, 9147–9155. https://doi.org/10.1021/es050889p

Oremland, R.S., Stolz, J.F., 2003. The ecology of arsenic. Science (80-.). 300, 939–944. https://doi.org/10.1126/science.1081903

Raiswell, R., Canfield, D.E., Berner, R.A., 1994. A comparison of iron extraction methods for the determination of degree of pyritisation and the recognition of iron-limited pyrite formation. Chem. Geol. 111, 101–110.

Ravel, B., Newville, M., 2005. ATHENA, ARTEMIS, HEPHAESTUS: data analysis for X-ray absorption spectroscopy using IFEFFIT. J. Synchrotron Radiat. 12, 537–541.

Schaedler, F., Kappler, A., Schmidt, C., 2018. A revised iron extraction protocol for environmental samples rich in nitrite and carbonate. Geomicrobiol. J. 35, 23–30.

Sherman, D.M., Randall, S.R., 2003. Surface complexation of arsenic(V) to iron(III) (hydr)oxides: Structural mechanism from ab initio molecular geometries and EXAFS spectroscopy. Geochim. Cosmochim. Acta 67, 4223–4230. https://doi.org/10.1016/S0016-7037(03)00237-0

Smedley, P.L., Kinniburgh, D.G., 2002. A review of the source, behavior and distribution of arsenic in natural waters. Appl. Geochemistry 17, 517–568. https://doi.org/10.1016/S0883-2927(02)00018-5

Stookey, L.L., 1970. Ferrozine---a new spectrophotometric reagent for iron. Anal. Chem. 42, 779–781.

Stuckey, J.W., Schaefer, M. V., Kocar, B.D., Benner, S.G., Fendorf, S., 2016. Arsenic release metabolically limited to permanently water-saturated soil in Mekong Delta. Nat. Geosci. 9, 70–76. https://doi.org/10.1038/ngeo2589

Sullivan, C., Tyrer, M., Cheeseman, C.R., Graham, N.J.D., 2010. Disposal of water treatment wastes containing arsenic - A review. Sci. Total Environ. 408, 1770–1778. https://doi.org/10.1016/j.scitotenv.2010.01.010

Thompson, A., Chadwick, O.A., Boman, S., Chorover, J., 2006. Colloid mobilization during soil iron redox oscillations. Environ. Sci. Technol. 40, 5743–5749. https://doi.org/10.1021/es061203b

Turner, T., Wheeler, R., Stone, A., Oliver, I., 2019. Potential Alternative Reuse Pathways for Water Treatment Residuals: Remaining Barriers and Questions—a Review. Water. Air. Soil Pollut. 230. https://doi.org/10.1007/s11270-019-4272-0

Van Le, A., Straub, D., Planer-Friedrich, B., Hug, S.J., Kleindienst, S., Kappler, A., 2022. Microbial communities contribute to the elimination of As, Fe, Mn, and NH4+ from groundwater in household sand filters. Sci. Total Environ. 838, 156496. https://doi.org/10.1016/j.scitotenv.2022.156496

Vaxevanidou, K., Christou, C., Kremmydas, G.F., Georgakopoulos, D.G., Papassiopi, N., 2015. Role of indigenous arsenate and IRON(III) respiring microorganisms in controlling the mobilization of arsenic in a contaminated soil sample. Bull. Environ. Contam. Toxicol. 94, 282–288. https://doi.org/10.1007/s00128-015-1458-z

Vaxevanidou, K., Giannikou, S., Papassiopi, N., 2012. Microbial arsenic reduction in polluted and unpolluted soils from Attica, Greece. J. Hazard. Mater. 241–242, 307–315. https://doi.org/10.1016/j.jhazmat.2012.09.048

Viollier, E., Inglett, P.W., Hunter, K., Roychoudhury, A.N., Van Cappellen, P., 2000. The ferrozine method revisited: Fe (II)/Fe (III) determination in natural waters. Appl. geochemistry 15, 785–790.

Voegelin, Andreas; Kaegi, Ralf; Berg, Michael; Nitzsche, Katja Sonja; Kappler, Andreas; Lan, Vi Mai; Trang, Pham Thi Kim; Göttlicher, Jörg; Steininger, R., 2014. Solid-phase characterisation of an effective household sand filter for As, Fe and Mn removal from groundwater in Vietnam. Environ. Chem. 11, 566–578. https://doi.org/10.1071/EN14011

Webb, S.M., 2005. SIXpack: a graphical user interface for XAS analysis using IFEFFIT. Phys. Scr. 2005, 1011.

Winkel, L.H.E., Trang, P.T.K., Lan, V.M., Stengel, C., Amini, M., Ha, N.T., Viet, P.H., Berg, M., 2011. Arsenic pollution of groundwater in Vietnam exacerbated by deep aquifer exploitation for more than a century. Proc. Natl. Acad. Sci. U. S. A. 108, 1246–1251. https://doi.org/10.1073/pnas.1011915108

Yao, Y., Mi, N., He, C., Yin, L., Zhou, D., Zhang, Y., Sun, H., Yang, S., Li, S., He, H., 2020. Transport of arsenic loaded by ferric humate colloid in saturated porous media. Chemosphere 240. https://doi.org/10.1016/j.chemosphere.2019.124987

Zhao, J., Chen, S., Hu, R., Li, Y., 2017. Aggregate stability and size distribution of red soils under different land uses integrally regulated by soil organic matter, and iron and aluminum oxides. Soil Tillage Res. 167, 73–79. https://doi.org/10.1016/j.still.2016.11.007

Zhu, Y.G., Xue, X.M., Kappler, A., Rosen, B.P., Meharg, A.A., 2017. Linking Genes to Microbial Biogeochemical Cycling: Lessons from Arsenic. Environ. Sci. Technol. 51, 7326–7339. https://doi.org/10.1021/acs.est.7b00689

SUPPLEMENTARY INFORMATION

S1. Quantification of the elemental composition (Fe, Al, P, As, Mn) of samples by microwave digestion

Samples were digested in the Microwave Accelerated Reaction System, MARS 6 (CEM, USA) with 20 minutes of ramp time and 30 minutes of holding time at 180°C. Afterward, the digested samples were transferred into a 50 ml Falcon tube and adjusted to a total volume of 50 ml by adding milliQ water. Samples were centrifuged at 16,873 g for 15 minutes (Thermo Scientific Sorvall LYNX6000), then 100 µl of the supernatant was collected and diluted 100-fold in 1% HNO_3. Samples were stored at 4°C in the dark until analysis via the Agilent 7900 ICP-MS (Agilent Technologies, Santa Clara, CA). Typical long-term reproducibility is ±10%.

S2. Preparation of artificial rainwater

The composition of the artificial rainwater (ARW) was prepared based on report from Viet et al. 2001(Viet et al., 2001) (Table S1). Two liters of ARW were prepared and then flushed with N_2 to remove O_2 from solution and the headspace. Afterwards, the anoxic ARW was sterilized by autoclaving at 121°C for 40 minutes.

Table S1. Composition of artificial rainwater (ARW) medium, designed based on report from Viet et al. 2001 (Viet et al., 2001).

Composition	Concentration/ Value
NH_4Cl (mg/L)	20
$CaSO_4.2H_2O$ (mg/L)	21
$MgCl_2.6H_20$ (mg/L)	3.5
$NaNO_3$ (mg/L)	17
KNO_3 (mg/L)	8
pH	5.3

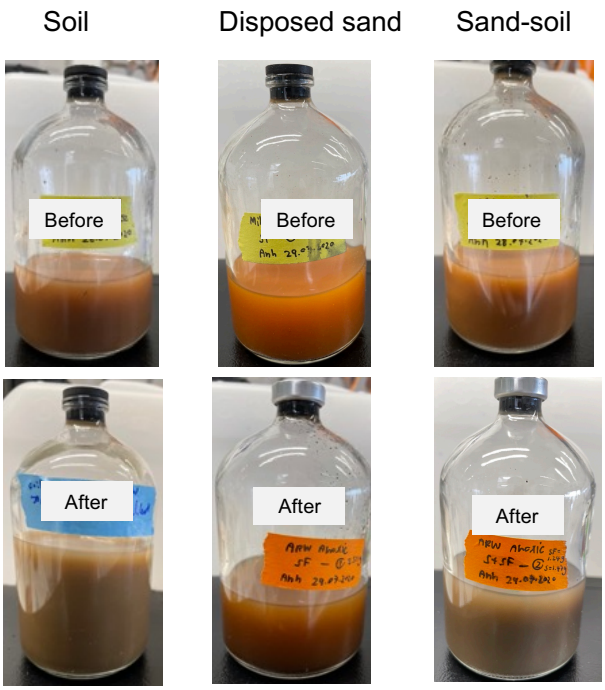

Figure S1. Color changes of the microcosms before and after 130 days of incubation. All bottles (soil, disposed sand, sand-soil mixture) turned darker indicating reducing conditions were present in all the microcosms.

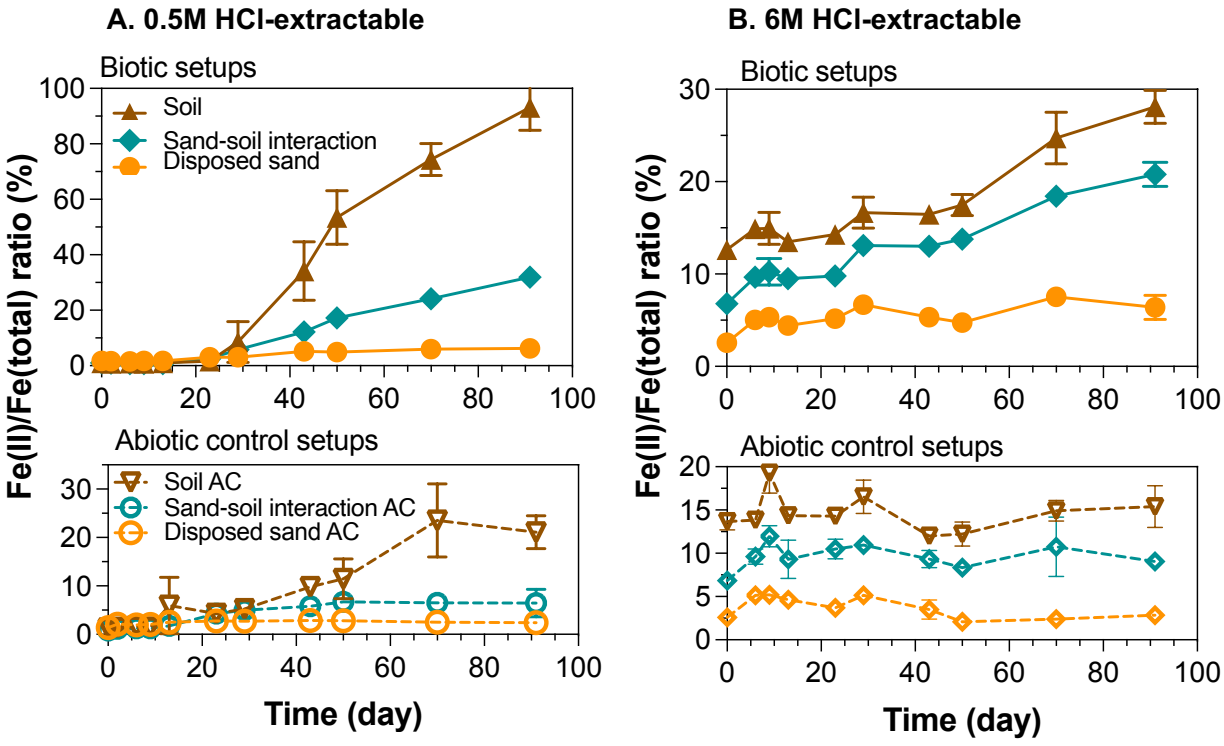

Figure S2. Changes of extractable Fe(II)/Fe(total) ratios over incubation time. The Fe(II)/Fe(total) ratio from highly reactive/poorly crystalline Fe phase extracted by 0.5 M HCl (A) and Fe(II)/Fe(tot) from more crystalline Fe phase extracted by 6 M HCl (B). All samples were analyzed in triplicate and error bars indicate standard deviation.

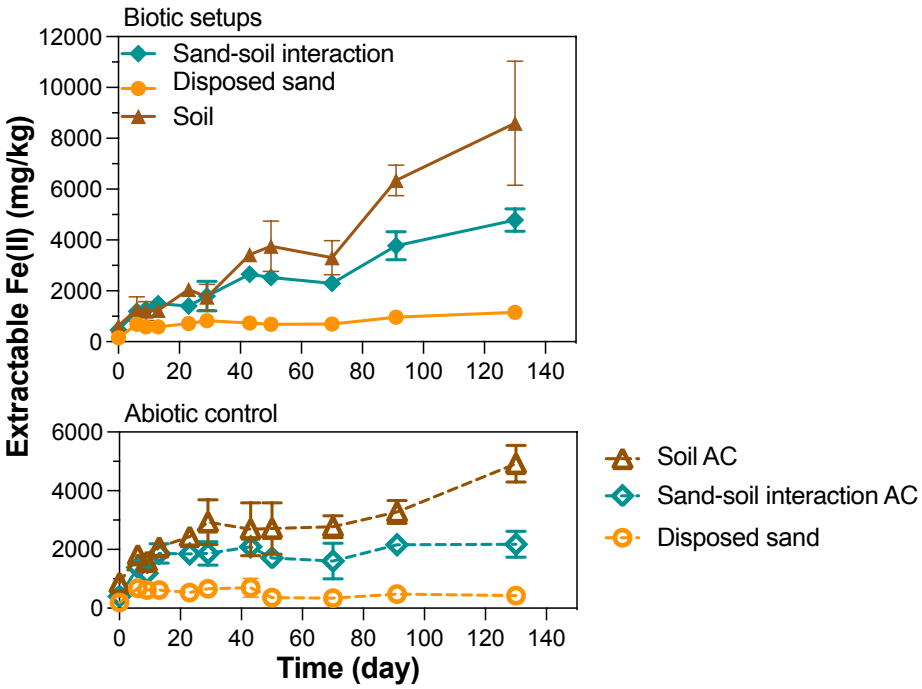

Figure S3. Quantification of changes in crystalline Fe(II) over time from 6 M HCl extraction in soil, disposed sand, sand-soil mixture microcosms and their abiotic controls (AC). All samples were analyzed in triplicate and error bars indicate standard deviation.

To compare sand-soil interaction with “no-interaction” case, we calculated the ratio of Fe(III) reduction, Fe mobilization and As mobilization values in the sand-soil interaction microcosms over corresponding values in the no-interaction case as percentages (Figure S4 A, B, C). Interestingly, the presence of sand-soil interaction did not promote Fe(III) reduction during the first 30 days. We attributed this to a lag phase before microbial Fe(III) reduction became dominant in all biotic microcosms. After 30 days, up to 40% of Fe(III) reduction was promoted by sand-soil interaction in comparison to the no-interaction case (Figure S4-A). Similarly, the interaction promoted more As mobilization (up to 91%) than in the absence of sand-soil interaction (Figure S4-B). However, Fe mobilization was not promoted in the mixture (Figure S4-C).

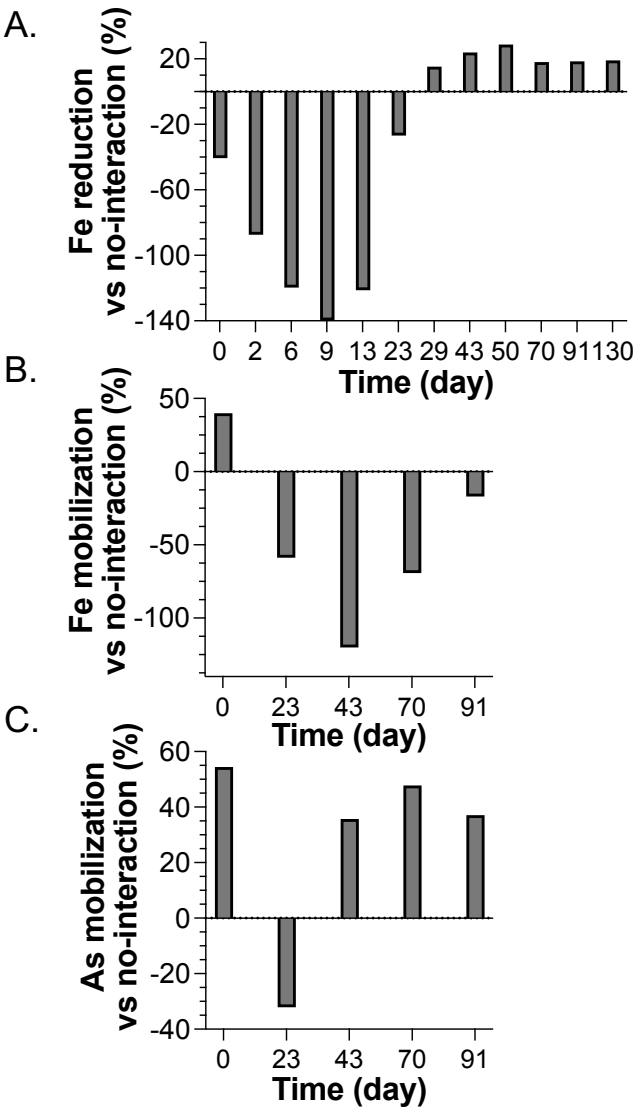

Figure S4. Comparison of Fe and As dynamics with the presence and absence of the sand-soil interactions. The percentage differences of Fe(III) reduction (A), dissolved Fe (B), and As (c) between presence and absence of sand-soil interactions. All samples were analyzed in triplicate, and error bars indicate standard deviation.

Fitting results of Moessbauer spectroscopy in the disposed sand, soil and sand-soil mixture samples

Table S2. Fitting results of Moessbauer spectroscopy. δ – center shift; ΔE_Q – quadrupole splitting; SD (ΔE_Q) – standard deviation of quadrupole splitting; H – hyperfine field; SD(H) – standard deviation of hyperfine field; R.A. – Relative area; red. χ2 – goodness of fit

Sample/info	*δ* (mm/s)	*ΔE$_Q$* (mm/s)	H (T)	SD(H) (T)	R.A. %	Error	Red. χ2
Sand day0 – 77 K							0.81
Short-range-order (SRO) Fe(III) (oxyhydr)oxide / phyllosilicate	0.41	0.69			100	4.9	
Sand day 0 – 5 K							1.76
Fe(III) phyllosilicate	0.57	0.89			5.26	0.66	
Fe(II) phyllosilicate / adsorbed*	1.23	2.91			5.34	0.67	
SRO Fe (III) (oxyhydr)oxide	0.48	-0.27	46.6	4.0	89.4	8.90	
Sand day 30 – 77 K							0.63
SRO Fe(III) (oxyhydr)oxide	0.47	0.84			100		
Sand day 30 – 5 K							0.71
SRO Fe (III) (oxyhydr)oxide	0.48	-0.057	46.2	3.0	100		
Sand day 100 – 77 K							0.49
SRO Fe(III) (oxyhydr)oxide	0.48	0.80			85.6	4.0	
Fe(II) phyllosilicate / adsorbed	1.15	2.90			14.4	4.0	
Sand day 100 – 5K							0.77
SRO Fe(III) (oxyhydr)oxide**	0.44	-0.053	47.1	3.5	100		
Soil day 0 – 77 K							0.83
SRO Fe(III) (oxyhydr)oxide / phyllosilicate	0.48	0.76			29.1	1.3	
Fe(II) phyllosilicate / adsorbed	1.23	2.86			16.0	1.1	
Goethite	0.46	-0.21	47.3	4.61	48.1	1.9	
Hematite	0.49	-0.17	53.3	0.24	6.8	1.8	
Soil day 0 – 5 K							0.86
Fe(III) phyllosilicate	0.52	0.90			25.4	1.4	
Fe(II) phyllosilicate	1.23	2.88			13.8	1.4	
Goethite	0.46	-0.26	49.5	1.67	50.2	2.0	
Hematite	0.47	-0.17	53.6	0	10.6	2.0	
Soil day 30 – 77 K							0.57
SRO Fe(III) (oxyhydr)oxide / phyllosilicate	0.48	0.76			32.5	3.1	
Fe(II) phyllosilicate / adsorbed	1.25	2.81			17.3	2.3	
Goethite	0.47	-0.20	47.4	3.30	40.8	4.6	
Hematite	0.47	-0.18	53.1	0.25	9.4	4.7	
Soil day 30 – 5 K							0.72
Fe(III) phyllosilicate	0.55	0.80			20.7	2.6	
Fe(II) phyllosilicate / adsorbed	1.24	2.80			15.4	2.8	
Goethite	0.48	-0.24	49	1.94	47.6	4.7	
Hematite	0.44	0.07	54	1.08	16.2	5.0	

Soil day 100 – 77 K							0.69
SRO Fe(III) (oxyhydr)oxide / phyllosilicate	0.47	0.73			22.9	2.1	
Fe(II) phyllosilicate / adsorbed	1.24	2.84			27.3	2.5	
Goethite	0.49	-0.26	48.27	3.90	44.0	4.2	
Hematite	0.42	-0.15	53.5	0.20	5.8	3.1	
Soil day 100 – 5 K							0.63
Fe(III) phyllosilicate	0.54	0.94			21.8	2.8	
Fe(II) phyllosilicate / adsorbed	1.24	2.91			20.1	2.9	
Goethite	0.45	-0.27	49.6	1.53	45.0	4.7	
Hematite	0.47	-0.17	53.4	0.56	13.1	5.1	
Sand-soil day 0 – 77 K							0.75
SRO Fe(III) (oxyhydr)oxide / phyllosilicate	0.48	0.82			50.8	2.7	
Fe(II) phyllosilicate / adsorbed	1.21	2.88			13.7	1.3	
Goethite	0.46	-0.16	48.4	5.68	35.5	3.3	
Sand-soil day 0 – 5 K							0.92
Fe(III) phyllosilicate	0.41	0.95			12.2	1.5	
Fe(II) phyllosilicate / adsorbed	1.34	2.59			13.7	1.8	
SRO Fe(III) (oxyhydr)oxide	0.45	0.16	46.3	5.28	40.7	5.1	
Goethite	0.49	-0.24	49.6	2.60	33.4	5.2	
Sand-soil day 30 – 77 K							0.63
SRO Fe(III) (oxyhydr)oxide / phyllosilicate	0.48	0.83			54.5	2.7	
Fe(II) phyllosilicate / adsorbed	1.18	2.88			7.5	1.8	
Goethite	0.51	-0.12	48.7	5.36	38.0	2.8	
Sand-soil day 30 – 5 K							0.64
Fe(III) phyllosilicate	0.33	0.78			10.5	2.7	
Fe(II) phyllosilicate / adsorbed	1.25	2.90			12.0	3.6	
SRO Fe(III) (oxyhydr)oxide	0.36	0.08	45.0	6.25	40.5	9.1	
Goethite	0.51	-0.17	49.3	2.50	37.0	8.1	
Sand-soil day 100 – 77 K							0.73
SRO Fe(III) (oxyhydr)oxide / phyllosilicate	0.36	0.95			39.6	1.7	
Fe(II) phyllosilicate / adsorbed	1.43	2.50			21.8	1.5	
Goethite	0.42	-0.28	48.1	5.23	38.6	2.1	
Sand-soil day 100 – 5 K							0.66
Fe(III) phyllosilicate	0.39	0.97			12.4	2.2	
Fe(II) phyllosilicate / adsorbed	1.26	2.86			17.1	2.9	
Goethite	0.48	-0.31	49.68	2.11	34.5	5.6	
SRO Fe(III) (oxyhydr)oxide	0.39	0.11	47.9	5.06	36.1	5.8	

(*) A small doublet corresponding to Fe(II) was fit in this spectrum. However, since the quality of the 5K spectrum is lower than the 77K and there was no Fe(II) observed at day 30, this is likely not a real feature

(**)The quality of the 5K spectrum is low, therefore we use the fit based on the 77K as there is a clear doublet denoting Fe(II)

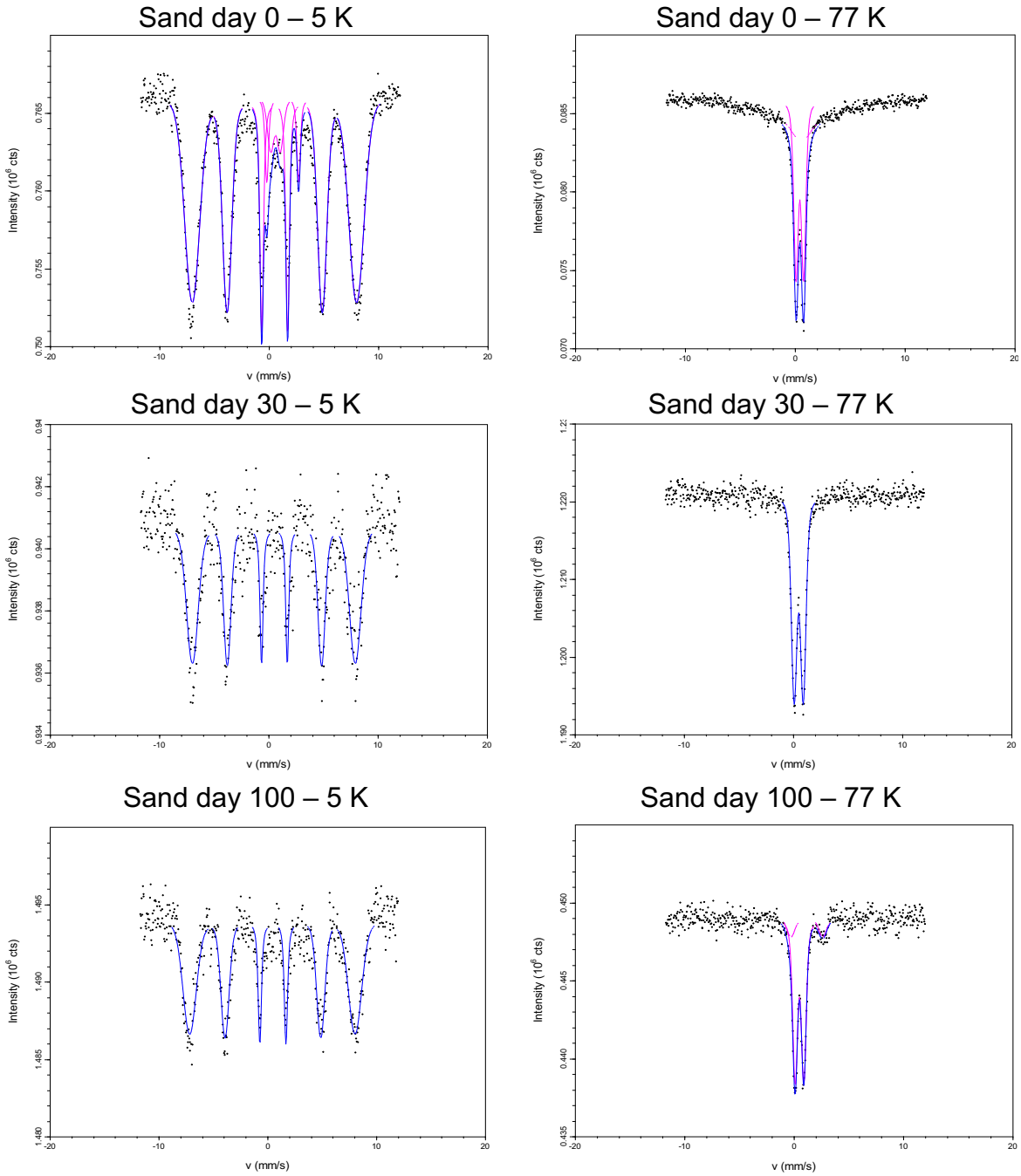

Figure S5. Moessbauer spectra collected at 5 K and 77 K at days 0, 30 100 from disposed sand incubation.

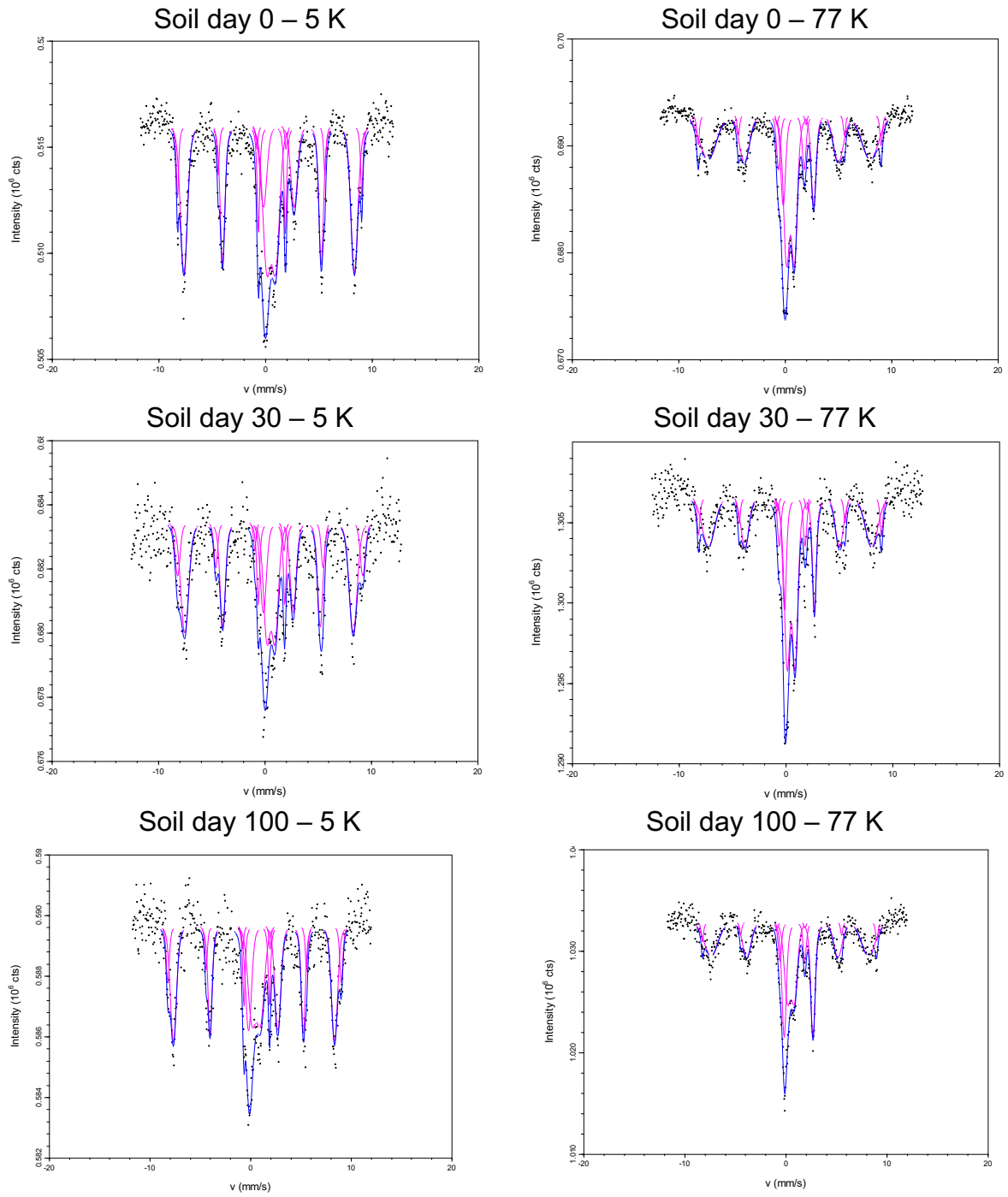

Figure S6. Moessbauer spectra collected at 5 K and 77 K at days 0, 30 100 from floodplain soil incubation.

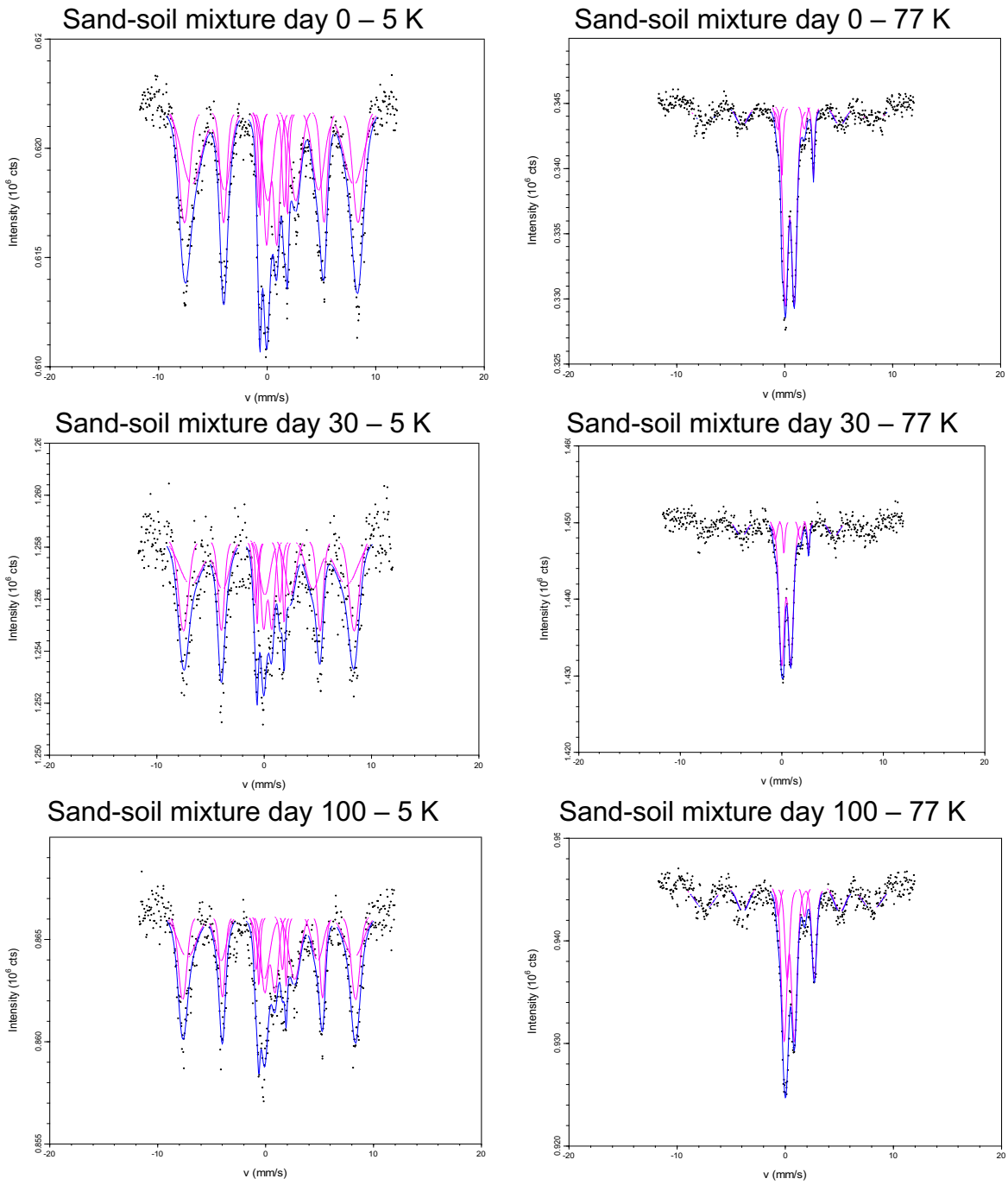

Figure S7. Moessbauer spectra collected at 5 K and 77 K at days 0, 30 100 from 1:1 sand-soil mixture incubation.

S3. X-ray absorption spectroscopy

Method: The double Si (220) monochromator was detuned by 35%. A germanium filter was placed in front of the detector to minimize scatter. To avoid thermal disorder, scans were run under helium cooling at 25 K. To prevent photo-damage of the sample and subsequent oxidation of As, the focused beam (1 mm x 1 mm) was moved across the sample in 1 mm increments between repetitive scans. For each sample or standard, six to nine scans were recorded. Faulty channels of the 30-element germanium detector array were manually removed in Sixpack (Webb, 2005) leaving around 25 channels to work with, followed by deadtime correction and averaging of channels.

Shell by shell fits were done with Artemis (Ravel and Newville, 2005). Theoretical shell amplitudes and phase parameters were generated using Feff6, using Scorodite ($AsFeO_4$), synthesized arsenate and arsenite model compounds. The number of atoms, Debye Waller factor and the interatomic distances were obtained from non-linear squares fits to the EXAFS signal for each individual theoretical path.

Table S3. Results of the Linear Combination Fitting (LCF) of the As K-edge XANES and EXAFS of the As in Sand, Soil and mixture of Soil-sand.

Day	Samples	LCF	As(V) (%)	As(III) (%)	Sum (%)	R-factor (x10^3)
0	Sand	XANES	91.7	8.3	100.0	2.4
		EXAFS	81.7	8.2	89.9	62.0
30		XANES	78.3	21.7	100.0	1.9
		EXAFS	61.6	31.3	92.9	55.8
84		XANES	68.1	31.9	100.0	0.9
		EXAFS	52.2	40.3	92.5	51.6
0	Soil	XANES	90.1	9.9	100.0	3.3
		EXAFS	73.1	17.4	90.5	79.7
30		XANES	85.3	14.7	100.0	3.0
		EXAFS	68.3	21.2	89.5	79.7
84		XANES	66.4	33.6	100.0	1.0
		EXAFS	52.2	39.2	91.4	61.2
0	Soil-sand	XANES	94.3	5.7	100.0	0.3

	EXAFS	82.8	9.6	92.4	62.169
30	XANES	86.6	13.4	100.0	0.2
	EXAFS	74.8	16.2	91.0	64.5
84	XANES	62.3	37.7	100.0	0.5
	EXAFS	48.8	44.2	93.0	51.2

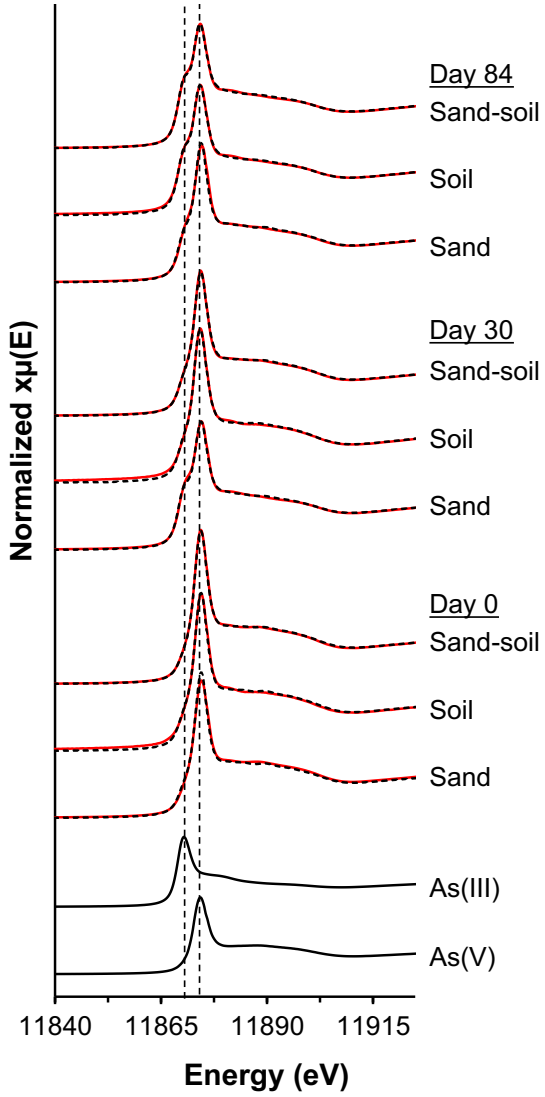

Figure S8. As K-edge XANES of As(V) and As (III) in disposed sand, soil and sand-soil mixture microcosms recorded over 3 time points, i.e., days 0, 30 and 84. Experimental and linear combination fit curves are plotted as black and red lines, respectively.

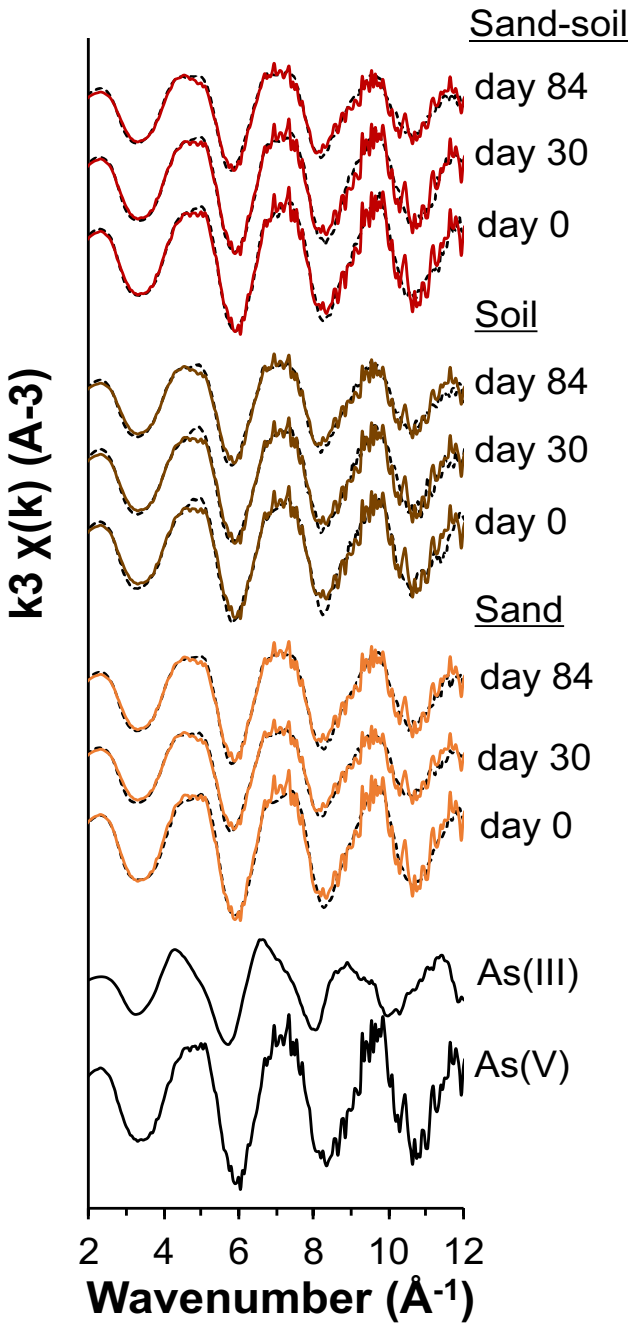

Figure S9. Arsenic *k*3-weighted EXAFS of disposed sand, soil and sand-soil mixture microcosms recorded over 3 time points, i.e. days 0, 30 and 84. Standards for As(III) and As(V) were used for fitting. Experimental and linear combination fit curves are plotted as black and red lines, respectively.

Table S4. Results of the shell-by-shell fitting analysis of the As K-edge EXAFS of the As in Sand, Soil and mixture of Soil-sand.

Sand	**day**	**0**	**30**	**84**
As-O	*N*	4.0±0.1	4.0±0.1	4.0±0.1
	R(Å)	1.70±0.01	1.70±0.01	1.71±0.01
	σ^2 *(Å^2)*	0.0014±0.0004	0.0034±0.0008	0.0013±0.0006
As-Fe1	*N*	1.0±0.1	1.0±0.1	1.0±0.1
	R	2.89±0.1	2.89±0.1	2.89±0.1
	σ^2 *(Å^2)*	0.0087±0.0058	0.0103±0.0058	0.0101±0.003
As-Fe2	*N*	1.0±0.1	1.0±0.1	1.0±0.5
	R	3.30±0.01	3.33±0.01	3.32±0.01
	σ^2 *(Å^2)*	0.0087±0.0058	0.0103±0.0010	0.0101±0.0058
Soil	**day**	**0**	**30**	**84**
As-O	*N*	4.0±0.1	3.6±0.5	4.0±0.1
	R(Å)	1.70±0.01	1.70±0.01	1.71±0.01
	σ^2 *(Å^2)*	0.0019±0.0004	0.0013±0.0005	0.0034±0.0004
As-Fe1	*N*	0.4±0.2	1.0±0.1	1.0±0.1
	R	2.94±0.2	2.85±0.05	2.89±0.1
	σ^2 *(Å^2)*	0.0019±0.0004	0.0098±0.005	0.0104±0.0058
As-Fe2	*N*	0.6±0.1	0.5±0.3	1.0±0.1
	R	3.28±0.01	3.29±0.07	3.34±0.01
	σ^2 *(Å^2)*	0.0019±0.0004	0.0098±0.0058	0.0104±0.0058
Sand-soil	**day**	**0**	**30**	**84**

	N	4.0±0.1	4.0±0.1	4.0±0.1
As-O	*R(Å)*	1.70±0.01	1.70±0.01	1.72±0.01
	$\sigma^2(Å^2)$	0.0013±0.0004	0.0022±0.0004	0.0013±0.0004
	N	0.4±0.1	1±0.1	1.0±0.1
As-Fe1	*R*	2.91±0.1	2.86±0.1	2.88±0.1
	$\sigma^2(Å^2)$	0.0045±0.0035	0.0101±0.0010	0.0097±0.0013
	N	1.0±0.5	1.0±0.2	1.0±0.5
As-Fe2	*R*	3.30±0.03	3.30±0.01	3.34±0.01
	$\sigma^2(Å^2)$	0.0045±0.0035	0.0101±0.0010	0.0097±0.0010

S4. Single particle ICP-MS

Samples were analyzed as detailed in our previous publication (Mansor et al., 2021). All samples were analyzed in one day of an analytical session in time-resolved analysis mode on an Agilent 7900 ICP-MS instrument (Agilent Technologies, Santa Clara, CA) with a RF power setting of 1550 V and a sampling depth of 8 mm. Standards (0-500 ppb Fe/As/Al in 1% HNO_3) were freshly diluted just before analysis. Samples were diluted anoxically by a factor of 1000 with anoxic milliQ water under anoxic condition and mixed by three times inversion just before uptake on the instrument. The transport efficiency (TE) was determined to be 0.036 by comparing the median intensity of 50 nm Au NPs to dissolved Au (0-50 ppb) based on the particle mass method (Heather E. Pace et al., 2011), consistent with our previous study (Mansor et al., 2021). Masses of ^{27}Al, ^{56}Fe, ^{75}As and ^{197}Au were monitored using an integration time of 0.1 ms, an acquisition time of 30 s, and a sample flow rate of 0.466 ml/min in Gas mode (helium flow = 4.3 ml/min). Sequential analysis with a time gap of 10 s between elements was employed for multielement analysis of the same sample. Data analysis was performed via a custom Python script using criteria of signals above 3 standard deviations and 3 minimum consecutive points to be recognizable as a particle (Mansor et al., 2021). Detection limits are provided in Table S5.

Water and acid blanks were monitored in-between samples and allowed to return to background levels before proceeding to the next sample. Particle blanks were highest

for Fe, with ~25 particles detectable on average. However, this accounted for a maximum of 5% (by number) and 2% (by mass) of the total particles detectable in samples. In comparison, typically zero particles (maximum 2 particles occasionally) were detected in blanks for As and Al. Analysis of a quality control standard every 10 samples – to check for instrument drift – showed that the values for Fe, As and Al were stable within ± 15%. Therefore, no correction was applied for blank contamination or instrument drift.

Our analysis likely underestimates the mass of colloidal Fe, As and Al. The smallest particles are below the detection limit of spICP-MS (Table S5) and incomplete particle ionization is known to occur for certain elements with increasing particle size (Jiménez-Lamana et al., 2018). Additionally, the lack of element-specific particle size standards makes it difficult to evaluate quantitative detection of different elements. Therefore, the reported colloidal masses should be considered semi-quantitative but comparable between samples that were treated the same way.

Samples showed higher detection limits compared to blanks, and the minimum detection limits decreased with sampling time (Table S6, S7). The increase in the minimum detection limits results from high frequency of particles with tailing effects and/or high ionic concentrations that increase the baseline's noise. The former was predominant in Day 0 samples while the latter was more important for Day 30 and 100 samples. Nevertheless, they do not change our observation that colloidal particles decreased over time (Figure. S11).

Table S5: Minimum detection limits for the analyzed masses on spICP-MS under reported operating condition as determined from blank analyses.

Mass	DL element mass per particle (fg)	DL size (nm)	Assumptions for size calculation
^{27}Al	8.70	200	Al_2O_3, f_{Al} = 0.529, ρ = 3.95 g/cm^3
^{56}Fe	0.17	55	Ferrihydrite, f_{Fe} = 0.523, ρ = 3.8 g/cm^3
^{75}As	0.81	-	-
^{197}Au	0.03	15	Au NPs, f_{Au} = 1 , ρ = 19.3 g/cm^3

Table S6: The mass and size range of colloidal Fe particles detected for each sample. Error bars represent standard deviation from triplicate microcosms. The minimum values reflect the minimum detection limits specific to each sample. Numbers in grey denote the equivalent particle size assuming spherical ferrihydrite particles.

Day	Mass of Fe per particle (fg) *Particle size (nm)*					
	Sand		**Soil**		**Sand-soil mixture**	
	Min	**Max**	**Min**	**Max**	**Min**	**Max**
0	2.9 ± 1.4	340.3 ± 32.4	4.5 ± 2.1	190.5 ± 17.1	3.8 ± 2.8	312.1 ± 76.5
	137 ± 21	*688 ± 22*	*160 ± 25*	*567 ± 16*	*146 ± 36*	*665 ± 53*
30	0.5 ± 0.1	208.4 ± 19.7	4.9 ± 1.3	152.1 ± 7.9	0.3 ± 0.0	72.8 ± 8.4
	78 ± 8	*584 ± 18*	*167 ± 15*	*526 ± 9*	*72 ± 1*	*411 ± 16*
100	0.4 ± 0.0	212.5 ± 20	0.6 ± 0.1	68 ± 9.8	0.3 ± 0.0	78.8 ± 3.8
	75 ± 1	*588 ± 18*	*85 ± 7*	*401 ± 19*	*70 ± 0*	*423 ± 6*

Table S7: The mass range of colloidal As particles detected for each sample. Error bars represent standard deviation from triplicate microcosms (duplicate from soils, due to low particle detection in the samples). The minimum values reflect the minimum detection limits specific to each sample.

Day	Mass of As per particle (fg)					
	Sand		**Soil**		**Sand-soil mixture**	
	Min	**Max**	**Min**	**Max**	**Min**	**Max**
0	1.2 ± 0.0	12.8 ± 2.4	1.3 ± 0.0	8.5 ± 0.0	1.2 ± 0.0	14 ± 2.8
30	1.4 ± 0.1	11.1 ± 3.2	1.9 ± 0.2	4.9 ± 1.6	1.6 ± 0.1	4.8 ± 1.4
100	1.3 ± 0.0	16.4 ± 10.2	-	-	2.7 ± 0.4	2.7 ± 0.4

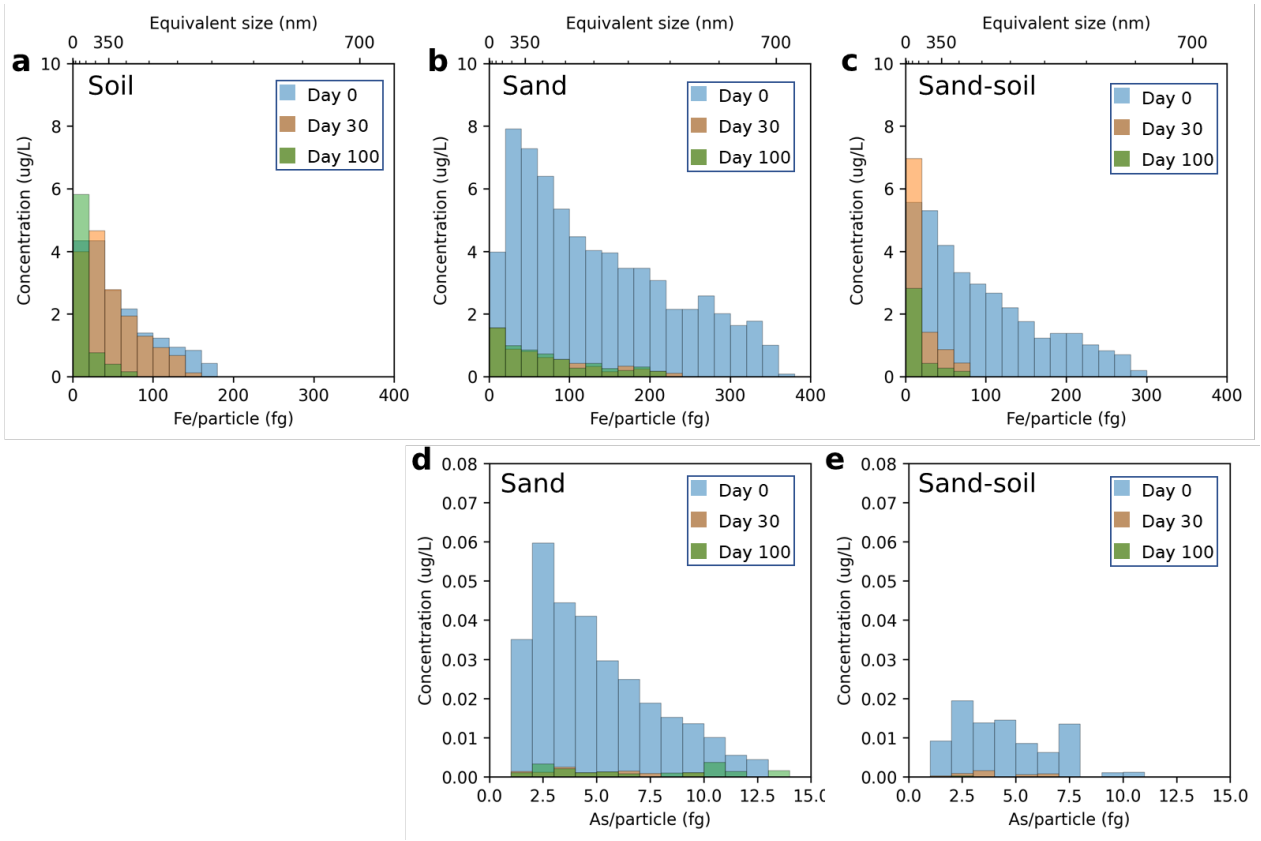

Figure S10: Particle mass distribution of (a-c) Fe and (d-e) As in the colloidal fraction. Colloidal As distribution data for soils are not shown due to limited detection that was not significant compared to blanks.

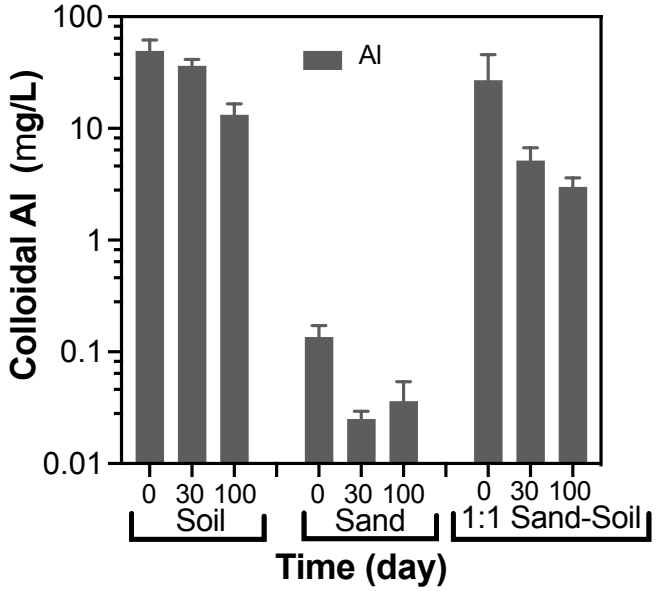

Figure S11. Changes of colloidal mass concentration of Al in soil, disposed sand and sand-soil mixture microcosms over incubation time.

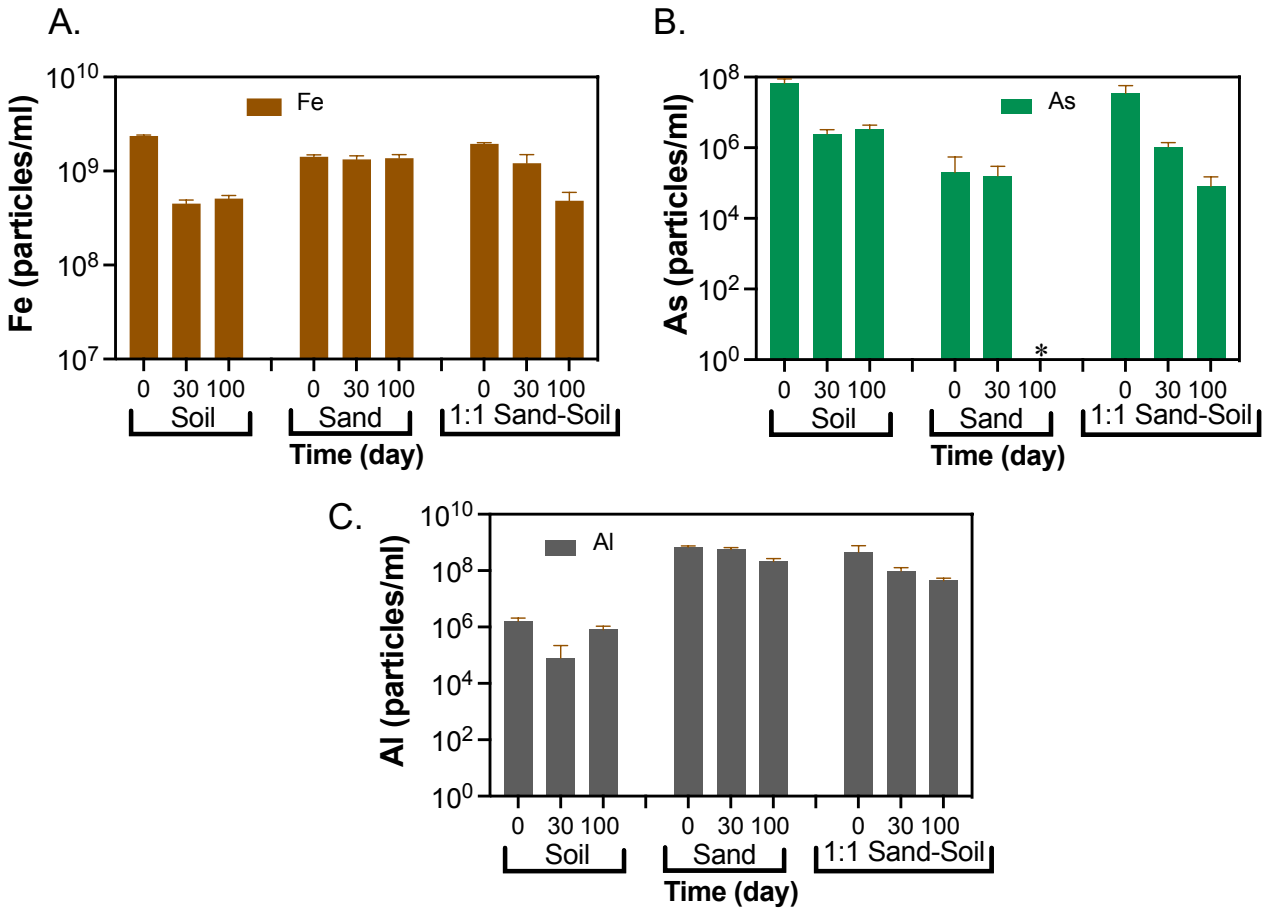

Figure S12. Changes of particle number concentrations of colloidal Fe (A), As (B), and Al (C) in the microcosms. (*) No colloidal particles containing As were detected in sand microcosm at day 100.

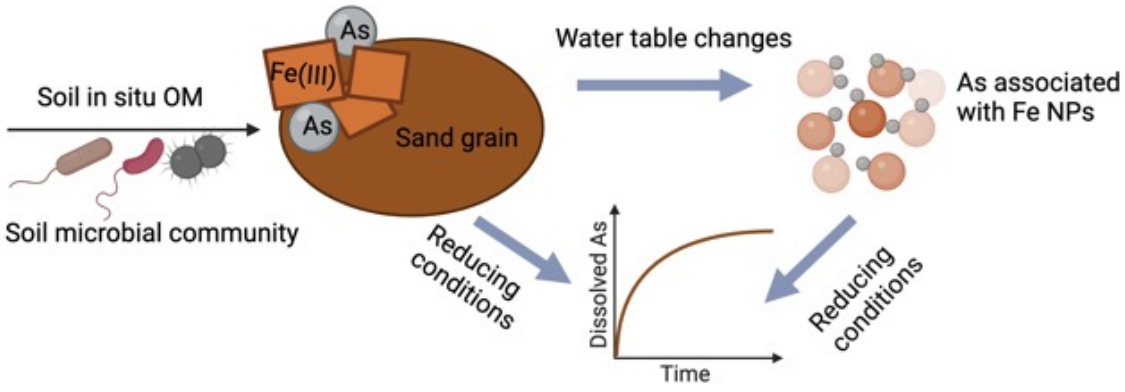

Figure S13. Overview contributions of Fe and As reduction in the bulk phase as well as Fe and As colloid removal over time to As mobilization under flood-inducing conditions.

References

Jiménez-Lamana, J., Abad-Álvaro, I., Bierla, K., Laborda, F., Szpunar, J., Lobinski, R., 2018. Detection and characterization of biogenic selenium nanoparticles in selenium-rich yeast by single particle ICPMS. J. Anal. At. Spectrom. 33, 452–460.

Mansor, M., Drabesch, S., Bayer, T., Van Le, A., Chauhan, A., Schmidtmann, J., Peiffer, S., Kappler, A., 2021. Application of Single-Particle ICP-MS to Determine the Mass Distribution and Number Concentrations of Environmental Nanoparticles and Colloids. Environ. Sci. Technol. Lett. https://doi.org/10.1021/acs.estlett.1c00314

Pace, H.E., Rogers, N.J., Jarolimek, C., Coleman, V.A., Higgins, C.P., Ranville, J.F., 2011. Determining transport efficiency for the purpose of counting and sizing nanoparticles via single particle inductively coupled plasma mass spectrometry. Anal. Chem. 83, 9361–9369. https://doi.org/10.1021/ac201952t

Ravel, B., Newville, M., 2005. ATHENA, ARTEMIS, HEPHAESTUS: data analysis for X-ray absorption spectroscopy using IFEFFIT. J. Synchrotron Radiat. 12, 537–541.

Viet, P.H., Tuan, V. V, Hoai, P.M., Anh, N.T.K., Yen, P.T., 2001. Chemical composition and acidity of precipitation: A monitoring program in northeastern Vietnam, in: Acid Rain 2000. Springer, pp. 1499–1504.

Webb, S.M., 2005. SIXpack: a graphical user interface for XAS analysis using IFEFFIT. Phys. Scr. 2005, 1011.

Chapter 6: Conclusions and Outlook

Household sand filters are the conventional and popular treatment method for removing As(III) and co-contaminants such as Fe(II), Mn(II), and NH_4^+ from groundwater. For more than 30 years, millions of people in the Red River delta, Vietnam have used this filtered water for cleaning and drinking purposes. Arsenic removal mechanisms account for a complex interplay of abiotic and biotic processes (Voegelin et al., 2014). However, the identification of core microbial communities in sand filters that contribute to the contaminant's removal was missing. Previous works evaluated sand filter performance at a specific time point (Berg et al., 2006; Luzi et al., 2004; Nitzsche et al., 2015a; Voegelin et al., 2014). Therefore, questions such as how long the sand filter can perform and whether any long-term risk threatens the filtered water quality remained unknown. Finally, As-bearing sand materials are disposed into soils every few months and can potentially act as a secondary As contamination source (Luzi et al., 2004). Thus, the environmental risk of disposal of As-bearing filter materials must be studied.

This Ph.D. dissertation has successfully tackled three mentioned knowledge gaps. The outcomes revealed core microbial communities potentially oxidizing Fe(II), Mn(II), NH_4^+, NO_2^-, and CH_4^+ in all studied household sand filters. The combination of abiotic and biotic processes assured the high removal efficiency of Fe and As over time and highlighted the role of Mn oxides in controlling the Fe and As retention under saturated (O_2-depleted) conditions. For the first time, the environmental risk of open disposal of As-bearing filter material was quantified. The key findings of each work package, proposed future experiments, and approaches are described as follows.

6.1. Sand filters shared core microbial communities potentially oxidizing Fe(II), Mn(II), NH_4^+, NO_2^- and CH_4^+ (chapter 2).

6.1.1. Key findings

Field-base studies on sand filter performances and analyzing microbial communities of household sand filters running under different geochemical compositions highlight that core microbial communities in sand filters potentially comprised of Fe(II)−, Mn(II) −, NH_4^+ −, NO_2^- − and CH_4^+ − oxidizing microorganisms (Figure 1).

- Microaerophilic Fe(II) oxidation by *Sideroxydans* was dominat in sand filters fed by low-As and high-Fe groundwater. Besides, putative nitrate reduction coupled to Fe(II) oxidation (NRFeOx) by *Gallionellaceae* might occurred in the O_2-depleted zone of the sand filters.
- *Hyphomicropbiaceae* were suggested as the main Mn(II)-oxidizers since they contained the Mn(II)- oxidizing gene moxA and were previously used as model organisms for studying Mn (II) oxidation (Larsen et al., 1999; Ridge et al., 2007).
- Sequences affiliating with typical nitrifiers, such as *Nitrosomonadaceae* (ammonium-oxidizing bacteria), *Nitrososphaeraceae* (ammonium-oxidizing archaea), and *Nitrospiraceae* (nitrite-oxidizing bacteria), were accounted for 13.5± 8.4 % of relative microbial abundance in sand filters.
- Unexpectedly, a high relative abundance of putative methanotrophs was detected in all sand filters, such as *Methylococcaceae* (10.3 ± 6.1 %) and *Methylomonaceae* (4.5 ± 2.8 %). Methane monooxygenase genes (*pmoA*) were further quantified, suggesting microbial methane oxidation in household sand filters.

Overall, the findings suggest that Fe(II)- and Mn(II) -oxidizers complement abiotic oxidation in household sand filters, thus contributing to the excellent Fe, Mn, and As removal efficiencies. In contrast, nitrification occurred during filtration, causing an elevated NO_3^- concentration (up to 20 mg-N/L) in the effluent, thus raising a potential concern for the water quality when being used for drinking.

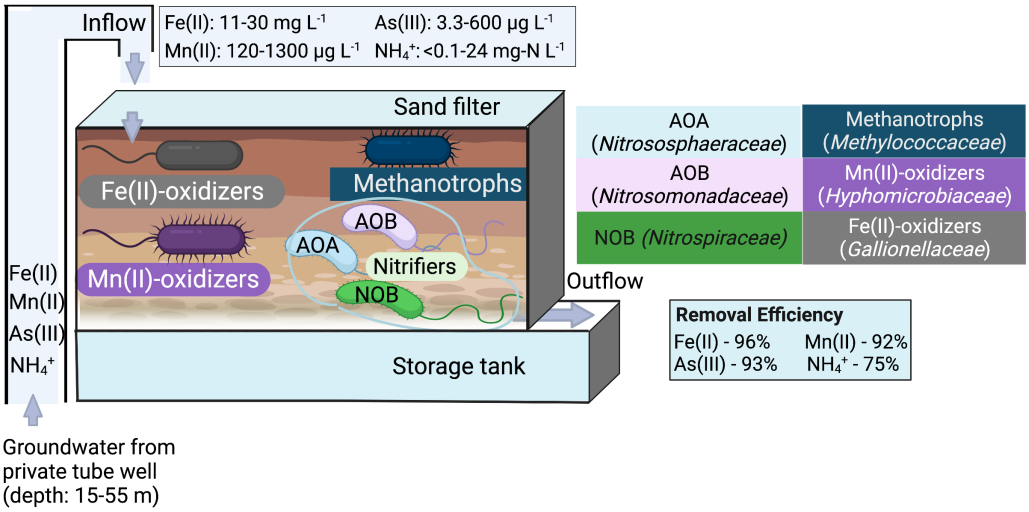

Figure 1. Summary of core microbial communities shared in household sand filters operating under various groundwater compositions and the filters removal efficiency (Van Le et al., 2022b)

6.1.2. Proposed future experiments.

Analysis of the microbial ecology of household sand filters has uncovered many novel microbial processes and microorganisms, such as complete ammonia oxidation (comammox) (Daims et al., 2016; Palomo et al., 2016) or novel neutrophilic iron and manganese oxidizing bacteria (Gülay et al., 2013; Hu et al., 2020). However, microbial community analysis methods such as 16S rRNA gene sequencing only can identify "the present members" and is not sufficient to fully understand the rules governing community assembly, metabolic functions and to discover potential novel processes (especially related to NH_4^+, Mn(II) and Fe(II) oxidation), therefore, the following further studies are proposed:

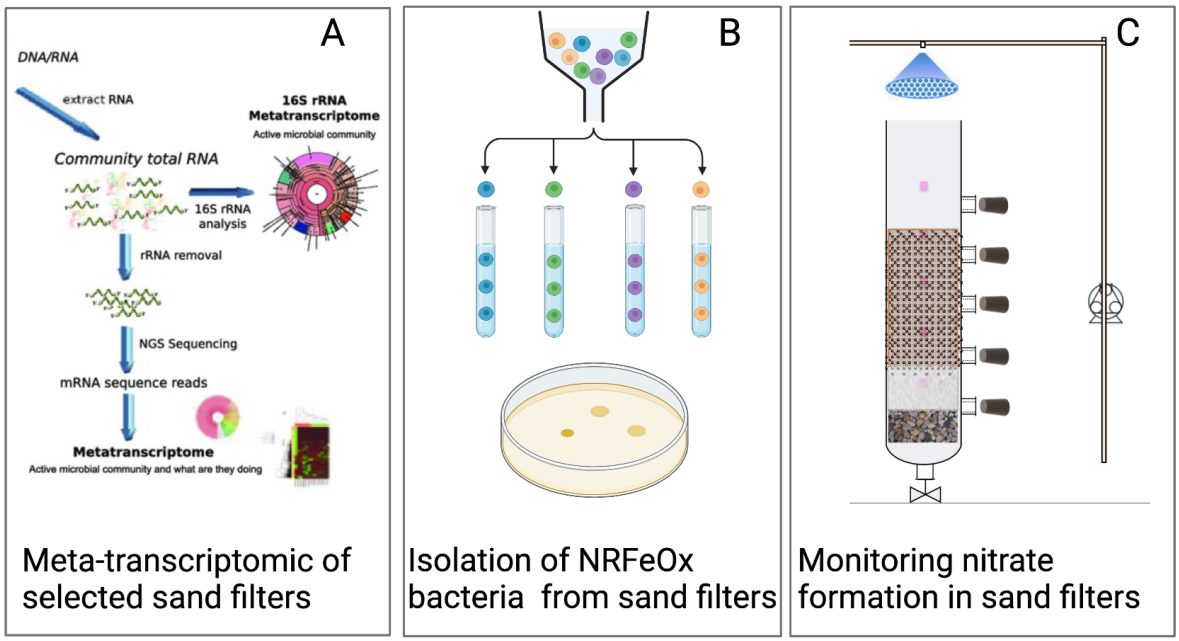

Figure 2. Proposed further experiments to (A) better understand the metabolic function of household sand filter's microbial communities and how it correlates to contaminants removal in sand filters; (B) isolation of NRFeOx bacteria from household sand filters; and (C) monitoring of nitrate formation over time and evaluating whether isolated NRFeOx bacteria from sand filters can reduce the nitrate mobilization to the filtered water.

i) Identification of key metabolic functions from sand filter's microbial communities by performing meta-transcriptomic (Figure 2A). The results can better conclude the contribution of microbial activities to sand filter performance, especially for Mn and As oxidation pathways. Microbial manganese and arsenic oxidizing processes are mediated by a diverse microbial community with flexible metabolic functions that do not solely use Mn(II) or As(III) for energy generation (Hu et al., 2020; Zhu et al., 2017).

Therefore, using the solely 16S rRNA sequencing-based approach might “miss” on their contribution.

ii)) Isolation of bacteria mediating nitrate reduction coupled to Fe(II) oxidation (NRFeOx) from household sand filters (Figure 2B). The work proposed that *Gallionellaceae* in sand filters might belong to NRFeOx bacteria; thus, they can reduce the nitrate produced by nitrification in filtered water in the O_2-depleted zone of sand filters.

iii) Evaluation to which extent the nitrate formation due to nitrification can affect the filtered water quality, and whether NRFeOx bacteria could potentially remove nitrate in the filtered water. A column experiment is proposed to run in the lab with or without spiking isolated NRFeOx bacteria. Concentration of NH_4^+, NO_2^- and NO_3^- is quantified over time (Figure 2C).

6.2. Manganese redox cycling controls iron and arsenic retention in household sand filters (chapter 3).

6.2.1. Key findings

Operation of the household sand filter starts with (oxic) unsaturated conditions followed by saturated conditions, in which semi-oxic to anoxic zones are formed along sand layers. When the filter surface gets clogged (every 3-6 months), 10- 20 cm of top sand is scraped off for unclogging. Thus, sand filters are usually operated under the cycle of unsaturated to saturated flow for many years.

Under unsaturated conditions, we found Fe, As, and Mn removal was stable and effective, averaging efficiency of 99, 93, and 91%, respectively. In the solid phase, As(V)-bearing Fe(III) (oxyhydr)oxides and Mn(III/IV) oxides dominated in unsaturated sand materials (Figure 3).

Under saturated conditions, Fe and As removal remained the same (99 and 95%), while Mn(II) was leached from the sand column to column effluent. Up to 46 and 15% of Fe(III) and As(V) were reduced in the anoxic zone (5-10 cm), and the presence of Mn(II) was confirmed.

The results suggest that Mn oxides that formed during unsaturated conditions were acting as a secondary hosting phase and oxidant for Fe(II) and As(III)/(V) under saturated conditions (Figure 3). Overall, the results proved the stability and efficiency

of household sand filters regarding As and Fe removal over a long operational time and highlighted the risk of Mn mobilization when the filter runs under unsaturated flow for a longer time.

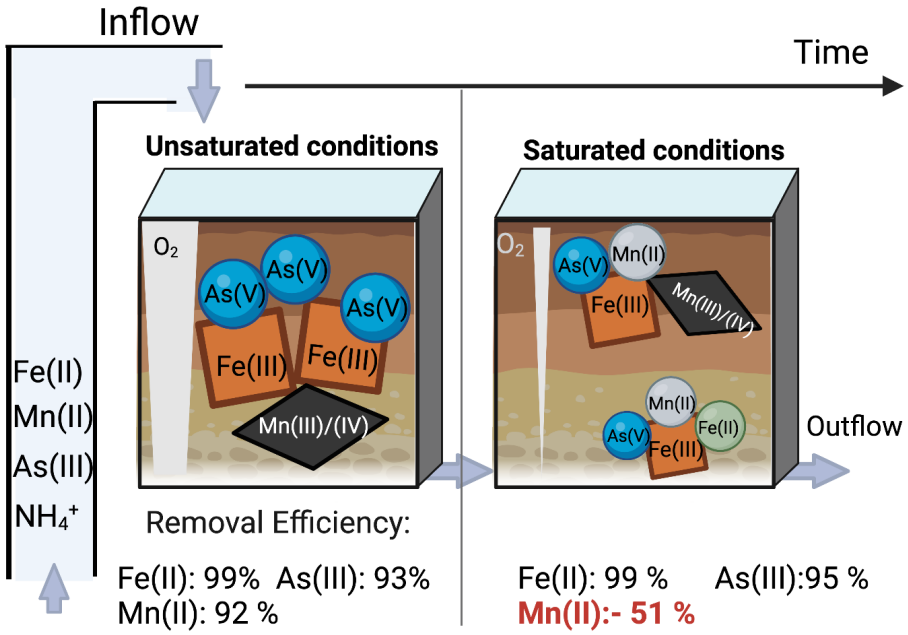

Figure 3. Summary of spatial-temporal distribution of solid-associated Fe, As, and Mn in the household sand filter when operating under unsaturated and saturated conditions and their correlation with aqueous Fe, As, and Mn removal efficiency.

6.2.2. Proposed future works.

A sustainable approach enhances arsenic removal by household sand filters.

Both field and lab experiments monitoring As removal over a long operational time confirmed that As residual concentration was still higher than 10 µg/L (drinking water standard by WHO). Thus, the next step is to upgrade current household sand filters to enhance As adsorption capacity in which the technology should base on local, affordable and sustainable resources.

Countries vulnerable to As contamination, such as Vietnam, India, and Bangladesh, produce the most rice worldwide, generating massive paddy rice biomass such as rice straw, rice husk, and rice kernel. Therefore, we propose to employ biochar recovered from paddy rice biomass as As adsorbent materials. This proposal is based on and supported by our observation in field campaigns 2018 and 2020, which many filter users added a thick layer of “burnt rice husk” on top of their household filters as extra filter materials (Figure 4A). This rises a concern regarding As treatment effectiveness

and pose a potential risk of toxic As(III) release under anoxic conditions caused by redox reactions triggered by organic carbon in this material. Therefore, replacement the “burnt rice husk” with a certified biochar material is necessary and can largely be implemented in the Red River delta.

Pristine biochar reveals a lower adsorption capacity for toxic metals (Amen et al., 2020), including arsenic. However, various modifications of biochar have been proposed, such as nano Fe or Fe oxides coating on the surface of biochar (Figure 4B) (Hu et al., 2015; Shaheen et al., 2022; Zhang et al., 2022; Zhou et al., 2014). The Fe-modified biochar shows a great potential to remove As (Amen et al., 2020; Hu et al., 2015; Zhang et al., 2022), inorganic-N contaminants (Zhang et al., 2020) and pharmaceutical products (Herrera et al., 2022) in the aquatic environment.

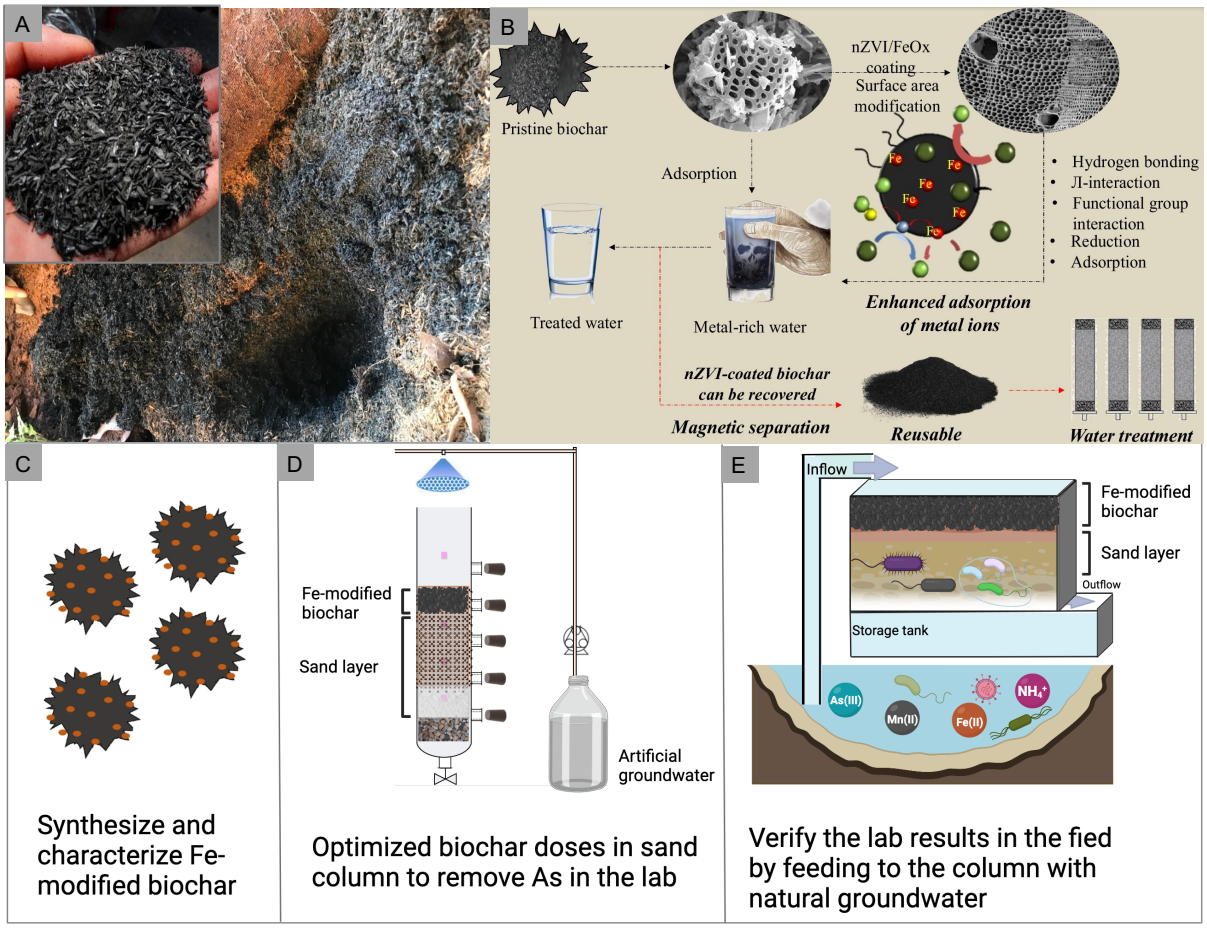

Figure 4. “Burnt rice husk” added on top of various household sand filters in Vietnam (A). Summary of preparation and possible application of Fe-modified biochar (including nano zerovalent iron (nZVI) or iron oxides (FeOx)) for toxic elements removal proposed by (Shaheen et al., 2022) (B). Proposed next steps to enhance As removal by sand filters include

synthesizing and characterizing Fe-modified biochar (C), optimization of biochar doses in sand column (D), and verification of the lab results in the field (E).

Therefore, to enhance the water quality by sand filtration applied to remove arsenic, we propose to synthesize and characterize the Fe-modified biochar (Figure 4B) as an amendment to sand filters, followed by optimization of the dosage of synthesized biochar in the sand columns (Figure 4C) and lastly validate the lab results by testing in the field in which Fe-modified biochar is added into the household sand filter. Their performance will be evaluated over time (Figure 4D).

6.3. Environmental risk of As mobilization from disposed sand filter materials (chapter 4 & 5).

6.3.1. Key findings

Around 3.1 million active household sand filters are in the Red River delta (Van Le et al., 2022a). Due to the high frequency of filter clogging, every 3-6 months, sand materials are scrapped off from the top layer and directly disposed on top of floodplain soils. These staggering amounts of disposed filter materials might act as secondary As contaminant sources.

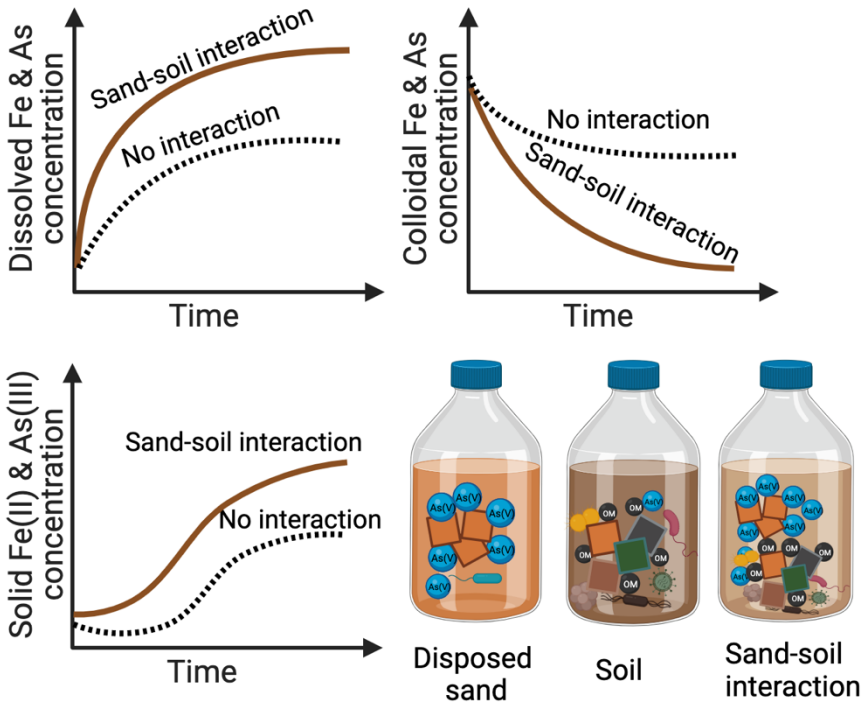

Figure 5. Summary of Fe and As reduction and mobilization in solid, aqueous, and colloidal phases when incubated disposed sand material into the soil under reducing conditions (Van Le et al., 2022a).

We proved that mixing filter materials with floodplain soil (termed sand-soil interaction) mimicking disposal of filter materials into the soils, promoted microbial reduction of As-bearing Fe(III) (oxyhydr)oxides under reducing conditions. The processes reduced Fe(III) and As(V) by 10 and 32% in the solid phase, respectively, and up to 210 µg/L of As was detected in the aqueous phase. Additionally, the work successfully optimized the application of spICP-MS to quantify the Fe and As in the colloidal phase (Mansor et al., 2021). Flood events and heavy rainfall release an elevated amount of Fe colloids into the porewater or stormwater, stressing the role of colloidal transport for As-bearing Fe colloids. We found that up to 77-100% of colloidal Fe and As were decreased shortly after starting the incubation. Similar results were also observed by (Ghosh et al., 2006) , studying the mobilization of As-bearing waste in mature landfill conditions. The finding suggests that As mobilization of colloids is essential when disposing of As-bearing waste to the environment, but its importance decreases over time.

6.3.2. Proposed future works.

Due to changes in precipitation frequency throughout the year, factors such as redox fluctuation, flow conditions, and hydraulic retention times can control As mobilization from disposed sand materials. Therefore, we propose the following steps:

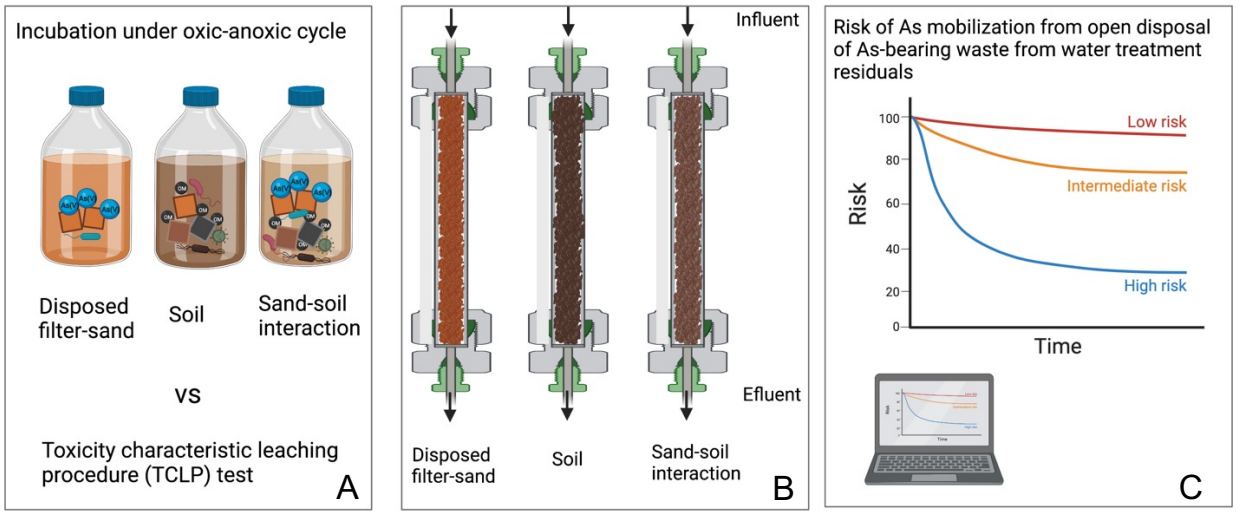

Figure 6. Proposed further experiments to (A) evaluate the influent of redox cycling (A), hydraulic retention times (B) to As mobilization from disposed sand materials. The results are interpolated into a risk analysis model to predict As mobilization due to open disposal.

i) Quantification of As mobilization from disposed sand, soil, and their mixture in redox cycling microcosm experiments. The results can be compared to standard leaching

tests, which are applied to classify hazardous waste such as the toxicity characteristic leaching procedure (TCLP) (Figure 6A).

ii) How colloidal transport contributes to arsenic mobilization from disposed sand, soil, and their mixture should be investigated further as a column experiment (Figure 6B).

iii) Last, the results of microcosm and column experiments can be included into a statistical model to predict the risk of As mobilization from open disposal of sand filter materials (Figure 6C).

6.4. References

Amen, R., Bashir, H., Bibi, I., Shaheen, S.M., Niazi, N.K., Shahid, M., Hussain, M.M., Antoniadis, V., Shakoor, M.B., Al-Solaimani, S.G., Wang, H., Bundschuh, J., Rinklebe, J., 2020. A critical review on arsenic removal from water using biochar-based sorbents: The significance of modification and redox reactions. Chem. Eng. J. 396. https://doi.org/10.1016/j.cej.2020.125195

Berg, M., Luzi, S., Trang, P.T.K., Viet, P.H., Giger, W., Stüben, D., 2006. Arsenic removal from groundwater by household sand filters: Comparative field study, model calculations, and health benefits. Environ. Sci. Technol. 40, 5567–5573. https://doi.org/10.1021/es060144z

Ghosh, A., Mukiibi, M., Sáez, A.E., Ela, W.P., 2006. Leaching of arsenic from granular ferric hydroxide residuals under mature landfill conditions. Environ. Sci. Technol. 40, 6070–6075. https://doi.org/10.1021/es060561b

Herrera, K., Morales, L.F., Tarazona, N.A., Aguado, R., Saldarriaga, J.F., 2022. Use of Biochar from Rice Husk Pyrolysis: Part A: Recovery as an Adsorbent in the Removal of Emerging Compounds. ACS Omega 7, 7625–7637. https://doi.org/10.1021/acsomega.1c06147

Hu, W., Liang, J., Ju, F., Wang, Q., Liu, R., Bai, Y., Liu, H., Qu, J., 2020. Metagenomics Unravels Differential Microbiome Composition and Metabolic Potential in Rapid Sand Filters Purifying Surface Water Versus Groundwater. Environ. Sci. Technol. 54, 5197–5206. https://doi.org/10.1021/acs.est.9b07143

Hu, X., Ding, Z., Zimmerman, A.R., Wang, S., Gao, B., 2015. Batch and column sorption of arsenic onto iron-impregnated biochar synthesized through hydrolysis. Water Res. 68, 206–216. https://doi.org/10.1016/j.watres.2014.10.009

Larsen, E.I., Sly, L.I., McEwan, A.G., 1999. Manganese (II) adsorption and oxidation by whole cells and a membrane fraction of Pedomicrobium sp. ACM 3067. Arch. Microbiol. 171, 257–264.

Luzi, S., Berg, M., Trang, P.T.K., Viet, P.H., Schertenleib, R., 2004. Household sand filters for arsenic removal: An option to mitigate arsenic from iron-rich groundwater.

Mansor, M., Drabesch, S., Bayer, T., Van Le, A., Chauhan, A., Schmidtmann, J., Peiffer, S., Kappler, A., 2021. Application of Single-Particle ICP-MS to Determine the Mass Distribution and Number Concentrations of Environmental Nanoparticles and Colloids. Environ. Sci. Technol. Lett. https://doi.org/10.1021/acs.estlett.1c00314

Nitzsche, K.S., Lan, V.M., Trang, P.T.K., Viet, P.H., Berg, M., Voegelin, A., Planer-Friedrich, B., Zahoransky, J., Müller, S.K., Byrne, J.M., Schröder, C., Behrens, S., Kappler, A., 2015. Arsenic removal from drinking water by a household sand filter in Vietnam - Effect of filter usage practices on arsenic removal efficiency and microbiological water quality. Sci. Total Environ. 502, 526–536. https://doi.org/10.1016/j.scitotenv.2014.09.055

Ridge, J.P., Lin, M., Larsen, E.I., Fegan, M., McEwan, A.G., Sly, L.I., 2007. A multicopper oxidase is essential for manganese oxidation and laccase-like activity in Pedomicrobium sp. ACM 3067. Environ. Microbiol. 9, 944–953.

Shaheen, S.M., Mosa, A., Natasha, Abdelrahman, H., Niazi, N.K., Antoniadis, V., Shahid, M., Song, H., Kwon, E.E., Rinklebe, J., 2022. Removal of toxic elements from aqueous environments using nano zero-valent iron- and iron oxide-modified biochar: a review. Biochar 4, 1–21. https://doi.org/10.1007/s42773-022-00149-y

van Kessel, M.A.H.J., Speth, D.R., Albertsen, M., Nielsen, P.H., Op den Camp, H.J.M., Kartal, B., Jetten, M.S.M., Lücker, S., 2015. Complete nitrification by a single microorganism. Nature 528, 555–559. https://doi.org/10.1038/nature16459

Van Le, A., Marie Muehe, E., Drabesch, S., Lezama Pacheco, J., Bayer, T., Joshi, P., Kappler, A., Mansor, M., 2022a. Environmental Risk of Arsenic Mobilization from Disposed Sand Filter Materials. Environ. Sci. & Technol. 0. https://doi.org/10.1021/acs.est.2c04915

Van Le, A., Straub, D., Planer-Friedrich, B., Hug, S.J., Kleindienst, S., Kappler, A., 2022b. Microbial communities contribute to the elimination of As, Fe, Mn, and NH4+ from groundwater in household sand filters. Sci. Total Environ. 838, 156496. https://doi.org/10.1016/j.scitotenv.2022.156496

Voegelin, A., Kaegi, R., Berg, M., Nitzsche, K.S., Kappler, A., Lan, V.M., Trang, P.T.K., Göttlicher, J., Steininger, R., 2014. Solid-phase characterisation of an effective

household sand filter for As, Fe and Mn removal from groundwater in Vietnam. Environ. Chem. 11, 566–578.

Zhang, M., Song, G., Gelardi, D.L., Huang, L., Khan, E., Mašek, O., Parikh, S.J., Ok, Y.S., 2020. Evaluating biochar and its modifications for the removal of ammonium, nitrate, and phosphate in water. Water Res. 186. https://doi.org/10.1016/j.watres.2020.116303

Zhang, W., Cho, Y., Vithanage, M., Shaheen, S.M., Rinklebe, J., Alessi, D.S., Hou, C.H., Hashimoto, Y., Withana, P.A., Ok, Y.S., 2022. Arsenic removal from water and soils using pristine and modified biochars. Biochar 4. https://doi.org/10.1007/s42773-022-00181-y

Zhou, Y., Gao, B., Zimmerman, A.R., Chen, H., Zhang, M., Cao, X., 2014. Biochar-supported zerovalent iron for removal of various contaminants from aqueous solutions. Bioresour. Technol. 152, 538–542. https://doi.org/10.1016/j.biortech.2013.11.021

Zhu, Y.G., Xue, X.M., Kappler, A., Rosen, B.P., Meharg, A.A., 2017. Linking Genes to Microbial Biogeochemical Cycling: Lessons from Arsenic. Environ. Sci. Technol. 51, 7326–7339. https://doi.org/10.1021/acs.est.7b00689

Statement of personal contribution

The German Research Foundation funded this work (Deutsche Forschungsgemeinschaft, DFG), project number (DFG, KA1736/41-1). Prof. Andreas Kappler, the main supervisor throughout the project, designed the conceptual background for this project. Besides, Dr. Stephan Hug (Eawag) is the second supervisor who reviews research outlines and publications. Apart from chapter 4, which was conceptualized and written by Dr. Muammar Mansor, other experiments and chapters were either conceptualized by myself or with Prof. Kappler and were carried out and written by me.

In detail, the contributions of people other than Prof. Kappler or myself were:

Field Work: The fieldwork in 2018 and 2020 required extensive planning and preparation. I was supported by Vietnamese colleagues/ collaborators: Pham Vy Anh (Vietnam Institute of Industrial Chemistry), Prof. Viet, Prof. Trang, Duyen, The Anh (KLATEFOS) Hanoi University of Science. The sampling campaign 2020 also included the help of master student P. Tutiyasarn (Elly) from the University of Tuebingen.

Chapter 2. Prof. Britta Planer-Friedrich and technician Stefan Will helped with As analysis by ICP-MS. Stephan Hug supported XRF analysis in Eawag. Ellen Röhm performed nitrate and nitrite, and ammonium analysis. Franziska Schädler advised on DNA extractions, and Student Assistance (hiwi) Caroline Schlaiss helped with qPCR-related works. Daniel Straub processed sequencing data. Jun-Prof. Dr. Sara Kleindienst and all other co-authors contributed to manuscript revisions and/or wrote parts of the manuscript. Infrastructural support of this work included the Deutsche Forschungsgemeinschaft (DFG) under Germany's Excellence Strategy, cluster of Excellence EXC2124, project ID 390838134. Daniel Straub was funded by the University of Tuebingen Institutional Strategy (DFG, ZUK63). Sara Kleindienst is supported by an Emmy- Noether fellowship from the DFG (grant number 326028733).

Chapter 3. Assoc. Prof. Marie Muehe helped with synchrotron-related works (including sample preparation, measurement, and data analysis). Dr. Sam Webb and Dr. Saron Bone helped at SSRL with beamline support (proposal number 5587). Sören Drabesch analyzed As, Fe, Mn by ICP-MS. Dr. Stefan Fisher conducted SEM/EDS. Column experiments were operated with the help of student assistant P. Tutiyasarn (Elly) in the lab and field. Julian Sorwat analyzed aqueous Mn(II) by MPAES. All co-

authors contributed to manuscript revisions and/or wrote parts of the manuscript. Infrastructural support of this work included the Deutsche Forschungsgemeinschaft (DFG) under Germany's Excellence Strategy, cluster of Excellence EXC2124, project ID 390838134; Tübingen Structural Microscopy Core Facility (Funded by the Federal Ministry of Education and Research (BMBF) and the Baden-Württemberg Ministry of Science as part of the Excellence Strategy of the German Federal and State Governments) and Stefan Fisher was funded by the DFG (INST 37/1027-1 FUGG).

Chapter 4. The works were conceptualized, analyzed, and written by Dr. Muammar Mansor in corporation with Prof. Andreas Kappler and Prof Stefan Peiffer. Sören Drabesch, Timm Bayer, Anh Van Le, Ankita Chauhan, and Johanna Schmidtmann provided samples, helped with sample preparation, and revised the manuscript. Infrastructural support of this work included Deutsche Forschungsgemeinschaft (DFG, German Research Foundation) under Germany's Excellence Strategy, cluster of Excellence EXC2124, Project 390838134. This work was funded by the DFG Project 391977956 (SFB 1357) and KA 1736/66-1, KA 1736/51-1, and KA 1736/48-1 and Cluster of Excellence: EXC 2124: Controlling Microbes to Fight Infection, Tübingen, Germany.

Chapter 5. Assoc. Prof. Marie Muehe helped with synchrotron-related works (including sample preparation, measurement, and data analysis). Dr. Latimer and Dr. Juan S. Lezama Pacheco helped at SSRL with beamline support (proposal number 5587). Sören Drabesch analyzed As, Fe, Mn by ICP-MS. Dr. Prachi Joshi and Timm Bayer conducted Mössbauer analysis. The microcosms experiments were operated by the help of student assistants P. Tutiyasarn (Elly) and Thomas Schlereth. Muammar Mansor helped with spICP-MS analysis and conceptualized the experiment and manuscript. All co-authors contributed to manuscript revisions and/or wrote parts of the manuscript. Infrastructural support of this work included the Deutsche Forschungsgemeinschaft (DFG) under Germany's Excellence Strategy, cluster of Excellence EXC2124, project ID 390838134.

I state hereby that I have not plagiarized or copied any of the text. Chapter 2 was published in Science of The Total Environment journal. Chapter 3 is in preparation for submission to the Water Research X journal. Thus it might be published with minor variations elsewhere in the future. Chapter 4 was published in Environmental Science and Technology Letter Journal, and Chapter 5 was published in Environmental Science and Technology Journal.